

# **The Role of Endoglin in Endothelial and Mesenchymal cells during Development, Maintenance and Repair of the Heart**

**Esha Singh**

Thesis submitted for the degree of  
**Doctor of Philosophy**

**Institute of Genetic Medicine  
Faculty of Medical Sciences  
Newcastle University  
December 2019**

---

---

## Abstract

Mutations in the endoglin gene lead to Haemorrhagic Telangiectasia Type 1 (HHT1), an inherited vascular disease, demonstrating the importance of endoglin in the vasculature. Haplo-deficiency of endoglin also leads to reduced angiogenesis in mice in several pathologies, indicating a pro-angiogenic role for endoglin. However, the precise role of endoglin in development and maintenance of the vasculature is still unclear. The aim of this project therefore was to investigate the role of endoglin during vascular development and maintenance and whether its pro-angiogenic properties can be used to enhance cardiac recovery following myocardial infarction (MI).

Using immunofluorescence staining of mouse cardiac tissue, I showed high endoglin expression in coronary veins endothelial cells (ECs), capillaries & endocardium and weak expression in coronary arteries ECs, valve mesenchyme & in epicardially derived cells (EPDCs) during development. I hypothesised that during cardiac development endoglin is essential for EC proliferation and migration, and plays a key role during EPDC proliferation, migration and differentiation. Induced knockdown of endoglin in murine epicardial cells using *Wt1-Cre* led to a reduced number of EPDCs in E15.5 hearts but did not lead to any detectable vascular defects in E17.5 hearts.

In contrast, EC-specific endoglin knockdown in the first week of postnatal life (which is known to lead to retinal AVMs) was associated with the development of eccentric cardiomyopathy and cardiomyocytes (CM) hypertrophy, but no obvious coronary vasculature defects. Deletion of endoglin in venous ECs and capillaries in first week of postnatal life also led to development of AVMs in P11 retinas coupled with the development of cardiac hypertrophy. A similar eccentric cardiomyopathy phenotype with CM hypertrophy was observed after endoglin deletion in adult ECs (*Eng-iKO<sup>EC</sup>*). Microbeads were used to show increased vascular shunting in the systemic but not the pulmonary vasculature of *Eng-iKO<sup>EC</sup>* mice. Ultimately *Eng-iKO<sup>EC</sup>* mice developed high output heart failure due to reduced vascular resistance caused by systemic AVMs. This data confirms that endoglin is vital for maintaining the adult vasculature.

Finally, I analysed the role of endoglin in a heterogeneous population of cardiac derived stem cells known as cardiosphere derived cells (CDCs). CDCs express endoglin which I showed is vital for their pro-angiogenic paracrine effect when delivered to the infarcted heart. Furthermore, endoglin not only promotes paracrine mediated proliferation of ECs in the infarct zone but also helps in maturation of the neo-vasculature by recruitment of smooth muscle cells.

In conclusion, the results from this thesis show the critical importance of endoglin in the development and maintenance of the vasculature.

---

## **Declaration**

The work described in this thesis was undertaken in the laboratory of Prof. Helen M. Arthur at the Institute of Genetic Medicine, Newcastle University for the fulfilment of the requirements for the degree of Doctor of Philosophy.

The results described in the thesis was my own work and I have correctly acknowledged the contributions of others where appropriate in the text. No material within this thesis has been submitted by me for a degree or diploma or other qualification in this or any other University. This thesis does not exceed the word limit prescribed by the Faculty of Medical Sciences.

**Esha Singh**

December 2019

---

## Acknowledgement

I would like to first thank my supervisor Prof. Helen Arthur for the opportunity to perform this research in her laboratory. I would also like to thank Prof. Arthur for her continuous support, guidance and expertise which helped me to be a better scientist today. Next, I would like to thank my co-supervisor Dr. Helen Phillips for her expertise and support throughout my PhD.

Next, I would like to thank Dr. Rachael Redgrave for her encouragement and support, for all the coffees and lunches. It meant a lot. I would also like to thank Rachael for all discussions and ideas which helped me understand my work better, especially for the contributions for the work during CDCs mediated heart repair. Also thank you so much for performing the MI surgeries and the intraocular injections.

I would next like to thank Dr. Simon Tual-Chalot for collaborations and help especially during the endothelial endoglin study in adult and also for teaching me neonatal retina dissections. Next, I would like to thank Dr. Darroch Hall for preparing CDCs during MI surgeries and genotyping mice. I would next like to thank Dr. Kate Bailey for her help with Wt1-Cre optimisation and for her guidance during staining protocol optimisations. I would also like to thank Dr. Rebecca Dodds for her help with optimisation of Sm22a staining on wax sections. I would next like to thank Ms. Elizabeth Grealley for her the useful tips on sectioning and Ms. Kathleen Alison for her help in lab. I would also like to thank Dr. Gavin Richardson for showing me how to use Stero SV 11 microscope. Next, I would like to pass my sincere thanks to all the staff in the mouse unit especially Mr. Steve Smith for the endless help and guidance with mice. I would also like to give a big thank you to Ms. Lisa Hodgson for answering my continuous questions on microscopy. I learnt a lot from her as well as from the Microscope team at Carl Zeiss.

Finally, I would like to thank my family, my dad, my mum, my wife, brothers, aunts, cousins and all my dear friends (Monish, Avinash, Niki, Elena and Rachael) for giving me the strength and courage to be here today. I would especially like to thank two very important people in my life, my dad and my wife. Thank you, my sweet and wonderful father for being my inspiration, my rock and support throughout my life. And thank you to my beautiful wife, Jelena for being here for me, for listening to me endlessly, for holding me when I was sad, for making me laugh and for all love. This thesis is dedicated to you both because without you it would not be possible. I love you both so much!!

---

## Table of Contents

Abstract.....	ii
Declaration.....	iii
Acknowledgement.....	iv
Table of Contents .....	v
List of Figures.....	x
List of Tables.....	xvii
List of Abbreviations.....	xix
Chapter 1. Introduction .....	23
1.1. Heart Development .....	24
1.2. Vasculogenesis and Angiogenesis during Development .....	25
1.2.1. Anatomy of Mature Coronary Circulation .....	28
1.3. Cells in Coronary Vessels Development .....	31
1.3.1. Role of Epicardium in Coronary Vessel Development .....	32
1.3.2. Origin of the Endothelial Component of Coronary Vessels.....	37
1.4. TGF $\beta$ and Endoglin in Coronary Vasculature Development.....	40
1.4.1. TGF $\beta$ Ligands and its Receptors .....	40
1.4.2. Endoglin: TGF $\beta$ type 3 co-receptor.....	42
1.5. TGF $\beta$ and Endoglin in Coronary Vessel Development .....	45
1.5.1. TGF $\beta$ and Endoglin in Endothelial Cells .....	45
1.5.2. TGF $\beta$ Ligands and Receptors in Vasculature Development .....	48
1.5.3. TGF $\beta$ Signalling during EMT .....	50
1.6. Hereditary Haemorrhagic Telangiectasia (HHT).....	51
6.1.1. Role of TGF $\beta$ Signalling in HHT .....	53
6.1.2. Treatment for HHT.....	54
1.7. Myocardial Infarction .....	56
1.7.1. Importance of TGF $\beta$ during Heart Repair .....	57
1.7.2. Cell Mediated Therapy in Post-MI.....	59
1.8. Aims.....	61

---

1.9. Hypotheses .....	61
Chapter 2. Materials and Methods .....	62
2.1. Mouse Strains and Genotyping .....	63
2.1.1. Mouse Strains.....	63
2.1.2. Tamoxifen .....	66
2.1.3. Dissection of Embryos, Pups and Adult Hearts .....	67
2.2. Processing, Fixing and Embedding of Tissue .....	69
2.2.1. Paraffin Embedding .....	69
2.2.2. Embedding for Cryo Sectioning .....	69
2.3. Genotyping .....	70
2.3.1. Genotyping using Mouse Tissue.....	70
2.3.2. Genotyping using Mouse Tissue Section.....	73
2.4. Sectioning.....	73
2.4.1. Paraffin Wax Sectioning .....	73
2.4.2. OCT Cryo-Sectioning .....	73
2.5. Staining.....	74
2.5.1. Haematoxylin and Eosin (H&E) Staining.....	74
2.5.2. Immunohistochemistry (IHC) using DAB.....	74
2.5.3. Immunofluorescence on paraffin embedded sections.....	76
2.5.4. Immunofluorescence on OCT embedded sections.....	76
2.5.5. Immunofluorescence on Whole-mount Retinas.....	79
2.6. Intra-Ocular BMP9 Injection.....	80
2.7. Injection of Microbeads.....	80
2.7.1. 15 $\mu\text{m}^3$ Red Fluorescence Microbeads Perfusion .....	80
2.7.2. 45 $\mu\text{m}^3$ Green Fluorescence Microbeads Perfusion.....	81
2.7.3. 15 $\mu\text{m}^3$ and 45 $\mu\text{m}^3$ beads perfused Organs: Tissue Mounting .....	81
2.8. CDC Culture.....	82
2.9. MI Surgery and Intra-Myocardial Injection .....	83
2.10. Microscopy .....	84

---

---

2.10.1. Organs/ Embryo Imaging .....	84
2.10.2. Imaging Retinas .....	84
2.10.3. Bright-field and Fluorescence Microscopy .....	85
2.10.4. Imaging and Analysis .....	86
2.11. Statistical Analysis .....	86
Chapter 3. Endoglin Expression in the Heart from Embryo to Adult.....	88
3.1. Introduction.....	89
3.2. Results.....	90
3.2.1. Staining Optimisation.....	90
3.2.2. Expression of Endoglin in Coronary Vessels during Embryogenesis.....	93
3.2.3. Endoglin in Mesenchymal Cells of Embryonic Mice Heart.....	105
3.2.4. Endoglin Expression in Coronary Arteries, Veins and Capillaries .....	111
3.2.5. Expression of Endoglin in Postnatal Mice Hearts.....	114
3.2.6. Expression of Endoglin in Adult Mice Hearts.....	117
3.3. Discussion.....	121
3.3.1. Endoglin in Coronary Endothelial Cells.....	121
3.3.2. Endoglin in Cardiac Mesenchymal Cells .....	122
Chapter 4. Role of Endoglin and TGF $\beta$ R2 in Epicardial Derived Cells during Heart Development	124
4.1. Introduction.....	125
4.1.1. Endoglin and TGF $\beta$ Signalling in EMT .....	125
4.2. Results.....	127
4.2.1. Wt1 <sup>Cre-ERT2</sup> Optimisation and Lineage Tracing .....	127
4.2.2. Expression of Endoglin in EPDCs <i>in vivo</i> .....	135
4.2.3. Effect of Epicardial Specific Endoglin Knockdown on Coronary Vessel Development.....	140
4.2.4. Effect of Epicardial Specific <i>Tgfb2</i> Knockdown on Coronary Vessels Development.....	145
4.3. Discussion.....	150

---

---

4.3.1.	Specificity of Wt1-Cre <sup>ERT2</sup> .....	150
4.3.2.	Role of Endoglin in EPDCs .....	151
4.3.3.	Role of TGFβR2 in Epicardium and EPDCs .....	152
Chapter 5.	Role of Endoglin in Endothelial Cells during Development and in Adult Life	155
5.1.	Introduction .....	156
5.1.1.	Endoglin in Coronary Vessel Development.....	156
5.1.2.	Endoglin and the Developing Retinal Vasculature .....	158
5.1.3.	Endoglin and Quiescent Adult Vasculature .....	159
5.2.	Results .....	160
5.2.1	Optimisation of <i>Dll4in3</i> <sup>Cre-ERT2</sup> activation .....	160
5.2.2	Effect of Endothelial Specific Endoglin Knockdown on Coronary Vessel Development in the Foetal and Neonatal Heart.....	163
5.2.3	Effect of Endothelial Specific Endoglin Knockdown on the Neonatal Retinal Vasculature.....	175
5.2.4	To investigate the effect of exogenous BMP9 treatment on AVM formation in Eng-iKO <sup>EC</sup> mice – A Pilot Study .....	178
5.2.5	Effect of Venous Endothelial Specific Endoglin Knockdown on AVM formation in Neonates using <i>Apj</i> <sup>Cre-ER</sup> .....	182
5.2.6	Effect of Endoglin Knockdown in Adult Quiescent Endothelial Cells using VE-Cad <sup>Cre-ERT2</sup> .....	196
5.3.	Discussion .....	209
5.3.1	Endoglin in coronary ECs during cardiac development .....	209
5.3.2	BMP9 mediated rescue of AVM phenotype .....	211
5.3.3	Origin of AVMs: Arterial, Venous or Both .....	212
5.3.4	Endoglin in Vascular Maintenance in Adult Mice.....	213
Chapter 6.	Role of Endoglin in CDC Promoted Angiogenesis in Post-MI Hearts.....	217
6.1.	Introduction .....	218
6.1.1.	Cardiospheres Derived cells in Therapeutic Angiogenesis Post-MI .....	218
6.1.2.	Role of Endoglin in CDCs: Pilot study.....	219
6.2.	Results .....	221

---

---

6.2.1. Experimental setup and optimisation of CD31 quantification .....	221
6.2.2. Pro-angiogenic effect of CDCs is Endoglin Dependent .....	224
6.2.3. Endoglin Promotes Vessel Maturation in the Infarct Border Zone .....	225
6.3. Discussion .....	233
Chapter 7. Final Discussion and Future Work .....	238
APPENDIX .....	243
REFERENCES .....	249

---

## List of Figures

Figure 1.1: Schematic of mice heart development.....	24
Figure 1.2: Process of Vasculogenesis and Angiogenesis .....	26
Figure 1.3: Coronary circulation tree .....	28
Figure 1.4: Coronary arteries and their attachment at the aorta (ostium). .....	29
Figure 1.5: Coronary arteries .....	30
Figure 1.6: Coronary Veins.....	31
Figure 1.7: Development of Coronary Vasculature .....	32
Figure 1.8: Layers of the Heart .....	33
Figure 1.9: Heart with epicardium from two different sources.....	33
Figure 1.10: During Epicardial EMT, TGF $\beta$ signalling occurs via ALK5 Mediated Type 1 Receptor .....	35
Figure 1.11: Fate of epicardial cells: Epicardial cells undergo EMT under the influence of signalling proteins to form EPDCs .....	35
Figure 1.12: Potential origin of coronary endothelial cells through three different progenitor cells .....	39
Figure 1.13: Different waves of Coronary Vessels formation during mouse heart development and in post-natal life.....	40
Figure 1.14: Structure of TGF $\beta$ receptor .....	41
Figure 1.15: Structure of Endoglin .....	43
Figure 1.16: Molecular structure of different endoglin isoforms.....	44
Figure 1.17: Dual role of canonical TGF $\beta$ / BMP signalling in endothelial cells .....	46
Figure 1.18: Endoglin in TGF $\beta$ mediated angiogenesis .....	47
Figure 1.19: Arteriovenous Malformation in HHT.....	52
Figure 1.20: Phases of Cardiac Healing.....	57
Figure 1.21: Role of TGF $\beta$ during Cardiac Healing .....	58
Figure 1.22: Direct and indirect mechanism of cell-mediated heart repair .....	59
Figure 2.1: Transgenic Rosa26 locus with floxed stop eYFP gene .....	63

---

Figure 2.2: Floxed <i>Endoglin</i> gene showing the <i>LoxP</i> sites flanking exon 5 and 6 .....	64
Figure 2.3: Floxed <i>Tgfb<math>\beta</math>2</i> gene showing the <i>LoxP</i> sites flanking exon 4.....	64
Figure 2.4: Transgenic Rosa26 locus with mTmG reporter sequence .....	66
Figure 2.5: ‘Petal’ shape appearance of freshly dissected neonate retina .....	68
Figure 2.6: Cartoon of a sample preparation for imaging whole organs and lung slices using M2 axio-imager microscope .....	81
Figure 2.7: Image of an adult mouse heart after a MI surgery. MI was induced by ligating the LAD and confirmation of MI was established blanching of the myocardium .....	84
Figure 2.8: Bleed through check for Carl Zeiss M2 Axioimager Filter Sets.....	87
Figure 3.1: Co-localisation of rat and goat anti-CD105 antibodies on E15.5 and E17.5 heart sections .....	92
Figure 3.2: Quantification of cytoplasmic endoglin expression/staining intensity using the spline contour function of Zen lite 2012 software.....	94
Figure 3.3: Endoglin is expressed in the endocardium and endothelium of nascent blood vessels in E11.5 mouse hearts.....	95
Figure 3.4: At E13.5 endoglin expression was observed in the endocardium, endothelium of nascent coronary vessels and in non-ECs.....	97
Figure 3.5: At E15.5 strong endoglin expression is observed in the endocardium, endothelium of coronary vessels and at lower levels in the presumed EPDCs.....	100
Figure 3.6: At E17.5 endoglin expression is predominantly expressed in the endocardium and endothelium of coronary vessel.....	103
Figure 3.7: Valvular mesenchymal cells express low levels of endoglin compared to adjacent endocardial cells .....	106
Figure 3.8: Similar Level of Endoglin Expression Observed in Valvular Mesenchymal Cells and Presumed EPDCs.....	107
Figure 3.9: At E11.5, SM22 $\alpha$ expression was observed in the major arteries of the embryos. ....	108
Figure 3.10: Presumed EPDCs in E13.5, E15.5 and E17.5 mouse hearts express low levels of endoglin and SM22 $\alpha$ .....	109

---

---

Figure 3.11: The number of presumed EPDCs expressing low levels of endoglin peaks at E15.5 during mouse heart development .....	110
Figure 3.12: At E17.5 endoglin is predominantly expressed within the endothelium of the coronary vessels and is expressed at higher levels in veins compared to arteries and presumed EPDCs.....	112
Figure 3.13: Significantly higher endoglin expression is observed in ECs of coronary veins and capillaries compared to coronary arteries in P21 hearts .....	115
Figure 3.14: Arteries and veins distinction in the adult heart using elastin auto-fluorescence and endomucin marker.....	118
Figure 3.15: In healthy adult mice heart, a higher level of endoglin is expressed by endothelial cells of coronary veins and capillaries in comparison to coronary arteries .....	119
Figure 3.16: Dynamic Expression of Endoglin in Coronary ECs throughout development and in adult heart.....	121
Figure 3.17: Endoglin is strongly expressed in the coronary ECs compare to a weaker expression in the mesenchymal cells .....	123
Figure 4.1: Analysis of $Wt1^{Cre-ERT2}$ activity using $Rosa26^{eYFP}$ reporter .....	128
Figure 4.2: Strong eYFP expression was observed in the epicardium and in the EPDCs after activation of $Wt1^{Cre-ERT2}$ .....	129
Figure 4.3: $Wt1^{Cre-ERT2}$ activation to detect EPDCs in the hearts of E15.5 $Wt1^{Cre-ERT2}; Rosa26^{eYFP/eYFP}$ embryos .....	130
Figure 4.4: Cartoon image of transverse section of an embryonic heart section .....	131
Figure 4.5: $Wt1^{Cre-ERT2}$ lineage tracing using the optimised activation protocol .....	134
Figure 4.6: Mouse lines used to study and knockdown the expression of endoglin in epicardium and EPDCs <i>in vivo</i> .....	135
Figure 4.8: A cartoon and an example image of a z-stack .....	136
Figure 4.9: EPDCs express endoglin <i>in vivo</i> .....	137
Figure 4.10: Endoglin knockout in the EPDCs led to a significantly reduced number of EPDCs in $Eng-iKO^{epi}$ mutants compared to age matched controls .....	139
Figure 4.11: Staging control and $Eng-iKO^{epi}$ mutant embryos using hind limb development .....	140

---

---

Figure 4.13: Normal heart morphology of control and <i>Eng-iKO<sup>epi</sup></i> mutant embryos at E17.5. .....	141
Figure 4.14: specific endoglin knockdown did not lead to vasculature or structural defects.. .....	143
Figure 4.15: Epicardial Specific <i>Tgfb2</i> knockout using <i>Wt1<sup>Cre-ERT2</sup></i> mouse line.....	145
Figure 4.16: Confirmation of the presence of <i>Tgfb2-iKO<sup>epi</sup></i> recombined gene in epicardial and epicardially derived cells from tissue sections .....	146
Figure 4.17: Epicardial Specific <i>Tgfb2</i> knockout using <i>Wt1<sup>Cre-ERT2</sup></i> did not have any effect on development of the mouse hear .....	147
Figure 4.18: Epicardial specific <i>Tgfb2</i> knockdown did not lead to any vasculature related defects.....	148
Figure 4.19: Summary of TGF $\beta$ signalling in EPDCs in the presence and absence of Endoglin or TGF $\beta$ R2.....	154
Figure 5.1: Depletion of <i>Endoglin</i> using <i>VE-Cad<sup>Cre-ERT2</sup></i> even at later stages led to rapid embryonic lethality .....	157
Figure 5.2: <i>Dll4in3<sup>Cre-ERT2</sup></i> cloned sequence and its insertion into mouse genome .....	158
Figure 5.3: BMP9 mediated signalling in ECs via ALK1 and endoglin mediated signalling. .....	159
Figure 5.4: Knockdown of <i>Endoglin</i> in ECs lead to High Output Heart Failure .....	160
Figure 5.5: Optimisation of <i>Dll4in3<sup>Cre-ERT2</sup></i> activation .....	161
Figure 5.6: <i>Dll4in3<sup>Cre-ERT2</sup></i> activation and analysis at different time points in heart development. .....	162
Figure 5.7: Mapping the expression pattern of <i>VE-Cad<sup>Cre-ERT2</sup></i> in neonate mouse hearts using <i>Rosa26<sup>eYFP</sup></i> reporter mice.....	163
Figure 5.8: Endothelial specific <i>Endoglin</i> knockdown using <i>Eng<sup>fl/fl</sup>; VE-Cad<sup>Cre-ERT2</sup></i> mouse line. .....	164
Figure 5.9: Activation of <i>VE-Cad<sup>Cre-ERT2</sup></i> at P2 & P4 showed strong expression of eYFP in coronary endothelium of P7 hearts.....	165
Figure 5.10: Endothelial specific <i>Endoglin</i> knockdown using <i>VE-Cad<sup>Cre-ERT2</sup></i> led to development of enlarged hearts in P7 <i>Eng-iKO<sup>EC</sup></i> mice compared to controls.....	166

---

---

Figure 5.11: Cartoon image of coronal P7 heart section.....	167
Figure 5.12: Lack of <i>Endoglin</i> in ECs did not lead to any coronary vasculature related defects in P7 <i>Eng-iKO<sup>EC</sup></i> hearts.....	168
Figure 5.13: Endothelial specific <i>Endoglin</i> knockdown led to cardiomyocyte hypertrophy in P7 <i>Eng-iKO<sup>EC</sup></i> hearts compared to controls .....	171
Figure 5.14: Endothelial specific <i>Endoglin</i> knockdown led to an enlarged heart. ....	174
Figure 5.15: Cartoon of neonate retina showing vasculature structure and progression .....	175
Figure 5.16: Endothelial specific <i>Endoglin</i> knockdown led to development of AVMs in P7 <i>Eng-iKO<sup>EC</sup></i> retinas.....	177
Figure 5.17: Intraocular exogenous treatment of BMP9 did not rescue the AVMs phenotype in P7 <i>Eng-iKO<sup>EC</sup></i> .....	179
Figure 5.18: Intraocular injection of PBS and BMP9 at P5 exacerbates the AVMs phenotype in P7 <i>Eng-iKO<sup>EC</sup></i> mice.....	180
Figure 5.19: Optimisation of <i>Apj<sup>Cre-ER</sup></i> activation using <i>Rosa26<sup>mTmG</sup></i> reporter mice.....	183
Figure 5.20: Activation of <i>Apj<sup>Cre-ER</sup></i> by tamoxifen injection at P5 or P6 showed GFP expression in veins and capillaries of P8 retina .....	185
Figure 5.21: Activation of <i>Apj<sup>Cre-ER</sup></i> at P6 by tamoxifen leads to GFP reporter expression in coronary veins and capillaries but not arteries of P8 hearts.....	186
Figure 5.22: Mouse models used to study the effect of venous ECs specific <i>Endoglin</i> knockdown.....	187
Figure 5.23: Endothelial specific <i>Endoglin</i> knockdown using <i>VE-Cad<sup>Cre-ERT2</sup></i> and <i>Apj<sup>Cre-ER</sup></i> lead to enlarged hearts in both males and females at P11 <i>Eng-iKO<sup>EC</sup></i> and <i>Eng-iKO<sup>V</sup></i> mice compared to controls.....	188
Figure 5.24: Cartoon of retina vasculature development in mice [adapted from (301, 304)]. New born mice retinas are avascular .....	189
Figure 5.25: <i>Endoglin</i> knockdown using <i>VE-Cad<sup>Cre-ERT2</sup></i> and <i>Apj<sup>Cre-ER</sup></i> led to formation of AVMs in P8 and P11 retinas.....	191
Figure 5.26: In-depth coding showed the AVMs observed in P11 <i>Eng-iKO<sup>EC</sup></i> and <i>Eng-iKO<sup>V</sup></i> retinas had developed in the primary plexus.....	192

---

---

Figure 5.27: <i>Endoglin</i> knockdown using <i>VE-Cad</i> <sup>Cre-ERT2</sup> and <i>Apj</i> <sup>Cre-ER</sup> leads to development of wider veins and AVMs in P8 and P11 retinas .....	194
Figure 5.28: <i>Endoglin</i> knockout in adult quiescent ECs using <i>VE-Cad</i> <sup>Cre-ERT</sup> .....	196
Figure 5.29: <i>Endoglin</i> knockdown in ECs using <i>VE-Cad</i> <sup>Cre-ERT2</sup> leads to enlarged adult hearts five weeks after <i>Endoglin</i> knockdown .....	197
Figure 5.30: Morphological characteristic used to identify arteries and veins in heart, lungs and liver.....	199
Figure 5.31: Different levels of <i>Endoglin</i> knockdown was observed in the arteries and veins of heart, lungs and liver using <i>VE-Cad</i> <sup>Cre-ERT</sup> .....	200
Figure 5.32: Depletion of <i>Endoglin</i> in adult quiescent ECs using <i>VE-Cad</i> <sup>Cre-ERT2</sup> leads to cardiac hypertrophy.....	202
Figure 5.33: Injection of fluorescently labelled microsphere to investigate the presence of AVMs in pulmonary or systemic circulation. ....	203
Figure 5.34: Knockdown of <i>Endoglin</i> in quiescent ECs using <i>VE-Cad</i> <sup>Cre-ERT2</sup> did not lead to formation of AVMs in the lungs. ....	205
Figure 5.35: Knockdown of <i>Endoglin</i> in quiescent ECs using <i>VE-Cad</i> <sup>Cre-ERT2</sup> cause systemic vasculature related abnormalities .....	208
Figure 5.36: Endothelial <i>Endoglin</i> knockdown in adult ECs leads to development of AVMs in pubis symphysis .....	214
Figure 5.37: Summary of TGFβ/BMP9 signalling in quiescent endothelial cells in the presence and absence of endoglin .....	216
Figure 6.1: Derivation of murine CDCs .....	219
Figure 6.2: Characterisation of endoglin expression in CDCs and knock-down .....	220
Figure 6.3: Effect of endoglin knockout on CDC mediated heart repair, pilot data results ...	221
Figure 6.4: Experimental Design: Immunofluorescent Staining .....	222
Figure 6.5: Knockout of <i>Endoglin</i> in CDCs leads to loss of the pro-angiogenic effect of control donor cells 4 weeks post-MI.....	226
Figure 6.6: Major vascular and ventricular remodelling was observed in all 4-weeks post-MI hearts.....	227

---

---

Figure 6.7: Whole-view tiled image of 4-weeks sham and MI hearts showing the analysis area..	229
Figure 6.8: <i>Endoglin</i> loss in donor CDCs led to a reduction of muscularised vessels in the trans- border region of 4 weeks post-MI hearts .....	230
Figure 6.9: Quantification showed a significant reduction in percentage of muscularised vessels in MI hearts after transplantation of Eng-iKO CDCs. ....	233

---

## List of Tables

Table 1.1: Molecules Involved in EPDCs differentiation during coronary vasculature development. ....	36
Table 1.2: Defects in mice and humans due to knockout or depletion of TGF $\beta$ ligands and/or its receptors [adapted from (66)]. ....	49
Table 1.3: Clinical classification of Myocardial Infarction [taken from (201)].....	56
Table 2.1: Paraffin Embedding Protocol .....	69
Table 2.2: OCT Embedding Protocol.....	69
Table 2.3: PCR Reaction .....	71
Table 2.4: PCR Conditions and Primer sequences (for PCR reaction temperature, refer to table 2.4).....	71
Table 2.5: Primary Antibody Details for IHC-DAB Staining.....	75
Table 2.6: Secondary Antibody Details for IHC-DAB Staining.....	75
Table 2.7: Secondary Antibody and Isolectin Details .....	76
Table 2.8: Primary Antibody Details for Immunofluorescence .....	78
Table 2.9: Secondary Antibodies Details for Immunofluorescence.....	79
Table 2.10: Antibodies details for Whole-mount Immunofluorescence .....	80
Table 2.11: Carl Zeiss Axioimager M2 Filter Set Details.....	85
Table 3.1: Antibodies used to characterise expression of endoglin in developing, postnatal and adult mouse heart. Antibodies details are summarised in Table 2.8. ....	91
Table 4.1: Combinations of Wt1 <sup>Cre-ERT2</sup> with different Cre-Activated Rosa26 Reporters from different genetic background [adapted from (253)] .....	127
Table 4.2: The activation of Wt1 <sup>Cre-ERT2</sup> using three different tamoxifen regimes (2 Subcut, 3 Subcut & 3 IP) showed a similar density of YFP positive EPDCs at E15.5. ....	131
Table 4.3: Antibodies used to for lineage tracing of EPDCs after activation of Wt1 <sup>Cre-ERT2</sup> using the optimised protocol. Antibodies details are summarised in Table 2.8.....	133
Table 4.4: EPDCs differentiation into Cardiac Cell Types at E17.5.....	135
Table 4.5: Data summary of <i>in vivo</i> expression of endoglin in EPDCs of E15.5 control and Eng-iKO <sup>epi</sup> mutant embryos. ....	138

---

Table 4.6: Concentrations of DNA in Tgfb $\beta$ 2-iKO <sup>epi</sup> and littermate control embryonic heart sections.....	145
Table 5.1: Data summary of heart and retinal phenotype in pups with endoglin knockout in all ECs (Eng-iKO <sup>EC</sup> ) and venous & capillary ECs (Eng-iKO <sup>V</sup> ) .....	193
Table 5.2: Results summary of tail vein injection of 2x10 <sup>5</sup> (200 $\mu$ l) 15 $\mu$ m <sup>3</sup> red fluorescently labelled microspheres in control and Eng-iKO <sup>qEC</sup> female mice .....	204
Table 5.3: Results summary of 45 $\mu$ m <sup>3</sup> green fluorescently labelled microspheres (5.5x10 <sup>4</sup> ) entrapment in organs of female controls and Eng-iKO <sup>qEC</sup> mice injected via left ventricle...	207
Table 6.1: Summary of ImageJ area analysis of CD31 stained heart sections 4 weeks post-MI and cell delivery .....	224
Table 6.2: Summary of the average number of muscularised/ $\alpha$ SMA positive vessels in the trans-border zone 4wks post-MI with and without CDCs, with and without endoglin KO.....	232
Table 6.3: Summary of density of muscularised vessels per FOV in the trans-border zone 4-weeks post-MI hearts with and without CDCs, with and without endoglin KO .....	232

---

## List of Abbreviations

µl	Micro litre
µm	micro meter
µm <sup>3</sup>	micro meter cube
4-OH	4-hydroxy tamoxifen
a	artery
AKT	Protein kinase B
ALK	activin receptor-like kinase
ASF	alternate splicing factor
AV	Atrioventricular
AVMs	Arterio Venous Malformations
BM-MSCs	Bone Marrow Mesenchymal Stem Cells
BMP	Bone Morphogenetic Proteins
BMPR2	Bone Morphogenetic Protein Receptor 2
BSA	Basal Serum Albumin
Bves	Blood vessel epicardial substance
CADUCEUS	CARDiosphere-Derived aUTologous stem CELls to reverse ventricular dySfunction
CDCs	Cardiosphere Derived Cells
Cdh5	Cadherin 5
CEM	Complete Explant Media
CGM	Cardiosphere Growth Media
CHD	Congenital Heart Disease
CM	cardiomyocytes
CO <sub>2</sub>	Carbon Dioxide
Conc.	Concentration
Ctl	Control
CVD	Cardiovascular disease
DAB	3,3'-Diaminobenzidine
DILV	double-inlet left ventricle
Dll	Delta like ligand
DMEM	Dulbecco's Modified Eagle Media
DNA	Deoxyribonucleic acid
DORV	Double Outlet Right Ventricle
E	Embryonic Day
ECM	Extra Cellular Matrix
ECs	Endothelial Cells
EDCs	Explant Derived Cells
EDTA	Ethylene diamine tetra acetic acid
EGF	Epidermal Growth Factor
eGFP	enhanced Green Fluorescent Protein
EMT	Epicardial to Mesenchymal Transition
EndMT	Endothelial to Mesenchymal Transition

endo	endocardium
Eng	Endoglin
EPDCs	Epicardially derived Cells
epi	epicardium
EPO	Erythropoietin
EPOR	Erythropoietin Receptor
ERK	Extracellular Signal Kinases
ERT	Oestrogen Receptor Tamoxifen
EtOH	Ethanol
eYFP	enhanced Yellow Fluorescent Protein
FCS	Foetal Calf Serum
FGF	Fibroblasts Growth Factor
FOG	Friend of GATA
FOV	Field of view
g	Gravitational
G	Gauge
GDF	Growth & Differentiation Factors
GFP	Green Fluorescent Protein
GI	Gastro-Intestinal
GS-IB4	Griffonia Simplicifolia Isolectin B4
H&E	Haematoxylin and Eosin
H <sub>2</sub> O <sub>2</sub>	Hydrogen Peroxide
HCl	Hydrochloric Acid
HGF	Human Growth Factor
HHT	Hereditary Haemorrhagic Telangiectasia
HIF	Hypoxia Induced Factor
HOHF	High Output Heart Failure
hr	Hour
IA	Intussusceptive Angiogenesis
IAA	Interrupted Aortic Arch
Id	Inhibitor of DNA binding
IHC	ImmunoHistoChemistry
IO	Intraocular
IP	Intra-Peritoneal
IVS	Interventricular Septum
JNK	c-Jun N-terminal Kinases
KCl	Potassium Chloride
kDa	Kilo Dalton
KH <sub>2</sub> PO <sub>4</sub>	Monobasic potassium phosphate
kPa	Kilo Pascal
LA	Left atria
LAD	Left Artery Descending
LCA	Left Coronary Artery
LCx	Left Circumflex artery

LPS	LipoPolySaccharides
LV	Left Ventricle
M	Molar
MAP	Mitogen-Activated Protein
MeOH	Methanol
mG	membrane-targeted enhanced Green Fluorescent Protein
MI	Myocardial Infarction
mid-myo	mid-myocardium
mins	Minutes
ml	Mili Litre
MRTG	Myocardin Related Transcription Factor
mT	membrane-targeted tandem dimer Tomato
n/a	Not applicable
Na <sub>2</sub> HPO <sub>4</sub>	Sodium phosphate dibasic
NaCl	Sodium Chloride
NaOH	Sodium Hydroxide
NCC	Neural Crest Cells
Neg	Negative
NPHS	Nephrin
O/N	Overnight
°C	Degree Centigrade
OFT	OutFlow Tract
OR	Orphan Region
P	Postnatal
PBS	Phosphate Buffer Saline
PBST	Phosphate Buffer Saline Triton X-100
PCR	Polymerase Chain Reaction
PDGF	Platelet-Derived Growth Factor
PDGFR $\beta$	Platelet-Derived Growth Factor Receptor beta
PFA	Paraformaldehyde
PI3K	Phosphatidylinositol 3-Kinase
Pos	Positive
PPCI	Percutaneous Coronary Intervention
PTA	Persistent Truncus Arteriosus
qEC	Quiescent Endothelial cells
qPCR	quantitative Polymerase Chain Reaction
RA	Right Atria
RCA	Right Coronary Artery
RFP	Red Fluorescent Protein
RhoK	Rho-associated protein Kinase
RNA	Ribonucleic Acid
RT	Room Temperature
RV	Right Ventricle
SF	Splicing Factor

SL	Semilunar
SM	Smooth muscle
SMCs	Smooth Muscle Cells
SRF	Serum Response Factor
SRY	Sex-determining Region Y
Subcut	Subcutaneous
sub-endo	sub-endocardium
sub-epi	sub-epicardium
SV	Sinus Venous
TAE	Tris Acetate EDTA
TBS	Tris Buffer Saline
TBS-Tx	Tris Buffer Saline Triton X-100
TGF $\beta$ r	Tumour Growth Factor Beta Receptor
TGF $\beta$	Tumour Growth Factor Beta
UV	Ultraviolet
v	vein
VCAM	Vascular Cell Adhesion Membrane 1 Protein
VEGF	Vascular Endothelial Growth Factor
VEGFR2	Vascular Endothelial Growth Factor Receptor
VSD	Ventricular Septal Defect
vSMCs	vascular Smooth muscle cells
WGA	Wheat Germ Agglutinin
Wks	Weeks
WT	Wild Type
Wt1	Wilms' tumour 1
YFP	Yellow Fluorescent protein
ZP	Zona Pellucida
$\alpha$ SMA	alpha Smooth Muscle Actin
$\mu$ M	micro Molar

---

# **Chapter 1. Introduction**

## 1.1. Heart Development

The heart is the first organ to form in a vertebrate embryo. It has a mesoderm origin and requires various progenitor cells during the course of development. The mouse and the avian heart have been intensively studied as models of cardiac development [reviewed in (1, 2)]. In mammals, heart development begins with the formation of a cardiac crescent at the midline of the embryo at embryonic day 7.5 (E7.5) in mice. At around E8.0, the crescent then transforms into the linear tube which consists of a myocardial layer and an inner endocardial layer, separated by cardiac jelly (3). This linear tube then undergoes the process of looping between E8.5 to E10.0 in mice to form a primitive heart structure (Figure 1). The tube is elongated by the addition of progenitor cells (second heart field cells) at the atrial and venous poles of the heart. By E9.5, various other structures start to appear, including sinus venosus (SV, draining systemic blood into the common atrial chamber), atrioventricular (AV) canal (initial connection between common atrial chamber and left ventricle) and bulboventricular canal (connection between the primitive ventricles). The outflow tract (OFT) also connects to the primitive right ventricle by E9.5. Subsequently, the atrial chambers expand on both sides of the atrial pole while ventricle development occurs in the looping region via the process of ballooning. During ballooning, the interventricular septum (IVS) starts to form between the ventricles. Around the same time, formation of the endocardial cardiac cushions occurs in the AV canal (develop into AV valves) and in the common OFT [develop into semilunar (SL) valves]. Endocardial cushion formation is followed by the septation of the OFT and valve formation. Finally, the heart is remodelled to form the four chambered heart (Figure 1.1) [reviewed in (1, 2)].

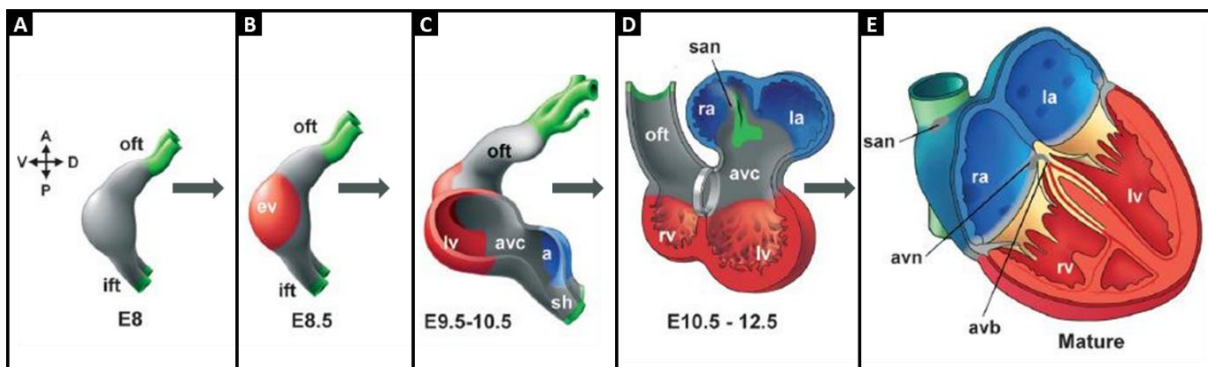


**Figure 1.1: Schematic of mice heart development [adapted from (4)]:** Heart development begins with a formation of a cardiac crescent around E7.5/ E8.0 in mouse (A). This then forms a linear tube like structure (B) which then undergoes the process of looping (C) and ballooning (D) to form a four-chamber heart (E). Abbreviations: OFT - Outflow tract; IFT - Inflow tract; EV - embryonic ventricle; a - atria; AVC - Atrioventricular canal; SH - sinus horns; SAN - Sinoatrial node RA - Right Atria; RV - Right Ventricle; LA - Left Atria; LV - Left Ventricle

---

## 1.2. Vasculogenesis and Angiogenesis during Development

The circulatory system provides the required nutrients and gasses for the growing embryo. The formation of vessels occurs by three processes: first vasculogenesis followed by angiogenesis and finally arteriogenesis. By definition, vasculogenesis is “the *de novo* formation of blood vessels by the formation of primary endothelial plexus” (5). Angiogenesis is “the process of blood vessel formation from these pre-existing plexus and expansion of the vasculature” (5). Primitive arteries are then matured to cope with the circulatory system by the process of arteriogenesis [reviewed in (6-8)].

Vasculogenesis begins in the embryonic mesoderm, extra-embryonic yolk sac, allantois and placenta (9), with the formation of blood island-like structures around E6.5 in the yolk sac just after the formation of the cardiac crescent (10). Hemangioblasts in the extra-embryonic yolk cells, give rise to these blood islands which later on fuse with each other to form the initial endothelial plexus (11). These blood islands consist of two types of precursor cells: angioblasts and haematopoietic cells. The angioblasts differentiate to form endothelial cells (ECs) which then form primitive tube-like structures in the embryo which then undergo network remodelling to form a secondary plexus (11, 12).

The process of coronary vasculogenesis is controlled by many factors. An *in vitro* analysis showed that vascular endothelial growth factor (VEGF) and its receptors are vital for the process of vasculogenesis (13, 14). VEGF-A, a vascular permeability factor (15) is important for vasculogenesis. VEGF is expressed in the extra-embryonic visceral endoderm and in the extra-embryonic mesoderm. At E8.5, strong VEGF expression is noted in the endodermal cells in contrast to the lower expression in the mesodermal cells during intra-embryonic endothelial plexus formation. Deletion of even one of the *VEGF* alleles led to embryonic lethality by E11 due to vasculogenesis defects (16, 17). The VEGF receptor 2 (also known as flk1) null mice resulted in absence of vasculogenesis causing complete embryonic lethality by E8.5 or E9.5 (18). On the other hand, the *VEGF receptor 1* (also known as flt1) null mice lack the proper organisation of the blood islands causing disruption in the localization of angioblasts and ECs (19). Remodelling and expansion of the vessels via angiogenesis can occur either by sprouting angiogenesis or by intussusceptive angiogenesis (IA) (Figure 1.2). In mice, angiogenesis begins around E9.5 and is responsible for the formation of majority of blood vessels in an embryo [reviewed in (6, 7)].

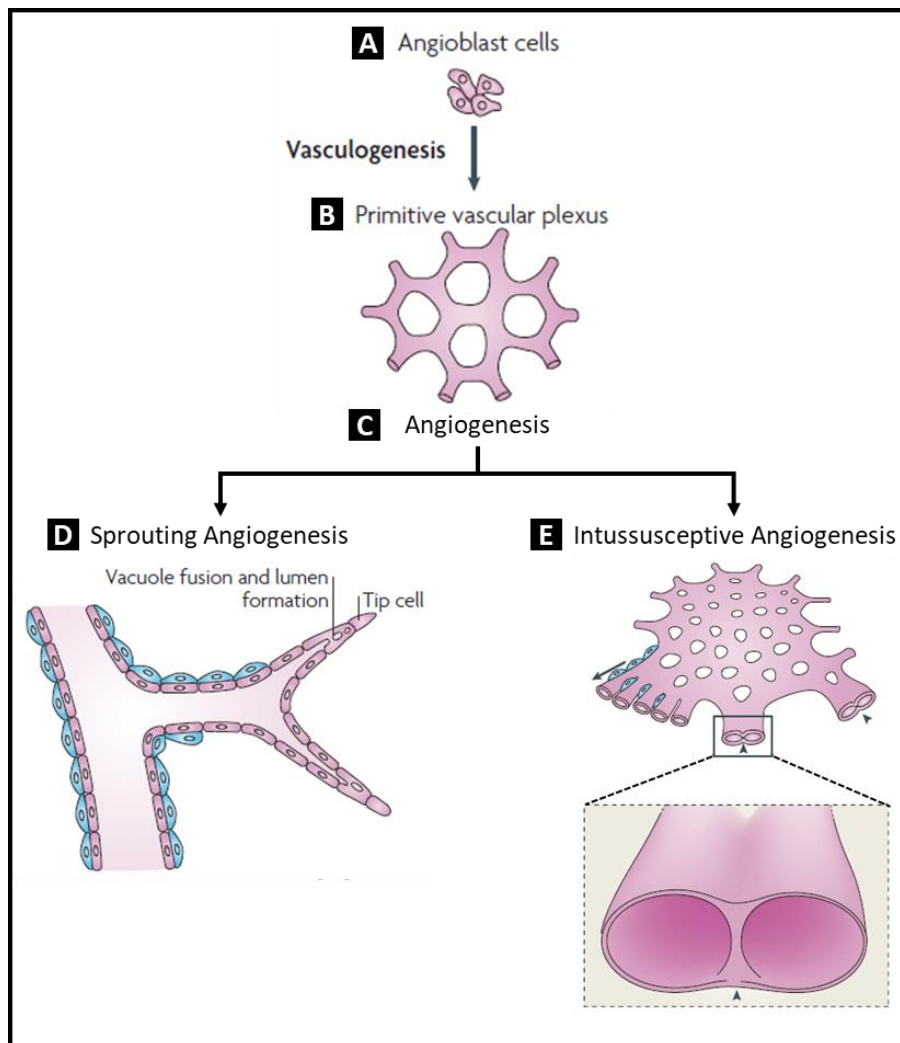


**Figure 1.2: Process of Vasculogenesis and Angiogenesis [adapted from (20)]:** Formation of blood vessels in embryos start by recruitment of angioblasts (A) to form initial endothelial plexus (B) by the process of vasculogenesis. These initial plexuses are then expanded and remodelled via angiogenesis process (C). Vessels expansion by angiogenesis can occur by two ways: (D) Sprouting angiogenesis or (E) intussusceptive angiogenesis.

The mechanisms of angiogenesis have been reviewed extensively (6-8, 21, 22). Briefly, in sprouting angiogenesis (Figure 1.2D) new capillaries develop by the formation of endothelial sprouts from the pre-existing vessels. This process is initiated by degradation of the basement membrane of the nascent vessels and migration of ECs in response to the angiogenic stimuli (e.g. hypoxia or VEGF). The ECs align and form a stalk like structure. The tip of this stalk like structure contains specialised ECs, known as “tip cells”. These tip cells respond to the angiogenic stimulus and migrate towards it. This migration of the tip cell ECs is paired with proliferation of the stalk ECs which results in the formation of a vessel lumen. The vessel is then stabilised by deposition of vascular smooth muscle cells (vSMCs) and adventitial fibroblasts. Blood flow in these vessels begins soon after the formation of the lumen. While in case of IA (Figure 1.2E), the expansion of the vascular network occurs by division of the pre-existing vessel by forming a tissue column in the middle [reviewed in (6, 7)]. In mouse, the process of coronary vasculogenesis is completed by mid-gestation while the process of

---

angiogenesis and arteriogenesis of the vessels continue until three weeks of postnatal life [reviewed in (23)].

Many signalling molecules have been shown to play an important role during the process of angiogenesis including VEGF (discussed above) and Notch signalling pathway. Notch signalling controls sprouting of the ECs. In vessels, Notch receptor 1 and 4 are expressed in the endothelium while Notch receptor 3 is expressed in vSMCs. Various ligands of Notch signalling have been also observed in vessels including *Jagged1*, *Jagged2*, *Delta like ligand (Dll) 1*, *Dll3* and *Dll4* (24). *Notch1* null mice die by E11 due to vessel degradation and abnormal vessel remodelling although the initial primary endothelial plexus was formed normally (25). Homozygous deletion of both *Notch1* and *Notch4* showed severe defects as compared to *Notch1* deletion alone including defects in the major vessels (25). Continuous Notch-4 signalling in ECs led to embryonic lethality by E10 due to impaired vessel formation (26). *Dll4* has been shown to bind to both Notch 1 and 4 (expressed in ECs) and is critical for angiogenesis as deletion of a single allele of *Dll4* resulted in embryonic lethality by E10.5 due vascular remodelling defects (27). The expression of *Dll4* and Notch signalling has been shown to be controlled by VEGF (28) and blockage of VEGF has been shown to cause reduced levels of *Dll4* in vessels and inhibited sprouting (29). Notch signalling has also been shown to act as a negative feedback of the VEGF signalling as activation of Notch signalling in ECs led to reduced VEGF receptor 2 (VEGFR2) (29).

Once the vasculature is formed, it undergoes maturation. This step is critical for stabilisation of vessels and for proper functioning of the vessels. During this phase, vSMCs and fibroblasts are deposited over the endothelium. Improper or incomplete deposition of either of vSMCs or fibroblasts can lead to hyper-permeable vessels which can lead to the formation of oedema leading to developmental defects. Several factors are involved during the maturation of vessels as well. For instance, platelet derived growth factor (PDGF) is important for recruitment of vSMCs. Mice lacking PDGFB or PDGF receptor  $\beta$  (PDGFR $\beta$ ) led to embryonic lethality due to reduced number of vSMCs causing hyper-permeable vessels and oedema (30).

Another factor which plays a major role during vasculature development is hypoxia. Hypoxia-inducible factor (HIF) is a transcription factor and consists of two subunits: HIF-1 $\beta$  and HIF-1 $\alpha$ . Under normal oxygen levels (normoxia), HIF-1 $\alpha$  is degraded, while in hypoxic conditions HIF-1 $\alpha$  is expressed during development or in ischemic conditions (31). Embryos lacking HIF-1 $\alpha$  die by mid-gestation, because of vasculature related abnormalities in yolk sac and in the

embryo (32), while overexpression of HIF-1 $\alpha$  led to an increase in various factors including VEGF and PDGF causing significant increase in neovascularisation (31).

### 1.2.1. Anatomy of Mature Coronary Circulation

The fate of blood vessels is decided by the expression of ephrin family protein and their Eph receptors. Endothelium expression of ephrinB2 is seen in developing arteries while expression of its receptor EphB4 is restricted to endothelium of the developing veins (33). Lack of any of these two led to embryonic lethality by E10.5 due to vascular defects in both the yolk sac and embryo itself. It is also shown that Ephrin guides the arteriovenous anastomoses by inhibition of ECs stimulation by VEGF and angiopoietin1 (33, 34). Arteries and veins also show differential expression of members of the Notch signalling family. For example, Notch3, Dll4 and Gridlock expression is restricted to arteries. In addition, Neuropilin-1 expression is restricted to endothelium of the arteries while Neuropilin-2 expression is shown to be restricted to venous endothelium (35).

The mature mammalian coronary circulation consists of two parts: an arterial system and a venous system (Figure 1.3). The major arteries and veins branch out to form various small vessels which then give rise to capillaries to supply blood to cardiomyocytes (36).

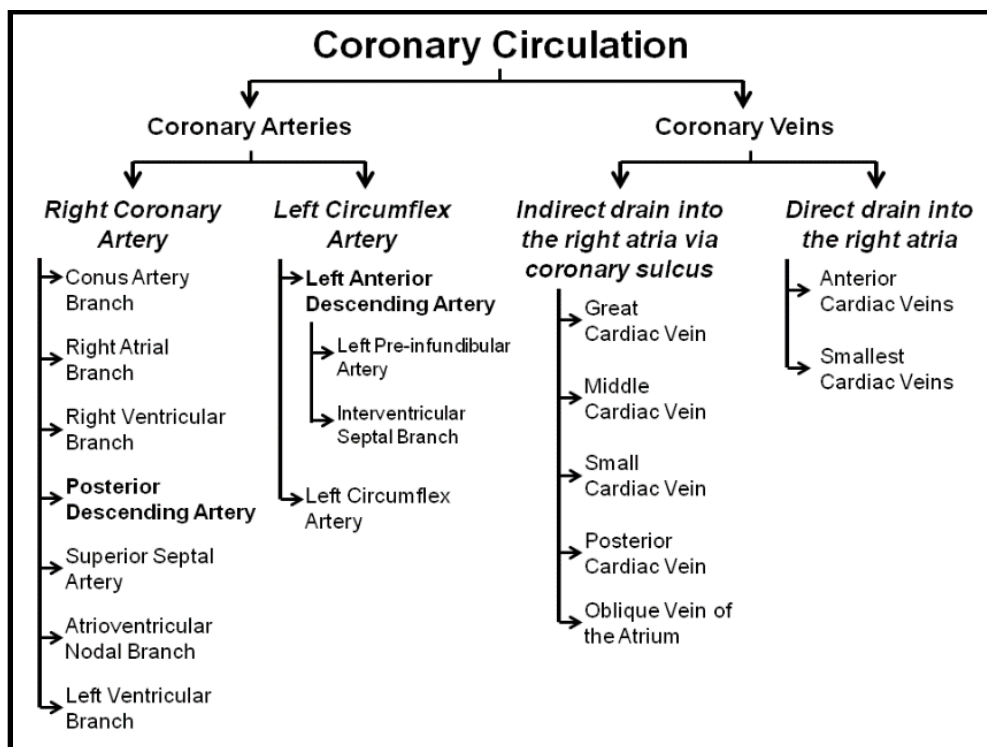
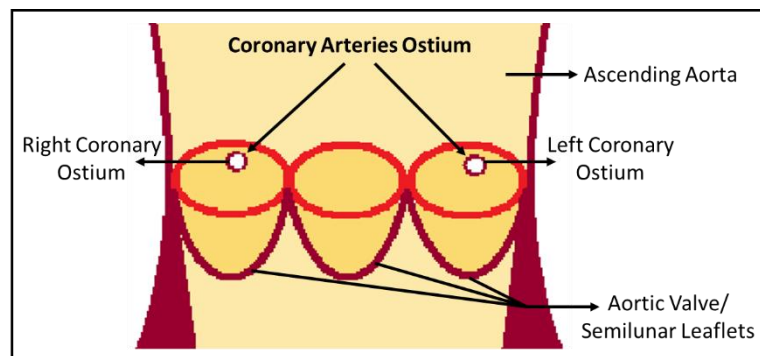


Figure 1.3: Coronary circulation tree [Based on the data from (36, 37)]

---

### 1.2.1.1. Coronary Arteries

Coronary arteries supply oxygenated blood to myocardium and are connected to the aorta via the coronary ostium (Figure 1.4). These arteries do not grow out of the aorta rather they grow into the aorta at their ostium (38). There is variability from person to person between the precise anatomy of coronary arteries and their connection to the aorta.



**Figure 1.4: Coronary arteries and their attachment at the aorta (ostium).**

There are two main coronary arteries (Figure 1.5): right coronary artery (RCA) and left coronary artery (LCA). The RCA during its course from the ostium to the crux (the point where the AV groove meets the interventricular groove) gives rise to multiple branches which further branch out to give oxygenated blood to the majority of the right side of the heart (Figure 1.5). Clinically, the RCA is divided into three parts: first segment, mid segment and distal segment (36).

The LCA also known as the left main coronary artery travels laterally between the base of the pulmonary trunk and left atrium (Figure 1.5). The LCA and its branches [the Left Anterior Descending artery (LAD) and the Left Circumflex artery (LCx)] are responsible for majority of circulation of the left side of the heart (Figure 1.5). The LAD is responsible for supply blood to the left ventricular (LV) and IVS in human (36). In contrast, IVS is supplied by a separate septal coronary artery in mice originating from the right sinus of Valsalva or from the right coronary artery (39).

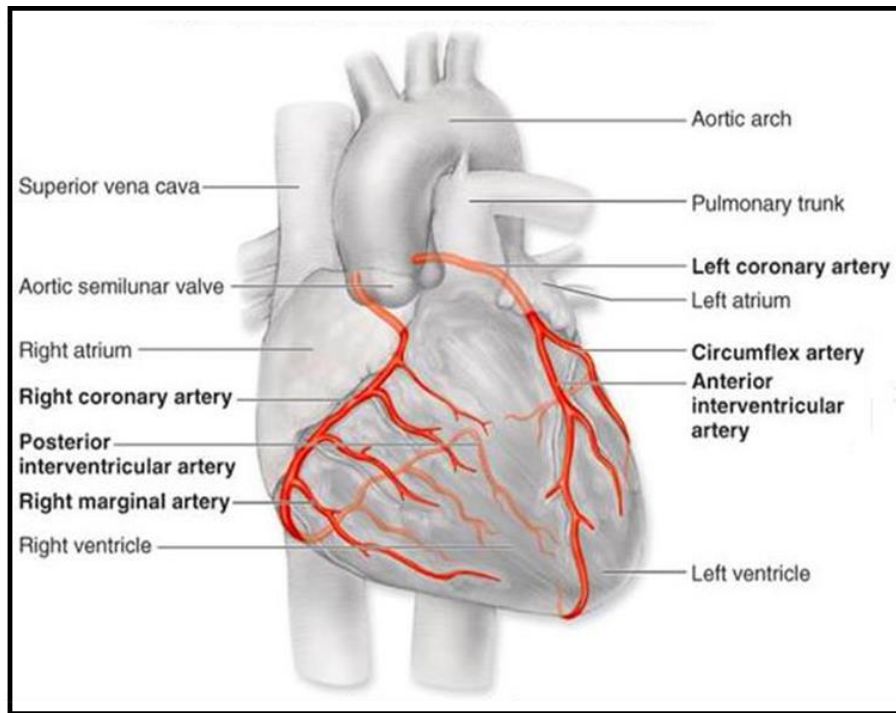


Figure 1.5: Coronary arteries [taken from (40)]

### 1.2.1.2. Coronary Veins

The coronary veins drain the deoxygenated blood and metabolic waste from the heart into the right atria of the heart. The blood pressure in coronary veins is low compared to the coronary arteries. The coronary veins also contain valves to prevent the back flow of blood. Presence of these valves and lower blood pressure reduce the risk of stress related injuries in veins in comparison to arteries. These factors also make coronary veins less prone to atherosclerotic plaque (41, 42).

The majority of the coronary veins drain the venous blood in the coronary sinus with some draining directly into the right atria (Figure 1.6). The coronary sinus then empties the blood into the right atria (37, 41, 42).

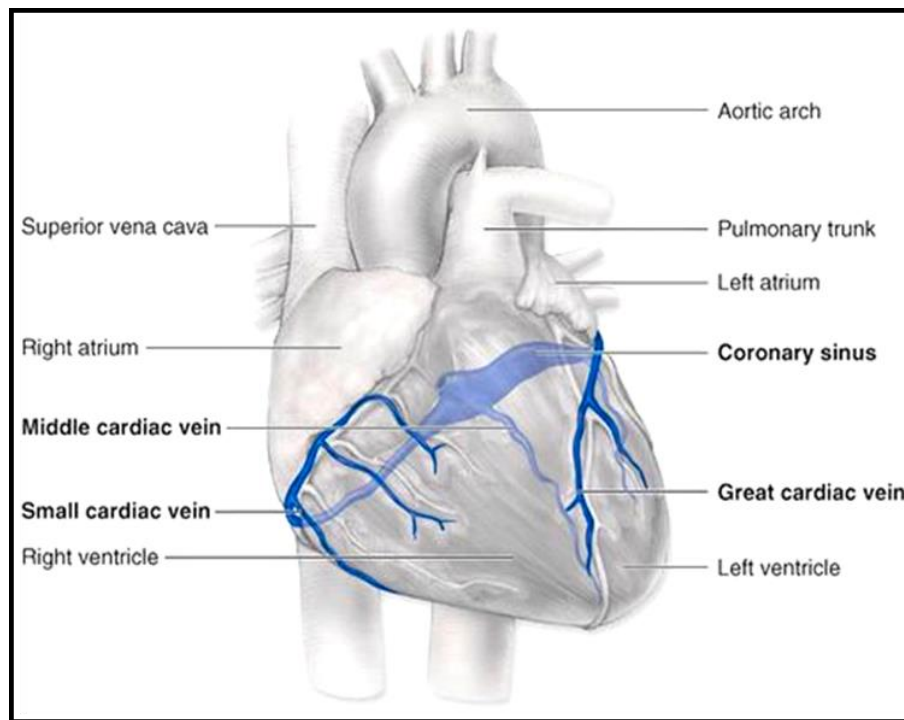
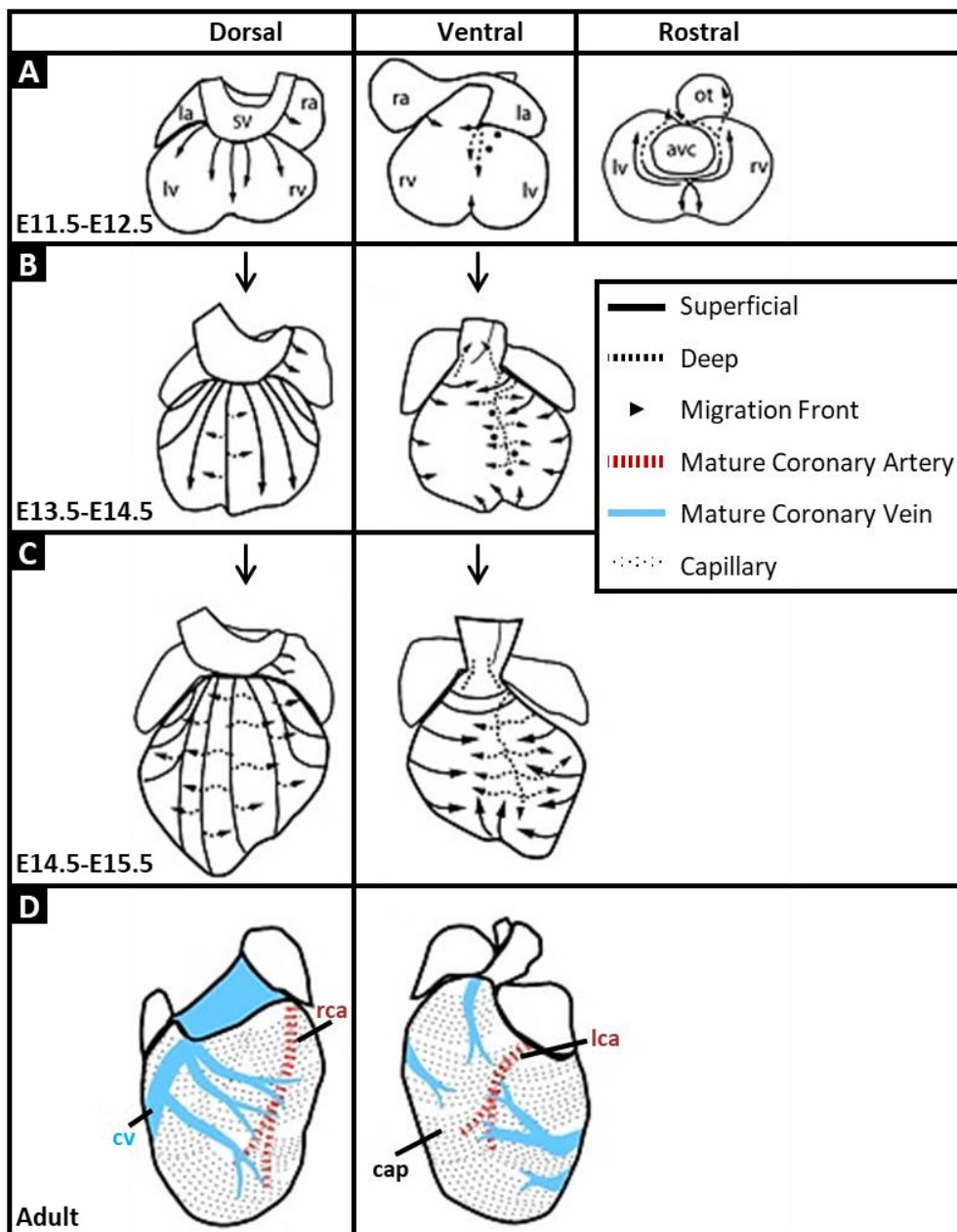


Figure 1.6: Coronary Veins [taken from (40)]

### 1.3. Cells in Coronary Vessels Development

The need of blood circulation within the myocardium is no different from other parts of the body; it is required to exchange gases and nutrients. At the beginning of heart development, at the primitive heart tube stage (E9.5 in mouse; Figure 1.1), there is no need for coronary vessels as nutrients and gases can be exchanged through simple diffusion. But as the thickness of the myocardium increases and the simple tubular structure turns into a complex organ, the need for a coronary circulation becomes critical as without the gases and nutrient exchange, the myocardial cells will die due to ischemia and necrosis. Development of the coronary vasculature in mouse begins with formation of vascular plexus around E11.5 (Figure 1.7) and continues through the process of angiogenesis until three weeks in post-natal life (43, 44). In an adult heart, nearly of all the cardiomyocytes are closely associated with coronary capillaries (45, 46). Coronary vessels are primarily composed of three types of cells: ECs, vSMCs and adventitial fibroblasts. The origin of these cells from different progenitor cells is discussed below.



**Figure 1.7: Development of Coronary Vasculature [adapted from (43)].** (A) During the process of coronary vessel development, endothelial cells (ECs) first start to migrate from sinus venosus on to the myocardium around E11.5. These ECs migrate into the myocardium from the sub-epicardial side. (B) ECs originating from the endocardium migrate inwards around E14.5. (C) After anastomosis of the coronaries with aorta, coronary vessels can be observed throughout the myocardium around E15.5. (D) These vessels then under maturation to form the coronary vessel network observed in the adult hearts Abbreviations: *la* – Left Atria; *sv* – Sinus venosus; *ra* – Right Atria; *lv* – Left Ventricle; *rv* – Right Ventricle; *ot* – Outflow tract; *avc* – Atrioventricular canal; *rca* – Right Coronary Artery; *lca* – Left coronary artery; *cv* – coronary vein; and *cap* – Capillaries.

### 1.3.1. Role of Epicardium in Coronary Vessel Development

The epicardium is the outer layer of the heart, covering the myocardium (Figure 1.8); it consists of connective tissue and epithelial cells. The epicardium is derived from an extra-cardiac cell population known as the proepicardium [reviewed in (47-49)].

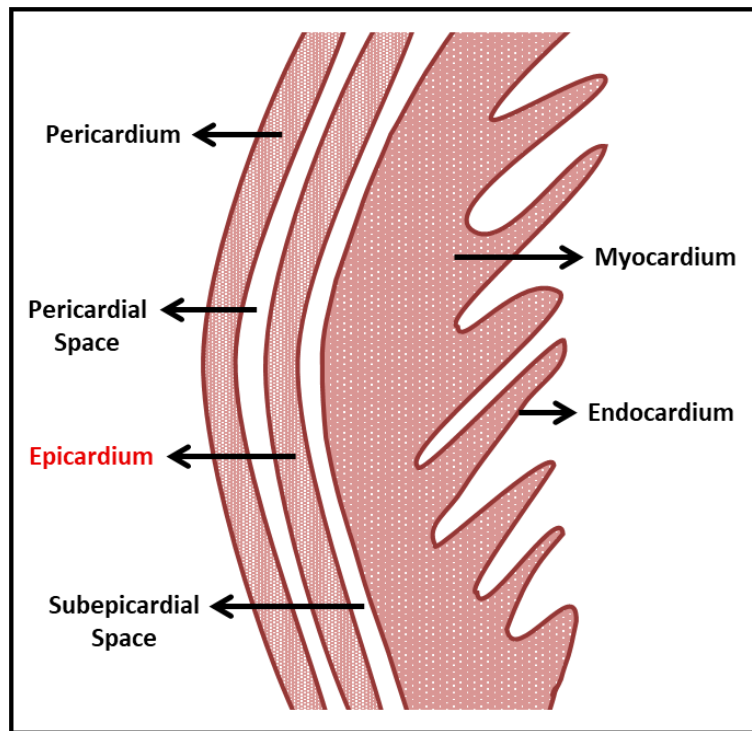


**Figure 1.8: Layers of the Heart [based on data from (47)].** The trabecular layer of the heart consists of two layers: myocardium and endocardium. The myocardium is covered by next layer called as the epicardium. The myocardium and epicardium are separated by a sub-epicardial space filled with extracellular matrix. The epicardium is covered by another layer called as the pericardium.

The proepicardium cells that originate from the splanchnic mesoderm near the inflow region of the heart forms the epicardium that covers the heart chambers (Red, Figure 1.9) while proepicardial cells generated from the splanchnic mesoderm near the outflow pole form epicardium over the OFT (Green, Figure 1.9) (50).

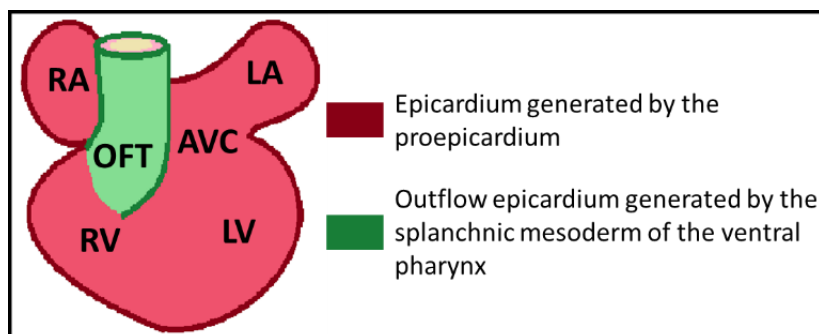


**Figure 1.9: Heart with epicardium from two different sources (Red and Green) [Adapted from (47)].** Abbreviations: RA – Right Atria; RV – Right Ventricle; LA – Left Atria; LV – Left Ventricle; AVC – Atrioventricular Canal; OFT – Outflow Tract.

The process of epicardium formation has been extensively reviewed (23, 47-50). Briefly, formation of the epicardium begins around during the process of looping of the heart with the migration of the proepicardial progenitor cells on the surface of the heart. In mice, migration of these progenitor cells occurs via formation of protrusions at the posterior surface of the pericardial cavity which cross the coelom to reach the surface of the heart at E9.5 (51, 52). The septum transversum releases free-floating aggregates of epicardial cells that float across and

---

attach onto the myocardium and subsequently spread out to form the complete epicardium (53). The AV and the interventricular grooves are the initial regions to be covered by this single layer of epicardial cells in mice. The ventricles are covered next, followed by the atria and then the OFT. The whole heart in mice is covered by epicardium by E10.5 (53). OFT epicardial cells generally do not undergo EMT while the epicardial cells over the heart chamber do undergo EMT to form mesenchymal like cells known as epicardially derived cells (EPDCs) (50).

### **1.3.1.1. Epicardial EMT & Importance in Coronary Vessel Development**

The epicardium and the myocardium are not in direct contact but are separated by the sub-epicardial space filled with extracellular matrix (ECM) produced by the epicardium and myocardium by E12.5 in mice (Figure 1.8) (46). This sub-epicardial space is rapidly filled by EPDCs formed by epicardial to mesenchymal transition (EMT) of epicardium cells. The EPDCs first fill the sub-epicardial space then start to invade the myocardium around E12.0 (54). This process of myocardial invasion of EPDCs occurs in parallel to myocardial wall thickening and is important for myocardium layer compaction and maturation (49).

Not all of the epicardial cells undergo EMT, according to Pérez-Pomares and de la Pompa (55); epicardial cells which can undergo EMT are either genetically predisposed or exposed to local signals. Several signalling pathways are involved in the activation of epicardial cell EMT. These signals work in a coordinated manner to down-regulate epithelial cell markers, promote mesenchyme marker expression, reorganise the cytoskeleton and the ECM. The *Wilms' tumor 1* (*Wt1*) gene plays a major role in the EMT of epicardial cells; it is expressed in the early proepicardium, in the epicardium and in EPDCs (56, 57). During the process of epicardial EMT, TGF $\beta$  (Transforming Growth Factor Beta) signalling also plays an important role by activating ALK5 receptor [activin receptor-like kinase, TGF $\beta$  type 1 receptor (58-60)] and promotes expression of genes such as *Pai-1* and *Snail* (Figure 1.10A). These genes in turn suppresses epicardial markers such as  $\beta$ -catenin & VCAM-1 (vascular cell adhesion protein-1) and promotes the expression of mesenchymal markers such as phalloidin &  $\alpha$ SMA (Figure 1.10B) (61-69). The Role of TGF $\beta$  during EMT process is discussed below in section 1.5.3.

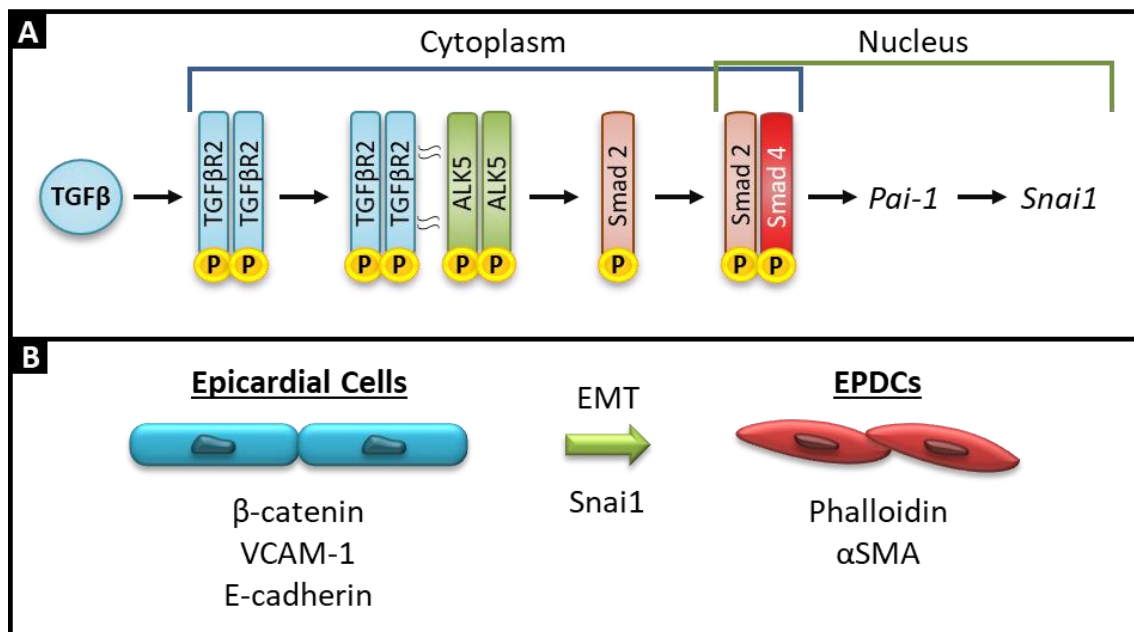


**Figure 1.10: During Epicardial EMT, TGFβ signalling occurs via ALK5 Mediated Type 1 Receptor [adapted from (20, 64)]. (A) Activated TGFβ ligand activate TGFβR2 which in turn phosphorylates ALK5 type 1 receptor. This pathway then leads to expression of Pai-1 and Snai1 which in turns promotes the epicardial cell EMT. (B) Snai1 triggers the expression of mesenchymal marker such as phalloidin and αSMA in EPDCs and inhibit the expression epicardial markers such as β-cateinin and VCAM-1.**

### 1.3.1.2. EPDCs in Coronary Vessel Development

Lineage tracing experiments using both avian and mammalian models showed that EPDCs differentiate majorly into vSMCs of coronary vessels and fibroblast cells (Figure 1.11) (54, 70-75). In avian models, a significant percentage of ECs also arise from differentiated EPDCs (76, 77) while in mammals, only a minimal percentage of EPDCs differentiate into ECs (43, 44, 73, 78, 79). Furthermore, some studies have shown that EPDCs also differentiate into cardiomyocytes (78, 80, 81) however this contribution is still debatable (82, 83).

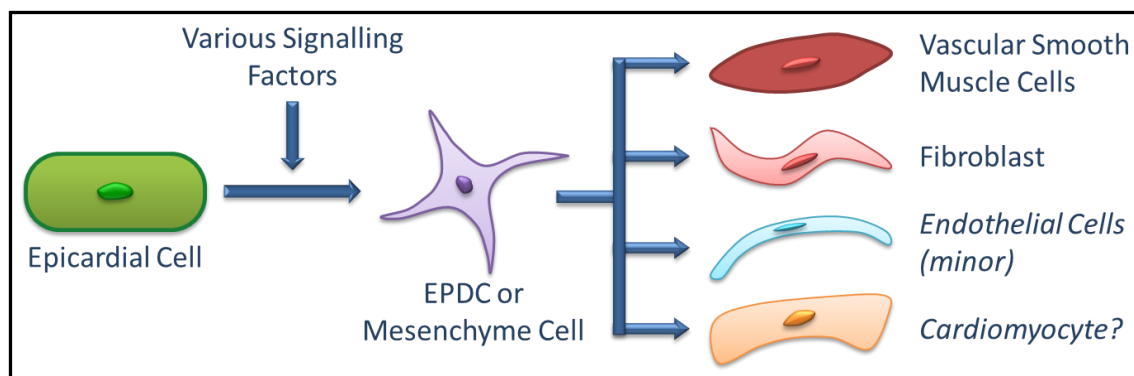


**Figure 1.11: Fate of epicardial cells:** Epicardial cells undergo EMT under the influence of signalling proteins to form EPDCs. These EPDCs then differentiate into vSMCs, fibroblasts, ECs (minor contribution in mammals) and may be cardiomyocytes depending upon the interaction with various signalling factors.

The differentiation of EPDCs begins as soon as they come in contact with the factors in the subepicardial space provided by the epicardium, EPDCs themselves, and the adjacent myocardium [reviewed in (23, 55, 84-86)]. Table 1.1 lists a few of the differentiating factors

and their expression pattern in developing heart. These factors are essential during the EPDCs differentiation and can cause to mild to severe phenotypic effects in their absence (Table 1.1).

**Table 1.1: Molecules Involved in EPDCs differentiation during coronary vasculature development.**

Name	Expression	Phenotype in the coronary vascular system
<i>α4 integrin</i>	PEO & epicardium (87)	Mutant embryos lacked epicardium & suffer pericardium haemorrhage (88, 89)
<i>Bves</i>	PEO, migrating epicardium, EPDCs & vSMCs (90)	Treatment with anti-Bves antibodies inhibit epicardial migration of vasculogenic cells from the proepicardium <i>in vitro</i> . <i>In vivo</i> , lack of Bves leads to abnormal epithelial cell integrity (91, 92).
<i>Connexin43</i>	PEO, epicardium & vSMCs (93)	Increased migration & proliferation rate of pro-epicardial cells. Abnormal migration of fibroblast & vSMCs, resulted in multiple coronary artery patterning defects (93)
<i>EPO &amp; EPOR</i>	EPOR expressed in epicardium & pericardium (94)	Detached epicardium, abnormal vascular network & reduced number of cardiomyocytes (94)
<i>Ets-1/Ets-2</i>	EPDCs & cushion mesenchyme (95)	Thinner epicardium, reduced number of EPDCs, lack of vSMCs in the peripheral coronary arteries, disorganised coronary arteries & capillaries (95)
<i>FGF</i>	Several FGF ligands & receptors are expressed in pro-epicardium (96)	Neutralizing antibodies to basic FGF inhibit capillary formation & arteriolar growth [reviewed in (97)].
<i>FOG-2</i>	At E8.5, in ventral tube & septum transversum. Later on, in atria, ventricles & pericardium (98)	FOG-2 knockdown mutants displayed intact epicardium however coronary vasculature was absent due to lack of sub-epicardial mesenchyme & endothelium (98).
<i>GATA-4</i>	Epicardium, endocardium & myocardium of developing heart (99)	Incorrect cardiac looping, lack of epicardium due improper pro-epicardium migration, thin myocardium & lack of endocardial cushions (99).
<i>MRTF A &amp; B</i>	Epicardium, EPDCs & endocardium (100)	Detached & disorganised epicardium, reduced EPDCs migration, incomplete coronary vessels penetration over ventricles & reduced number of pericytes (100).
<i>NPHS1</i>	Epicardium & coronary vessels during embryonic development (101)	Nephrin knockout embryos showed abnormal epicardial cell morphology & reduced number of coronary vessels (101)
<i>rhoA-RhoK</i>	Myocardium (atria & ventricles), trabeculae, endocardial cushions & OFT (102)	Treatment with inhibitor Y27632, hindered cardiac looping process, prevented expression of coronary vSMCs makers on migrating EPDCs & trabeculae formation (102, 103).
<i>SRF</i>	Epicardium, EPDCs & vSMCs (100)	Prevent vSMCs marker expression <i>in vitro</i> & <i>in vivo</i> . <i>In vivo</i> time course study revealed failed EPDCs migration (100, 103, 104).
<i>VCAM-1</i>	Cardiomyocytes (105)	Lack epicardium, thinner myocardium & suffer from pericardium haemorrhage (106).
<i>VEGF -A</i>	ECs of highly vascular regions of the developing heart (16, 107)	Neutralizing antibodies to VEGF inhibit capillary formation and arteriolar growth. Regulated endogenous VEGF is vital for vascular patterning and lumen size regulation. Changes in the expression pattern led to severe cardiac abnormalities including absence of coronary plexus & was fatal by E12.5 to E14.5 (108-111).
<i>VEGF-B</i>	Developing myocardium, OFT, dorsal aorta & pericardium (112)	Healthy and fertile, however reduced heart size & impaired coronary growth post MI (113).
<i>VEGF-C</i>	Epicardium (44)	Absence inhibited coronary growth in dorsal & lateral side of developing heart (44).

<i>VEGFR1</i> ( <i>Flt1</i> )	ECs (16, 19, 114)	Essential during the organization of embryonic vasculature, however is not important for ECs differentiation. The absence of VEGFR1 induces an overproduction of endothelial cells and vessel malformation (19)
<i>VEGFR2</i> ( <i>Flk1</i> )	ECs & endocardium (16, 115)	Endocardium specific knockdown led to lack of coronary plexus, defective coronary arterial network & pericardium haemorrhage (111)
<i>Wt1</i>	PEO, epicardium & EPDCs (56, 116, 117)	Epicardial cells fail to undergo EMT (116, 118)
<i>Abbreviations:</i> <i>Bves</i> – Blood vessel epicardial substance; <i>EPO</i> – Erythropoietin; <i>EPOR</i> - EPO Receptor; <i>FGF</i> – Fibroblasts Growth Factor; <i>FOG-2</i> – Friend of GATA, <i>MRTF</i> – Myocardin related transcription factor; <i>NPHS1</i> – Nephren; <i>RhoK</i> – Rho-associated protein kinase; <i>SRF</i> – Serum Response Factor; <i>VCAM</i> – Vascular Cell Adhesion Molecule; <i>VEGF</i> – Vascular Endothelial Growth Factor; <i>VEGFR</i> – VEGF Receptor; <i>Wt1</i> – Wilms tumor 1		

### 1.3.2. Origin of the Endothelial Component of Coronary Vessels

The development of coronary vessels starts around E11.5 in mice (43, 44). As the cardiac development progresses, the coronary arterial network is formed in the myocardium while coronary veins are formed in the sub-epicardial space (43, 119). The origin of coronary ECs is controversial. However, results from the past two decades showed that coronary ECs potentially arise from three different sources (Figure 1.14): (i) SV [sinus venosus, (41, 42, 67)]; (ii) endocardium (67, 99, 108) and (iii) epicardium (41, 42, 61, 66, 67).

Red-Horse *et al.* (43) performed immuno-histochemical and clonal analysis to determine the origin of the ECs of the coronary vessels. Using the *apelin-nlacZ* knock-in mouse to specifically mark coronary ECs in mouse embryo hearts, followed by Xgal wholemount analysis at various time points (E11.5 to E15.5) they showed that coronary vasculature formation begins near the SV. Red-Horse *et al.* (43) also showed that the interaction between the SV and the ventricular epicardium is important for ECs sprouting from the SV via their functional culture assay on E10.5 *apelin-nlacZ* mice hearts (43). Furthermore, this SV origin of the coronary vasculature was confirmed by repeating the experiment using VE-cadherin-creER; brainbow transgenic mice that marked the VE-cadherin<sup>+</sup> ECs clones with different multicolour markers. The marker analysis showed that VE-cadherin<sup>+</sup> cells originate in the SV and migrate into the myocardium between E12.5 to E14.5 (43).

These VE-cadherin<sup>+</sup> cells expressed venous markers (like EphB4) when they sprout from the SV but as these ECs migrate towards the myocardium and differentiate to form coronary arteries ECs, venous marker expression was reduced and expression of arterial marker like *ephrinB*, *Dll4* and *Notch4* increased. The ECs that remain in the sub-epicardial region form mature coronary veins (43). During the histological analysis of *apelin-nlacZ* mice, Red-horse and

---

colleagues (43) also found isolated clusters of ECs in the interventricular groove at E15.5. These clusters have been termed as blood islands in the past and have an unknown origin. In this study, it is speculated that these clusters may have an endocardial origin (43).

Chen *et al.* (44) and Tian *et al.* (79) supported this SV and endocardial contribution to coronary ECs using immuno-histochemical and clonal analysis of *Apln<sup>CreERT2</sup>*; embryo hearts at various stages of development (E11.5 to E15.5) using different reporters (*Rosa26<sup>LacZ</sup>*, *Rosa26<sup>RFP</sup>* and *Rosa26<sup>mTmG</sup>*). They showed that the majority of coronary vessel ECs (both arteries and veins) are formed by the sub-epicardial ECs of the nascent coronary plexus. The sub-epicardial vessels migrate into the myocardium to form coronary arteries and the vessels that remained in the sub-epicardial space contributes to the formation of coronary veins (79). During these clonal analysis studies, they found that the ECs in the IVS do not form from the sub-epicardial ECs. They speculated that these ECs or blood islands in the IVS may have an endocardial origin(79).

In a contrasting study, Wu *et al.* (111) used various *in-vivo* and *in-vitro* analyses to show that ECs of coronary arteries primarily arise from the endocardium of the heart. They showed that the endocardium of the heart is not terminally differentiated but retains angiogenic potential. Immuno-histochemical and clonal analysis of endocardial cells and their descendants using a *Nfatc1-cre* mouse line (*Nfatc1* is an endocardial specific marker in the heart) from E11.5 to E16.5 revealed that approximately 80% of coronary artery ECs have an endocardial origin while only a third of coronary vein ECs were derived from endocardium (111). However this conclusion was challenged by a recent publication showing nascent expression of *Nfatc1-Cre* in SV (120).

Using a more endocardial specific promoter (*Npr3*) to drive Cre expression, Zhang *et al.* (120) showed GFP (Cre-reporter) expression only in the ventricular endocardium until E10.5 (120). As the development of coronary vessels development begins, GFP expression was observed in these vessels at E14.5 and E15.5. However, in contrast to earlier studies significantly reduced number of coronary vessels ECs were observed to arise via the endocardial route (120). A majority of these endocardially originating coronary vessel ECs were observed in the IVS with very few vessels in the free ventricle walls (120).

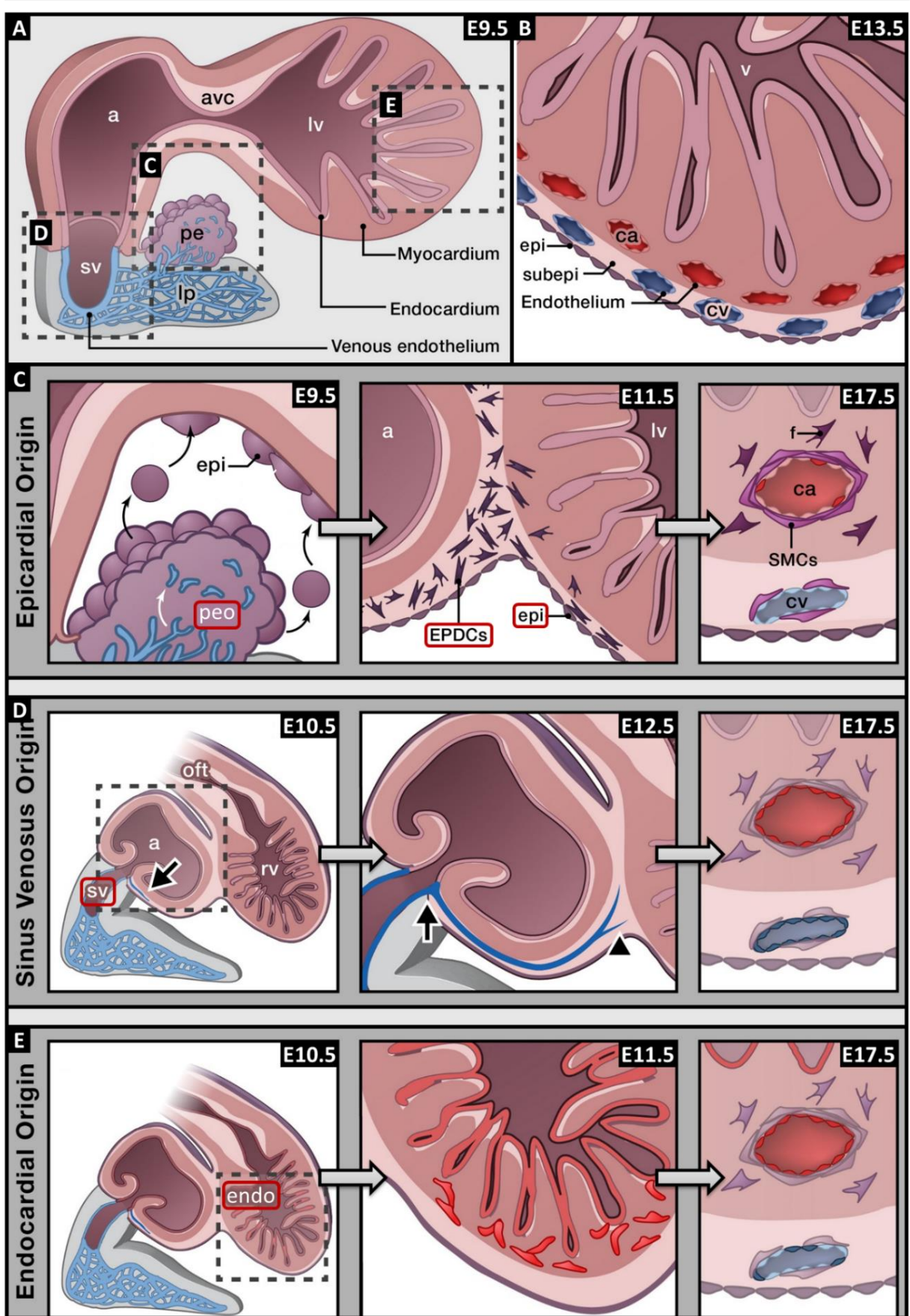


**Figure 1.12: Potential origin of coronary endothelial cells through three different progenitor cells [adapted from (121)].** Cartoon showing embryonic heart structure at (A) E9.5 and (B) E13.5. (C) **Epicardial Origin:** At E9.5, progenitor cells migrate towards developing heart to form epicardium. The epicardial cells then undergo EMT to form EPDCs around E11.5. These EPDCs then invade the myocardium and differentiate primarily into SMCs and fibroblasts with a minor contribution towards ECs. (D) **Sinus Venosus Origin:** SV is potentially the major source of coronary ECs. At E10.5, ECs migrate from SV endothelium towards atria (black arrow) and

ventricular (black arrowhead) myocardium contribute towards most of the coronary ECs in the free ventricular walls. These migrating ECs initially observed to express venous ECs markers. However, as ECs to migrate deeper into the myocardium, venous markers are replaced with atrial markers. Thus, indicating origin of coronary atrial ECs via coronary vein ECs. **(E) Endocardial Origin:** There is controversial evidence regarding the percentage of ECs originating via endocardium. It is speculated that endocardium either undergo budding, sprouting or EndMT to form coronary ECs. It is also suggested that the endocardium contributes towards coronary ECs primarily in the IVS during development and in trabeculae compaction during postnatal heart development. *Abbreviations: A – Atria; AVC – AtrioVentricular Canal; CA – Coronary Arteries; CV – Coronary Veins; EPDCs – EPicardially Derived Cells; Epi – Epicardium; LP – Liver Permodia; LV – Left Ventricle; OFT – OutFlow Tract; PEO – ProEpicardial Organ; RV – Right Ventricle; SMCs – Smooth Muscle Cells; SV – Sinus Venosus.*

In a study by Tian et al. (122), it is postulated that formation of the coronary vessels occurs in three waves (Figure 1.13). They showed that, the first wave for coronary development starts around E10.5, second wave starts around E13.5 in parallel to myocardium thickening and the final wave starts in early post-natal life in parallel to trabeculae compaction (122). They also proposed that coronary vessels formed in the outer part of free ventricular wall are formed during the first wave, vessels in the IVS are formed during the second wave while the vessels in the trabeculated myocardium are formed during the third wave in post-natal life (122).

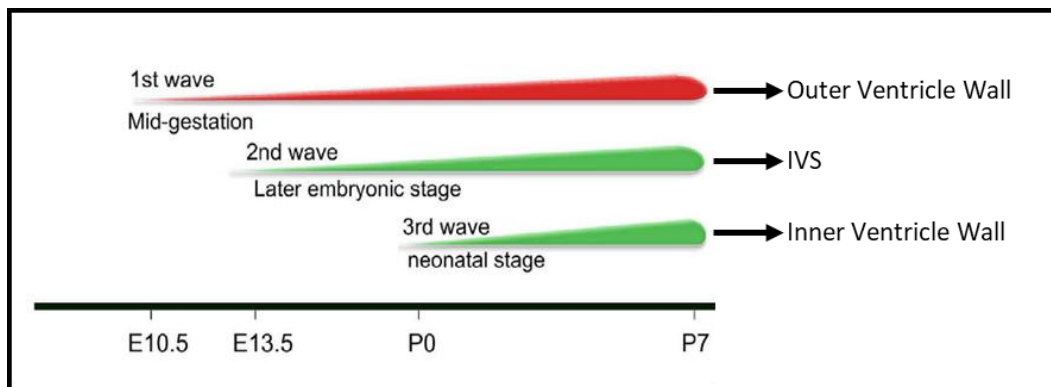


**Figure 1.13: Different waves of Coronary Vessels formation during mouse heart development and in post-natal life [adapted from (122)].** During coronary vessels development, vessels in the outer ventricle wall are formed during the first wave; during second wave, in the IVS and in the third wave in the inner ventricle wall.

## 1.4. TGF $\beta$ and Endoglin in Coronary Vasculature Development

### 1.4.1. TGF $\beta$ Ligands and its Receptors

TGF $\beta$  signalling is known to be involved in regulation of many cellular functions including proliferation, differentiation, migration and survival of many cell types. In mammals, TGF $\beta$  superfamily consist of various ligands including TGF $\beta$ s, bone morphogenetic proteins (BMPs) and growth & differentiation factors (GDFs). These ligands are formed in latent form and are activated prior to signalling by cleavage of the latent unit with the help of proteases such as proprotein convertases [reviewed in (123-125)]. During the signalling cascade, activated ligand binds to a high affinity TGF $\beta$  type 2 receptor which then recruits and phosphorylates a specific TGF $\beta$  type 1 receptor. Canonical signalling involves phosphorylation of SMADs by the type 1

receptor while non-canonical signalling occurs by phosphorylation of ERK, PI3K/AKT, JNK or p38 MAP kinases [reviewed in (123, 125, 126)].

In mammals, there are seven kinds of type 1 receptors (ALK 1, 2, 3, 4, 5, 6 and 7) and five kinds of type 2 receptors (TGFB $\beta$ 2, BMPR2, ACVR2A, ACVR2B and AMHR2) [reviewed in (123-125)]. The molecular structure of both TGF $\beta$  type 1 and type 2 receptors are quite similar (Figure 1.14A). The extra-cellular domain of both receptors consists of a small cysteine rich region followed by a single trans-membrane sequence. The intracellular domain of both the receptors consists of serine/threonine kinases. In case of type 1 receptor, a GS domain is also present (site for phosphorylation by type 2 receptor). The two type 1 and 2 receptors exist as homodimers (monomers linked by disulphide bonds) on the cell surface. During signalling, these homodimers combine to form a heterodimer complex [reviewed in (123, 125)].

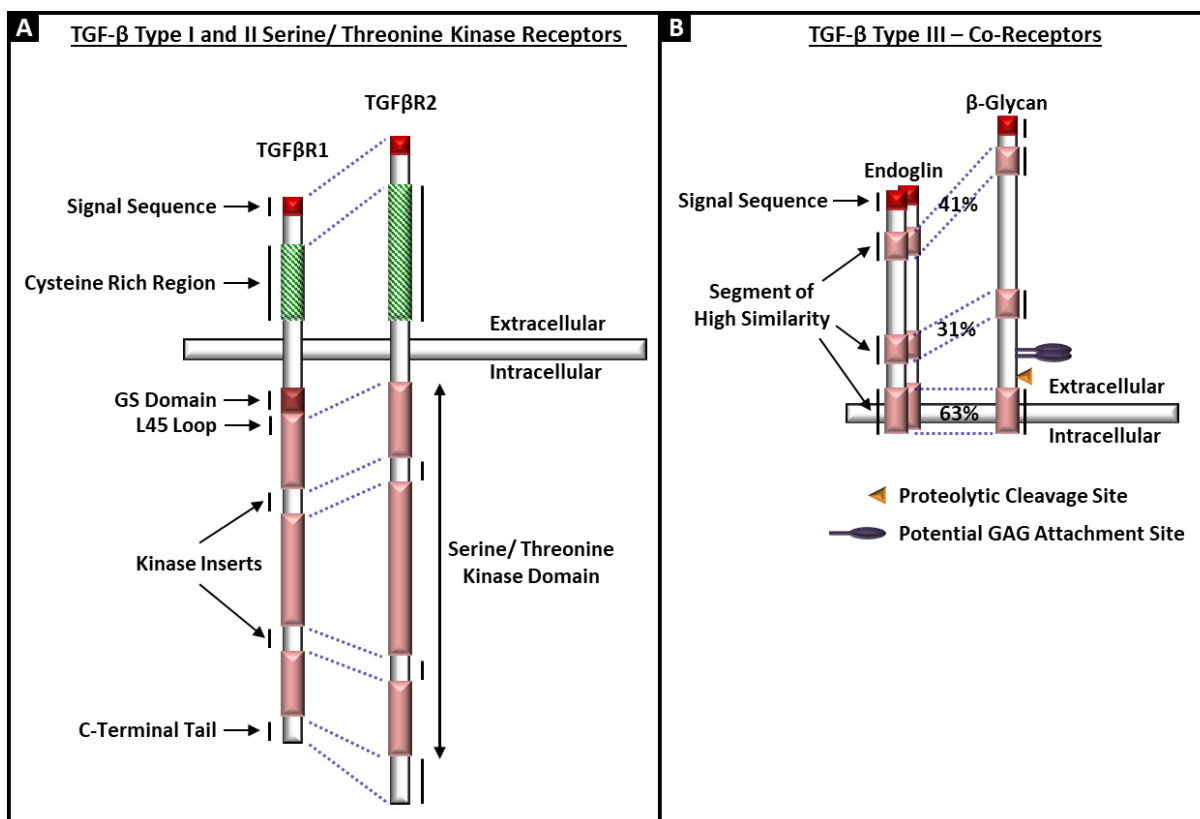


**Figure 1.14: Structure of TGF $\beta$  receptor [adapted from (123)]. (A) Cartoon of TGF $\beta$  type 1 and 2 receptor showing extracellular and intracellular domain of the receptors. (B) Cartoon of TGF $\beta$  type 3/ co-receptor: Endoglin and  $\beta$ -glycan.**

During the TGF $\beta$  signalling process, type 3 co-receptors ( $\beta$ -glycan and endoglin) are also involved. The interaction of type 1 and type 2 TGF $\beta$  receptors is influenced by type 3 co-receptors. The two co-receptors,  $\beta$ -glycan and endoglin are trans-membrane receptors with similar molecular structure. In both co-receptors, a large extracellular domain is present followed by a hydrophobic transmembrane domain and a short intracellular domain (Figure

---

1.14B). In case of endoglin, monomer units are linked via disulphide bonds while  $\beta$ -glycan monomer units are connected by non-covalent interactions [reviewed in (123, 125)].

### 1.4.2. Endoglin: TGF $\beta$ type 3 co-receptor

Endoglin also known as CD105 is critical for proper angiogenesis. Knockout of *endoglin* leads to complete mortality around E10.5 due to angiogenic defects (problems with SMCs recruitment) in both the embryo (heart & body) and the yolk sacs (127-129).

Human *endoglin* is an 180KDa homodimeric disulphide linked trans-membrane glycoprotein (130). The 14 exon *endoglin* gene in humans is located on chromosome 9q34 and encodes a protein of 658 amino acids (131) and belongs to the ZP (zona pellucida) family of proteins. The structure of human endoglin has recently studied in a great detail by Saito *et al.* (130). Structurally, human endoglin is composed of a large extracellular domain, followed by a single transmembrane domain and a small intracellular domain (Figure 1.15). The extracellular N-terminal consists of an orphan region (OR1 & OR2 with 18% identical sequence and 102 overlapping residues) while the C-terminal consist of ZP domain [~260 amino residues, (130) and reviewed in (126, 131-133)]. Endoglin has shown to have higher affinity towards BMP9/BMP10 (130, 134). During the signalling pathway the highly conserved Q270 and I271 residues of OR1 domain of endoglin had shown to be essential for binding with conserved regions of BMP9/10 (130). Once BMP9/10 binds to the OR1, the ZP domain next aids in dimerization of the complex (130). In humans, the extracellular domain also contains an Arg-Gly-Asp (RGD) tripeptide and glycosylation sites (four N-linked and one O-linked) and is a cell-recognition site for various cell adhesion proteins present in the ECM (126, 130-133). This RGD peptide is absent in murine, porcine, rat and canine endoglin. In ECs, the two monomer units of the homodimeric endoglin protein are arranged in an anti-parallel fashion to form a dome like structure with a cavity at one end [reviewed in (126, 131-133)].

The intracellular domain of endoglin contains a PDZ domain-binding motif (Ser-Ser-Met-Ala) which regulates EC migration by interacting with the scaffolding protein synectin [GAIP (G $\alpha$ -interacting protein) – interacting protein C-terminus, GIPC]. The intracellular domain of endoglin does not have any enzymatic motifs but contains many serine/threonine residues. The phosphorylation of these residues by TGF $\beta$  receptors occurs at specific sites. In ECs, TGFBR2 phosphorylates endoglin at Ser<sup>634</sup> and Ser<sup>635</sup> followed by phosphorylation on Thr<sup>640</sup>, Thr<sup>647</sup> and Thr<sup>654</sup> by ALK1. On the other hand, ALK5 phosphorylates endoglin at Ser<sup>646</sup> and Ser<sup>649</sup>. The

---

reason for the phosphorylation of these endoglin residues is still unclear but is said to be crucial for TGF $\beta$  mediated signalling in ECs [reviewed in (126, 133)].

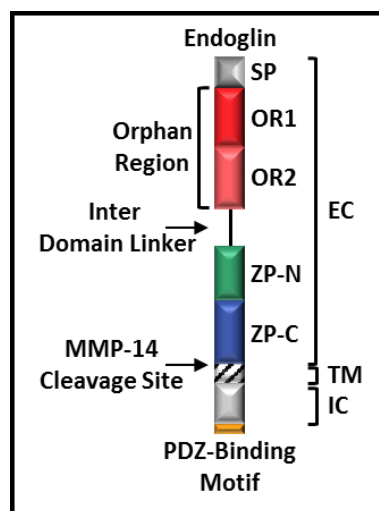


**Figure 1.15: Structure of Endoglin [adapted from (126, 130)].** The extracellular (EC) region of the endoglin protein composed of orphan regions (OR1 and OR2) at the N-terminal end followed by a zona pellucida region (ZP-N and ZP-C) at the C-terminal end. The endoglin protein also consist of a trans-membrane region followed by small intra-cellular (IC) domain comprises of PDZ motifs.

There are two isoforms of endoglin observed in humans, L-endoglin (long-endoglin) and S-endoglin (short-endoglin) with differences in the length of their intracellular domain, distribution in tissues and degree of phosphorylation (Figure 1.16). L-endoglin has an intracellular domain of 47 residues is present dominantly in the ECs and promotes angiogenesis (Figure 1.16A). While S-endoglin on the other hand contains only 14 residues (Figure 1.16C), is expressed significantly in lungs and liver and has been shown to have an anti-apoptotic effect. S-endoglin is formed by alternate splicing mechanism regulated by ASF (alternate splicing factor) and SF-2 (splicing factor-2) in quiescent ECs. The L and S isoform of endoglin only have 7 amino acid residues in common [reviewed in (126, 131, 132)].

The extracellular domain of endoglin, known as sol-endoglin (soluble-endoglin, Figure 1.16B) can also be found in the circulation. Sol-endoglin is shed from the cells and has been shown to have an anti-angiogenic effect [reviewed in (126, 132)]. The mechanism of formation of sol-endoglin is not clear but it is proposed that exposure of TNF $\alpha$  (Tumour Necrosis Factor- $\alpha$ , an inflammatory cytokine) can lead to shedding of endoglin from ECs via MMP14 (matrix metalloproteinase 14) cleavage at 586-587 residues *in vitro* (135, 136).

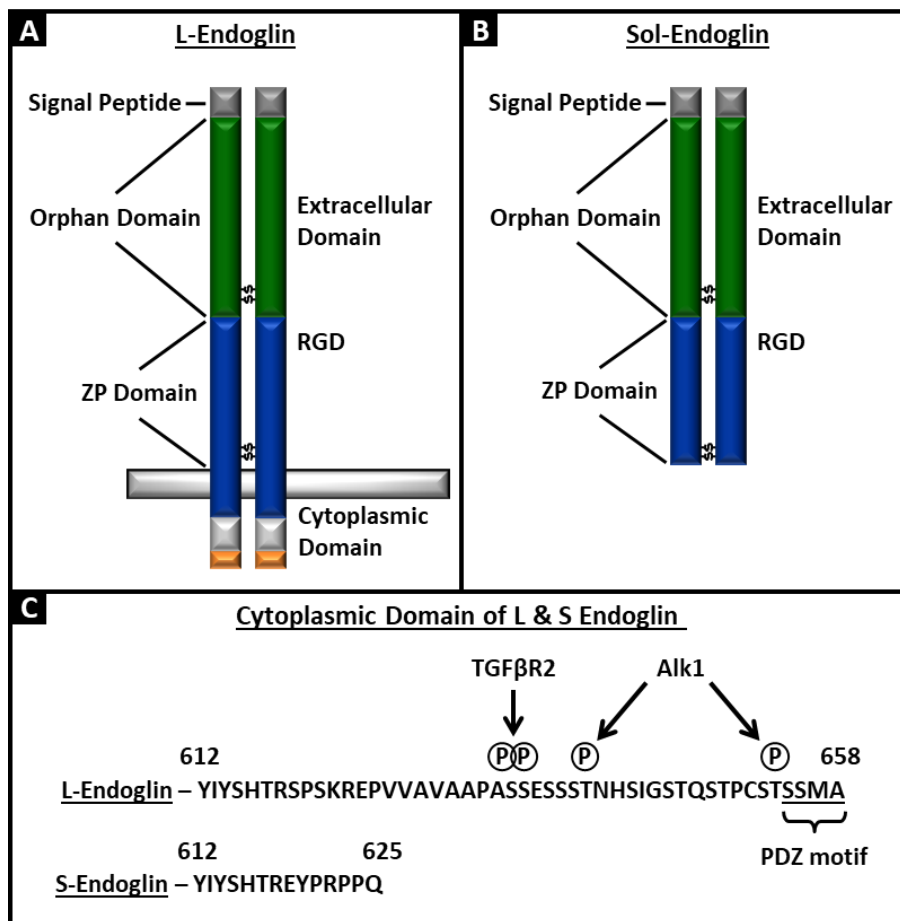


**Figure 1.16: Molecular structure of different endoglin isoforms [adapted from (131)]. (A) Structure of pro-angiogenic, long endoglin isoform. (B) Shedding of L-endoglin from ECs leads to formation anti-angiogenic, soluble endoglin isoform. (C) Anti-angiogenic, short endoglin structure is similar to L-endoglin with a smaller intracellular domain.**

### 1.4.2.1. Cellular Expression of Endoglin

Previous studies have shown the expression of endoglin in the ECs of various specific vessels of developing mouse embryo e.g. dorsal aorta, branchial arches, inter-somatic vessels, cardinal vein, optic vessels and yolk sac (127, 129, 137). During development, endoglin is also highly expressed in ECs of the endocardium and in the cardiac cushions (138). Endoglin expression is also observed in the syncytiotrophoblasts of the placenta and in case of pre-eclampsia the level of Sol-endoglin is highly elevated (139). In the haematopoietic system, endoglin is involved in efficient myelopoiesis and erythropoiesis. Endoglin is also shown to be expressed in adult bone marrow haematopoietic stem cells and termed as a functional marker of long-term repopulating haematopoietic stem cells (140). In postnatal and adult life, the expression of endoglin is more restricted. Pulmonary blood vessels express high levels of endoglin (141) while the expression of endoglin in some quiescent ECs is very low. This expression of endoglin in adult ECs increases during active phases of angiogenesis like wound healing, heart repair and tumour angiogenesis. (131). Other cell types like activated monocytes express endoglin and the level

---

of endoglin increases during monocyte to macrophage transition. Endoglin is also said to play an important role during monocyte mediated vascular repair (131).

## **1.5. TGF $\beta$ and Endoglin in Coronary Vessel Development**

The development of the coronary vessels is a complex process and involves not only different cell populations (discussed above in section 1.2) but also different signalling pathways that regulate the complex series of events required to form the mature coronary vasculature.

### **1.5.1. TGF $\beta$ and Endoglin in Endothelial Cells**

The TGF $\beta$  signalling pathway plays an important role in coronary vessel development. In ECs, canonical TGF $\beta$  signalling via SMADs phosphorylation plays a dual role (Figure 1.17). There are three different types of SMADs: (i) receptor regulated (R-SMADs 1, 2, 3, 5, & 8) which interacts with and are phosphorylated by TGF $\beta$  type 1 receptors; (ii) common mediator (Co-SMAD 4), which interacts with phosphorylated R-SMADs to facilitate transport to the nucleus and (iii) inhibitory SMADs (I-SMADs 6 & 7), competitively inhibit interaction between R-SMADs and Co-SMAD [reviewed in (123-126)].

During the *activation phase* of angiogenesis, EC proliferation and migration is promoted by TGF $\beta$  signalling via phosphorylation of SMAD1/5/8 via an ALK1 BMPR2 complex (Figure 1.17). The phosphorylated SMAD1/5/8 then combines with SMAD4 and translocates to the nucleus to initiate transcription of pro-angiogenic genes such as inhibitor of DNA binding 1 (Id-1) [reviewed in (123-126, 142)]. Id-1 promotes EC proliferation and migration via inhibition of basic helix-loop-helix proteins [reviewed in (123, 143)].

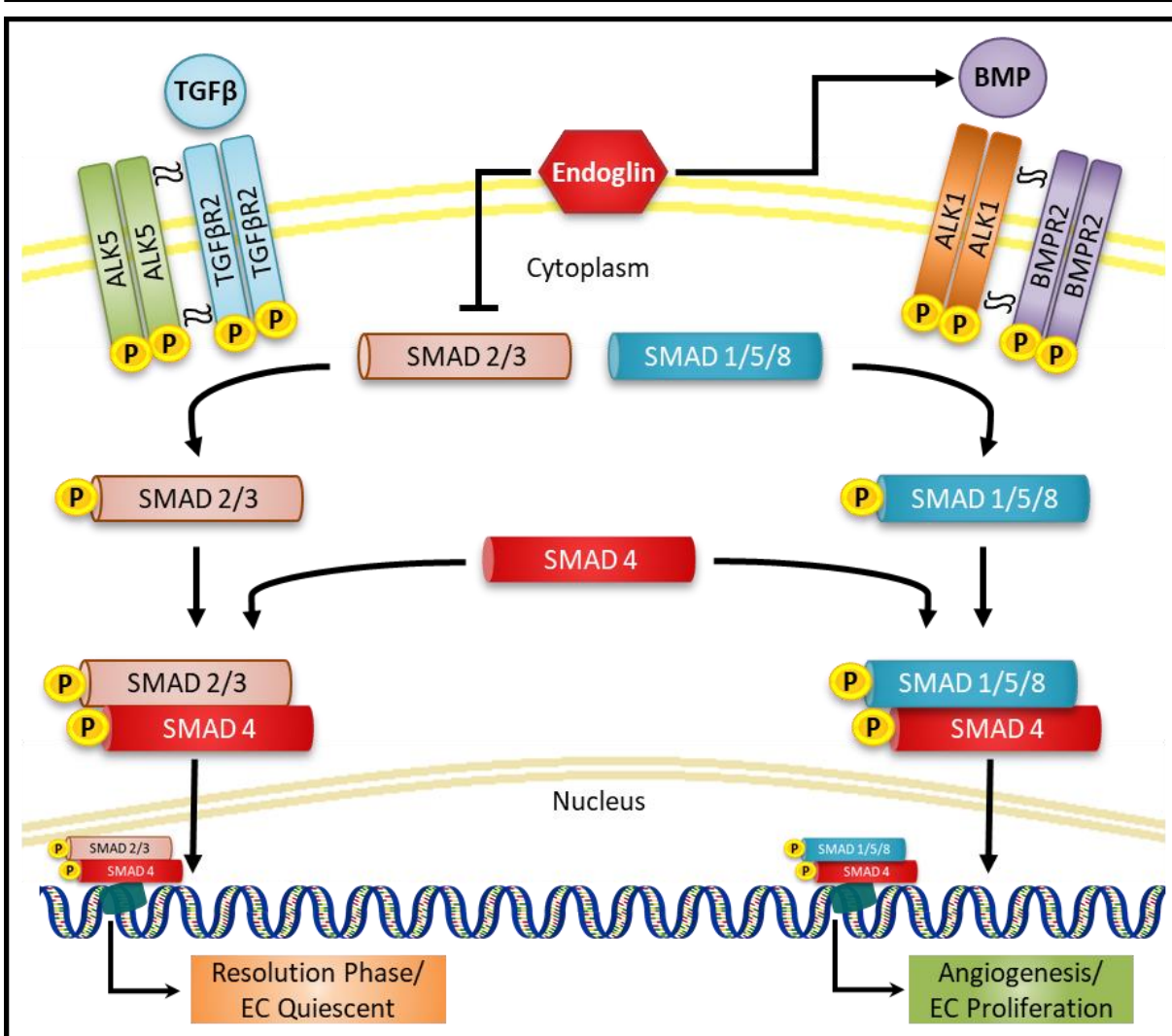


**Figure 1.17: Dual role of canonical TGF $\beta$ / BMP signalling in endothelial cells [adapted form (20)].** TGF $\beta$  signalling initiates by auto-phosphorylation of type 2 serine/threonine kinase under the influence of active TGF $\beta$ /BMP ligands. This interaction of TGF $\beta$  ligand and type 2 receptor is mediated by TGF $\beta$  type 3 receptors. This ligand and type 2 receptor complex then phosphorylate type 1 receptor to form heterodimer complex. This heterodimer complex then phosphorylates receptor SMADs (1/5/8 or 2/3) which then combines with common-mediator SMAD4. This phosphorylated SMADs complex then translocates into the nucleus and trigger transcription of effector genes. In ECs, TGF $\beta$  signalling plays a dual role. In proliferative phase of ECs, active BMP ligands combine with BMPR2 and ALK1 receptor to phosphorylate SMAD1/5/8 which leads to transcription of pro-angiogenic genes such as Id1 (142). This pro-angiogenic effect of TGF $\beta$ /BMP ligands is promoted by endoglin. Endoglin promotes the binding of active ligands to type 2 receptor and ALK1 while suppressing ALK5 mediated pathway at SMADs level. In contrast, during resolution phase EC or in quiescent ECs, active TGF $\beta$  ligands signals via SMAD2/3 by interacting with TGF $\beta$ R2 and ALK5 heterodimer complex to transcribe effector genes such as PAI-1 (142).

In the *resolution phase* of angiogenesis, EC proliferation and migration is inhibited and basement membrane is reformed. The vessels are then stabilised by mesenchymal cell recruitment and their differentiation into vSMCs and fibroblasts. This maturation of vessels is promoted by TGF $\beta$  signalling via ALK5 type 1 receptor (Figure 1.17). During the signalling process, TGF $\beta$ R2 auto-phosphorylates under the influence of activated TGF $\beta$  ligand. This phosphorylated receptor then recruits the ALK5 type 1 receptor and phosphorylates it at the GS motif. This heterodimer complex then phosphorylates SMAD2/3 which then forms a complex with SMAD4 and translocates into the nucleus to initiate transcription of effector genes such as

plasminogen activator inhibitor type 1 (PAI-1) [reviewed in (123-126, 142, 144)]. *In vitro* studies showed that PAI-1 inhibits ECs proliferation and migration by interrupting FGF-2 (145) and/ or VEGFR2 (146) mediated angiogenesis.

A balance between the two TGF $\beta$  mediated pathways is vital for proper vascular development and for maintenance during adulthood. The balance between these pathways is maintained by endoglin (144, 147). *In vitro* analysis showed that endoglin is highly expressed in actively proliferating ECs (144). Endoglin was also shown to be an essential component for efficient ALK1 mediated signalling and ECs without endoglin failed to proliferate. Endoglin stimulates TGF $\beta$ /ALK1 mediated SMAD1/5 phosphorylation, indirectly inhibiting the TGF $\beta$ /ALK5 pathway (Figure 1.18). Lebrin *et al.* (144) also saw that reduction in endoglin levels led to reduced ALK5 levels suggesting a regulatory adaptation response by the ECs.

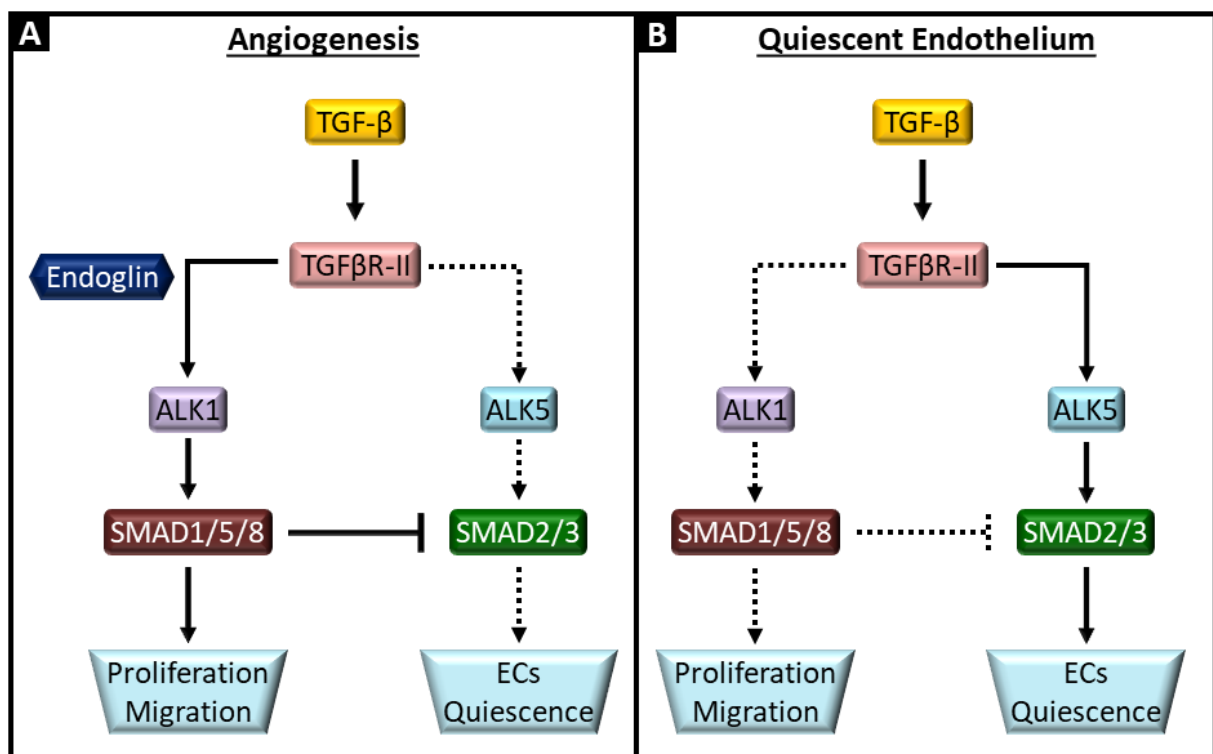


**Figure 1.18: Endoglin in TGF $\beta$  mediated angiogenesis [adapted from (144)]. (A) Endoglin promotes ECs proliferation via ALK1 type 1 receptor and inhibiting ALK5 mediated pathway at SMAD levels. (B) While in quiescent ECs, ALK5 mediated pathway is active.**

Hypoxia is amongst the major stimuli which promote endoglin expression in ECs. Various other factors have been observed to initiate the expression of endoglin and these include TGF $\beta$ , BMP9 and activated ALK1 [reviewed in (123)]. During TGF $\beta$  mediated signalling in ECs, endoglin indirectly helps in the binding of the TGF $\beta$  ligands to specific TGF $\beta$  receptors. In the presence of TGF $\beta$ R2, endoglin is known to bind to TGF $\beta$ 1 and TGF $\beta$ 3 (142, 148, 149).

---

Recently, it has become clear that endoglin binds BMP9 and BMP10 ligands at much higher affinity compared to TGF $\beta$  ligands (130, 134). *In vitro* analysis in my host laboratory showed that loss of *endoglin* in mesenchymal cells led to reduced levels of phosphorylated SMAD1/5/8 and this loss was partially rescued by treatment with active BMP9 ligands (150). In contrast, sol-endoglin has been observed to reduce TGF $\beta$  ligand availability by binding to the ligand [reviewed in (123, 126, 128)].

### **1.5.2. TGF $\beta$ Ligands and Receptors in Vasculature Development**

TGF $\beta$  signalling pathway plays an essential role during angiogenesis (20, 123, 125, 126, 148). For instance, TGF $\beta$ /ALK5 signalling has been shown to be important for the normal attachment of epicardium over the myocardium (60). Knockout of *Alk5* in epicardial cells using *Gata5-Cre* led to formation of thinner myocardial growth with reduced proliferation rate due to improper attachment of epicardium (60). The *Alk5*-KO embryos at E18 showed ventral body gastroschisis and an increased number of capillaries in the myocardium. The coronary vessels had a defective vSMC layer due to improper vSMC differentiation. The cell adhesion molecule N-cadherin was also down-regulated in the mutant embryos along with reduced ZO1 junction protein signalling suggesting that ALK5 mediated TGF $\beta$  signalling is important for epicardium attachment (60).

Smooth muscle cell specific knockout of *Tgfb2* led to coronary vessel defects and embryo lethality prior to birth (151-153). Immuno-histochemical analysis of mutant embryos at various time points (E11.5 to E18.5) after partial knockout of *Tgfb2* using *SM22 $\alpha$ -Cre* showed various defects related to cardiac and vascular development. Severe myocardial hypoplasia was seen due to impairment of EPDC differentiation into vSMCs leading to lack of coronary vasculature formation (153).

Global knockouts of TGF $\beta$  and its receptors cause embryonic lethality at mid-gestation due to major angiogenesis defects. For instance, homozygous knockout of *Tgfb2* in mice resulted in embryonic lethality by E10.5 mainly due to haematopoiesis and vasculogenic defects in the yolk sac (154). In contrast, genetic depletion of individual ligands has more minor defects, likely due to some compensatory or overlapping functions in angiogenesis (Table 1.2). In the case of mice that are null for the *Tgfb1* ligands, the phenotype is dependent on genetic modifiers. Knockout of *Tgfb1* in mice of a mixed genetic background led to death of 50% embryos in utero due to angiogenic defects and the rest survived to approximately 3 weeks postnatally and died from auto-immune defects (155-157). *Tgfb2* null mice show perinatal mortality due to various

heart defects including incomplete ventricular septation, double-outlet right ventricle (DORV), interrupted aortic arch (IAA) (158, 159). While in *Tgfb3* null mice, hypoplasia of ventricular wall was observed along with some minor defects including position of aortic arch but no major heart defects are reported (160).

Global knockout of *endoglin* is embryonic lethal at E10.5 due to defects in yolk sac vasculature and developing hearts. The embryos displayed fragile vessels due to lack of SMC recruitment (127, 128, 161). A similar phenotype was observed after global deletion of *Alk1* (147) with embryonic lethality at E10.5. These embryos also failed to recruit vSMCs leading to formation of fragile and dilated vessels. Furthermore, *Alk1* knockout embryos displayed significantly fewer capillaries compared to controls (147). The summary of various defects in mouse and humans caused due to systemic and cell specific knockdown of TGF $\beta$  ligands or its receptors is shown below in Table 1.2.

**Table 1.2: Defects in mice and humans due to knockout or depletion of TGF $\beta$  ligands and/or its receptors [adapted from (66)].**

Target Gene	Cell Specificity and Cre line	Mouse: Viability and Cardiovascular Phenotype	Human Related CHD
<i>Tgfb1</i>	Systemic	1. Modifier dependent phenotype; 2. Embryonic lethal at E10.5 – angiogenic defects; 3. Postnatal lethal – major autoimmune response	
<i>Tgfb2</i>	Systemic	Perinatal lethal – OFT & aortic arch malformations, VSD & DORV	DORV; IAA; VSD
<i>Tgfb3</i>	Systemic	Perinatal lethality – thin ventricular walls & cleft palate	Ventricular Hypoplasia
<i>Tgfb1</i>	Systemic	Embryonic lethal at E10.5 – angiogenic defects	
<i>Tgfb1</i>	NCC (Wnt1-Cre)	Perinatal lethal – PTA	PTA
<i>Tgfb1</i>	Cardiomyocytes (Nkx2.5-Cre)	Viable – majority normal	None?
<i>Tgfb1</i>	Endothelium & Endocardium (Tie1/Tie2-Cre)	1. Embryonic lethal at E13.0 – reduced AV cardiac cushion, thin & poorly trabeculated myocardium; 2. Embryonic lethal at ~E11.0 – angiogenic defects.	Ventricular Hypoplasia
<i>Tgfb1</i>	Epicardium (Gata5-Cre)	Embryonic lethal at E10.5 – coronary vessel defects & thin myocardium	Ventricular hypoplasia
<i>Tgfb2</i>	Systemic	Embryonic lethal at E10.5 – angiogenesis defects	
<i>Tgfb2</i>	NCC (Wnt1-Cre)	Perinatal lethal – OFT defects & aortic elastin defects.	IAA, PTA, Aortic Dilatation
<i>Tgfb2</i>	Cardiomyocytes (Mlc2v/ cTcT-Cre)	Viable – majority normal	None?
<i>Tgfb2</i>	Endothelium & Endocardium (Tie1/Tie2-Cre)	1. Embryonic lethal at E10.0 to E12.0 – angiogenic & inferior AV cushion defects; 2. Embryonic lethal at E15.5 when Cre activated at E11.5, VSD & cerebral haemorrhage	VSD
<i>Tgfb2</i>	vSMCs & Epicardium (SM22 $\alpha$ -Cre)	1. Embryonic lethal at ~ E17.0 – VSD, aortic dilatation & coronary vessel defects; 2. Embryonic lethal at ~ E12.0 – underdeveloped heart & angiogenic defects	1. VSD, aortic dilatation; 2. Ventricular Hypoplasia
<i>Endoglin</i>	Systemic	1. Embryonic lethal at ~ E11.0 – reduced cardiac cushion cellularity & angiogenic defects; 2. Postnatal endothelial specific deletion – AVMs	HHT1

$\beta$ -glycan	Systemic	1. Embryonic lethal at E14.5 – reduced number of coronary vessels, DORV, VSD & thin myocardium; 2. Embryonic lethal between E16.0 & birth – poorly formed IVS & non-compacted myocardium	DORV, VSD, Ventricular Hypoplasia
<i>Abbreviations:</i> AV – AtrioVentricular; AVMs – ArterioVenous Malformations; CHD – Congenital Heart Disease; DORV – Double Outlet Right Ventricle; E – Embryonic Day; HHT – Hereditary Haemorrhagic Telangiectasia; IAA – Interrupted Aortic Arch; NCC – Neural Crest Cells; OFT – OutFlow Tract; PTA – Persistent Truncus Arteriosus; VSD – Ventricular Septal Defect; vSMCs – Vascular Smooth Muscle Cells.			

### 1.5.3. TGF $\beta$ Signalling during EMT

The process of EMT of endocardial and epicardial cells is important for development of the valves and coronary vasculature (section 1.3.1.1). The expression of TGF $\beta$ 2 ligand is shown in the myocardium around the endocardial cushions and in the migrating mesenchymal cells while TGF $\beta$ 3 expression is only observed in the mesenchymal cells in later stages (162). This expression in TGF $\beta$ 2 in mesenchymal cells continue during the whole process of AV valve formation (162). Mouse models with global knockdown of Tgf $\beta$ 2 led to perinatal mortality due to defects in EMT dependent organs such as heart, lungs and limbs (163). *In vitro* studies by Sanford *et al.* (162), showed that blocking Tgf $\beta$ 2 but not Tgf $\beta$ 3 inhibited EMT (162). However, they suggested that the later expression of Tgf $\beta$ 3 is also vital for correct AV valve remodelling (162).

During the process of EMT, Tgf $\beta$ r2 is also expressed in AV cushion mesenchymal cells and is necessary for migration & activation of EMT by Tgf $\beta$  ligands (58, 59). *In vitro* studies using collagen gel assay on AV explants from E9.25 embryos from *Tgf $\beta$ r2<sup>fl/fl</sup>*; *Tie2-Cre* mouse line showed that in the absence of Tgf $\beta$ r2, endocardial cells failed to undergo EMT (59). However, depletion of Tgf $\beta$ r2 *in vivo* using *Tie2-Cre* mouse line did not affect the EMT process in AV cushions but did lead to reduced proliferation of mesenchymal cells in AV cushions (59). Jiao *et al.* (59) also showed that Tgf $\beta$  is essential for remodelling of AV canal & cardiac looping *in vivo* and in its absence, E12.5 embryos displayed double-inlet left ventricle (DILV).

The TGF $\beta$  co-receptor  $\beta$ -glycan is necessary during the process of EMT. Immunohistochemical analysis on chick hearts showed expression of  $\beta$ -glycan in the endocardial cell adjacent to AV cushions and in the migrating mesenchymal cells (164). *In vitro* analysis on AV cushion explants from stage 14-18 chick embryos showed that blocking of  $\beta$ -glycan using antisera reduced numbers of mesenchymal cells due to inhibition of endocardial EMT (164). Global knockdown of  $\beta$ -glycan led to poorly developed IVS, thin non-compacted myocardium in E14.5 to E18.0 embryos (165, 166). Furthermore, Compton *et al.* (166) showed that knockdown of  $\beta$ -

---

*glycan* led to reduced number of coronary vessels in E14.5 embryos along with various heart defects including DORV and detached epicardium.

*In vitro* analysis by Bax *et al.* (64) has shown that adult EPDCs after EMT attain a spindle like structure (similar to SMCs) and start to express endoglin while expression of *VCAM1* is inhibited via an ALK5 mediated pathway (64). Inhibition or knockdown of endoglin did not prevent TGF $\beta$  mediated EMT *in vitro*, and the authors concluded that endoglin is probably not involved during the beginning of epicardial EMT but is potentially important during mesenchymal cells differentiation following EMT (64). This hypothesis was tested in the current study during coronary vasculature development *in vivo*.

## **1.6. Hereditary Haemorrhagic Telangiectasia (HHT)**

Hereditary haemorrhagic telangiectasia (HHT) also known as Osler-Weber-Rendu disease is an autosomal dominant vasculature related disorder and affects 1 in 5000 individuals (167). Genetically, in over 80% cases HHT is caused due to haplo-deficiency of either *endoglin* or *ALK1* gene. This results in two main variants of HHT: (i) HHT1, caused due to mutations in *endoglin* gene (168); and (ii) HHT2, caused due to mutations in *ALK1* gene (also known as *ACVRL1*) (169).

The HHT patients clinically presents with epistaxies (nosebleeds), telangiectasias and arteriovenous malformations (AVMs). In normal individuals, the arteries and veins are not directly linked but are separated via a mesh of capillary bed which helps gas and nutrient exchange with the tissues (Figure 1.19A). However, in HHT patients, there are localised AVMs where arteries and veins are directly connected bypassing the capillary bed (Figure 1.19B). These AVMs range from small to large size and are found primarily in brain, lungs & liver. The location and size of these AVMs determine disease severity. For instance, larger AVMs in liver are reported to lead to high output heart failure (HOHF) (170-172). The smaller AVMs also called telangiectases are formed due to dilation of post-capillary venules which eventually connect with arterioles and present as red spots on skin or mucosal surface (173). The vessels within a telangiectasis are quite fragile and are prone to rupture or haemorrhage. As a consequence, HHT patients are also suffer from anaemia (174).

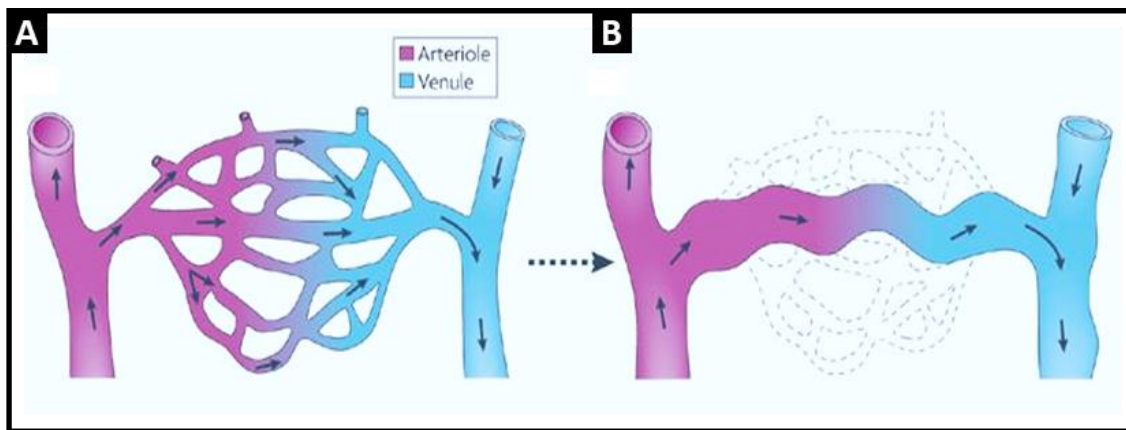


**Figure 1.19: Arteriovenous Malformation in HHT [adapted from (20)].** (A) The normal capillary network present in most vascular beds and interconnects an arteriole and a venule. (B) Formation of an arteriovenous malformation in hereditary haemorrhagic telangiectasia (HHT).

HHT1 and HHT2 patients exhibit similar symptoms (e.g. AVMs and telangiectases). However, the occurrence of symptoms within HHT1 or HHT2 patients differ from individual to individual potentially due to environmental factors and genetic modifiers [reviewed in (175)]. Furthermore, HHT1 patients are prone to pulmonary and cerebral AVMs while in HHT2 patients gastrointestinal (GI) tract and liver AVMs are more common (176-179).

Clinically, a patient is diagnosed with HHT if at least three out of four Curacao criteria are met (174). These criteria are: (i) spontaneous recurrent epistaxies especially at night time; (ii) presence of telangiectases on lips, mouth, nose or inner mucosal lining; (iii) AVMs in visceral organs such as brain, lungs &/or liver; and (iv) family history. Further confirmation of HHT is made via genetic testing of the suspected or clinically diagnosed patients and family members (167, 174). AVMs are high risk symptom of HHT and depending on its location & size it can be fatal. For instance, pulmonary AVMs are asymptomatic until cyanosis, stroke (caused due to entrance of small clots from pulmonary circulation to systemic circulation via AV shunts instead of filtering through the capillary network) or brain abscess or AVMs in liver can lead to HOHF [reviewed in (178, 180-182)]. However, the mechanism behind AVMs formation is still elusive and there are many unanswered questions regarding their origin and tissue-specific locations.

Since the identification of the genes involved with HHT a lot of research has focused on understanding the mechanism behind the clinical phenotypes observed in HHT patients. As discussed in section 1.5.1, all the genes identified in HHT play a critical role during the angiogenesis process and are predominantly expressed in ECs [reviewed in (123-126, 175)]. This indicates that HHT is caused primarily due to defects in TGF $\beta$  signalling in ECs [reviewed in (20, 123, 126, 131, 175, 181-183)].

---

### 6.1.1. Role of TGF $\beta$ Signalling in HHT

TGF $\beta$  signalling plays a dual role in ECs (section 1.5.1). The TGF $\beta$ /ALK1 mediated signalling is vital for ECs proliferation and migration, while TGF $\beta$ /ALK5 signalling is crucial for recruitment of SMCs or pericytes to stabilise the vessels. An imbalance in this pathway in endothelial cells can potentially explain some of the vascular defects in HHT.

As over 80% of HHT patients suffer from haplo-deficiency of *endoglin* or *ALK1*, these two are considered as the most potent therapeutic targets. Many studies using genetic *in vivo* and *in vitro* models focusing of these two genes have shed some light regarding potential origin of AVMs [reviewed in (20, 126, 175, 181-183)]. It has been suggested that AVMs occur due to loss of arterial and venous identity of the vessels (184, 185). Urness *et al.* (185) observed that global knockdown of *Alk1* lead to formation of shunts between dorsal aorta & cardinal vein around E8.5 and which enlarged by E9.0. By E9.5, multiple AV shunts were observed, vSMC recruitment was impaired and led to embryonic lethality by E10.5 (185). Further immuno-histochemical analysis on E8.5 and E9.5 embryo sections also showed downregulation of arterial marker *Efnb2* in the affected vessels. They concluded that *Alk1* is necessary to establish arterial and venous identity of the vessels. Any disruption in vessel identity lead to formation of AV shunts (185).

In a study by Sorensen *et al.* (184), they analysed the effect of global endoglin loss on vessel identity. In comparison to *Alk1* null embryos, AV shunts were only observed between dorsal aorta & cardinal vein in global endoglin knockout embryos. These shunts were far less dilated and occurred slightly later (at E9.0). Furthermore, no loss of arterial identity was observed in the AV shunts after endoglin knockdown. However, haematopoietic clusters (functional marker of arterialisiation) were observed budding from the walls of the cardinal vein of E10 endoglin null embryos as well as higher expression of the arterial marker CD34 (184).

As majority of the vasculature appears normal in HHT1 and HHT2 patients, it supports the idea that haplo-deficiency of the affected genes alone does not cause AVMs. A trigger such as injury (186), inflammation, angiogenic stimuli (187-190) possibly combined with a further somatic mutation (190) is required which leads to formation of AVMs [reviewed in (175, 191)]. Mahmoud *et al.* (188) using wholemout immuno-histochemical studies showed formation of AVMs in P7 neonatal retinas after using conditional deletion of endoglin in EC at P2 and P4 using *Cdh5(PAC)Cre<sup>ERT2</sup>* mice. They showed that the AVMs originated due to increased ECs proliferation in the absence of endoglin however no change in the phosphorylation of

---

Smad1/2/3/5/8 was observed. These AVMs expressed venous marker *EphB4* but arterial vessel identity remained unchanged. However, veins were observed to be significantly dilated and the retina vasculature progression was significantly delayed (188).

In another study, AVMs were reported in P6 retinas by wholemount immuno-histochemical analysis after *Alk1* knockdown at P4 in ECs using *Cdh5(PAC)Cre<sup>ERT2</sup>* mice (187). Dilated veins were observed as well as loss of the arterial identity of the vessels with no difference in the venous marker EphB4. They also observed a reduction in the phosphorylation of Smad1/5/8 (187). However, the retina vasculature progression was unaffected, but an increased number of branch points were observed in the *Alk1* null retinas. Tual-Chalot *et al.* (187) speculated that the increased number of branch points coupled with reduced phosphorylation of Smad1/5/8 was potentially due to lack of BMP9 & BMP10 mediated signalling. A similar increase in the number of branch points were observed in BMP10 depleted BMP9 knockout P6 retinas (192).

### **6.1.2. Treatment for HHT**

HHT patients in most cases, initially present with nosebleeds caused by telangiectasias while the formation of AVMs in GI tract, brain, lungs or liver occur much later in life (193). These AVMs can be detected via CT scan or Doppler ultrasound and in certain cases, can be treated by embolization performed under general anaesthesia (194, 195).

Recently, VEGF neutralising antibody, bevacizumab has been shown to be quite effective in epithaxies treatment in HHT patients (196, 197). However, the mechanism behind this improvement is unclear. Han *et al.* (198), used an HHT2 mouse model to understand the mechanism behind VEGF neutralising antibodies. They showed using intravital hyperspectral imaging system with dorsal window chamber that in the absence of *Alk1* in ECs, AVMs are formed in presence of an angiogenic stimuli (wound) and these AVMs were formed by development of new connections between vessels rather than by regression of pre-existing capillary network (198). They next showed the VEGF can trigger AVM formation in subcutaneously injected PLGA implant (containing VEGF or lipopolysaccharides) in *Alk1-iKO* mice. While in the presence of VEGF neutralising antibody (G6.31), the formation of AVMs in LPS implants was inhibited (198).

Han *et al.* (198) also showed that treatment with VEGF neutralising antibody (G6.31) not only inhibited VEGF induced AVM formation but also the ones initiated due to a wound or in *Alk1* knockdown in mice. In this study AVMs formation was classified into three phases: (i) initiation (2-4 days after wounding); (ii) maturation (4-6 days after wounding) and (iii) maintenance (7-

---

9 days after wounding). They showed that, treatment with G6.31 antibody during the initiation phase only led to formation of a few small AV shunts; treatment during maturation phase decreased total number of AV shunts as well as regressing those that were still developing. While treatment during maturation phase did not affect the large AVMs, however small and intermediate regressed slightly.

Ola *et al.* (199) showed the effect of *Vegfr2* knockdown was analysed in *Alk1-iKO* mice. During this study, they showed AVMs near the centre of P5 retinas in *Alk1-iKO* pups as well as BMP9/10 antibody treated pups. Retinas in both groups also showed increased vessel area and branch points near the angiogenic front (199). In addition to retinas, AV shunts were also observed in the GI tract of these mice. Quantification of AVMs (in both retinas and GI tract) showed a higher probability of AV shunts in *Alk1-iKO* mice compared to BMP9/10 antibody treated group (199). The qPCR analysis on isolated and primary cultured lung ECs from *Alk1-iKO* mice showed a downregulation of *Alk1*, *Eng* and *Vegfr1* but no change in *Vegfr2* was observed. Furthermore, downregulation of arterial markers such as *Notch1* & *Jag1* and an upregulation in venous marker *EphB4* was also observed in these cells (199). This reduction in *Vegfr1* as well as *Jagged1* potentially led to enhanced VEGF signalling leading to formation of AVMs.

To test this hypothesis, Ola *et al.* (199) first showed an increased phosphorylation of VEGFR2 and downstream genes pERK and pAKT in siRNA mediated *Alk1* depleted HUVECs (199). Next, they tested the effect of *Vegfr2* depletion (using *Vegfr2<sup>fl/fl</sup>*) *in vivo* in *Alk1-iKO* mice. A varying phenotype was observed in these mice depending on the level of *Vegfr2* deletion. A mild loss of *Vegfr2* led to almost normal retina vasculature was observed in P5 retinas. However, further depletion of *Vegfr2* significantly reduced angiogenesis in P5 retinas and in case of complete loss, no retina vasculature was observed (199). *In vitro* analysis showed BMP9 regulates activity of PI3K/AKT pathway. Next, *in vivo* inhibition of PI3K using an inhibitor (Wortmannin or Pictilisib) efficiently normalised the vasculature of P5 retinas of both *Alk1-iKO* and BMP9/10 antibody treated mice. Inhibition of PI3K also prevented AV shunt formation in GI tracts (199) and was able to promote regression of established retinal AVMs. These potentially make PI3K a novel target for treatment of AV shunts in HHT2 patients.

These studies have focused on rescue of the *Alk1* (HHT2) mutant phenotype with very little work on *endoglin* (HHT1). During the current study, I analysed the effect of BMP9 treatment to try and rescue AVM formation in P7 retinas in an established HHT1 mouse model (188). I also studied the effect of venous ECs endoglin knockdown on AVMs formation.

---

## 1.7. Myocardial Infarction

Cardiovascular disease (CVD) is the biggest cause of death worldwide. Presently, ~7 million people are living with CVD in the UK alone and one third of this population is suffering from coronary artery or ischemic heart disease (200). A heart attack is the most common cause of death in these patients (200). A healthy adult heart has high energy demand. To fulfil this demand, each cardiomyocyte (CM) is in the vicinity of a coronary capillary (45, 46). Blockage of any coronary artery supplying these capillaries leads to myocardial hypoxia or myocardial infarction (MI), also known as a ‘heart attack’ (201). The severity of MI differs depending on the location of the coronary artery involved, and whether occlusion is proximal or distal to the aortic ostia. Acute MI most frequently occurs due to the formation of a thrombus following local rupture of an atherosclerotic plaque in a coronary artery causing an arterial blockage. If left untreated, completely occluded vessels can be fatal (202). Clinically, MI is divided into 6 types as shown in Table 1.3 (201).

**Table 1.3: Clinical classification of Myocardial Infarction [taken from (201)].**

MI Classification	Symptoms
<b>Type 1</b>	Spontaneous MI related to ischemia due to a primary coronary event such as plaque erosion and/or rupture, fissuring, or dissection.
<b>Type 2</b>	MI secondary to ischemia due to either increased oxygen demand or decreased supply, e.g. coronary artery spasm, coronary embolism, anaemia, arrhythmias, hypertension, or hypotension.
<b>Type 3</b>	Sudden unexpected cardiac death, including cardiac arrest, often with symptoms suggestive of MI, accompanied by presumably new ST elevation, or new LBBB, or evidence of fresh thrombus in a coronary artery by angiography and/or at autopsy, but death occurring before blood samples could be obtained, or at a time before the appearance of cardiac biomarkers in the blood.
<b>Type 4a</b>	MI associated with PCI.
<b>Type 4b</b>	MI associated with stent thrombosis as documented by angiography or at autopsy.
<b>Type 5</b>	Myocardial infarction associated with CABG.
<i>Abbreviations: CABG – Coronary Artery Bypass Grafting; LBBB – Left Bundle Branch Block; MI – Myocardial Infarction; PCI – Percutaneous Coronary Intervention.</i>	

The death of cardiomyocytes (CM) post-MI is inevitable but for a better prognosis it is essential that CM loss is minimal. To reduce CM loss, acute MI patients are subjected to primary percutaneous coronary intervention (PPCI) to restore the blood supply to the affected region (203). Occurrence of MI results in a cascade of cellular responses to initiate heart repair. This process of heart repair is divided into three phases: the inflammatory phase; the proliferative phase and the maturation phase (Figure 1.20) (204-208). Briefly, in the inflammatory phase is an influx of innate immune cells attracted by the release of alarmins by necrotic CM (157). This phase lasts for 3 to 4 days in mice (207). The dead CM are then removed by phagocytes which

---

in turn suppresses the inflammatory response and promote cardiac healing by initiating the proliferative phase (204).

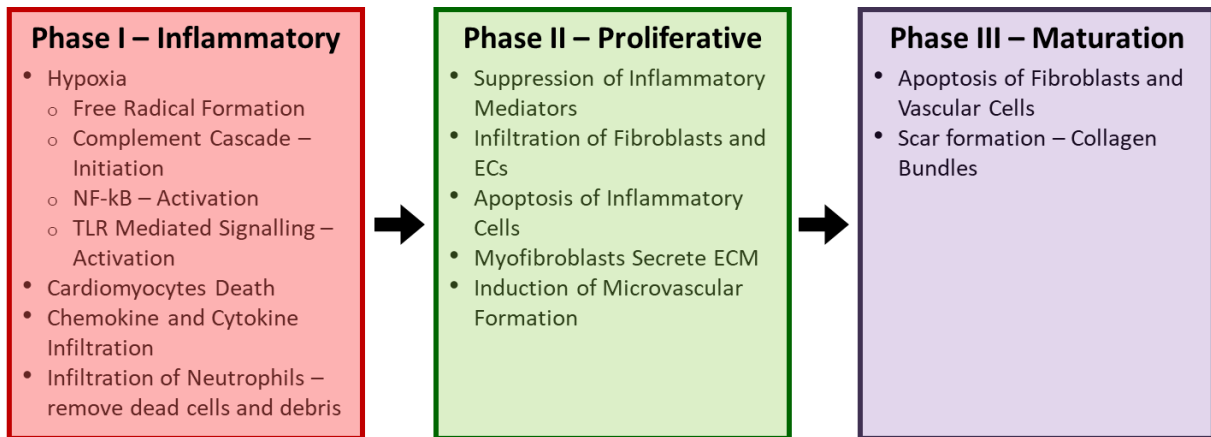


**Figure 1.20: Phases of Cardiac Healing [Reviewed in (204)].**

During the proliferative phase, ECM is secreted by myofibroblasts and new blood vessels are formed through the process of angiogenesis in the infarcted region (204). During cardiac remodelling, MI induced hypoxia in the heart leads to secretion of VEGF and activation of angiogenesis. The final phase of cardiac healing is the maturation phase. During this phase, a mature scar, rich in collagen, is formed and neo-vessels are stabilised through the process of arteriogenesis (204, 205).

### **1.7.1. Importance of TGF $\beta$ during Heart Repair**

The importance of TGF $\beta$  signalling in myocardial injury, repair and vascular remodelling has been extensively reviewed (204, 206, 207, 209-212). After MI, the expression of TGF $\beta$  is upregulated in hearts where it drives various functions in different cell types during the cardiac healing phase (Figure 1.21). For example, TGF $\beta$  is involved in promoting deposition of fibrous tissue in the infarcted area during the maturation phase of cardiac healing (204, 205, 211). TGF $\beta$  also plays an essential role during angiogenesis. In ECs TGF $\beta$  stimulates or inhibits angiogenesis depending upon whether it signals via TGF $\beta$ /Alk1 or TGF $\beta$ /Alk5 pathway, respectively (Figure 1.17).

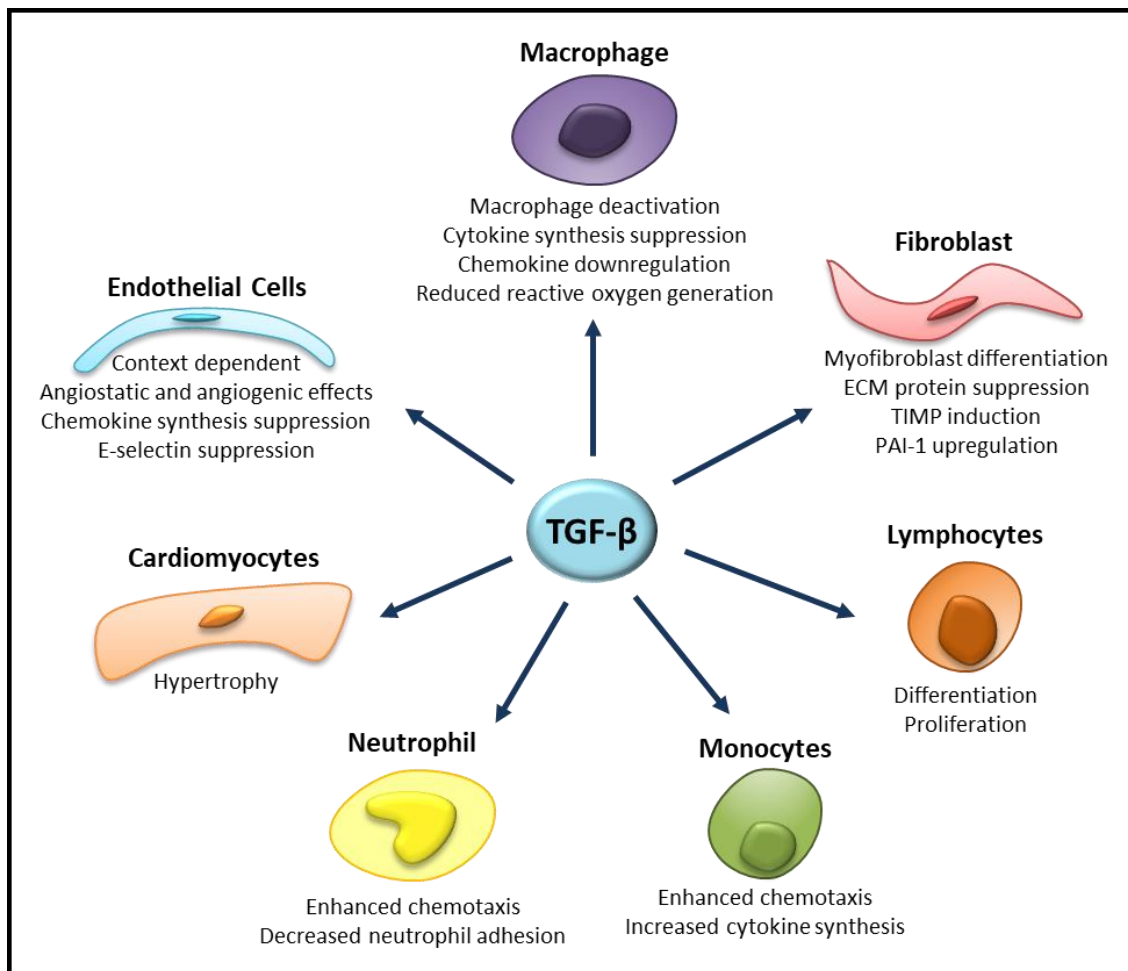


**Figure 1.21: Role of TGFβ during Cardiac Healing [adapted from (204)].**

The importance of TGFβ in heart repair has been shown by Frantz *et al.* (210) by blocking TGFβ ligand with an antibody before and after MI leading to high mortality. The left ventricle of these mice also showed higher dilation and lower contractibility. Thereby concluding that, auto and paracrine signalling by TGFβ plays a vital role in heart repair (210).

Endoglin plays an important role during TGFβ mediated angiogenesis (section 1.5.1). Expression of endoglin has also been observed to be elevated in injury state [reviewed in (131, 213, 214)]. In solid tumours, endoglin is also used as a biomarker for tumour angiogenesis with elevated levels correlated with increased metastasis [reviewed in (131, 213, 214)]. In clinical trials, anti-endoglin antibody (TRC105) has been used to reduce angiogenesis in tumour size [reviewed in (214)]. Currently, TRC105 is being used to treat hepatocellular carcinoma. In studies involving MI models, expression of endoglin was reported to be elevated in the ECs of infarcted region as well other types including myo-fibroblasts and SMCs (215-217). Mice heterozygous for endoglin showed reduced angiogenesis in the peri-infarct region (216) consistent with a role for endoglin in promoting angiogenesis in the infarct border zone.

The need for angiogenesis in post-MI cardiac healing is no different from any other wound healing process. Restoration of the blood flow is vital to exchange of nutrients and to promote survival of the nearby cells. During cardiac remodelling, MI induced hypoxia in the heart leads to secretion of VEGF. This leads to activation of the developmental like processes to promote angiogenesis (section 1.2). Angiogenesis and arteriogenesis are critical processes for healing but are generally insufficient at the endogenous level to preserve the CM which results in the necrosis of the heart muscle tissue and this may ultimately lead to heart failure (218). Ongoing research to promote angiogenesis in hearts and mechanisms to stabilise neovessels is therefore critically important (218).

### 1.7.2. Cell Mediated Therapy in Post-MI

To improve the outcomes post-MI, transplantation of stem cell or stem cell like cells has proved to be beneficial in augmenting heart repair. These cells have been shown to act via two main routes (Figure 1.22): (i) direct repair via cellular contribution or (ii) indirect contribution via secretion of paracrine factors (219).

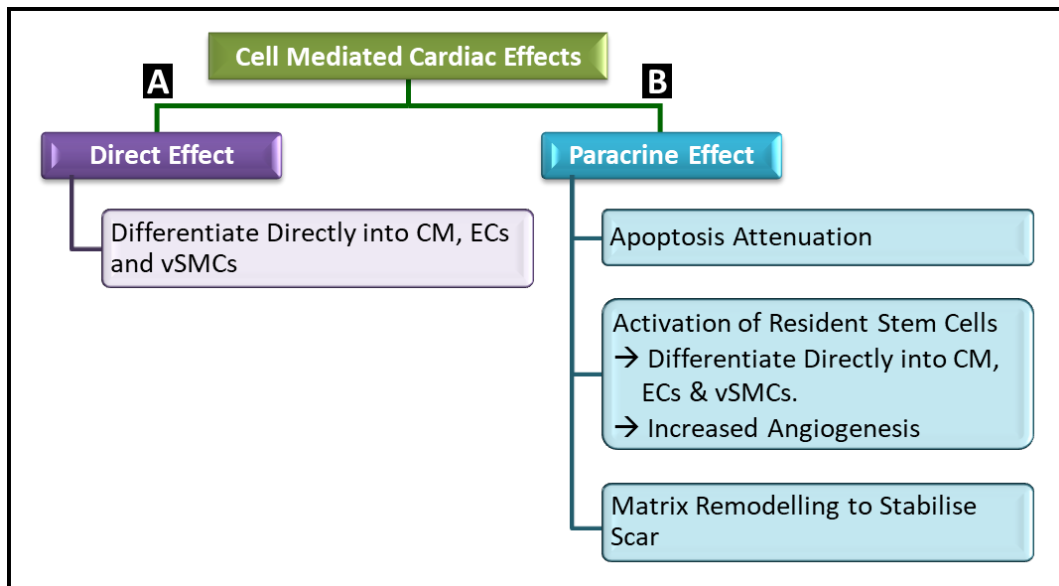


**Figure 1.22: Direct and indirect mechanism of cell-mediated heart repair [adapted from (219)].** Stem cells transplantation after MI could mediate cardiac healing in two ways: (A) Direct effect during which transplanted cell differentiate directly into cardiac cells. (B) Stem cells could also improve cardiac healing via paracrine mechanism. These could be reduction in cell apoptosis or secrete various cell signalling factors which could lead to activation of resident stem cell. These cells can then either differentiation into cardiac cell types or increase angiogenesis to promote cardiac healing. Stem cells could remodel matrix which could help to stabilise the scar.

Many cell types have been tested to exploit their cardiac regenerative potential [reviewed in (220)]. These cells include bone marrow mesenchymal stem cells (BM-MSCs), embryonic stem cells (ES cells) and cardiosphere derived cells (CDCs) (219). Amongst these cells, BM-MSCs and CDCs have been tested in clinical studies. Many clinical trials involving BM-MSCs showed

---

no global functional difference between control and treated group (221-224). However, in pre-clinical studies, CDCs showed promising results predominantly via paracrine mechanism resulting in reduced CM apoptosis, increased CM proliferation and angiogenesis, modulation of inflammatory phase and promotion of host healing process including pro-angiogenic factors [reviewed in (220)].

Injection of CDCs in post-MI hearts showed beneficial effects including improved heart function and reduction in scar size 3 weeks after MI in mice (225). CDCs are also observed to provide more paracrine contribution than direct cellular contribution in CDC mediated heart repair as few CDCs differentiated into CM or any other cardiac cell type (225). Furthermore, these paracrine benefits of CDCs have been studied using CDC-conditioned media (CDC-CM) *in vitro*, which showed an anti-apoptotic effect on neonatal rat ventricular myocytes by release of pro-angiogenic factors like VEGF and HGF (human growth factor). Similar beneficial effects of CDC-CM were seen *in vivo* upon immediate injection of CDC-CM in post-MI mice hearts (225).

Due to these beneficial effects of CDCs on cardiac function and angiogenesis, these cells are currently being investigated in multiple clinical trials (226-229), with a primary goal to reverse ventricular dysfunction after MI. CDCs are delivered to the heart by intracoronary injection and led to reduction in scar mass and increased viable myocardium mass. But unlike animal models, no significant change in the LV function was observed 6 and 12 months after the injection (226). This clearly shows the need to study these cells in more detail and to further characterise them in order to use them to their full potential.

---

## **1.8. Aims**

1. To investigate the role of Endoglin and TGF $\beta$ R2 in the epicardium and EPDCs during mouse heart development.
2. To investigate the role of Endoglin in coronary vessel endothelial cells during mice heart development.
3. To investigate the effect of Venous Endoglin knockdown on AVMs formation.
4. To study the occurrence AVMs/ shunts or dilated vessels in the lungs and liver in Eng-iKO adult mice.
5. To determine the role of Endoglin in CDC-mediated angiogenesis in the adult mouse heart after a myocardial injury.

## **1.9. Hypotheses**

1. Endoglin iKO (induced knockout) or TGF $\beta$ R2 iKO in epicardial cells and EPDCs during mice heart development will affect coronary vessel formation.
2. Endoglin iKO in coronary vessel ECs during mice heart development will affect coronary vessel formation.
3. Endoglin iKO in venous ECs leads to AVMs formation in neonatal retinas.
4. Systemic Eng-iKO using VE-Cad<sup>Cre-ERT2</sup> mouse line leads to HOHF in adult mice due to formation of AVMs or vasodilation in the peripheral vasculature.
5. Endoglin iKO in the CDCs will impede the process of angiogenesis during cell-mediated heart repair in an adult mouse heart post-myocardial injury by altering the profile of secreted pro-angiogenic factors.

---

## **Chapter 2. Materials and Methods**

---

## 2.1. Mouse Strains and Genotyping

All animal procedures were performed with local ethical approval and under UK Home Office licence and national guidelines for the care and use of laboratory animals were adhered to. Mice were housed in a ventilated, germ free facility in a 12-hour light-dark cycle and fed with standard diet and water.

### 2.1.1. Mouse Strains

**C57Bl/6 Mouse Line:** C57Bl/6 mice were provided by either in-house breeding or bought from Charles River Laboratories, UK. Mice from this line were used to study expression of *endoglin* in the developing & adult heart ([chapter 3](#)) and the role of endoglin in CDC promoted angiogenesis in the adult heart post-MI ([chapter 6](#)).

***Wt1<sup>Cre-ERT2/+</sup>; Rosa26<sup>eYFP/eYFP</sup>* Mouse Line:** *Wt1<sup>Cre-ERT2/+</sup>* mice (78) were provided by Dr Helen Phillips (Newcastle University, UK) and were crossed with in-house available C57Bl/6 background *Rosa26<sup>eYFP/eYFP</sup>* reporter mice (230). *Wt1<sup>Cre-ERT2</sup>* mice express tamoxifen inducible Cre recombinase (Cre-ERT2) enzyme under regulation of wilm's tumor 1 protein (78). *Rosa26<sup>eYFP</sup>* reporter mice express enhanced yellow fluorescence protein (eYFP) with a transcriptional stop sequence flanked by *loxP* sites (230). In the presence of an active Cre recombinase, the stop sequence is removed, which leads to expression of enhanced yellow fluorescent protein (eYFP) (Figure 2.1). Mice from this line were used to optimise the activation of *Wt1<sup>Cre-ERT2</sup>* and to study the expression of endoglin in EPDCs during heart development ([chapter 4](#)).

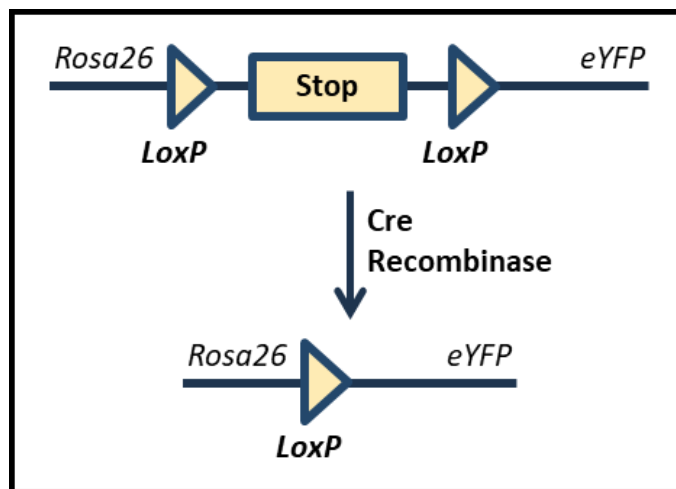


**Figure 2.1: Transgenic Rosa26 locus with floxed stop eYFP gene.** In the presence of active Cre recombinase, the stop sequence is removed which leads to expression of eYFP protein.

***Eng*<sup>fl/fl</sup>; *Wt1*<sup>Cre-ERT2/+</sup>; *Rosa26*<sup>eYFP/eYFP</sup> Mouse Line:** *Endoglin* floxed mouse was generated in my host laboratory by inserting *loxP* sites flanking exon 5 and 6 (231). In the presence of active recombinase Cre enzyme, exon 5 and 6 are removed leading to the production of truncated non-functional endoglin protein (Figure 2.2). *Eng*<sup>fl/fl</sup> mice were crossed with *Wt1*<sup>Cre-ERT2/+</sup>; *Rosa26*<sup>eYFP/eYFP</sup> mice to generate an *Eng*<sup>fl/fl</sup>; *Wt1*<sup>Cre-ERT2</sup>; *Rosa26*<sup>eYFP/eYFP</sup> mouse line and were maintained in C57Bl/6 genetic background. Mice from this line were used to study the role of endoglin in EPDCs during heart development (chapter 4).

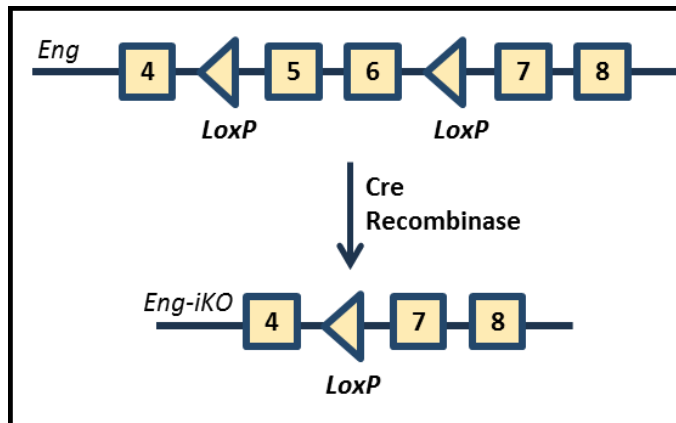


**Figure 2.2:** Floxed *Endoglin* gene showing the *LoxP* sites flanking exon 5 and 6. In the presence of Cre recombinase exon 5 and 6 are removed to form a truncated non-functional endoglin protein.

***Tgfb2*<sup>fl/fl</sup>; *Wt1*<sup>Cre-ERT2/+</sup>; *Rosa26*<sup>eYFP/eYFP</sup> Mouse Line:** *Tgfb2* floxed mice were available in-house, and were originally created by flanking exon 4 with *loxP* sites (232). In the presence of an active Cre recombinase exon 4 is removed, which leads to a frameshift mutation and formation of a non-functional transcript (Figure 2.3). These mice were crossed with *Wt1*<sup>Cre-ERT2/+</sup>; *Rosa26*<sup>eYFP/eYFP</sup> mice to generate a *Tgfb2*<sup>fl/fl</sup>; *Wt1*<sup>Cre-ERT2</sup>; *Rosa26*<sup>eYFP/eYFP</sup> mouse line and were back crossed 5 generations with C57Bl/6 mice. Mice from this line were used to study the role of *Tgfb2* in EPDCs during heart development (chapter 4).

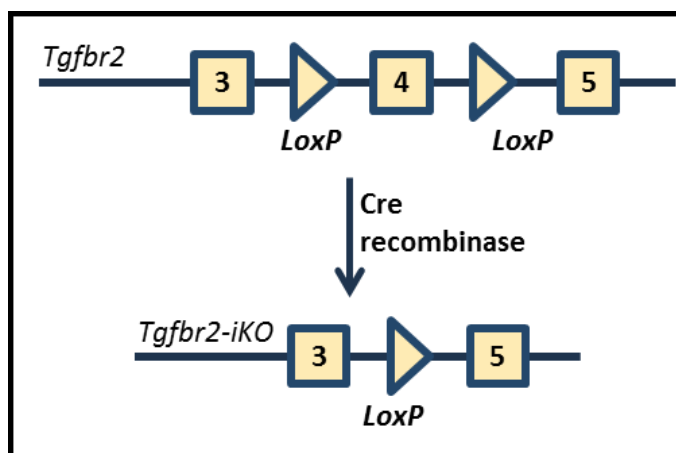


**Figure 2.3:** Floxed *Tgfb2* gene showing the *LoxP* sites flanking exon 4. In the presence of Cre recombinase exon 4 is removed leading production of a non-functional *Tgfb2* protein.

---

**Dll4in3<sup>Cre-ERT2/+</sup>; Rosa26<sup>eYFP/eYFP</sup> Mouse Line:** *Dll4in3<sup>Cre-ERT2</sup>* is an arterial endothelial cell specific Cre mouse line, provided by collaborator Dr Sarah de Val (Oxford University, UK). In this mouse line, a transcriptional enhancer in the highly conserved third intron of *Dll4* (233) is cloned upstream of Cre recombinase. Multiple copies of this sequence (*Dll4in3-Cre*) were then randomly inserted into a mouse genome to produce a transgenic mouse. Mice from this line were crossed with *Rosa26<sup>eYFP</sup>* reporter mice to generate a *Dll4in3<sup>Cre-ERT2/+</sup>; Rosa26<sup>eYFP/eYFP</sup>* mouse line. Activation of *Dll4in3<sup>Cre-ERT2</sup>* after tamoxifen injection leads to expression of eYFP protein in all Dll4in3 positive cells and daughter cells (Figure 2.1). Mice from this line were used to optimise activation of *Dll4in3-Cre* (chapter 5).

**VE-Cad<sup>Cre-ERT2/+</sup>; Rosa26<sup>eYFP/eYFP</sup> Mouse Line:** *VE-Cad<sup>Cre-ERT2</sup>* (also known as *Cdh5 (PAC)<sup>Cre-ERT2</sup>*) mice were obtained from Dr Ralf Adams (CRUK, UK). This line expresses inducible Cre recombinase under the control of the vascular endothelial cadherin (*VE-Cadherin* or *Cdh5*) promoter (234). These mice were crossed with *Rosa26<sup>eYFP</sup>* reporter mice to enable the labelling of all the VE-Cad expressing cells following tamoxifen treatment (Figure 2.1). Mice from this line were maintained in C57Bl/6 genetic background and were used to map the expression pattern of *VE-Cad<sup>Cre-ERT2</sup>* (chapter 5).

**Eng<sup>fl/fl</sup>; VE-Cad<sup>Cre-ERT2</sup> Mouse Line:** *VE-Cad<sup>Cre-ERT2</sup>* mice were crossed with *Eng<sup>fl/fl</sup>* mouse model to generate an *Eng<sup>fl/fl</sup>; VE-Cad<sup>Cre-ERT2</sup>* mouse line. In the presence of tamoxifen Cre-ERT2 is activated leading to knockdown of endoglin from all VE-Cad-Cre positive cells (Figure 2.2). This mouse line was used to study the role of *endoglin* in ECs (chapter 5).

**Apj<sup>Cre-ERT2/+</sup>; Rosa26<sup>mTmG/+</sup> Mouse Line:** *Apj<sup>Cre-ERT2</sup>* is an inducible Cre recombinase under the control of the *Apj* promoter. *Apj* is predominantly expressed in the venous ECs (43). *Apj<sup>Cre-ERT2</sup>* mice were crossed with a dual reporter *Rosa26<sup>mTmG</sup>* mice (235) to generate a *Apj<sup>Cre-ERT2/+</sup>; Rosa26<sup>mTmG/+</sup>* mouse line. *Apj<sup>Cre-ERT2</sup>; Rosa26<sup>mTmG</sup>* mice (43) were provided by Dr. Kristy Red-Horse (Stanford University, US). Cells expressing *Rosa26<sup>mTmG</sup>* reporter express red fluorescence in the absence of an active Cre recombinase, while in the presence of an active Cre recombinase, green fluorescence is emitted (Figure 2.4). Mice from this line were backcrossed for 5 generations with C57Bl/6 mice to generate a syngeneic line and were used to optimise the activation of *Apj<sup>Cre-ERT2</sup>* in neonates (chapter 5).

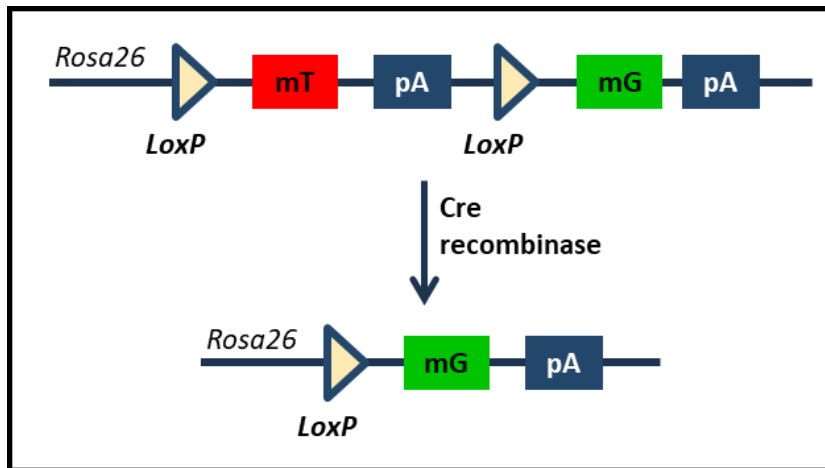


**Figure 2.4: Transgenic Rosa26 locus with mTmG reporter sequence.** Cells expressing mTmG reporter prior have red fluorescence due to expression of membrane-targeted tandem dimer Tomato (mT). In the presence of an active Cre recombinase the mT sequence is removed resulting in the expression of green fluorescence due to expression of membrane-targeted enhanced green fluorescent protein (mG).

***Eng<sup>fl/fl</sup>; Apj<sup>Cre-ERT2/+</sup>; Rosa26<sup>mTmG/+</sup>* Mouse Line:** To study the role of *endoglin* in *Apj<sup>Cre-ERT2</sup>* positive endothelial cells (chapter 5), *Apj<sup>Cre-ERT2/+</sup>; Rosa26<sup>mTmG/+</sup>* mice are crossed with *Eng<sup>fl/fl</sup>* mice to generate *Eng<sup>fl/fl</sup>; Apj<sup>Cre-ERT2/+</sup>; Rosa26<sup>mTmG/+</sup>* mouse line. In the presence of tamoxifen, *Apj-Cre* is activated which leads to knockdown of endoglin in *Apj-Cre* positive cells (Figure 2.2).

***Eng<sup>fl/fl</sup>; Rosa<sup>Cre-ERT2/Cre-ERT2</sup>; CAG<sup>GFP/GFP</sup>* Mouse Line:** CAG-farnesyl-eGFP mice were obtained from Prof Alexander Medvinski (Edinburgh University, UK). In these mice the expression enhanced green fluorescent protein (eGFP) is under control of the CAG promoter (a combination of the chicken beta actin promoter and the CMV promoter). The farnesyl group restricts location of the eGFP to the cell membrane (150). These mice were crossed with ubiquitously expressed *Rosa<sup>Cre-ERT2</sup>* mice line (obtained by from Di Li, Connecticut, USA) and in-house available *Eng<sup>fl/fl</sup>* mice to obtain *Eng<sup>fl/fl</sup>; Rosa<sup>Cre-ERT2/Cre-ERT2</sup>; CAG<sup>GFP/GFP</sup>* in C57Bl/6 genetic background. Mice from the resulting line were used to culture CDCs and study the importance of endoglin in these cells (Chapter 6).

### 2.1.2. Tamoxifen

To activate inducible Cre recombinase (Cre-ERT2), tamoxifen was injected. Tamoxifen was prepared in two stages during this study. First, 10 or 15mg of tamoxifen was dissolved in 100µl of absolute ethanol followed by the addition of 900µl of peanut oil to give a final concentration of 10 or 15mg/ml, respectively. Dose of tamoxifen and mode of injection depended upon the age of the mice.

- 
1. Pregnant females – 100µl tamoxifen is given from a 10mg/ml stock solution for 2 or 3 days (depending on experiment requirement), via subcutaneous or intraperitoneal (IP) route. Total dose: 2 to 3mg.
  2. Pups – 33 or 40µl tamoxifen is given from a 15mg/ml stock solution for 1 or 2 days (depending on experiment requirement) via subcutaneous route. Total dose: 0.5 to 1.2mg.
  3. Adult Mouse – 200µl tamoxifen is given from a 10mg/ml stock solution via IP route for 5 consecutive days. Total dose: 10mg.

### **2.1.3. Dissection of Embryos, Pups and Adult Hearts**

**Embryo Dissection:** The day of vaginal plug was considered as E0.5. The Cre-ERT2 was then activated on specific days by injecting tamoxifen via subcutaneous or IP route. The pregnant females were euthanized either via cervical dislocation or exposure to CO<sub>2</sub>. The embryos were then harvested from the peritoneal cavity of the mice following a standard dissection protocol. Briefly, lower abdominal skin and muscle was lifted using forceps and an incision was made to expose the embryos. Embryos were carefully transferred to a petri dish containing 1xPBS for imaging (Section 2.10.1) and then transfer to 0.2% or 4% PFA for fixation at 4°C O/N on an orbital shaker. In case of E15.5 and E17.5 embryos, embryonic hearts were harvested post fixation and then embedded either in paraffin or OCT (Section 2.2). Prior to fixing, forelimbs of the embryos were also harvested imaged and stored at -20°C for genotyping (Section 2.3.1).

**Pups Dissection:** The day pups were born was considered as P0. To activate Cre-ERT2 tamoxifen was injected via a subcutaneous route on specific days (for specific details of days and dose, refer to chapter 5). Pups were sacrificed by cervical dislocation. Pups' hearts were harvested by making an incision just below the diaphragm, followed by upward cut from within the thoracic cavity. The heart was carefully removed and put in a petri dish containing 0.1M potassium chloride to stop the heart in diastole. Blood was removed from the heart by gently squeezing the heart using wide forceps. Hearts were imaged (Section 2.10.1) and fixed either using 0.2% or 1% PFA at 4°C O/N on an orbital shaker followed by embedding in OCT over dry ice (Section 2.2.2).

**Retinal Dissection:** To harvest pups eyes the protocol described by Tual-Chalot *et al.* (236) was followed. Briefly, skin covering the eyes was removed using scissors. Eyes were then enucleated using forceps & scissors and placed in 24 well plate containing 4% PFA (in 2xPBS) at RT for 10mins. After 10mins, eyes were transferred to a 24 well plate containing cold 2x PBS. To dissect retinas from the eyes they were transferred to a petri dish using a wide bore

---

pipette. With the help of forceps and scissors, excess fat and the optic nerve was removed. Forceps were then carefully inserted between the retina and sclera. Sclera layer was carefully removed with minimal or no damage to the retina. If possible, the choroid layer was also removed at this stage. Next, the lens and hyaloids vessels were removed using forceps followed by 4 to 5 radial incisions to create a ‘petal’ shape (Figure 2.5). Excess PBS and remaining tissue debris were removed using a Pasteur pipette and cold 100% methanol (-20°C) was slowly added to fix and permeabilise the retinas. Retinas were then transferred to a 2ml tube and stored at -20°C in 100% methanol until further use. To genotype pups, tail tips or ears were harvested and stored at -20°C.



**Figure 2.5:** ‘Petal’ shape appearance of freshly dissected neonate retina (image courtesy of Kathleen R. Allinson).

**Adult Mice Dissection:** Adult mice with or without tamoxifen treatment were scarified following one of the three protocols according the experiment specification.

1. Cervical dislocation;
2. CO<sub>2</sub> chamber followed by cervical dislocation to confirm death; or
3. Intracardiac injection of euthatal.

Organs including brain, heart, lungs, liver, kidneys, aorta, mesenteric artery and gut were then harvested in 1xPBS at specific time points according to experimental requirements. Once harvested, heart and lungs were flushed with 1xPBS to remove blood. Images of freshly dissected hearts were taken (Section 1.1.2.10.1) and all the tissues were fixed in PFA (Section 1.1.2.2.2) prior to embedding.

## 2.2. Processing, Fixing and Embedding of Tissue

### 2.2.1. Paraffin Embedding

The method used to embed embryos and embryonic hearts in paraffin is summarised in Table 2.1. Once embedded, paraffin blocks were stored at room temperature until required.

**Table 2.1: Paraffin Embedding Protocol**

	<b>E15.5 (whole embryo)</b>	<b>E17.5 (chest cavity)</b>	<b>E17.5 (hearts)</b>
<b>4% PFA (At 4°C)</b>	2 nights	3 nights	1 nights
<b>Rinse in 1x PBS to remove PFA</b>			
<b>Transfer to 50% EtOH in dH<sub>2</sub>O (shaker)</b>	3 hours	3 hours	30 mins
<b>Transfer to 70% EtOH in dH<sub>2</sub>O (shaker)</b>	3 hours	3 hours	30 mins
<b>Replace 70% EtOH in dH<sub>2</sub>O (Can store like this at RT)</b>	3 hours	3 hours	30 mins
<b>Transfer to 95% EtOH in dH<sub>2</sub>O (shaker)</b>	3 hours	3 hours	30 mins
<b>Transfer to 100% EtOH (shaker)</b>	3 hours	3 hours	30 mins
<b>Replace 100% EtOH (shaker)</b>	Over night	Over night	1 hour
<b>Transfer to HistoClear (shaker)</b>	15 minutes	15 minutes	10 mins
<b>Replace HistoClear (shaker)</b>	15 minutes	15 minutes	10 mins
<b>HistoClear/wax (65°C oven)</b>	1 hour	1 hour	20 mins
<b>Paraffin Wax (65°C oven)</b>	1 hour	1 hour	30 mins
<b>Paraffin Wax (65°C oven)</b>	1 hour	1 hour	30 mins
<b>Paraffin Wax (65°C oven)</b>	1 hour	1 hour	30 mins
<b>Paraffin Wax (65°C oven)</b>	1 hour	1 hour	-

*For solution details, refer to Appendix 3*

### 2.2.2. Embedding for Cryo Sectioning

This method was used to embed embryos, embryonic hearts and adult tissue in OCT for cryo-sectioning are summarised in Table 2.2. E15.5 and E17.5 embryonic hearts were dissected out of chest cavity prior to embedding.

**Table 2.2: OCT Embedding Protocol**

	<b>E11.5 (Whole embryo)</b>	<b>E13.5 (Chest cavity only)</b>	<b>E15.5 &amp; E17.5 (Heart)</b>	<b>Adult Organs</b>
<b>Fix – 0.2% or 1% PFA (4°C with gentle rocking)</b>	1 night	1 night	1 nights	1 night
<b>Wash in 1x PBS to remove PFA</b>				
<b>15% Sucrose in 1xPBS at 4°C</b>	2 to 3 hours (until sunk)			n/a
<b>30% Sucrose in 1xPBS at 4°C</b>	n/a	n/a	n/a	1 night
<b>Embedded in OCT over dry ice for coronal or transverse sectioning and stored at -80°C.</b>				

*For solution details, refer to Appendix 3*

---

## **2.3. Genotyping**

### **2.3.1. Genotyping using Mouse Tissue**

To genotype mice or embryos, DNA was extracted from small tissue samples using alkaline lysis method. First, tissue samples were collected (ear clip for adult mouse, tail tip or ear clip for pups and limb for embryos) and submerged in 50 to 300 $\mu$ l of alkaline DNA extraction lysis buffer 1 (refer to Appendix 1). The samples were then incubated in a thermo-mixer at 95°C, 350 revolutions for 60mins to lyse the cells, vortexed for 15secs and neutralised by the addition of DNA extraction solution 2 (refer to Appendix 1) at a 1:1 ratio with lysis buffer 1. The samples were vortexed and centrifuged at 13,000g for 5mins. The supernatant was transferred to a fresh Eppendorf tube and stored at -20°C until use.

Genotyping was performed on this extracted DNA by PCR, using primers and PCR reaction conditions described in Table 2.3 and Table 2.4 using Bio Rad Tetrad Thermal Cycler. A minimum of 150 ng/ $\mu$ l of DNA was used as a template. The PCR products were separated on a 2% agarose gel containing 0.01% of ethidium bromide in 1x TAE buffer at 140 volts for 45mins. The DNA bands were observed in a UVP benchtop UV trans-illuminator.

*For DNA extraction lysis buffer and solution details, refer to Appendix 1.*

**Table 2.3: PCR Reaction**

Step		Reaction 1	Reaction 2	Reaction 3
1	Initialisation	5mins at 95°C	5mins at 95°C	2mins at 95°C
2	Denaturation	30secs at 95°C	30secs at 95°C	30secs at 95°C
3	Annealing	30secs at 62°C	30secs at 58°C	30secs at 60.0°C
4	Elongation	90secs at 72°C	90secs at 72°C	90secs at 72°C
5	Final Extension	5mins 72°C	5mins 72°C	5mins 72°C
6	Storage	15°C forever	15°C forever	15°C forever
7	No. of Cycles (2 to 4)	x35	x35	x35

**Table 2.4: PCR Conditions and Primer sequences (for PCR reaction temperature, refer to table 2.4)**

PCR	Primer	Sequence (5' – 3')	PCR Condition					Product Size
			Primer	Sterile dH <sub>2</sub> O	GoTaq Master Mix	DNA Volume	PCR Reaction	
Cre PCR	Cre Forward	GAACCTGATGGACATGTTTCAGG	0.10µl	3.60µl	5.00µl	1µl	Reaction 1	Cre = 320bp
	Cre Reverse	AGTGCGTTTCGAACGCTAGAGCCTGT	0.10µl					
	Myo Forward	TTACGTCCATCGTGGACAGC	0.10µl					
	Myo Reverse	TGGGCTGGGTGTTAGCCTTA	0.10 µl					
Eng PCR	Forward F6	GACGCCATTCTCATCCTGC	0.10µl	3.80µl	5.00µl	1µl	Reaction 2	Eng <sup>fl</sup> = 500bp
	Reverse R7	CCACGCCTTTGTCCTTGC	0.10µl					Eng <sup>+</sup> (WT) = 420bp
Eng iKO PCR	Forward F4	GGTCAGCCAGTCTAGCCAAG	0.10µl	3.60µl	5.00µl	1µl	Reaction 2	Eng <sup>-</sup> (iKO) = 602bp
	Reverse R7	CCACGCCTTTGTCCTTGC	0.10µl					
	Myo Forward	TTACGTCCATCGTGGACAGC	0.10µl					
	Myo Reverse	TGGGCTGGGTGTTAGCCTTA	0.10µl					
RFP PCR	RFP Forward	CCCATGGTCTTCTTCTGCAT	0.10µl	3.80µl	5.00µl	1µl	Reaction 2	RFP = 220bp
	RFP Reverse	AAGGTGTACGTGAAGCACCC	0.10µl					
Rosa PCR (multiplex)	R26 - WT	GCGAAGAGTTTGTCTCAACC	0.20µl	3.10µl	5.00µl	1µl	Reaction 2	R26 <sup>eYFP</sup> = 310bp
	R26 - Trans	GGAGCGGGAGAAATGGATATG	0.50µl					
	R26 - Gtrgeo	AAAGTCGCTCTGAGTTGTTAT	0.20µl					R26 <sup>+</sup> (WT) = 600bp

Rosa WT PCR	R26 - WT	GCGAAGAGTTTGCCTCAACC	0.10 $\mu$ l	3.60 $\mu$ l	5.00 $\mu$ l	1 $\mu$ l	Reaction 2	R26 <sup>+</sup> (WT) = 600bp
	R26 - Gtrgeo	AAAGTCGCTCTGAGTTGTTAT	0.10 $\mu$ l					Myo = 250bp
	Myo Forward	TTACGTCCATCGTGGACAGC	0.10 $\mu$ l					
	Myo Reverse	TGGGCTGGGTGTTAGCCTTA	0.10 $\mu$ l					
SRY PCR	SRY Forward	GACTAGACATGTCTTAACATCTGTCC	0.10 $\mu$ l	3.60 $\mu$ l	5.00 $\mu$ l	1 $\mu$ l	Reaction 1	SRY = 183bp
	SRY Reverse	CCTATTGCATGGACAGCAGCTTATG	0.10 $\mu$ l					Myo = 250bp
	Myo Forward	TTACGTCCATCGTGGACAGC	0.10 $\mu$ l					
	Myo Reverse	TGGGCTGGGTGTTAGCCTTA	0.10 $\mu$ l					
Tgfbr2 PCR	P3b – Forward	GAGAGTATTCCGGCTTGCAG	0.10 $\mu$ l	3.80 $\mu$ l	5.00 $\mu$ l	1 $\mu$ l	Reaction 2	Tgfbr2 <sup>fl</sup> (Trans) = 360bp
	P4b – Reverse	TGCTGATTTTGTGTTTGGAAAGG	0.10 $\mu$ l					Tgfbr2 <sup>+</sup> (WT) = 213bp
Tgfbr2 iKO PCR	P3b – Forward	GAGAGTATTCCGGCTTGCAG	0.20 $\mu$ l	3.60 $\mu$ l (DNA Conc. dependent)	10.00 $\mu$ l	150 to 200 ng/ $\mu$ l	Reaction 3	Tbr2 iKO = 450bp
	P5b – Reverse	AATGGAAGGGGAGTGAGGAC	0.20 $\mu$ l					Myo = 250bp
	Myo Forward	TTACGTCCATCGTGGACAGC	0.20 $\mu$ l					
	Myo Reverse	TGGGCTGGGTGTTAGCCTTA	0.20 $\mu$ l					

---

### **2.3.2. Genotyping using Mouse Tissue Section**

To extract DNA from OCT embedded tissue sections to confirm the knock down of Tgfbr2 expression (chapter 4), slides were removed from -80°C storage, left at room temperature for 60mins to dry followed by two 10min washes in sterile 1xPBS (pH 7.4) at RT to remove any traces of OCT. Slides were then dried and 50µl of DNA extraction lysis buffer 1 was added to the slides and the sections were scraped from the slides using a sterile scalpel. DNA extraction lysis buffer 1 containing tissue scrapes was collected in a 1.5ml Eppendorf tube. A minimum of two slides with around 10 to 12 sections each slide was used per sample. Once the samples were collected, tubes were placed in a thermo-mixer at 95°C, 350 revolutions for 30mins. Samples were then vortexed and briefly centrifuged at 13,000g to avoid cross-contamination. DNA extraction solution 2 was added to neutralise the solution (1:1 ratio to solution 1). Samples were vortexed then centrifuged at 13,000g for 5mins at RT. Approximately 3 quarters of the supernatant was transferred to a labelled fresh tube. Nucleic acid concentration was checked using a Nanodrop ND-1000 spectrophotometer (Thermo Scientific) to confirm successful DNA extraction. Around 150 to 200 ng/µl of DNA was used to perform Tgfbr2iKO and Cre PCR using conditions described in Table 2.3 and Table 2.4

*For DNA extraction lysis buffer and solution details, refer to Appendix 1.*

## **2.4. Sectioning**

### **2.4.1. Paraffin Wax Sectioning**

Embryos were sectioned in transverse/ coronal orientation into sister/ serial sections according to the need of the experiment. One day prior to sectioning, paraffin blocks containing embryos were cooled overnight at 4°C and kept on ice until use. 8µm thick sectioned were cut at 5° angle on a Leica RM2235 rotary microtome. The sections were hydrated on Histobond Twinfrosted adhesion slides using Millipore filtered H<sub>2</sub>O on a 37°C hot plate. Once hydrated, excess water was removed and slides were baked overnight in an oven at 37°C. All slides were stored in slide boxes at room temperature until further use.

### **2.4.2. OCT Cryo-Sectioning**

Cutting blade and tissue samples were cooled in a cryostat for 30mins prior to sectioning. 10µm thick sections were cut at 10° angle on Microm HM 560 CryoStart (Thermo Scientific) and at 5° angle on Leica CM1860 cryostat. Serial or sister sections in transverse or coronal orientation

---

were cut according to the experimental requirement. All the slides were left for at least 30mins at room temperature before storage at -80°C.

## **2.5. Staining**

### **2.5.1. Haematoxylin and Eosin (H&E) Staining**

To study the histology of embryonic hearts slides were stained with haematoxylin and eosin. Paraffin embedded tissue sections were first incubated in a 60°C oven for 1hr for dewaxing and increased fixing of tissue slides. The slides were then washed in histoclear twice at RT for 10mins each to remove wax followed by washing in 100% ethanol to remove histoclear (twice - 5mins each). Slides were next re-hydrated through a descending ethanol series (90%, 70% and 50% - 5mins each) and equilibrated in autoclaved Millipore filtered H<sub>2</sub>O. Once hydrated, slides were stained with haematoxylin (nuclear stain) for 2 to 10mins followed by a brief wash in acid-alcohol (appendix 1) solution (2 to 5dips). Slides were then washed under running tap water for 2 to 5mins (until sections turned dark blue). Next, sections were stained with 1% eosin to stain cytoplasm and blood cells for 2 to 5mins followed by washing in tap water by dipping (2 to 5 dips times three). Once stained, the slides were dehydrated using ascending ethanol series (50%, 70%, 95% and 100% - 5mins each) followed by histoclear for 10 minutes. These slides were then mounted with histomount and then kept in a fume hood overnight to set.

OCT embedded tissue sections were taken out of -80°C freezer and left in the slide mailer at RT for 30mins to avoid condensation. Next, slides were air dried for 30mins at RT to make sure the tissue was affixed on to slides. Sections were then fixed with 4% PFA for 10mins at RT followed by three washes in 1xPBS (5mins each). Slides were then stained with haematoxylin and eosin using the protocol described above.

*For solution and reagent details, refer to Appendix 1.*

### **2.5.2. Immunohistochemistry (IHC) using DAB**

Selected paraffin embedded tissue section slides were dewaxed and hydrated as described in section 2.5.1. Once hydrated, sections were equilibrated in 1x PBS and then subjected to antigen retrieval using 0.1M citrate buffer (pH 6) in the microwave set at high power for 15mins. The slides were first cooled at bench for 15mins, followed by 15mins under running tap water and then incubation with cold 3% hydrogen peroxide solution (appendix 1) for 10mins to inhibit endogenous peroxidase activity. Next, slides were rinsed in 18.2mq filtered H<sub>2</sub>O and were

washed in TBS-Tx (3 times – 7mins each). Slides were then subjected to antigen blocking buffer (10% FCS in TBS-Tx) for 2hrs at RT. Primary antibody (Table 2.5) appropriately diluted in blocking solution was added to sections; and blocking solution was added to negative control sections. The slides were next incubated in a levelled humidified chamber at 4°C overnight.

**Table 2.5: Primary Antibody Details for IHC-DAB Staining**

Cell Type	Antibody	Raised In	Type	Company	Cat. No.	Dilution
<b>GFP</b>	Anti-GFP	Rabbit	Polyclonal	Amsbio	TP401	1 in 200
<b>Smooth Muscle Cells</b>	Anti- $\alpha$ SMA	Mouse	Clone 1A4	Sigma-Aldrich	A5228	1 in 100

Next day, primary antibody was carefully drained, and the slides were washed three times in TBS-Tx for 7mins at RT (1st wash of negative controls were performed separately to avoid exposure to antibody). Once washes were complete, biotinylated secondary antibody (Table 2.6) was diluted in blocking solution and added to slides. Slides were then incubated in a levelled humidified chamber at RT for 2hrs.

**Table 2.6: Secondary Antibody Details for IHC-DAB Staining**

Antibody	Raised In	Company	Cat. No.	Dilution
<b>Biotinylated Anti-Rabbit IgG Antibody</b>	Goat	Vector Lab	BA-1000	1 in 300
<b>Biotinylated Anti-Mouse IgG Antibody</b>	Goat	Vector Lab	BA-9200	1 in 300

AB Complex (standard) was made 30mins prior to use according to manufacturer's instructions (appendix 3). Secondary antibody was carefully drained off the slides and the slides were again washed 3 times in TBS-Tx as above. The slides were then incubated with AB Complex in a levelled humidified chamber for 30mins at RT. AB complex was carefully drained off the slides and the slides were again washed 3 times in TBS-Tx as above. Liquid DAB was prepared (Appendix 1) and added over the sections. The sections were incubated with DAB for up to 20mins or until brown staining was observed. The DAB reaction was stopped by placing slides in 1x PBS. Slides were then counterstained in Mayer's Haematoxylin for 2mins and washed under running tap water for 5mins. Slides were dehydrated through an ascending ethanol series (50%, 70%, and 95% for 5mins each) and washed in 100% ethanol (twice for 5mins each). The slides were then washed in histoclear (twice for 10mins each), mounted using histomount and glass cover slides and left in fume cabinet overnight to set.

***For solution and reagent details – refer to Appendix 3.***

---

### 2.5.3. Immunofluorescence on paraffin embedded sections

Slides were dewaxed and hydrated using the protocol described in section 2.5.1. Hydrated sections were subjected to antigen retrieval using 0.1M citrate buffer (pH 6.3-4) in a pressure cooker. Approximately, 600ml of citrate buffer was warmed in a pressure cooker and a metal rack containing slides were completely submerged in the buffer with a set valve pressure of 80kPa. Samples were allowed to steam for 5mins prior to cooling under cold running tap water. Slides were left to cool for a further 20mins at RT. Next, slides were rinsed in sterile 18.2mq filtered H<sub>2</sub>O followed by three washes in 1xPBS (5mins each). Slides were then incubated in a blocking solution containing 10% FCS in TBS-Tx for 1hr at RT. Primary antibody, rabbit anti-Sm22 $\alpha$  (Abcam, cat. No. ab14106) was diluted (1 $\mu$ g/100 $\mu$ l) in blocking solution and then added to sections. Blocking solution was added to negative controls. The slides were then incubated in a humidified chamber at 4°C overnight on a level bench.

Next day, primary antibody was removed by rinsing the slides briefly in 1xPBS followed by 3 washes in 1xPBS (5mins each). Slides were next incubated with secondary antibody and Isolectin GS-IB4 appropriately diluted in blocking solution (Table 2.7) in a light protected humidified chamber for 3hrs at RT. Sections were then rinsed and washed as described above followed by mounting using Prolong Gold antifade reagent with DAPI and overnight incubation at 4°C to allow to set .

*For solution and reagent details – refer to Appendix 3.*

**Table 2.7: Secondary Antibody and Isolectin Details**

Antibody	Raised in	Company	Cat. No.	Dilution
Anti-Rabbit Alexa Fluor 488 Conjugated (H+L) Cross-Adsorbed	Goat	Life Technology	A-11008	1 in 200
Isolectin GS-IB4 from Griffonia simplicifolia, Alexa Fluor™ 594 Conjugate	n/a	Life Technology	I-21413	1 in 50

### 2.5.4. Immunofluorescence on OCT embedded sections

Slides were removed from -80°C freezer, kept at RT for 30mins within slide mailers to reduce condensation, and then air dried on a slide rack for a further 30 mins. Whilst drying, sections were traced around with a hydrophobic barrier pen. Depending upon the type of antibody used, sections were subjected to post-fixing using 4% PFA on slide (as summarised in (Table 2.8), followed by washing in 1xPBS 3 times (5mins each) at RT (only 1 wash required if tissue not post-fixed). The slides were then incubated with blocking solution containing 5% secondary antibody specific serum (donkey or goat serum), 1% BSA and 0.5% Tween 20 in 1xPBS for

---

2hrs in a humidified chamber at RT. Excess blocking solution was removed by gentle tapping and primary antibody appropriately diluted (Table 2.8) in blocking solution was added to slides and incubated on a level bench, overnight at 4°C.

Next day the primary antibody was carefully removed, and slides were rinsed briefly in 1xPBS followed by three washes in 1xPBS (5mins each). For some antibodies (please refer to Table 2.8), slides were washes in PBST (1xPBS + 0.25% Triton-X 100) solution for 5mins at RT to reduce non-specific staining. Slides were next incubated in a light protected humidified chamber with an appropriately diluted secondary antibody (Table 2.9) for 2hrs at RT or overnight at 4°C. The slides were then washed as mentioned above with minimal light exposure and mounted using Prolong Gold antifade reagent with DAPI.

***For solution details – Appendix 3.***

**Table 2.8: Primary Antibody Details for Immunofluorescence**

Cell Type	Antibody	Raised In	Type	Company	Cat. No.	Post-Fix on Slides	Dilution	Washes
Cardiomyocytes	Anti-Alpha Actin	Mouse	Clone EA-53	Sigma	A7732	4% PFA - 5mins at RT	1 in 200	PBS and PBST washes
	Anti-MF20	Mouse	Clone MF20	DSHB	MF 20	4% PFA - 5mins at RT	1 in 200	PBS and PBST washes
ECs	Anti-CD31 (15.625 µg/ml)	Rat	Clone MEC13.3	BD Pharmingen	550274	With and without 4% PFA for 5mins at RT	1 in 100	With or without PBS and PBST washes
	Anti-Podocalyxin (0.2 mg/ml)	Goat	Polyclonal	R&D Systems	AF1556	No post-fix	1 in 100	PBS and PBST washes
ECs & Mesenchymal Cells	Anti-Endoglin	Rat	Clone MJ7/18	eBioscience	14-1051-85	With and without 4% PFA for 5mins at RT	1 in 100	With or without PBS and PBST washes
	Anti-Endoglin (0.2 mg/mL)	Goat	Polyclonal	R & D	AF1320	With and without 4% PFA for 5mins at RT	1 in 25	With or without PBS and PBST washes
Fibroblasts	Anti-Vimentin	Chicken	Polyclonal	Abcam	ab24525	4% PFA - 5mins at RT	1 in 300	PBS and PBST washes
GFP	Anti-GFP	Chicken	Polyclonal	Abcam	ab13970	4% PFA - 5mins at RT	1 in 400 (embryo)	PBS and PBST washes
						4% PFA - 5mins at RT	1 in 100 (adult)	PBS and PBST washes
	Anti-GFP 647 Conjugated	Rabbit	Polyclonal	Life Technologies	A-31852	4% PFA - 5mins at RT	1 in 100	PBS and PBST washes
Smooth Muscle Cells	Alpha SMA Cy3	Mouse	Clone 1A4	Sigma Aldrich	C6198	No post-fix	1 in 100	PBS and PBST washes
	Anti-Sm22a	Rabbit	Polyclonal	Abcam	ab14106	4% PFA - 5mins at RT	1 µg	PBS and PBST washes
Venous EC & capillaries	Anti-Endomucin	Rat	Clone V.5C7	Santa Cruz Biotechnology	sc-53941	With and without 4% PFA for 5mins at RT	1 in 100	With or without PBS and PBST washes

**Table 2.9: Secondary Antibodies Details for Immunofluorescence**

Cell Type	Antibody	Raised In	Company	Cat. No.	Dilution
<b>Anti-Chicken</b>	Alexa Fluor 488 Conjugated (H+L)	Goat	Life Technologies	A-11039	1 in 200
	Alexa Fluor 568 Conjugated (H+L)	Goat	Life Technologies	A-11041	1 in 200
	Alexa Fluor 647 Conjugated (H+L)	Goat	Life Technologies	A-21449	1 in 200
<b>Anti-Goat</b>	Alexa Fluor 647 Conjugated (H+L) Cross-Adsorbed	Donkey	Life Technologies	A-21447	1 in 200
<b>Anti-Mouse</b>	Alexa Fluor 488 Conjugated (H+L) Highly Cross-Adsorbed	Goat	Life Technologies	A-11029	1 in 200
<b>Anti-Rabbit</b>	Alexa Fluor 488 Conjugated (H+L) Cross-Adsorbed	Goat	Life Technologies	A-11008	1 in 200
	Alexa Fluor 568 Conjugated (H+L) Cross-Adsorbed	Goat	Life Technologies	A-11011	1 in 200
	Alexa Fluor 568 Conjugated (H+L) Highly Cross-Adsorbed	Donkey	Life Technologies	A-10042	1 in 200
<b>Anti-Rat</b>	Alexa Fluor 488 Conjugated (H+L) Cross-Adsorbed	Goat	Life Technologies	A-11006	1 in 200
	Alexa Fluor 488 Conjugated (H+L) Highly Cross-Adsorbed	Donkey	Life Technologies	A-21208	1 in 200
	Alexa Fluor 568 Conjugated (H+L) Cross-Adsorbed	Goat	Life Technologies	A-11077	1 in 200
	Alexa Fluor 647 Conjugated (H+L) Cross-Adsorbed	Goat	Life Technologies	A-21247	1 in 200

### 2.5.5. Immunofluorescence on Whole-mount Retinas

Retinas were carefully transferred from the 2ml tube into a 24-well plate containing 2xPBS and washed for 10mins at RT with gentle agitation. Once washed, PBS was replaced with blocking solution containing 0.3% Triton X-100, 0.5% Tween-20, 1% BSA and 5% normal goat serum. Retinas are blocked in the blocking solution for 4hrs at RT with gentle agitation. Next, primary antibody appropriately diluted (Table 2.10) in blocking solution was added and retinas were left overnight in a cold-room at 4°C with gentle agitation.

Next day, retinas were washed 5 times in a PBSTTx solution at RT with gentle agitation (10mins each). Retinas were next incubated over-night with appropriately diluted secondary antibody and Isolectin (Table 2.10) in cold-room at 4°C with gentle agitation. Third day, retinas were washed again with 5 changes of PBSTTx as above. Once washed, retinas were transferred on to a slide with the help of a wide Pasteur pipette, excess wash solution was carefully drained, and retinas were mounted using 30 to 50µl of Prolong gold antifade reagent per retina.

*For solution details – refer to Appendix 3.*

**Table 2.10: Antibodies details for Whole-mount Immunofluorescence**

Cell Type	Antibody	Raised In	Type	Company	Cat. No.	Dilution
<b>Primary Antibodies</b>						
<b>ECs &amp; Mesenchymal Cells</b>	Anti-Endoglin	Rat	Clone MJ7/18	eBioscience	14-1051-85	1 in 100
<b>GFP</b>	Anti-GFP	Chicken	Polyclonal	Abcam	ab13970	1 in 300
<b>Smooth Muscle Cells</b>	Alpha SMA Cy3	Mouse	Clone 1A4	Sigma Aldrich	C6198-.2ML	1 in 100
<b>Secondary Antibodies and Lectin Details</b>						
<b>Endothelial Cells</b>	Isolectin GS-IB4 from Griffonia simplicifolia, Alexa Fluor 488 Conjugated	n/a	n/a	Life Technologies	I21411	1 in 50
<b>Anti-Rat</b>	Alexa Fluor 568 Conjugated (H+L) Cross-Adsorbed	Goat	Polyclonal	Life Technologies	A-11077	1 in 200
<b>Anti-Chicken</b>	Alexa Fluor 488 Conjugated (H+L)	Goat	Polyclonal	Life Technologies	A-11039	1 in 200

## 2.6. Intra-Ocular BMP9 Injection

BMP9 was injected into the left eye of the pups via intraocular (IO) route while PBS was injected into the right eye. IO injections were performed by Dr Rachael Redgrave on neonatal mice (day P4 or P5). During the procedure, mice were deeply anaesthetised with 4% isoflurane and were injected with 0.3µl of 1.5mg/ml BMP9 using a Hamilton syringe (27G needle). Once recovered from the anaesthesia, pups were returned to their mothers. Only the pups with successful injections were kept and others were euthanized by cervical dislocation.

## 2.7. Injection of Microbeads

Microbeads were injected into the circulation and to allow mapping of the vasculature as well as to identify the presence of any vascular abnormalities.

### 2.7.1. 15µm<sup>3</sup> Red Fluorescence Microbeads Perfusion

15µm<sup>3</sup> diameter red fluorescence microbeads (ThermoFisher, F21013) are normally trapped in the capillaries and were used to identify the presence of abnormal vessels. Microbeads were injected into the tail vein by Dr. Simon Tual-Chalot. To inject the beads into the tail vein injection, mice were terminally anesthetised using isoflurane and a catheter was placed in the tail vein using a 30G ½” needle. To confirm the catheter was correctly placed, saline was injected, and a small amount of blood was drawn. Once confirmed, 200µl of microbeads were slowly injected using a 1ml syringe with 30G ½” needle. Mice were scarified 1-minute post

---

injection by intra-cardiac injection of euthatal. Organs including brain, lungs, liver and kidneys were harvested in 1xPBS.

### 2.7.2. 45 $\mu\text{m}^3$ Green Fluorescence Microbeads Perfusion

To detect the presence of any abnormal vessels in brain, liver and kidneys, 45 $\mu\text{m}^3$  diameter green fluorescence microbeads (Polysciences, Inc., 18242-2) were injected into the LV of the mice by Dr. Simon Tual-Chalot. Mice were weighed then anesthetised using isoflurane. The heart was surgically exposed and 50 to 400 $\mu\text{l}$  of green microbeads were injected into the LV using a 1ml syringe with a 25G  $5/8$ " needle. During the procedure, heart rate was monitored, and mice were sacrificed 1-minute post injection by intra-cardiac injection of euthatal and organs were harvested in 1xPBS for imaging.

### 2.7.3. 15 $\mu\text{m}^3$ and 45 $\mu\text{m}^3$ beads perfused Organs: Tissue Mounting

During this experiment, to avoid any accidentally beads in-take after organ harvest, each organ was stored in separate vial in 1xPBS and prepared in separate petri-dishes for imaging. To capture the images the whole of organs, each organ was placed flat between two slides and secured between two slides using masking tape (Figure 2.6A). To image lung slices, the left lung lobe was frozen at -20°C for 45-60mins then sliced using mouse heart tissue slicer (Zivic Instruments, cat. no. HSMS005-1) into 1mm thick sections. The sliced lung tissue was next placed on slides in a chronological order, secured with coverslip and imaged (Figure 2.6B).

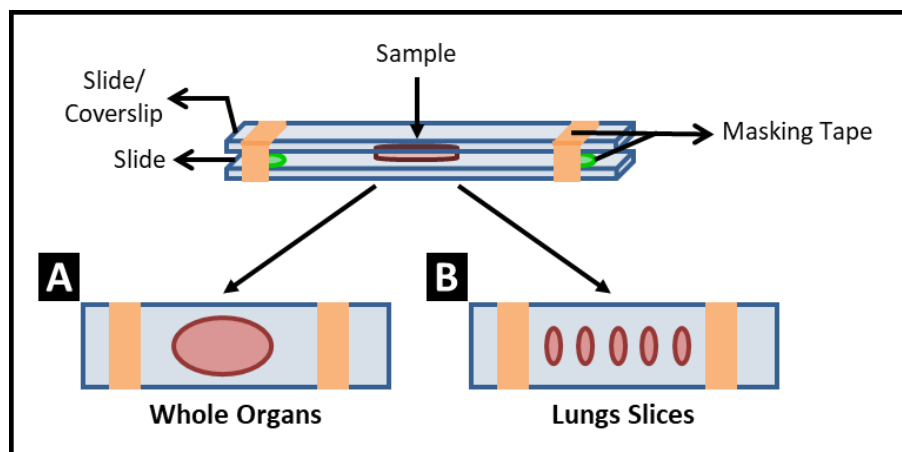


**Figure 2.6:** Cartoon of a sample preparation for imaging whole organs and lung slices using M2 axio-imager microscope. **(A)** To image whole organs (big red circles), organ was placed in the middle of a slide and a second slide was used to secured it in place with the help of some masking tape (orange). To be certain, the organ does not get crushed between slides, second slide was raised slightly using rolled up masking tape (green). **(B)** Sliced lungs were placed flat in a chronological order on a slide and secured in place with coverslip using masking tape.

---

## 2.8. CDC Culture

**Heart Dissection:** 3 to 6-weeks old *Eng<sup>fl/fl</sup>*; *Rosa<sup>CreERT2/CreERT2</sup>*; *CAG<sup>GFP/GFP</sup>* mice were culled via cervical dislocation and their hearts dissected using sterile instruments. Tissue was stored in ice cold culture media prior to processing in a tissue culture hood.

**Explant culture:** Dissected hearts were washed in sterile PBS (pH 7.2) 3 times to remove any traces of blood/ connective tissue/ media. The tissue was then minced into small 1-2mm<sup>3</sup> fragments in the presence of 1ml of pre-warmed (37°C) 0.05% Trypsin/EDTA for 5mins. Trypsinisation was stopped by adding 4ml of pre-warmed (37°C) culture media containing 20% foetal bovine serum (complete explant media, CEM). Tissue fragments were placed on fibronectin coated 60mm petri-dishes and cultured as explants in 2ml CEM in an incubator at 37°C with 5% CO<sub>2</sub>. Every 3 to 4 days, 1ml of fresh CEM was added to the culture dishes. Explant culture was carried for approximately 2 weeks and within this time a confluent layer of mesenchymal-like cells grew.

**Cardiosphere Culture:** These explant derived cells (EDCs) were harvested as follows; CEM was removed and dishes were rinsed with sterile PBS, this was followed by incubation with 1ml of versene for 3mins to enhance trypsin activity at 37°C. Next, dishes were incubated with 1.5ml of 0.05% Trypsin/EDTA for 5mins at 37°C and cells were removed by repeated trituration using 1ml pipette. To deactivate trypsin, 1ml of serum containing CEM was added to the plates and trituration was continued if needed. EDCs in suspension were transferred to falcon tube and centrifuged for 8mins at 800g. The supernatant was carefully discarded, and the cell/ explant pellet was re-suspended in 5ml of CEM and passed through a 70µM filter to remove explants/ debris. A 20µl sample of cell suspension was used to count the cells using a haemocytometer, while the filtered cell suspension was centrifuged again at 800g for 8mins. The supernatant was discarded, and cells were re-suspended in a specific, growth-factor enriched cardiosphere growth media (CGM) at a cell density of 5-7.5x10<sup>5</sup> cells per ml. 400µl of cell suspension was seeded per well of a poly-D-lysine coated 24 well plate and incubated at 37°C incubator with 5% CO<sub>2</sub>. Following 4 days of culture an additional 200µl CGM was added to each well and on day 6-8, cardiospheres were harvested.

**Cardiosphere Harvesting:** To remove cardiospheres, 0.5-1ml of PBS was added per well followed by gentle trituration to remove loosely adherent cardiospheres, which were transferred to a 50ml falcon tube. Cardiospheres were then allowed to settle at the bottom of the tube, the supernatant was carefully discarded. Cardiospheres were re-suspended in CEM prior to being

---

plated onto fibronectin coated tissue culture flasks and incubated in 5% CO<sub>2</sub> incubator at 37°C with growth media changes every 2 to 3 days.

**CDCs Passaging:** Old growth media was discarded, and flasks rinsed briefly with pre-warmed sterile PBS. The flask was then incubated with accutase (10ml per T75 flask) for 5 to 10mins at RT. Cells detachment was visually checked under inverted microscope. The subsequent cell suspension was transferred to a 50ml falcon tube and centrifuged at 800g for 8mins. The supernatant was carefully discarded, and the cell pellet was re-suspended in 1ml CEM using a P200 pipette to break up any cell clumps. A 20µl sample from this solution was used to calculate cell density using a haemocytometer. Approximately 5x10<sup>5</sup> cells per 15ml of CEM were seeded per T75 flask and kept in 37°C/ 5% CO<sub>2</sub> incubator. Media was changed every 3 to 4 days and cells were passaged at 80-90% confluency.

**Endoglin knockdown:** To knockdown endoglin in CDCs, cells were incubated with culture media containing 3µM 4-hydroxy tamoxifen (4-OH) for 96hrs. An additional 4 days of standard culture was additionally required to allow for turn-over of existing endoglin protein.

**CDC Injections for Post-MI injections:** Media was removed from the control and Eng-iKO T75 flasks (passage 2) and the flasks were briefly washed with 10ml PBS to remove any media traces. Flasks were then incubated with accutase (10ml per T75 flask) for 5 to 10mins at RT to detach cells. Flasks were gently knocked and triturated to encourage cell detachment (checked under microscope to confirm). The cell suspension was then collected in a 50ml falcon tube and flasks were rinsed with 10ml of CEM (also collected). The cell-suspension was then centrifuged for 10mins at 800g (repeated if necessary). Supernatant was carefully removed, and cell pellet was then re-suspended in 50 to 100µl of PBS (depending upon the pellet size). A 10µl sample was diluted in PBS and used for cell counting using the haemocytometer. The cell suspension was then re-suspended in more PBS to attain a cell concentration of 5x10<sup>5</sup> cells per 10µL. This cell suspension was then transferred to a screw cap vial and to deliver to FGU surgery suite on ice for intra-myocardial injections (5µL injections at two sites).

*For media details – refer to Appendix 4.*

## **2.9. MI Surgery and Intra-Myocardial Injection**

Myocardial surgeries were performed by Dr. Rachael Redgrave. Briefly, approximately 12-14 weeks old C57Bl/6 male mice were pre-medicated with analgesic (fentanyl/fluanisone, 0.4ml/kg) and anesthetized using isoflurane. Mice then underwent left-side thoracotomy and an

---

acute MI was achieved by permanent ligation of the LAD (left anterior descending) coronary artery using 7-0 prolene suture. Once confirmation of the MI was established by visible blanching of the myocardium (Figure 2.7); two intra-myocardial injection of PBS, control CDC or Eng-iKO CDCs ( $5 \times 10^5$  cells/ $10 \mu\text{l}$ ) at the infarct border (237). Following injection, the mouse chest was closed, and animals were allowed to recover in a warm oxygenated recovery chamber. Sham mice underwent the same thoracotomy but there was no ligation of the coronary vessel. At 4 weeks post-surgery, mice were euthanized by cervical dislocation, hearts were harvested, and atria were removed prior to embedding.

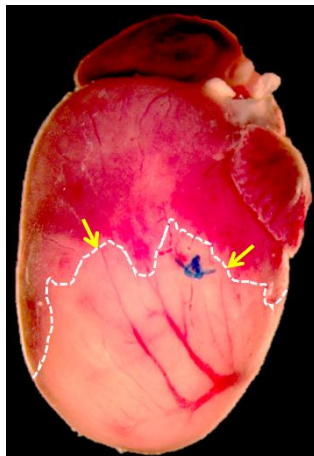


**Figure 2.7:** Image of an adult mouse heart after a MI surgery (image courtesy Dr. Rachael Redgrave). MI was induced by ligating the LAD and confirmation of MI was established blanching of the myocardium (under the white dotted line). Yellow arrows show the site of intra-myocardial injections.

## 2.10. Microscopy

### 2.10.1. Organs/ Embryo Imaging

To image whole embryos/ organs a stereo dissecting microscope (Stemi SV 6 (Carl Zeiss) or MZ6 (Leica) was used. Once dissected, embryos/ organs were placed in a petri-dish containing 1xPBS and oriented to the desired position using forceps. For adult and neonatal heart imaging, an external measurement scale was used to determine heart size. To image fluorescent beads injected whole organs, tiled images were taken using Axioimager M2 (Carl Zeiss) microscope.

### 2.10.2. Imaging Retinas

To image whole mTmG retinas a Stemi SV 11 Apo stereo (Carl Zeiss) or Axioimager M2 (Carl Zeiss) microscope was used. Dissected retinas (section 2.1.3) were kept in 2xPBS and were not exposed to methanol to avoid interference with the fluorescent protein signal. During imaging, most of the PBS was removed to flatten the retina inside the well (12-well plate for SV 11 Apo stemi microscope) or on a slide (for Axioimager M2). To image retinas on SV 11 Apo stemi

microscope, flattened retinas were first focused using white light and were then exposed to UV light with red fluorescent protein (RFP) and GFP filter sets and visualised using Axioimager software. Individual channel images were taken at selected exposure times and these images were then overlaid using Adobe Photoshop software. To image retinas using Axioimager M2, a tiled image (9 to 12 tiles) was taken using Carl Zeiss filter set 10 and filter set 31 (Table 2.11) at x5 magnification. Once imaged, retinas were stored in 100% methanol (see section 2.1.3).

### 2.10.3. Bright-field and Fluorescence Microscopy

To image stained slides (bright-field and fluorescence), Carl Zeiss Axioimager M2 microscope equipped with low and high-power objectives (x5, x10, x20, x40 and x63) was used. Fluorescence imaging was done using the filter sets mentioned in Table 2.11. During fluorescence imaging apotome was used along with focus off-set strategy for individual channels. To capture digital images, microscope was connected to image processor computer installed with Zen Pro software. To take bright-field images, 1.4megapixel AxioCam ICc1 R4 colour camera was used and for fluorescence images 1.4megapixel AxioCam MRm Rev.3 monochrome camera was used.

**Table 2.11: Carl Zeiss Axioimager M2 Filter Set Details.**

Microscope Filter Sets			Fluorophore Used in Experiments		
Detail	Excitation wavelength (nm)	Emission wavelength (nm)	Detail	Max. Excitation wavelength (nm)	Max. Emission wavelength (nm)
<b>Filter Set 49</b>	300 to 380	420 to 470	DAPI	359	461
<b>Filter Set 10</b>	450 to 495	510 to 560	FITC	495	519
			Alexa 488	495	519
<b>Filter Set 31</b>	550 to 585	595 to 650	Cy3	548	561
			Alexa 568	578	603
			Alexa 594	590	617
<b>Filter Set 50</b>	620 to 660	665 to 720	Alexa 647	650	665

To confirm there was no bleed through between different filter sets (Table 2.11), OCT embedded sections were stained with rat anti-CD105 primary antibody. To visualise, goat anti-rat secondary antibody conjugated with either Alexa 488, Alexa 568 or Alexa 647 fluorophore (Figure 2.8) was used. Once stained, exposure for each filter set was set using a positive section (Figure 2.8 A, E and I) and then each section was imaged using all four filter sets mentioned in the Table 2.11.

---

#### **2.10.4. Imaging and Analysis**

To analyse the whole section or whole organ, tiled image was created using Carl Zeiss Axioimager M2 microscope and Zen Pro software. Z-stack imaging allows analysis of expression of markers across all three axes (X-Y, X-Z and Y-Z) of a section. To take Z-stacks, Carl Zeiss Axioimager M2 microscope with Zen Pro/ Zen 2012 software was used. Z-stack imaging is used to confirm the expression of endoglin in EPDCs (Chapter 4) and confirm the presence of AVMs P11 retinas (Chapter 5).

During this project, data was generated by manual counting, intensity analysis; area and length measurements. To perform manual counting, 'Event' function of Zen Pro software was used. To perform line and area intensity analysis using Zen Pro software 'Draw Spline Contour' function was used. To measure length and area Zen Pro function, 'Line' and 'Draw Rectangle' was used. To perform intensity analysis using ImageJ software 'Limit to Threshold' function. To measure area using ImageJ software 'Perimeter' function was used. Prior to analysing any fluorescently stained images, same white and balance was set for all images.

#### **2.11. Statistical Analysis**

Unless otherwise stated all the experiments used at least three biological replicates. To perform statistical analyses GraphPad Prism software was used. To compare two independent groups, unpaired students t-test was used. In case where a single parameter was compared between multiple groups, one-way ANOVA with a Bonferroni post hoc test was performed to check for significance. To compare two parameters within a group, two-way ANOVA was performed followed by Bonferroni test. Significance was observed if p value was recorded to be less than 0.05.

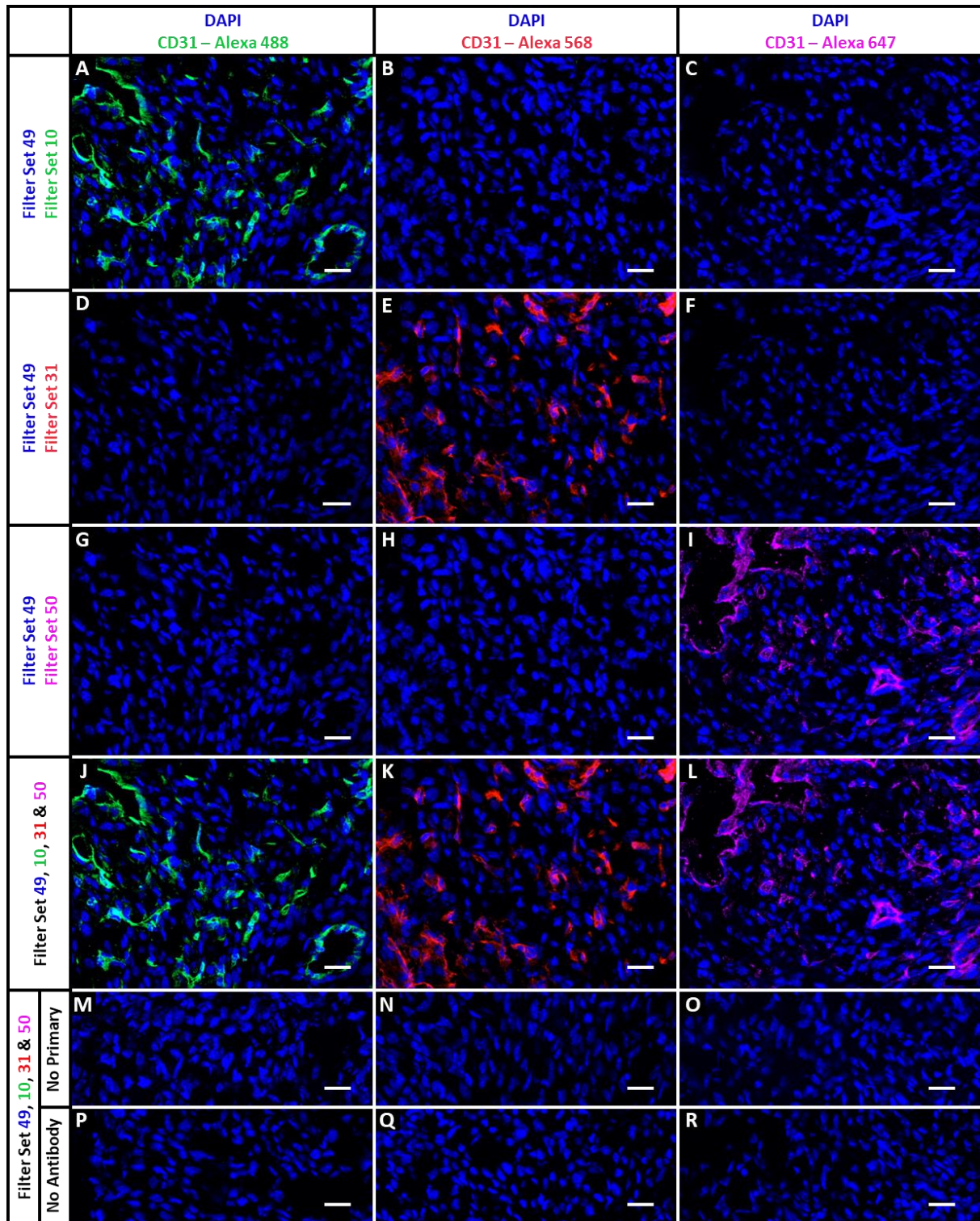


**Figure 2.8: Bleed through check for Carl Zeiss M2 Axioimager Filter Sets.** E17.5 OCT embedded heart sections stained with rat anti-CD105 primary antibody. To detect the primary antibody, heart sections were stained with goat anti-rat secondary antibody conjugated with Alexa 488 (**A,D&G**) Alexa 568 (**B,E&H**) or Alexa 647 (**C,F&I**) and counter-stained with DAPI (blue) to mark nuclei. Exposure times for each filter set was set using the sections shown in A, E and I. (**B&C**) Showing no bleed through from Alexa 568 and Alexa 647 conjugated secondary antibody stained sections in filter set 10. (**D&F**) Similarly, no bleed through was observed from Alexa 488 and Alexa 647 conjugated secondary antibody stained sections in filter set 31. (**G&H**) Showing no bleed through from Alexa 488 and Alexa 568 conjugated secondary antibody stained sections in filter set 50. (**J to L**) Merged channel images showing no bleed through of fluorophores between the three filter sets. (**M,O&Q**) No primary and (**N,P&R**) no antibody staining controls. Scale bar A to R = 20µm.

---

## **Chapter 3. Endoglin Expression in the Heart from Embryo to Adult**

---

### 3.1. Introduction

Endoglin is a TGF $\beta$  co-receptor that plays a vital role during angiogenesis (section 1.4.2 1.5.1). It is highly expressed in proliferating endothelial cells (ECs) (144, 238) while low levels of endoglin occur in quiescent ECs (141). In the heart, various studies have shown endoglin expression during development of cardiac valves, AV canal and endocardium or in pathological conditions. *In vivo* studies have showed expression of endoglin in the valvular mesenchymal cells during embryonic development (128, 138, 239, 240). In humans, endoglin is expressed in these cardiac valve mesenchymal cells, although this endoglin expression is downregulated during the latter phases of valve development (240). Using immunohistochemical and western blotting analysis, Qu *et al.* (240) showed the endoglin expression only in the primitive heart tube, ECs of coronary vessels and endocardium in 4 to 13-weeks old human embryos. They also showed endoglin expression in the mesenchymal cells of endocardial cushions [AV and semilunar (SL) valves] of 4 to 7-week old human embryos (240). St-Jacques *et al.* (138) used in situ hybridisation and immuno-histochemical analysis to show expression of endoglin in the mesenchymal cells of heart valves and in ECs of coronary arteries (138). Bourdeau *et al.* (161), also showed the presence of these endoglin expressing mesenchymal cells in the AV cushions of mice around E10.5 and were likely formed by endothelial to mesenchymal transition (EndMT) of adjacent endocardium. They also showed the expression of endoglin in the endocardium from E9.5 onwards (161).

A similar pattern of endoglin expression was observed by Jonker and Arthur (137) with strong expression of endoglin in E9.5 endocardium and in heart valves at E12.5 & E13.5. Furthermore, endoglin expression was observed in the vascular endothelium of E12.5 and 13.5 embryos and observed strongest endoglin expression in capillaries, intermediate levels in arteries and weakest in veins (137). In a recent study, endoglin is also used as an early cardiac vascular marker at E8.5 and by E10.5 was observed in the endocardium & coronary vessel endothelium (241).

Expression of endoglin has also been reported in chicks (242). At stage 15 in chicks, endoglin expression was shown in the endothelium of AV canal. At stage 17, expression of endoglin was also observed in the OFT endothelium, proepicardium and in the ECs of posterior cardinal veins (242); and by stage 18 endoglin was also detected in the mesenchymal cells located in the OFT and AV canal (242).

In adult porcine hearts, low level endoglin expression was observed in ECs, adventitial fibroblasts, and a minority of medial SMCs of normal hearts (215). However, 3, 7, and 14 days

---

after an arterial injury (balloon-injured) endoglin expression was significantly increased in ECs, myo-fibroblasts and medial SMCs. This expression of endoglin was significantly declined 28-days post injury. This showed that endoglin is necessary during the active angiogenic phase (215). They also showed similar endoglin expression pattern in normal and atherosclerotic human coronary arteries (215). Furthermore, they observed 95% of cultured human SMCs express endoglin on their cell surface (215).

Using situ hybridisation and immuno-histochemical analysis, Laake *et al.* (216) showed expression of endoglin primarily in the atria with low levels in ventricles of normal adult mice hearts (216). Endoglin expression was significantly increased in 1-week post-MI hearts in the infarcted region (216). Chen *et al.* (243), showed low level expression of endoglin mRNA and protein in cultured cardiac fibroblasts from adult male rats.

Apart from early to mid-development and in few injury model studies using adult hearts, the expression of endoglin has not been reported during the course of coronary vasculature development in mice. Therefore, the aim of this chapter was to determine the normal pattern, timing and relative intensity of endoglin expression in the heart and coronary vessels from early development to maturity. As coronary vessel development begins around E11.5 (43, 44), expression of endoglin was studied at different stages from E11.5 to adult in wildtype C57Bl/6 mice.

## **3.2. Results**

### **3.2.1. Staining Optimisation**

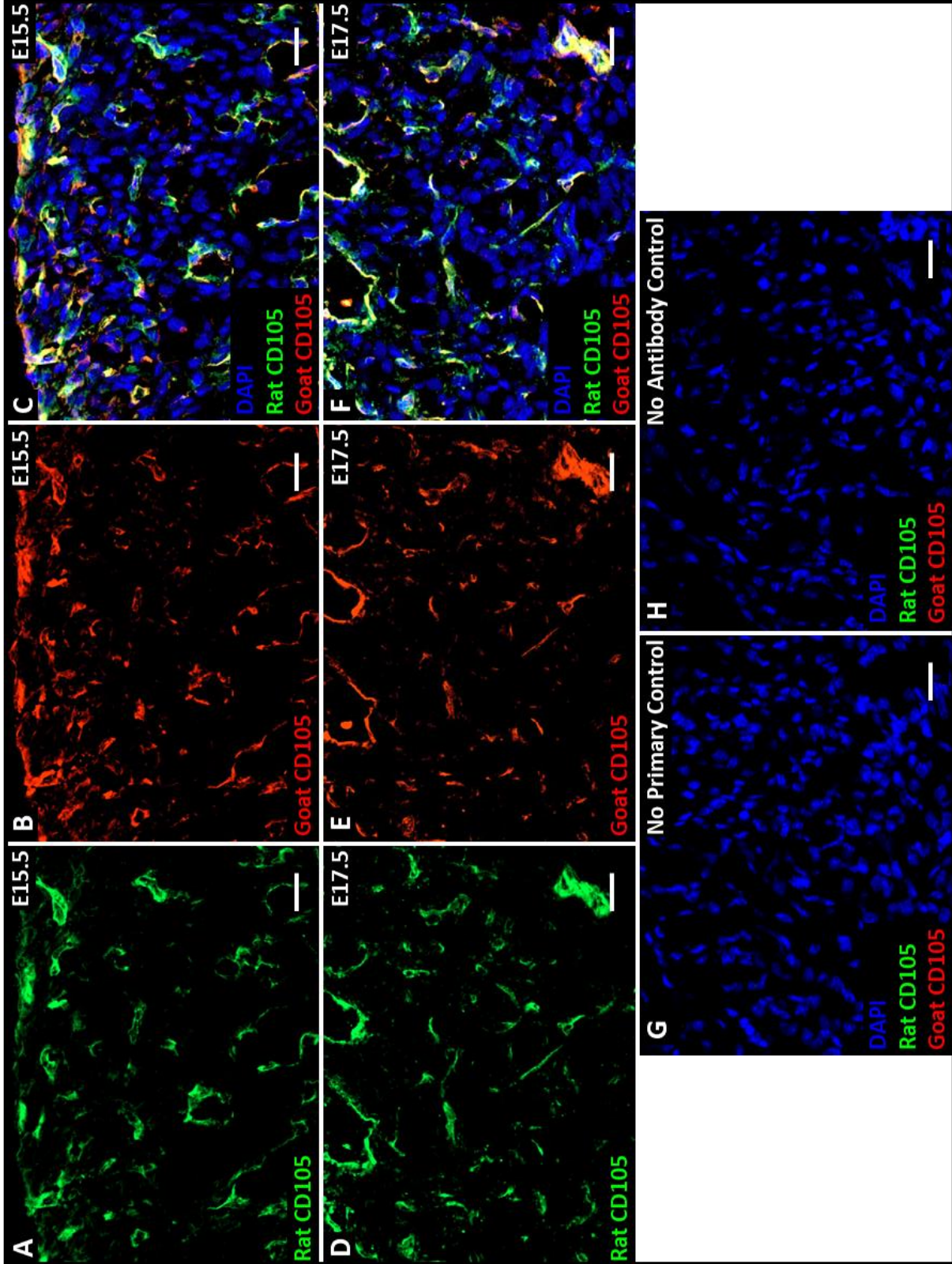
Freshly dissected hearts were fixed in 0.2% PFA overnight and embedded in OCT (section 2.2.2). Tissue was sectioned, and immuno-fluorescent staining was performed (as described in section 2.5.4) to evaluate endoglin expression in the heart with particular focus on the coronary arteries, and veins, using the markers summarised in Table 3.1.

**Table 3.1: Antibodies used to characterise expression of endoglin in developing, postnatal and adult mouse heart. Antibodies details are summarised in Table 2.8.**

<b>Antibody</b>	<b>Target protein</b>	<b>Raised In</b>	<b>Specificity within Heart</b>	<b>Age Range</b>
<b>Anti-CD31</b>	PECAM1	Rat	ECs & Endocardium (244)	All
<b>Anti-Endomucin</b>	EMCN	Rat	Venous ECs & Endocardial (245)	E17.5 and above
<b>Anti-SM22<math>\alpha</math></b>	TAGLN	Rabbit	vSMCs (246-248) & Mesenchymal Cells (249)	Coronary arteries specific from E13.5 to E17.5
<b>Anti-CD105</b>	ENG/ endoglin	Rat or Goat	Goal of this chapter (188, 241)	All

During the current study, two different anti-CD105 antibodies were used: rat anti-CD105 antibody (monoclonal antibody MJ7/18) and goat anti-CD105 antibody (polyclonal). To verify at the outset that both anti-CD105 antibodies identify the same cell types, double immunofluorescence staining was performed on E15.5 and E17.5 embryo sections (Figure 3.1), confirming that both goat and rat anti-CD105 antibodies show excellent co-localisation and can therefore be used interchangeably.

**Figure 3.1: Co-localisation of rat and goat anti-CD105 antibodies on E15.5 and E17.5 heart sections. E15.5 and E17.5 heart sections stained with rat anti-CD105 (green), goat anti-CD105 (red) antibodies and counterstained using DAPI (blue) to mark nuclei. Split channel images of (A-C) E15.5 and (D-F) E17.5 heart showing co-localisation of both anti-CD105 antibodies used during this study to detect endoglin. (G) No primary and (H) no antibody staining controls. Scale Bars: A-H – 20µm.**



---

To analyse the pattern of endoglin staining in heart in this chapter, images were taken from the mid plane of heart showing all four cardiac chambers (Figure 3.2A). Next, for intensity analysis images were taken from six regions of heart (boxed areas, Figure 3.2B) at x40 magnification to analyse endoglin staining intensity. These images were taken from three heart sections at least 30 to 70µm apart to avoid duplicate imaging of same cell. Furthermore, at each age three separate hearts were analysed. To calculate mean fluorescent endoglin intensity, a line was drawn along the cytoplasmic region of an endoglin expressing cell using the spline contour function of Zen Pro software (Figure 3.2C).

Endoglin expression was observed in both endothelial (CD31+ve) and some non-endothelial (CD31-ve) cells. To compare endoglin intensity between these two cell types, mean fluorescent endoglin intensity was measured from up to five CD31-ve; CD105+ve cells and 5 CD31+ve; CD105+ve per FOV (18 FOV per heart).

### **3.2.2. Expression of Endoglin in Coronary Vessels during Embryogenesis**

I first analysed the expression of endoglin in transverse sections of E11.5 (n=3) embryos using goat anti-CD105 and anti-PECAM1 antibodies. Tiled image of E11.5 embryos showed partial septation of the ventricle chambers (asterisk, Figure 3.3A) consistent with this stage of heart development (2, 250). Analysis of x40 immunofluorescence images of RV and LV free walls showed that expression of endoglin was restricted to endocardium (Figure 3.3) and ECs of newly developing coronary vessels in the apical half of the IVS (Figure 3.3).

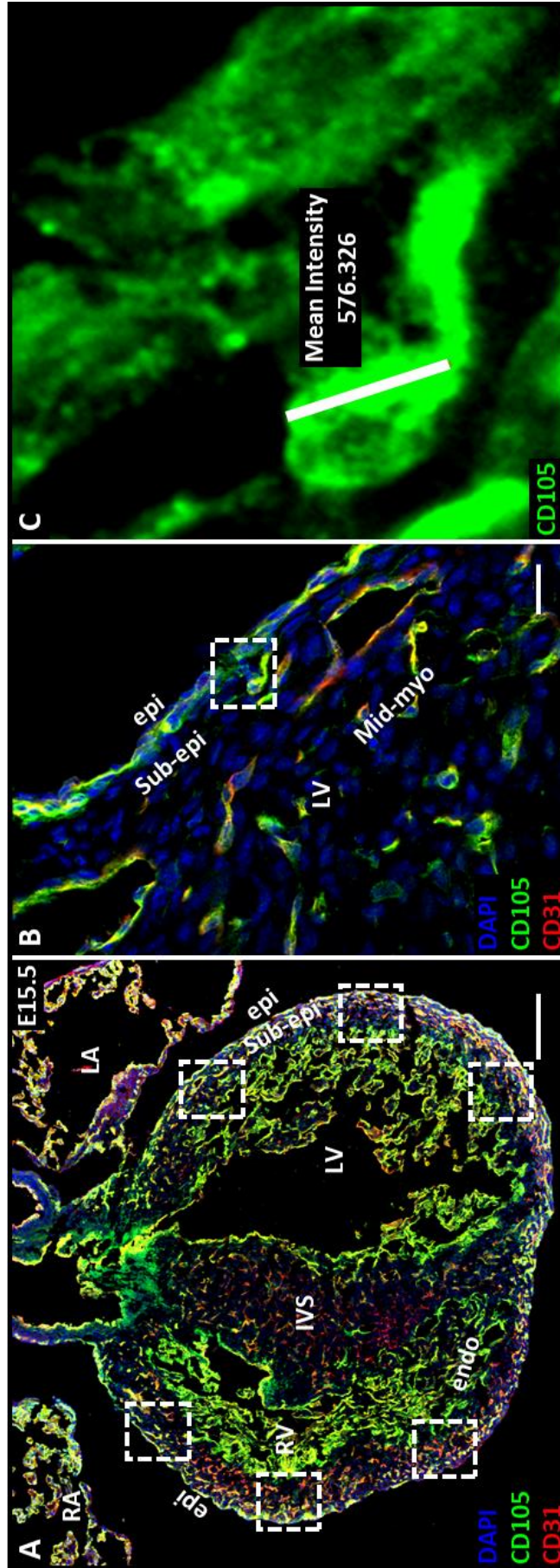


**Figure 3.2: Quantification of cytoplasmic endoglin expression/staining intensity using the spline contour function of Zen lite 2012 software.** (A) Overview image of an E15.5 heart section stained with anti-CD105 (green) and anti-CD31 (red) antibodies (nuclei counterstained with DAPI, blue) showing regions of the free RV and LV wall used for quantification to illustrate how 6 regions were selected from each section (white dotted boxes). Each region corresponded to a field of view (FOV) taken with x40 objective. (B) Example of an x40 objective image taken from free LV wall. (C) Digitally zoomed split channel image of a sub-epicardial EC (B, white box). The white line (drawn using spline contour function) indicates area measured to derive mean endoglin intensity value. This method was used to quantify endoglin intensity from E13.5 to 14wks hearts. Scale bar: A – 200µm and B – 20µm. Abbreviations: ECs – Endothelial Cells; endo – Endocardium; epi – Epicardium; IVS – Interventricular Septum; LA – Left Atria; LV – Left Ventricle; Mid-myo – Mid myocardium; RA – Right Atria; RV – Right Ventricle and Sub-epi – Sub-epicardium.

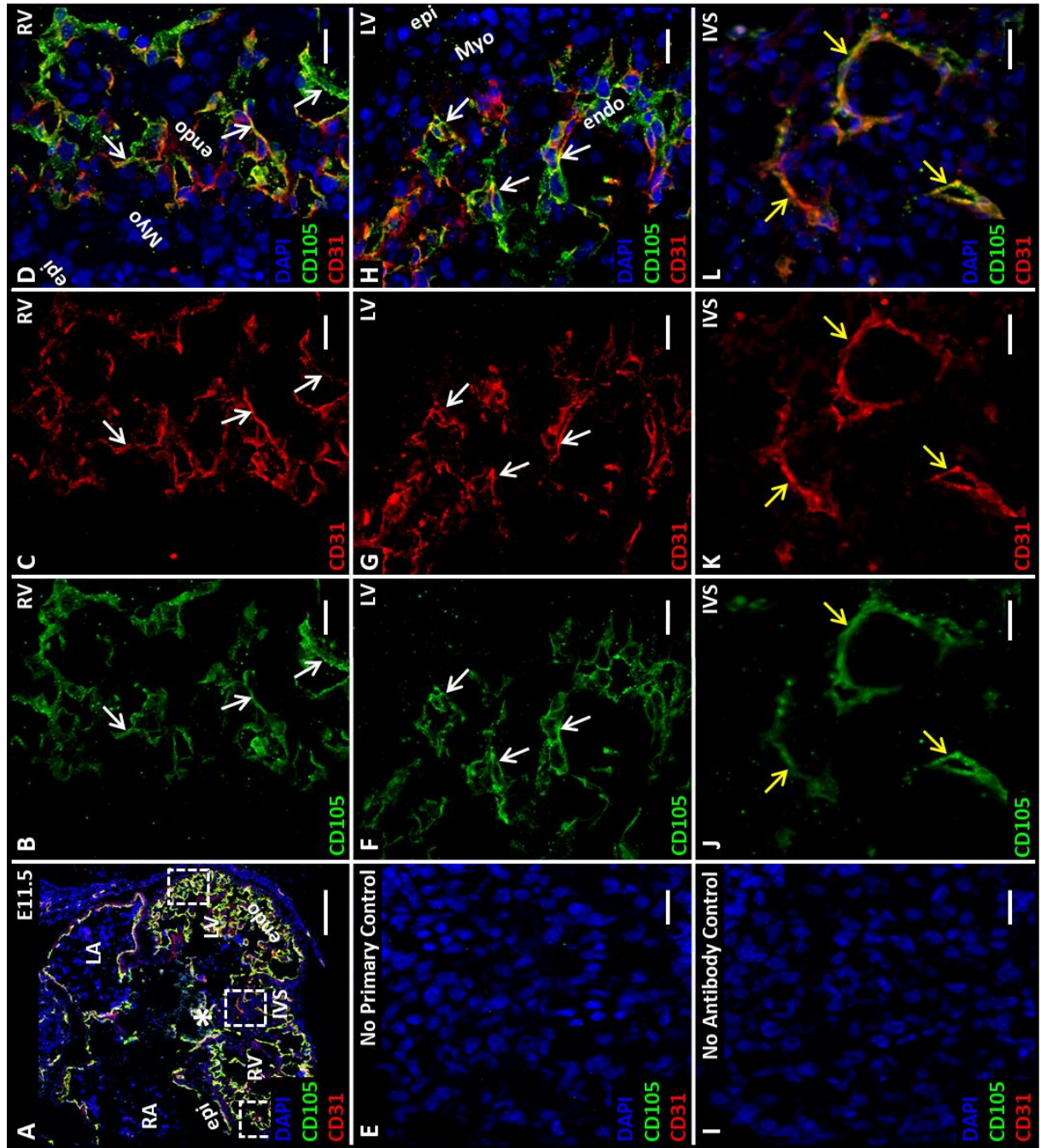


**Figure 3.3: Endoglin is expressed in the endocardium and endothelium of nascent blood vessels in E11.5 mouse hearts.** (A) Representative tiled image of a transverse section of an E11.5 embryo showing partially closed IVS (asterisk) stained with anti-CD105 (endoglin, green) and anti-CD31 (endothelium and ECs, red) antibodies. Nuclei stained using DAPI (blue). Split and merged channel images of RV wall (B-D), LV wall (F-H) and IVS (J-L) showed endoglin expression mainly in the CD31 positive endocardium (white arrows) and endothelium of newly developing blood vessels (yellow arrows), ( $n=3$ ). (E) No primary and (I) no antibody staining controls. Scale Bars: A – 200 $\mu$ m; B-L – 20 $\mu$ m. Abbreviations: ECs – Endothelial Cells; endo – Endocardium; epi – Epicardium; IVS – Interventricular Septum; LA – Left Atria; LV – Left Ventricle; Mid-my – Mid myocardium; RA – Right Atria and RV – Right Ventricle.

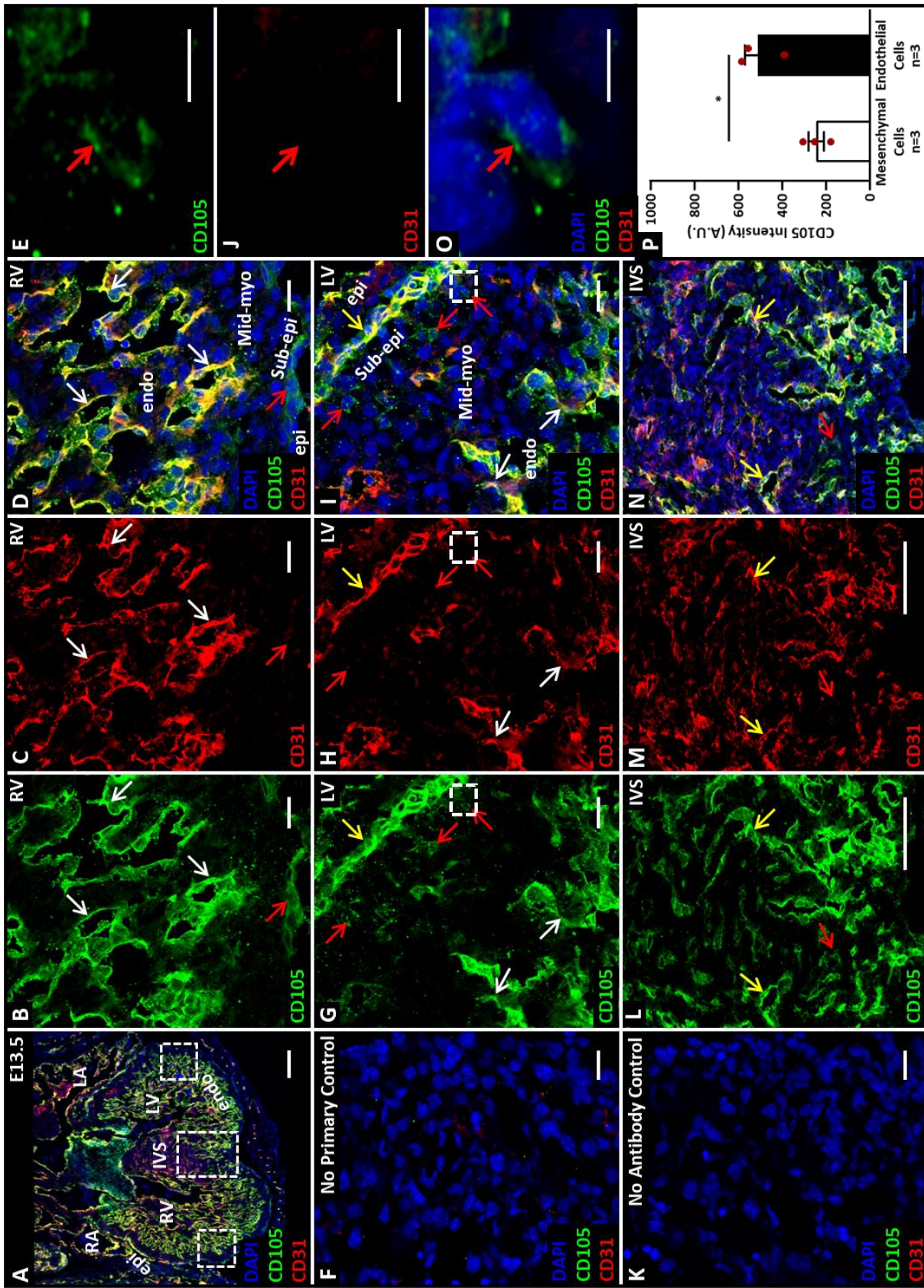
---

At E13.5, development of aortic arch and septation of the OFT into aorta & pulmonary trunk is complete (2, 250, 251). The septation of primitive ventricle into right & left ventricles are underway (2, 250). Coronary vessel development also continues over the dorsal and ventral surface of the heart (44).

Transverse sections of E13.5 hearts (n=3) were stained with goat anti-CD105 and anti-PECAM1 (CD31) antibodies. Tiled immunofluorescence images showed almost complete IVS consistent with this stage of development and the presence of the coronary vessels in the ventricles & IVS (Figure 3.4A). High-power images of free ventricle walls showed strong endoglin expression in the endocardium (white arrows, Figure 3.4) and ECs (yellow arrows, Figure 3.4).

However, cells with lower levels of endoglin expression that were also CD31 negative, were found in the IVS, sub-epicardial and mid-myocardial regions of the heart (red arrows, Figure 3.4). These cells could be mesenchymal cells as endoglin is a known mesenchymal marker (252) with potential origin from the epicardium (also known as epicardially derived cells, EPDCs). At this stage of development, EPDCs are expected to be migrating into the myocardium to support the developing coronary vasculature (section 1.3.1.1). Bax *et al.* (64) reported that EPDCs cultured *in vitro* in their mesenchymal state express endoglin, in agreement with the idea that these low endoglin expressing cells observed *in vivo* (Figure 3.7) may be EPDCs. In this chapter, these cells are referred to as “presumed EPDCs” from here on. Mean endoglin intensity was calculated using spline contour function of Zen Pro software as described in Figure 3.2. Endoglin fluorescent intensity analysis of the sub-epicardial ECs was observed to be two-fold higher compared to the presumed EPDCs at E13.5 (Figure 3.4M).

**Figure 3.4: At E13.5 endoglin expression was observed in the endocardium, endothelium of nascent coronary vessels and in non-ECs. (A)** Representative tiled image of a transverse E13.5 heart section stained with anti-CD105 antibody (endoglin, green) and anti-CD31 antibody (endocardium and ECs, red). Nuclei stained using DAPI (blue). Split and merged channel images of RV wall (**B-D**), LV wall (**G-I**) and IVS (**L-N**) showed strong endoglin expression in CD31 positive endocardium (white arrows) and ECs of newly developing blood vessels (yellow arrows). Low levels of endoglin were observed in CD31 negative, presumed EPDCs (red arrows). At E13.5, these presumed EPDCs were observed in the IVS, sub-epicardial and mid-myocardium region of the heart. (**E, J, O**) Split channelled, digitally zoomed image (dotted white box G-I) of a presumed EPDC. (**F**) No primary and (**K**) no antibody staining controls. (**P**) Quantification of mean fluorescence intensity levels show a significantly lower level of endoglin expression in presumed EPDCs (mesenchymal cells,  $245.0 \pm 36.43$ ;  $n = 3$ ) compared to sub-epicardial ECs ( $509.8 \pm 60.73$ ;  $n = 3$ ;  $p = 0.0201$ ). Data shown as mean  $\pm$  SEM and analysed using two tailed unpaired t-test (\*  $p < 0.05$ ). Scale Bars: A – 200 $\mu$ m; B-D, F-I & K – 20 $\mu$ m; J-N – 100 $\mu$ m; E, J, O – 10 $\mu$ m. Abbreviations: Endothelial Cells – ECs; endo – Endocardium; epi – Epicardium; EPDCs – Epicardially Derived Cells; IVS – Interventricular Septum; LA – Left Atria; LV – Left Ventricle; Mid-myo – Mid myocardium; RA – Right Atria; RV – Right Ventricle and Sub-epi – Sub-epicardium.

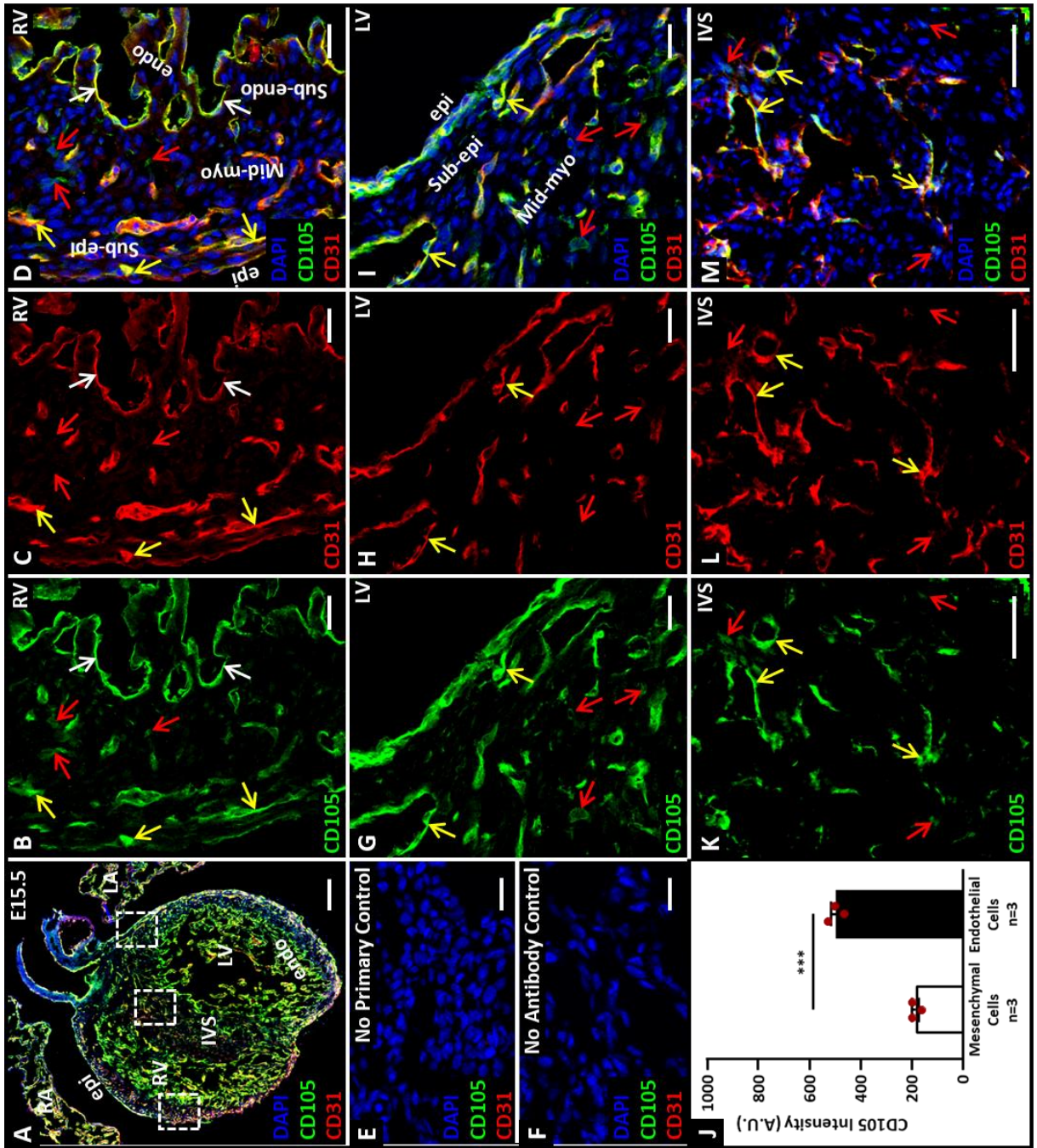


---

Next, the expression of endoglin was studied in E15.5 hearts. By this stage, the basic structure of the heart is almost complete. The right and left coronary arteries are connected at the base of the aorta thereby inducing blood flow in the nascent coronary plexus (38). This anastomosis of aorta and coronary vessels along with the hypoxia stimuli induced by myocardium thickening significantly promotes the growth of the coronary vasculature (43).

Coronal sections of E15.5 hearts (n=3) were stained with goat anti-CD105 and anti-CD31 antibodies. Tiled images show a four-chambered heart structure with thicker myocardium compared to E13.5 myocardium and presence of coronary vessels throughout the myocardium. High-power image analysis showed a similar pattern of endoglin expression to that previously seen in E13.5 embryonic mice hearts, with strong endoglin expression in endothelial (yellow arrows,) and endocardial cells (white arrows, Figure 3.5), but a three-fold lower endoglin expression in presumed EPDCs (red arrows, Figure 3.5 and Figure 3.5J). These presumed EPDCs were evenly dispersed throughout the myocardium, with some in clusters of 4 or more cells, and were more numerous at E15.5 in comparison to E13.5 (Figure 3.11).

**Figure 3.5: At E15.5 strong endoglin expression is observed in the endocardium, endothelium of coronary vessels and at lower levels in the presumed EPDCs.** (A) Representative tiled image of an E15.5 coronal heart section stained with anti-CD105 antibody (endoglin, green) and anti-CD31 antibody (endocardium and ECs, red). Nuclei stained using DAPI (blue). Split and merged channel images of RV wall (**B-D**), LV wall (**G-I**) and IVS (**K-M**) showed strong expression of endoglin in CD31 positive endocardium (white arrows) and ECs of developing blood vessels (yellow arrows). CD31 negative low endoglin expressing, presumed EPDCs (red arrows) were observed throughout the myocardium at this stage of development. (**E**) No primary and (**F**) no antibody staining controls. (**J**) Quantification of fluorescent intensity revealed significantly lower levels of endoglin expression in presumed EPDCs (mesenchymal cells,  $184.3 \pm 12.49$ ;  $n=3$ ) compared to sub-epicardial ECs ( $497.3 \pm 18.83$ ;  $n=3$ ;  $p = 0.0002$ ). Data shown as mean  $\pm$  SEM and analysed using two tailed unpaired t-test ( $*** p < 0.001$ ). Scale Bars: A – 200  $\mu$ m; B-I & K-M – 20  $\mu$ m. Abbreviations: ECs – Endothelial cells; endo – Endocardium; epi – Epicardium; EPDCs – Epicardially Derived Cells; IVS – Interventricular Septum; LA – Left Atria; LV – Left Ventricle; Mid-myo – Mid myocardium; RA – Right Atria; RV – Right Ventricle; Sub-endo – Sub-endocardium and Sub-epi – Sub-epicardium.



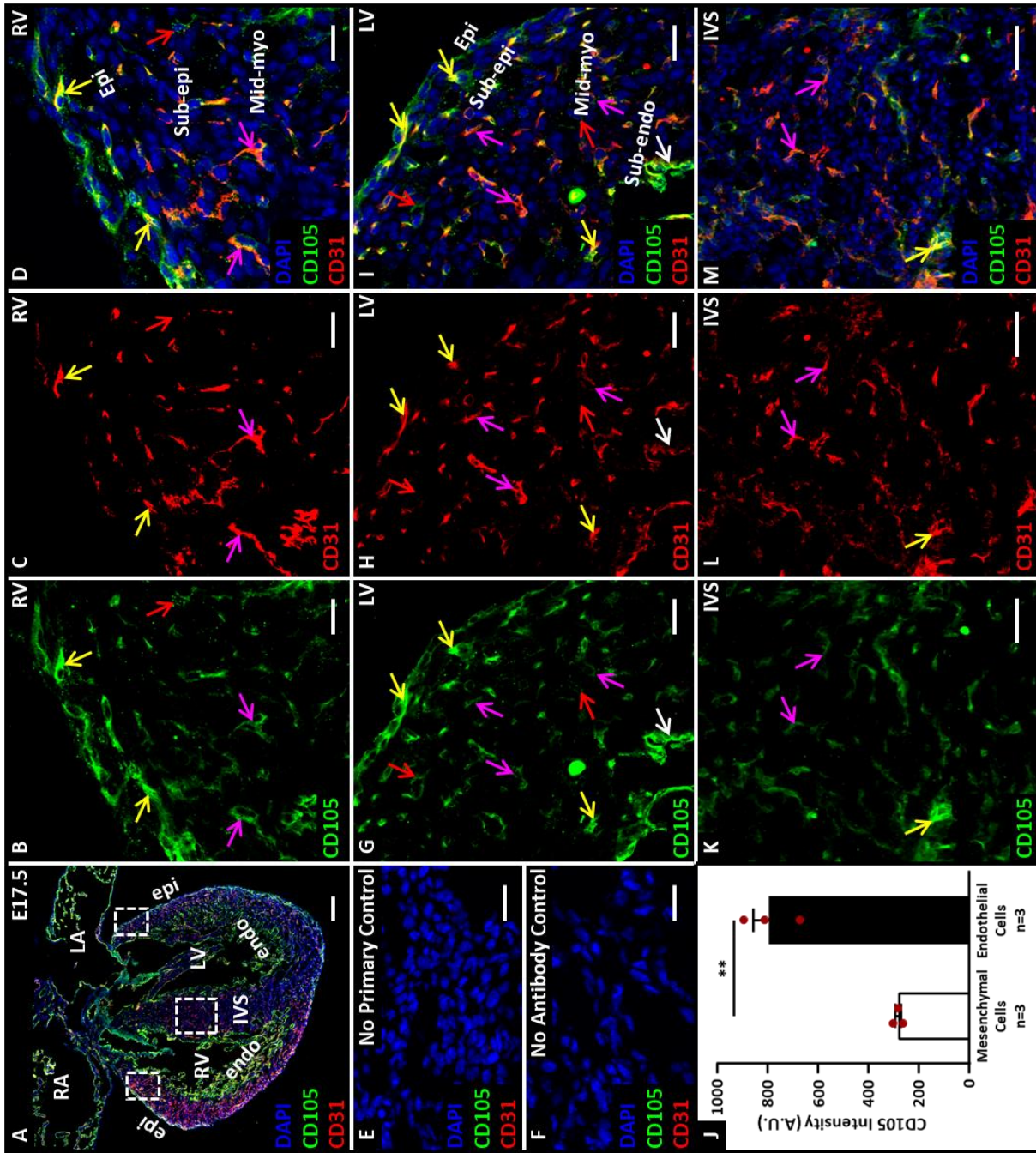
---

Next, expression of endoglin was studied at final stages of embryonic development at E17.5. At this stage, myocardium continues to thicken, valve mature (251) and is accompanied by differentiation of nascent vessels into coronary arteries and veins (43).

Coronal sections of E17.5 hearts (n=3) were stained with goat anti-CD105 and anti-CD31 antibodies. Analysis of high-power images now showed varying endoglin intensity in ECs. The endocardial cells (white arrows, Figure 3.6) and the ECs of sub-epicardial & sub-endocardial blood vessels (yellow arrows, Figure 3.6) continued to show strong endoglin expression, but vascular ECs in the mid-myocardium expressed lower levels of endoglin, although not as low as in presumed EPDCs (purple arrows, Figure 3.6). As the mid-myocardial vessels are arterial this difference in endoglin expression is further investigated in Section 3.2.4.

A significant reduction in the density of presumed EPDCs (red arrows, Figure 3.6) was observed throughout the myocardium at E17.5 in comparison to E13.5 and E15.5 hearts (Figure 3.11). Next, the expression of endoglin in presumed EPDCs and valve mesenchyme is studied in further detail.

**Figure 3.6: At E17.5 endoglin expression is predominantly expressed in the endocardium and endothelium of coronary vessel.** E17.5 embryonic heart sections were stained with anti-CD105 (endoglin, green) and anti-CD31 (red, to detect endocardium and ECs) antibodies. Nuclei were stained using DAPI (blue). (A) Representative tiled image of an E17.5 coronal heart section. Split and merged channel images of RV wall (B-D), LV wall (G-I) and IVS (K-M) showed co-expression of CD31 and CD105 in the endothelium of coronary vessels (yellow and purple arrows). Sub-epicardial coronary vessel (yellow arrows) express stronger levels of endoglin compared to mid-myocardial coronary vessels (purple arrows). Low numbers of presumed EPDCs (red arrows) were also observed throughout the myocardium. (E) No primary and (F) no antibody staining controls. (J) Mean fluorescent intensity quantification shows significantly lower levels of endoglin expression in presumed EPDCs (mesenchymal cells,  $282.9 \pm 11.40$ ;  $n=3$ ) compared to sub-epicardial ECs ( $793.4 \pm 65.20$ ;  $n=3$ ;  $p = 0.0015$ ). Data shown as mean  $\pm$  SEM and analysed using two tailed unpaired *t*-test (\*\*  $p < 0.01$ ). Scale Bars: A –  $200\mu\text{m}$ ; B-I & K-M –  $20\mu\text{m}$ . Abbreviations: ECs – Endothelial Cells; endo – Endocardium; EPDCs – Epicardially Derived Cells; IVS – Interventricular Septum; LA – Left Atria; LV – Left Ventricle; Mid-myo – Mid myocardium; RA – Right Atria; RV – Right Ventricle; Sub-endo – Sub-endocardium and Sub-epi – Sub-epicardium.



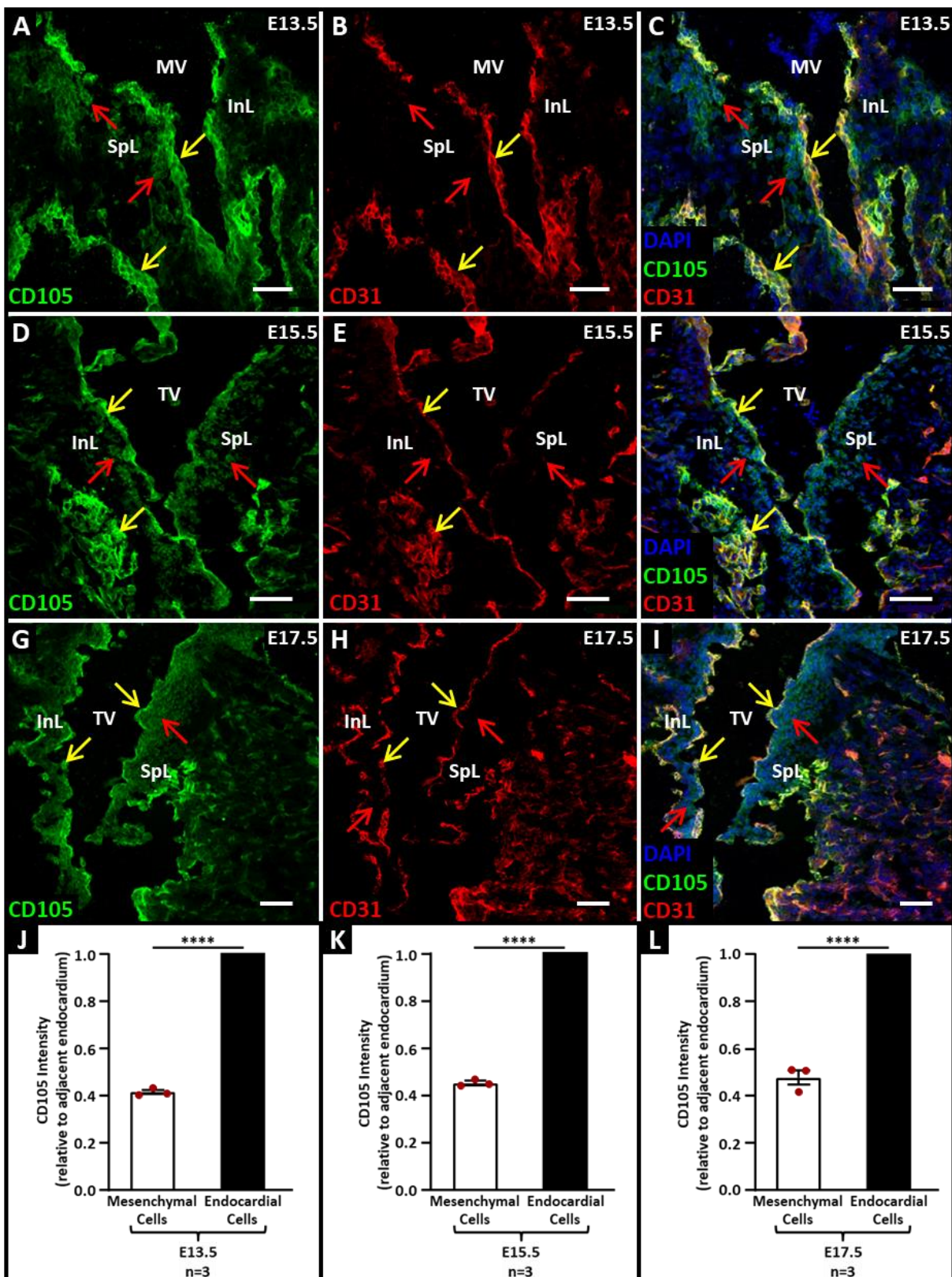
---

### 3.2.3. Endoglin in Mesenchymal Cells of Embryonic Mice Heart

Mesenchymal cells are vital for normal heart development (discussed in section 1.1). Epicardium provides mesenchymal cells (EPDCs) that differentiate into vSMCs required for coronary vessel maturation and cardiac fibroblasts (discussed in section 1.3.1.1 and 1.3.2). These EPDCs start to migrate into the myocardium around E13.5 (78, 253).

The endocardium is also known to provide mesenchymal cells required during AV & SL valve development (described in section 1.1.1) (254). Furthermore, mesenchymal cells are also known to express endoglin, (252). In this study, I analysed the intensity of endoglin expression in AV valve mesenchymal cells compared with presumed EPDCs and adjacent endocardium or vascular endothelium.

Development of AV valves begins around E11.5 with the formation of endocardial cushions populated by mesenchymal cells provided by the adjacent endocardium around E12.5 (2, 250). Valvular mesenchymal cells from E13.5 (n=3), E15.5 (n=3) and E17.5 (n=3) heart sections were next analysed to determine the relative endoglin expression. Analysis of immunofluorescence images showed expression of endoglin in CD31-ve valvular mesenchymal cells at all three stages of development (red arrows, Figure 3.7) consistent with the results observed by Qu *et al.* (240), Arthur *et al.* (128) and Nomura-Kitabayashi *et al.* (239). The mean endoglin fluorescent analysis also showed significantly reduced levels of endoglin expression in valvular mesenchymal cells compared to adjacent endocardial cells at E13.5, E15.5 and E17.5 (Figure 3.7J).



Next, endoglin expression in presumed EPDCs relative to adjacent ECs was compared with endoglin expression in valvular mesenchymal cells relative to the adjacent endocardium. The ratio of endoglin expression in both sets of mesenchymal cells compared to endothelial or endocardial cells was observed to be similar at approximately 0.4 (Figure 3.8).

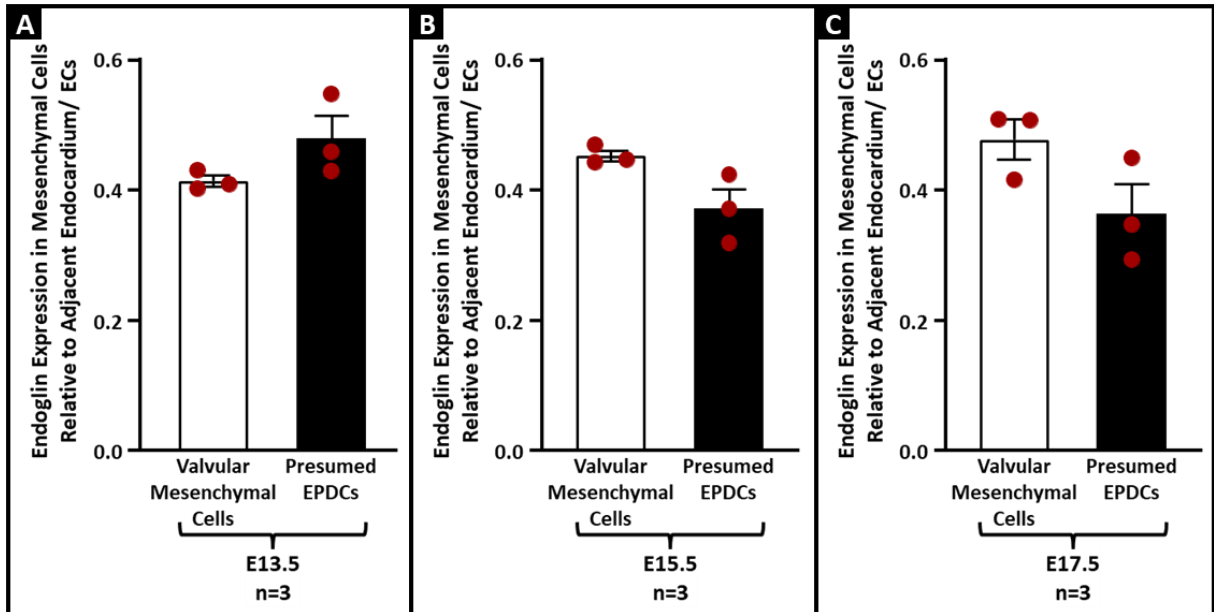


**Figure 3.8: Similar Level of Endoglin Expression Observed in Valvular Mesenchymal Cells and Presumed EPDCs.** The endoglin expression in valvular mesenchymal cells (relative to adjacent endocardium) at E13.5 ( $0.415 \pm 0.009$ ;  $n=3$ ;  $p = 0.1540$ ), E15.5 ( $0.453 \pm 0.008$ ;  $n=3$ ;  $p = 0.0620$ ) and E17.5 ( $0.478 \pm 0.031$ ;  $n=3$ ;  $p = 0.1070$ ) was similar to expression of endoglin in presumed EPDCs (relative to adjacent ECs) observed at respective ages (E13.5:  $0.480 \pm 0.036$ ,  $n=3$ ; E15.5:  $0.372 \pm 0.031$ ,  $n=3$  and E17.5:  $0.364 \pm 0.046$ ,  $n=3$ ). Data shown as mean  $\pm$  SEM and analysed using two tailed unpaired *t*-test. Abbreviations: ECs – Endothelial Cells and EPDCs – Epicardially Derived Cells.

To further confirm that these presumed EPDCs are mesenchymal cells, heart sections from E11.5, E13.5, E15.5 and E17.5 were also stained with anti-SM22 $\alpha$  and rat anti-CD105 antibodies. The SM22 $\alpha$  antibody is used to detect TAGLN gene and is also used as an early marker for mesenchymal cells and vSMCs in various studies (104, 249, 255). At E11.5, SM22 $\alpha$  expression was only seen in the dorsal aorta of a developing heart (red arrow, Figure 3.9). From E13.5 onwards, strong SM22 $\alpha$  expression was seen not only in the major vessels (aorta and pulmonary trunk) but also in newly muscularised vessels in the myocardium (yellow arrows,). Lower levels of SM22 $\alpha$  expression were also observed in all low endoglin expressing presumed EPDCs observed at E13.5, E15.5 and E17.5 (red arrow, Figure 3.10), consistent with their known mesenchymal identity (64).

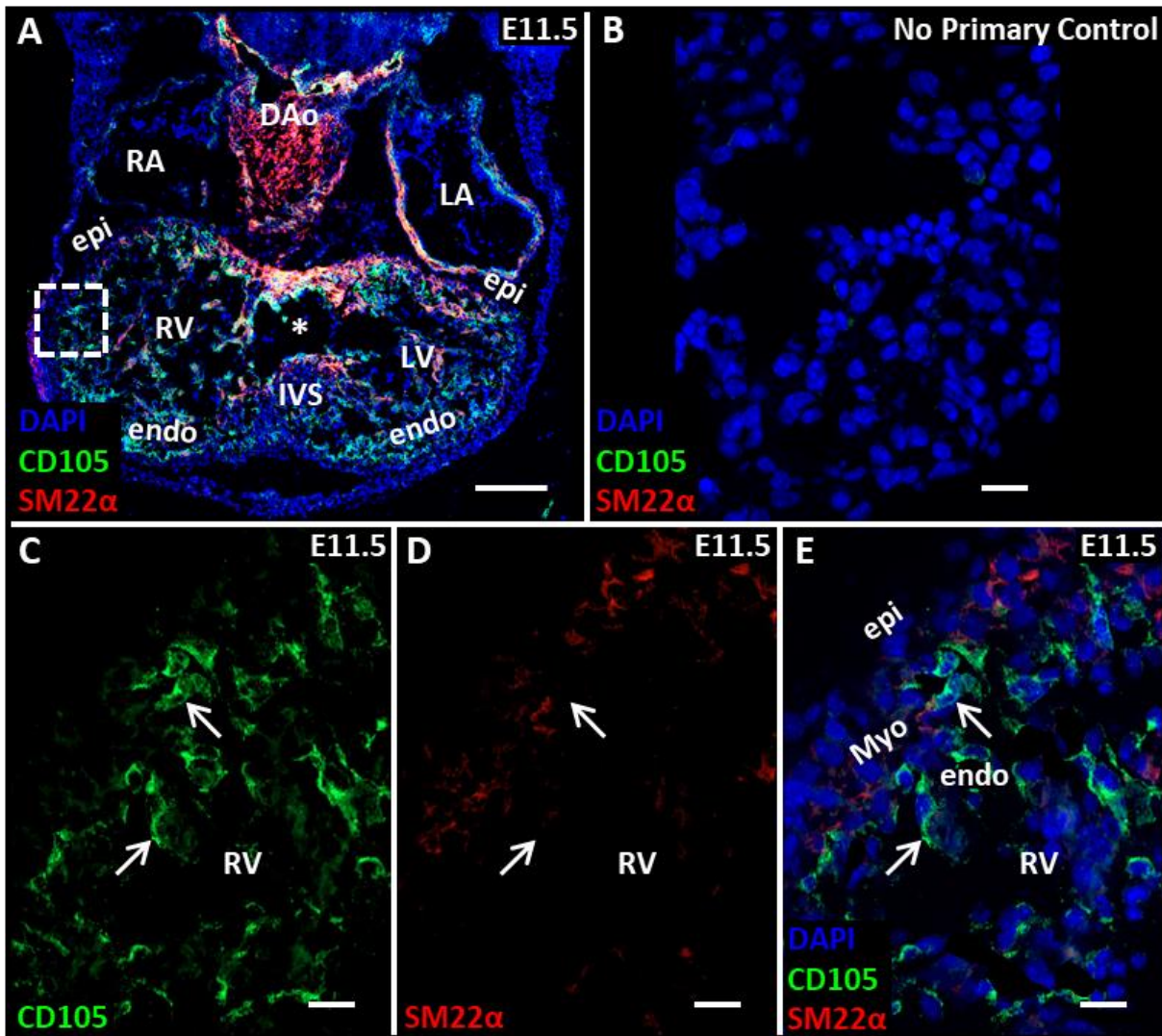


**Figure 3.9:** At E11.5, SM22 $\alpha$  expression was observed in the major arteries of the embryos. E11.5 transverse heart sections were stained with anti-CD105 (green), anti-SM22 $\alpha$  [vSMCs (bright red) and mesenchymal cells (weak red)] antibodies and counterstained with DAPI to mark nuclei (blue). **(A)** Representative tiled image of a transverse section of an E11.5 embryo showed partially formed IVS (asterisk) and strong expression of SM22 $\alpha$  in the dorsal aorta. **(C-E)** Split and merged channel images of free RV wall (white box A) showed expression of endoglin only in the endocardium (white arrows) and no SM22 $\alpha$  expression in the myocardium ( $n=3$ ). **(B)** No primary staining control. *Scale Bars: A – 200 $\mu$ m; B-E – 20 $\mu$ m. Abbreviations: DAo – Dorsal Aorta; endo – Endocardium; epi – Epicardium; IVS – Interventricular Septum; LA – Left Atria; LV – Left Ventricle; Myo – myocardium; RA – Right Atria and RV – Right Ventricle.*

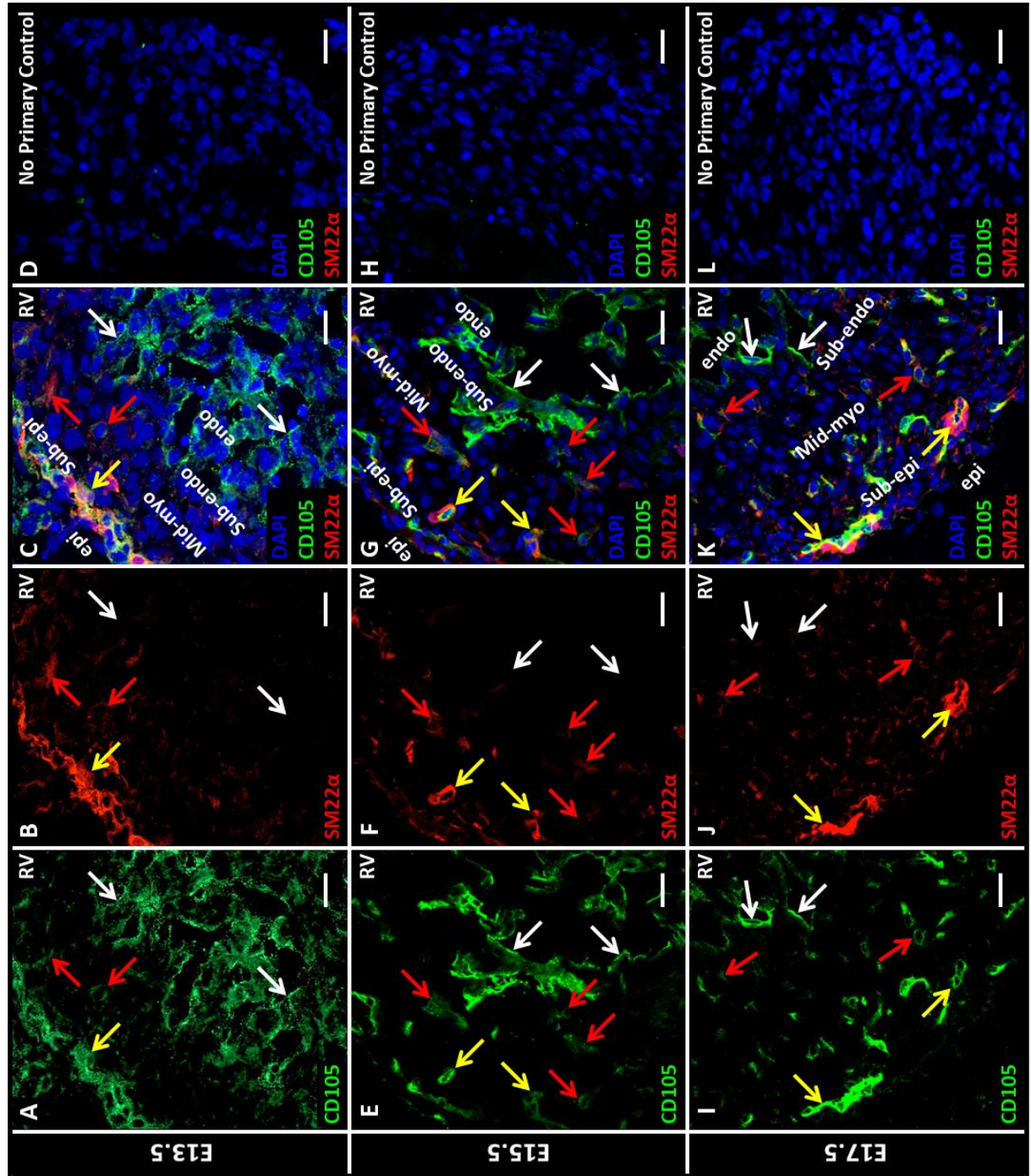


**Figure 3.10: Presumed EPDCs in E13.5, E15.5 and E17.5 mouse hearts express low levels of endoglin and SM22 $\alpha$ .** Embryonic heart sections were stained with anti-CD105 antibody (endoglin, green) and anti-SM22 $\alpha$  antibody [vSMCs (bright red) and mesenchymal cells (weak red)]. Nuclei stained using DAPI (blue). Split and merged channel image of (A-C) E13.5 (n=3), (E-G) E15.5 (n=3) and (I-K) E17.5 (n=3) hearts showed strong endoglin expression in the ECs of muscularised vessels (yellow arrows) and in the endocardium (white arrows). In contrast, low levels of endoglin and SM22 $\alpha$  expression was observed in presumed EPDCs (red arrows). (D,H,L) No primary staining controls. Scale bars: A to L – 20 $\mu$ m. Abbreviation: ECs – Endothelial Cells; endo – Endocardium; epi – Epicardium; EPDCs – Epicardially Derived Cells; Mid-myo – Mid myocardium; RV – Right Ventricle; Sub-endo – Sub-endocardium; Sub-epi – Sub-epicardium and vSMCs – Vascular smooth muscle cells.

Quantification of numbers of the “presumed EPDCs” at different ages (n=3, per group) was performed by counting the total number of presumed EPDCs (CD105+ve and CD31-ve) divided by total number of nucleated cells per FOV (6 FOV per section and 3 sections per heart). A dynamic change in the number of these CD105+ve presumed EPDCs was observed from E13.5 to E17.5 (Figure 3.11, C). The CD105+ve presumed EPDCs were first observed at E13.5 at a density of 1.1% myocardial cells and significantly increased in E15.5 hearts to 1.4% ( $p = 0.0012$ ) before dropping to 0.5% at E17.5 ( $p = <0.0001$ ). The analysis of E11.5 to E17.5 embryonic hearts showed that during development endoglin is expressed strongly by CD31+ve ECs and weakly in mesenchymal cells.

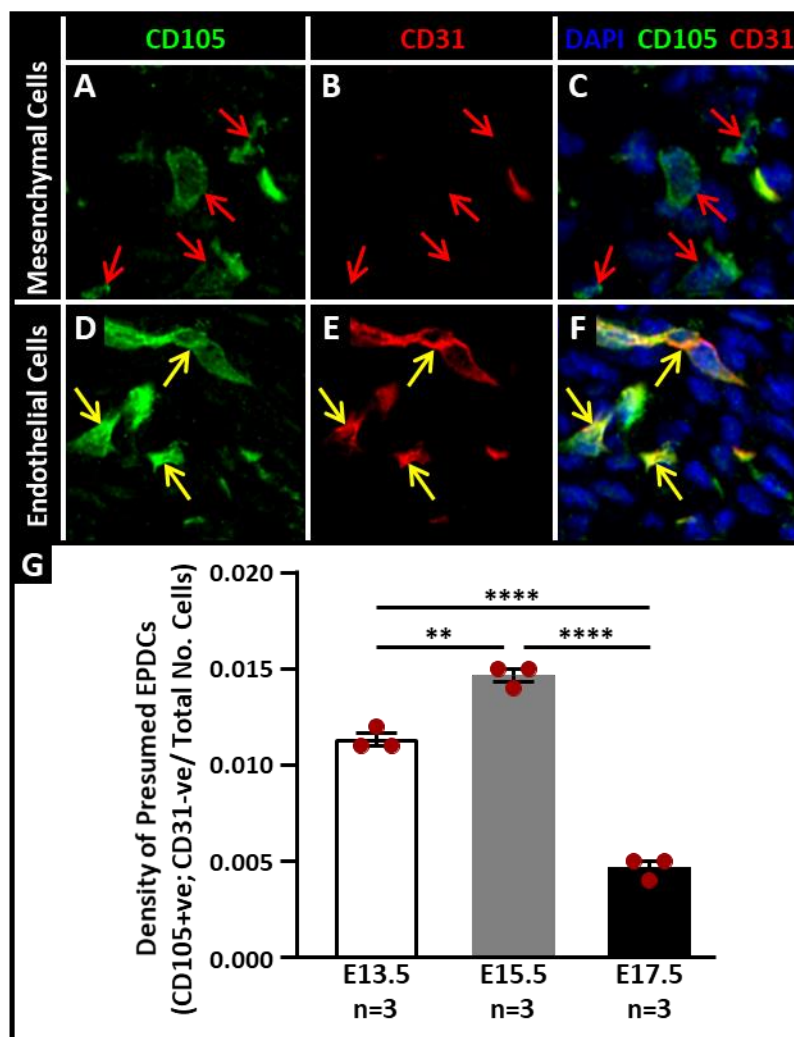


**Figure 3.11: The number of presumed EPDCs expressing low levels of endoglin peaks at E15.5 during mouse heart development.** E13.5 (n=3), E15.5 (n=3) and E17.5 (n=3) heart sections were stained with anti-CD105 (green) and anti-CD31 (red) antibodies. Nuclei stained with DAPI (blue). Digital zoomed split channel images of, (A-C) presumed EPDCs (CD31-ve cell with low levels of endoglin expression, red arrows) and (D-F) sub-epicardial ECs (CD31+ve cell expressing strong levels of endoglin, yellow arrows). (G) Quantification showing significantly increased and maximal density of presumed EPDCs at E15.5 ( $0.012 \pm 0.001$ , n=3) compared to E13.5 ( $0.015 \pm 0.001$ , n=3,  $p = 0.0012$ ) and with lowest density at E17.5 ( $0.005 \pm 0.001$ , n=3,  $p < 0.0001$ ). The density of presumed EPDCs was observed to significantly reduced at E17.5 compared to E13.5 ( $p < 0.0001$ ). Data shown as mean  $\pm$  SEM and analysed using one-way ANOVA (\*\*  $p < 0.01$  and \*\*\*\*  $p < 0.0001$ ). Abbreviations: ECs – Endothelial Cells and EPDCs – Epicardially Derived Cells.

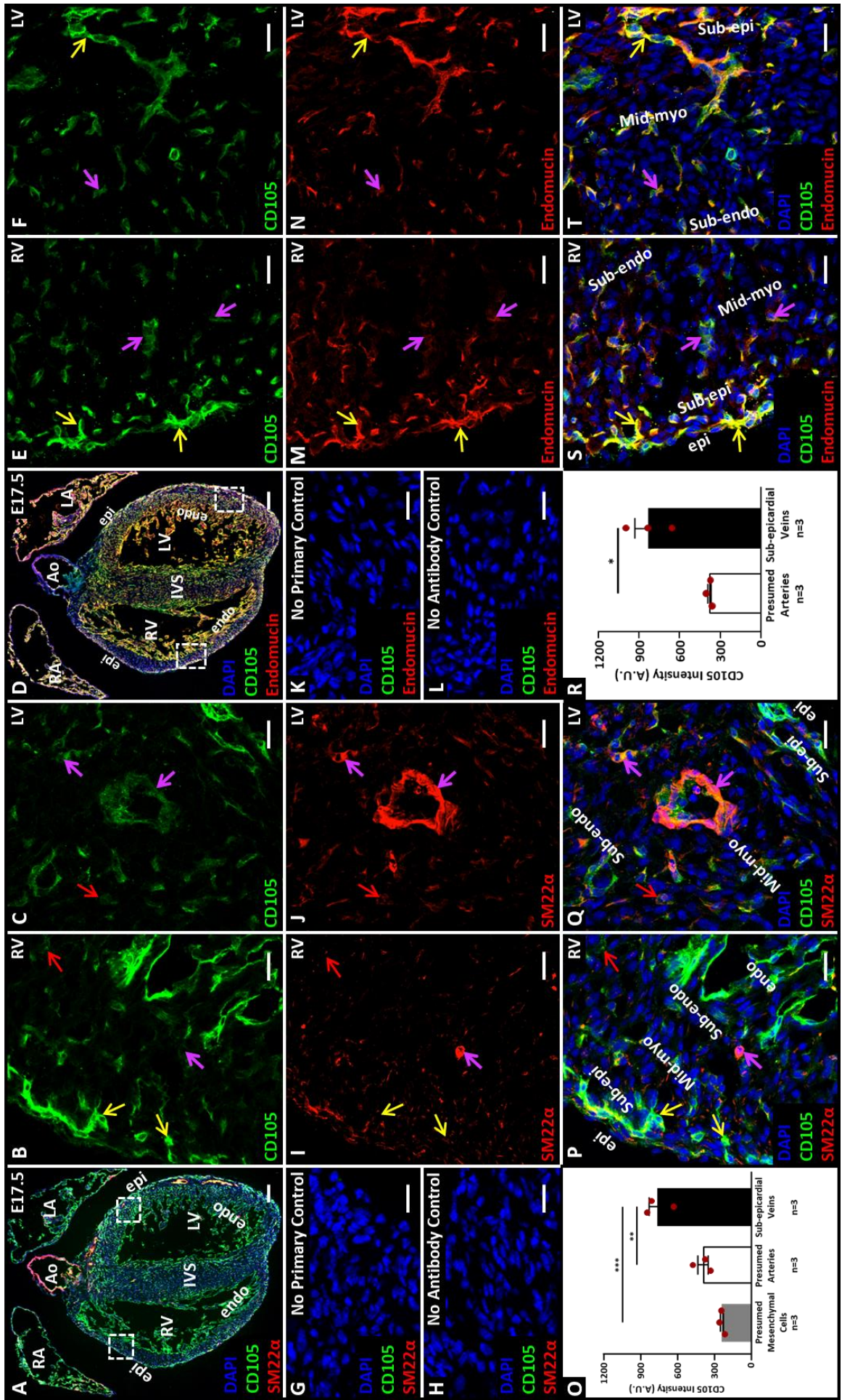
---

### 3.2.4. Endoglin Expression in Coronary Arteries, Veins and Capillaries

ECs of the coronary vessels in the sub-epicardium and sub-endocardium region of the heart at E17.5 expressed strong levels of endoglin while mid-myocardial coronary vessels express lower level of endoglin. As coronary arteries develop in the mid-myocardium region of the heart while coronary veins develop in the sub-epicardial and sub-endocardial region of the heart (43) this differential expression of endoglin could correspond to arterial and venous identity. Therefore, sister sections of the E17.5 hearts were stained to analyse whether this was the case. Furthermore, muscularisation of the arteries precedes the veins possibly due to increased pressure in arteries due to blood flow (256-258). Hence, SM22 $\alpha$  provides a useful marker to identify arteries (246-248).

The intra-myocardial vessels at E17.5 showed strong SM22 $\alpha$  staining (purple arrows, Figure 3.12, C,J,Q) whilst most of the sub-epicardial vessels were non-muscularised or have a very thin layer of vSMCs (yellow arrows, Figure 3.12, B,I,P). Conversely endomucin stains venous endothelium (245) and was therefore used to identify veins. At E17.5, sub-epicardial vessels showed strong expression of endomucin (yellow arrows, Figure 3.12, E,M,S) while mid-myocardial vessels showed weak endomucin expression (purple arrows, Figure 3.12, F,N,T). E17.5 heart sections stained with anti-CD105 and anti-SM22 $\alpha$  or anti-endomucin antibodies (Figure 3.12) revealed that endoglin was strongly expressed in venous ECs in the sub-epicardial region (yellow arrows, Figure 3.12), but expressed at significantly reduced levels in ECs of muscularised arteries in the mid-myocardium (purple arrows, Figure 3.12).

**Figure 3.12: At E17.5 endoglin is predominantly expressed within the endothelium of the coronary vessels and is expressed at higher levels in veins compared to arteries and presumed EPDCs.** Representative tiled images of E17.5 coronal heart sections stained with anti-CD105 (endoglin, green) and either with (A) anti-SM22 $\alpha$  [vSMCs (bright red) and mesenchymal cells (weak red)] or (D) anti-endomucin (veins & endocardium, red) antibodies. Nuclei stained with DAPI (blue). Split and merged channel images of RV (B,I,P) and LV (C,J,Q) walls showing reduced endoglin expression in the ECs of muscularised coronary vessels in the mid-myocardium, presumed arteries (purple arrows) compared to the ECs of non-muscularised vessels in the sub-epicardial region (yellow arrows), presumed veins. Low endoglin expressing presumed EPDCs with low levels of SM22 $\alpha$  were also observed throughout the myocardium at this stage of development (red arrows). (O) Mean endoglin fluorescent intensity analysis confirmed significantly increased endoglin expression in the sub-epicardial, non-muscularised “veins” ( $763.0 \pm 66.93$ ,  $n=3$ ) compared to the mid myocardial, muscularised “arteries” ( $393.2 \pm 42.08$ ,  $n=3$ ;  $p = 0.0039$ ). Endoglin expression was observed to be significantly lower in presumed EPDCs compared to “veins” ( $p = 0.0006$ ) and non-significantly lower than “arteries” ( $238.7 \pm 12.49$ ,  $n=3$ ;  $p = 0.1679$ ). Split and merged channel images of RV (E,M,S) and LV (F,N,T) wall showed strong endoglin expression in the ECs of sub-epicardial “veins” (strong endomucin expression, yellow arrows) while weak endoglin expression was seen in the ECs of mid-myocardium “arteries” (weak endomucin expressing, purple arrows). (R) Graphical display of fluorescence intensity measurements confirming significantly higher endoglin expression in the sub-epicardial “veins” ( $832.8 \pm 98.81$ ,  $n=3$ ) compared mid-myocardium “arteries” ( $380.4 \pm 13.56$ ,  $n=3$ ;  $p = 0.0105$ ). (G,K) No primary and (H,L) no antibody staining controls. Data shown as mean  $\pm$  SEM and analysed using two tailed unpaired t-test and one-way ANOVA (\*  $p < 0.05$  and \*\*  $p < 0.01$ ). Scale Bars: A & D – 200 $\mu$ m; B-D, E-F, G-N, P-Q & S-T – 20 $\mu$ m. Abbreviations: ECs – Endothelial Cells; endo – Endocardium; epi – Epicardium; EPDCs - Epicardially Derived Cells; IVS – Interventricular Septum; LA – Left Atria; LV – Left Ventricle; Mid-myo – Mid myocardium; RA – Right Atria; RV – Right Ventricle; Sub-endo – Sub-endocardium and Sub-epi – Sub-epicardium.



---

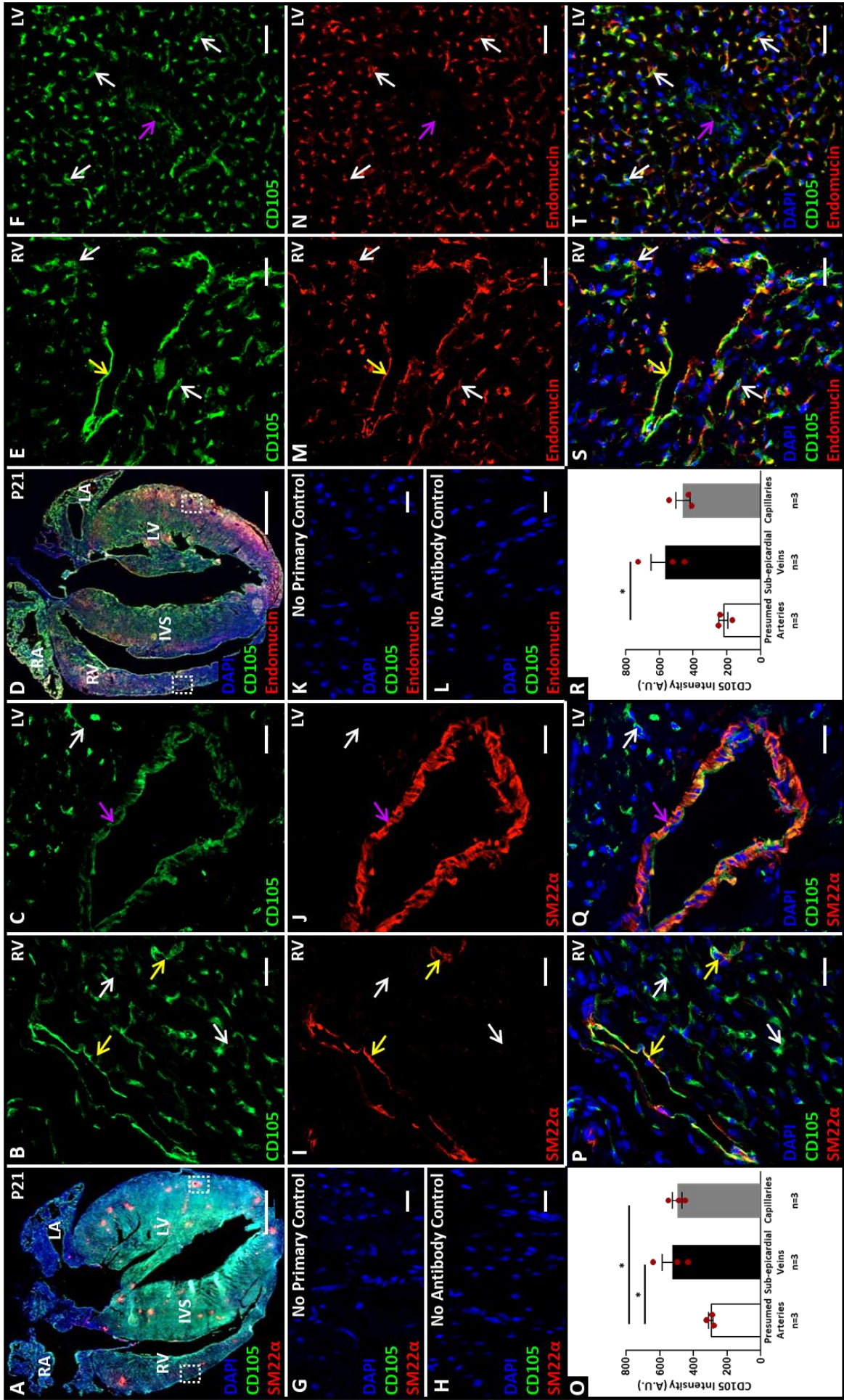
### 3.2.5. Expression of Endoglin in Postnatal Mice Hearts

Mouse heart development continues for 3wks in postnatal life (45). During this time the myocardium volumes increases significantly which in turn triggers the growth of the coronary vasculature (257). Interestingly, in post-natal and adult rodent hearts, arteries are still observed in the intra-myocardial space and veins are more superficially located in the sup-epicardial region (258).

To study the expression of endoglin at the final stages of heart development, coronal heart sections from P21 mice (n=3), were stained with rat anti-CD105 and anti-SM22 $\alpha$  antibodies. A tiled immunofluorescence image showed a typical P21 mice heart with thick ventricular myocardium with mature coronary vessels (Figure 3.13A). Mean fluorescent intensity analysis revealed strong endoglin expression in capillaries and in large sub-epicardial veins, identified by a flattened morphology and a thin vSMCs layer (Figure 3.13, I&P). In contrast, low endoglin expression was observed in highly muscularised intra-myocardial vessels (A to I, Figure 3.13). This endoglin expression pattern was similar to the one observed at E17.5 (Figure 3.12). Presumed EPDCs seen during the embryonic period (section 3.2.3, Figure 3.10) were not observed at P21.

To confirm this differential expression of endoglin in arteries, veins and capillaries, sister sections of P21 hearts were also stained with anti-endomucin and goat anti-CD015 antibody. Only sub-epicardial veins and intra-myocardial arteries were considered for quantification purposes. Mean endoglin fluorescence intensity analysis of high-power images of veins in the sub-epicardium showed strong expression of both endoglin and endomucin (yellow arrows, L-N Figure 3.13) while the intra-myocardial vessels (with big lumen) were negative for endomucin and expressed low levels of endoglin (purple arrows, Q-S Figure 3.13). Capillaries also showed strong expression of both endoglin and endomucin (44).

**Figure 3.13: Significantly higher endoglin expression is observed in ECs of coronary veins and capillaries compared to coronary arteries in P21 hearts.** Representative tiled image of P21 coronal heart sections stained with anti-CD105 (endoglin, green) and either with (A) anti-SM22 $\alpha$  (muscularised vessels, red) or (D) anti-endomucin (veins & endocardium, red) antibodies. Nuclei stained with DAPI (blue). Split and merged channel images of RV (B,I,P) and LV (C,J,Q) wall showed strong endoglin expression in the non-muscularised sub-epicardial veins (yellow arrows) and capillaries (white arrows) compared to muscularised intra-myocardial presumed arteries (purple arrows). (O) Quantification of fluorescent intensity showed significantly higher endoglin expression in ECs of sub-epicardial “veins” ( $523.6 \pm 61.37$ ,  $n=3$ ,  $p = 0.0211$ ) and capillaries ( $496.4 \pm 28.62$ ,  $n=3$ ,  $p = 0.0372$ ) compared to muscularised intra-myocardial “arteries” ( $297.8 \pm 13.05$ ,  $n=3$ ). Split and merged channel images of RV (E,M,S) and LV (F,N,T) wall showed endoglin expression in the ECs of non-muscularised sub-epicardial vein (endomucin positive, yellow arrows) and arteries (endomucin negative, purple arrows). Endoglin and endomucin expression was also observed in the capillaries (white arrows). (R) Fluorescent intensity measurements revealed significantly lower level of endoglin expression in intra-myocardial arteries ( $220.1 \pm 25.62$ ,  $n=3$ ) compared to ECs of sub-epicardial veins ( $567.4 \pm 83.74$ ,  $n=3$ ,  $p = 0.0139$ ) and non-significantly lower compared to capillaries ( $461.6 \pm 41.54$ ,  $n=3$ ,  $p = 0.0674$ ). The endoglin expression in sub-epicardial veins and capillaries were observed to be similar ( $p=0.6883$ ). (G,K) No primary and (H,L) no antibody staining controls. Data shown as mean  $\pm$  SEM and analysed using one-way ANOVA ( $*p < 0.05$ ). Scale Bars: A&D – Imm; B-C, E-F, G-N, P-Q & S-T – 20 $\mu$ m. Abbreviations: ECs – Endothelial Cells; IVS – Interventricular Septum; LA – Left Atria; LV – Left Ventricle; RA – Right Atria and RV – Right Ventricle.



---

### 3.2.6. Expression of Endoglin in Adult Mice Hearts

In adults, expression of endoglin was reported in the coronary capillaries (128, 216), but arterial and venous expression in the adult heart has not yet been established.

To distinguish between arteries and veins, coronal sections of 14-week hearts (n=3) were stained with anti-endomucin antibody (Figure 3.14) to identify veins. . In addition to this, several morphological characteristics are utilised to differentiate between arteries and veins. For instance arteries are known to be located deeper in the myocardial layer of mouse heart while veins are present in the sub-epicardial layer (258). Arteries also have thicker SMC layer compared to veins (259). Another distinct feature of arteries is presence of elastin, which is not found in veins (259). Therefore, a vein was only selected for quantification if it was: (i) located in the sub-epicardial region and had a visible lumen, (ii) showed no elastin auto-fluorescence and (iii) had thin or no vSMCs layer and are stained positive for endomucin (yellow arrows, Figure 3.14). To select an artery, the following criteria were used: (i) present in intra-myocardial space with visible lumen, (ii) presence of elastin auto-fluorescence in vessel wall and (iii) either possessed a thick vSMCs layer or was negative for endomucin (purple arrow, Figure 3.14).

Next, coronal sections of 14-weeks hearts were stained with anti-CD105 and anti-SM22 $\alpha$  or anti-endomucin antibodies. In a healthy adult mouse heart, expression of endoglin was observed to be restricted to the CD31 positive endocardium and ECs of coronary arteries, veins & capillaries (Figure 3.15), similar to P21 hearts (section 3.2.5, Figure 3.13) and the presumed EPDCs were absent, as expected.

Whole heart tiled immunofluorescence images showed a typical adult mouse heart with thick myocardium and a rich coronary vascular network (Figure 3.16, A&D). Mean endoglin fluorescent analysis of high-power images showed strong endoglin expression in the ECs of sub-epicardial non-muscularised and endomucin positive veins (yellow arrows, Figure 3.15) and capillaries (white arrows, Figure 3.15) compared to muscularised intra-myocardial arteries (purple arrows, Figure 3.15). There was approximately 50% reduction in the endoglin expression in the veins of adult hearts observed (Figure 3.13R) compared to P21 subepicardial veins (Figure 3.15R).

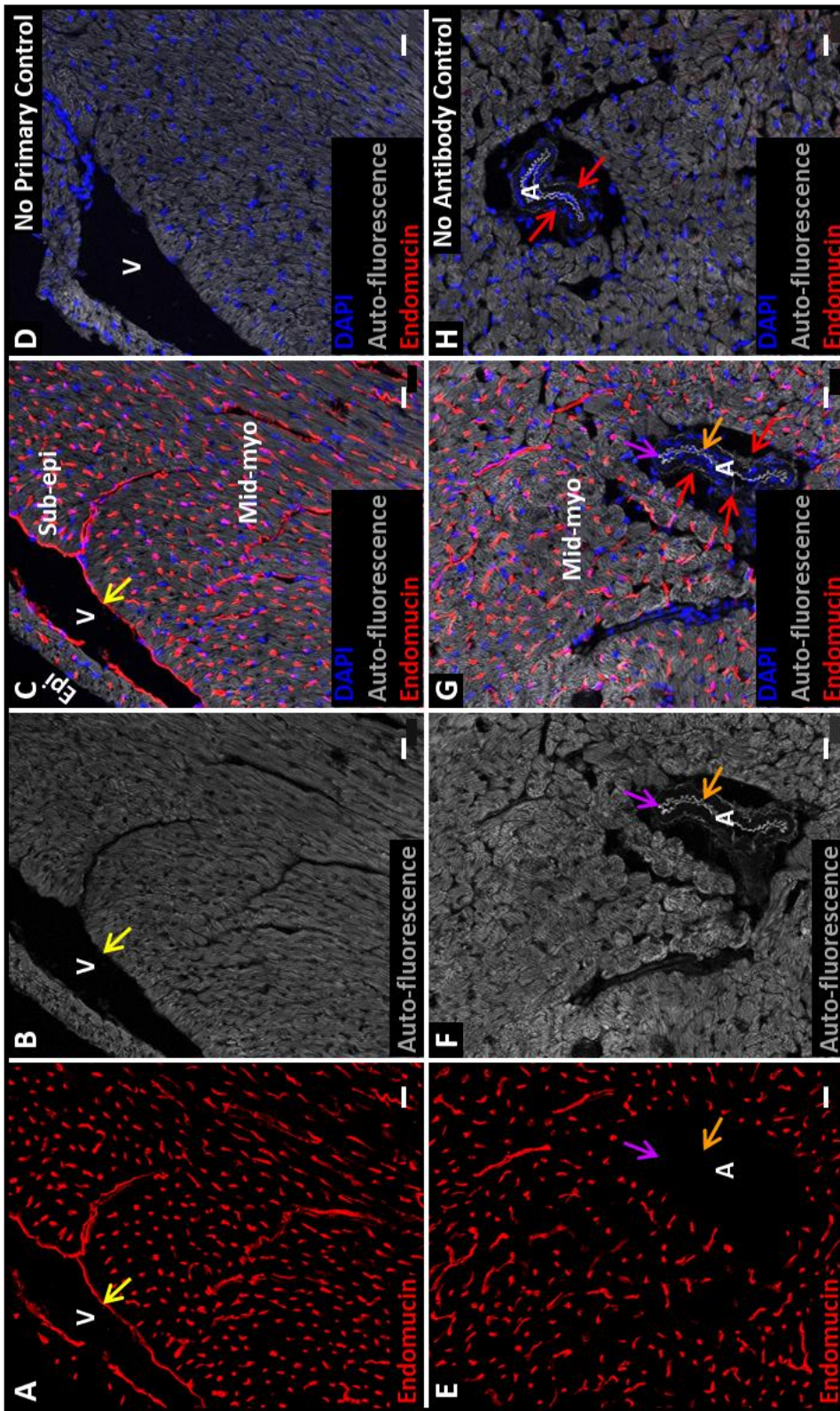
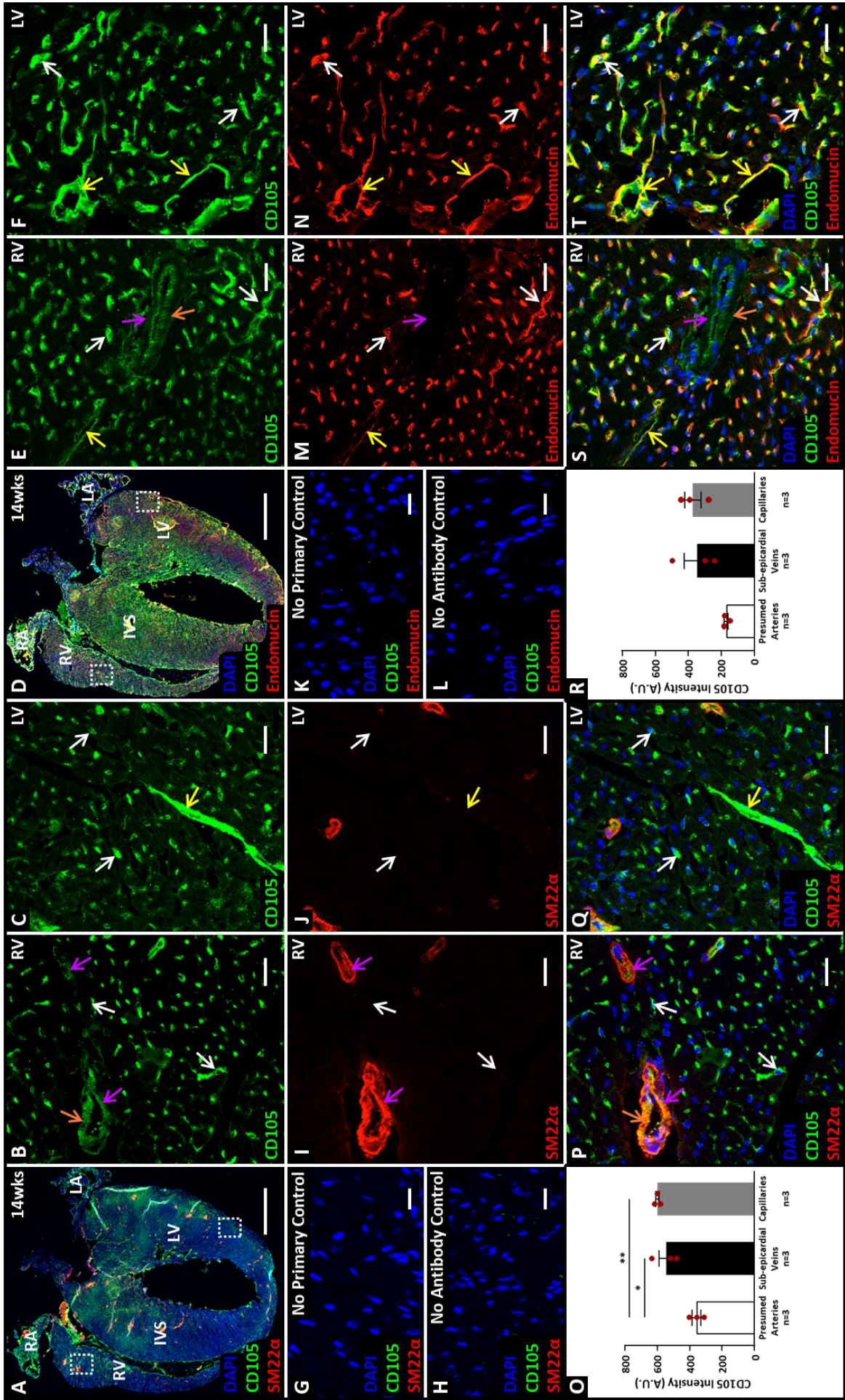


**Figure 3.14: Arteries and veins distinction in the adult heart using elastin auto-fluorescence and endomucin marker.** Adult heart section stained with anti-endomucin (red) to detect venous ECs and nuclei stained with DAPI (blue). Split channel images of an adult heart section showing example of (A-C) a sub-epicardial vein (endomucin positive, yellow arrow) and (E-G) a mid-myocardial artery (endomucin negative, purple arrow) selected for quantification. The sub-epicardial veins were observed here appear to be non-muscularised and devoid of elastin auto-fluorescence while mid-myocardial artery showed distinct elastin auto-fluorescence (orange arrows) and is possibly muscularised due the presence of multiple unstained nucleated cells (red arrows). (D) No primary and (H) no antibody staining controls. *Scale bars: A to H - 20µm. Abbreviations: A - Arteries; Epi - Epicardium; Mid-myo - Mid-myocardium Sub-epi - Sub-epicardium and V - veins.*

**Figure 3.15: In healthy adult mice heart, a higher level of endoglin is expressed by endothelial cells of coronary veins and capillaries in comparison to coronary arteries.** Representative tiled image of a 14wks coronal heart section stained with anti-CD105 (endoglin, green) and either with (A) anti-SM22 $\alpha$  (muscularised vessels, red) or (D) anti-endomucin (veins, red) antibodies. Nuclei stained with DAPI (blue). Split and merged channel images of RV (B,I,P) and LV (C,J,Q) wall showed lower levels of endoglin expression in the ECs of muscularised coronary arteries (purple arrows) with elastin auto-fluorescence (orange arrows) compared to the ECs of sub-epicardial non-muscularised veins (yellow arrows) and capillaries (white arrows). (O) Endoglin mean fluorescent intensity quantification showed significantly higher level of endoglin expression in ECs of sub-epicardial “veins” (545.8 $\pm$ 45.66,  $n=3$ ,  $p = 0.0164$ ) and capillaries (600.2 $\pm$ 11.42,  $n=3$ ,  $p = 0.0047$ ) compared to ECs of presumed intra-myocardial “arteries” (545.8 $\pm$ 45.66,  $n=3$ ). The expression of endoglin was observed to be similar in sub-epicardial “veins” compared to mid-myocardial “arteries” ( $p = 0.7948$ ). Split and merged channel images of RV (E,M,S) and LV (F,N,T) wall showed low levels of endoglin expression in the endomucin negative intra-myocardial arteries (purple arrows) with elastin auto-fluorescence (orange arrows) compared to the ECs of endomucin positive sub-epicardial veins (without elastin auto-fluorescence, yellow arrows) and capillaries (white arrows). (R) Fluorescent intensity quantification showed higher levels of endoglin expression in ECs of veins (346.5 $\pm$ 77.33,  $n=3$ ,  $p = 0.1801$ ) and capillaries (372.2 $\pm$ 49.36,  $n=3$ ,  $p = 0.1136$ ) compared to ECs of presumed “arteries” (171.9 $\pm$ 11.58,  $n=3$ ). The expression of endoglin was observed to be similar in veins and capillaries ( $p > 0.9999$ ). (G,K) No primary and (H,L) no antibody staining controls. Data shown as mean $\pm$ SEM and analysed using one-way ANOVA (\* $p < 0.05$ , \*\* $p < 0.01$ ). Scale Bars: A & J – 1000 $\mu$ m; B-D, F-J, L-N & P-T – 20 $\mu$ m. Abbreviations: ECs – Endothelial Cells; IVS – Interventricular Septum; LA – Left Atria; LV – Left Ventricle; RA – Right Atria; RV – Right Ventricle and Wks – Weeks.



---

### 3.3. Discussion

#### 3.3.1. Endoglin in Coronary Endothelial Cells

Prior to coronary vasculature development, endoglin expression is only observed in the endocardium of the heart (128, 137, 161). During this study, the expression of endoglin was consistently observed in the endocardium of all hearts analysed from embryo to adult. In addition, the coronary ECs (coECs) were observed to express endoglin from E11.5 (Figure 3.3) onwards throughout development (E13.5, Figure 3.4; E15.5, Figure 3.5 and E17.5, Figure 3.6), in post-natal (P21, Figure 3.13) and adult (Figure 3.15) mice hearts.

In the early stages of coronary vasculature development (E13.5, Figure 3.4 and E15.5, Figure 3.5), endoglin expression in all coECs was observed to be similar (Figure 3.16). These vessels could potentially be capillaries. As the development continues, the coronary vessels start to differentiate into arteries and veins. In this study, the earliest stage arterial and venous ECs could be differentiated was at E17.5 (Figure 3.12). As the ECs differentiate, the expression of endoglin in the arterial ECs in the mid-myocardial region was observed to decline (Figure 3.16). In contrast, endoglin expression in veins and capillaries remains high during coronary vessel development and begins to decline once heart development is complete [P21, (Figure 3.16)]. In adult heart, ECs express lower levels of endoglin but the endoglin expression in coronary veins and capillaries was still observed to be almost double than coronary arteries (Figure 3.16).

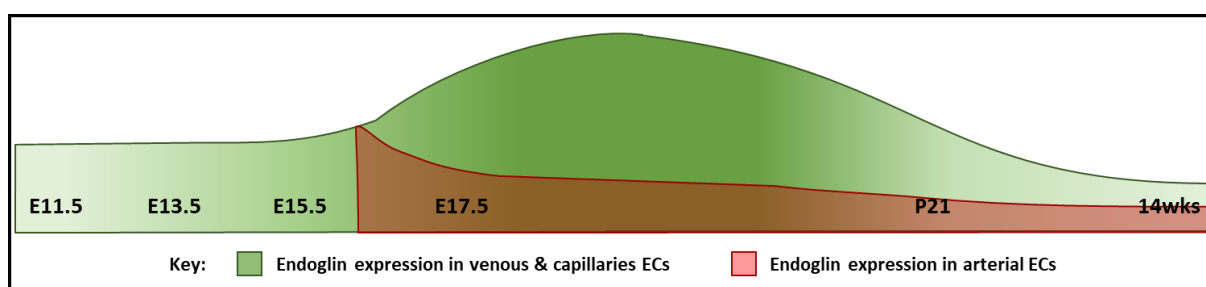


**Figure 3.16: Dynamic Expression of Endoglin in Coronary ECs throughout development and in adult hearts.** The expression of endoglin begins at similar level in all the coronary ECs at the beginning of coronary vasculature development (E11.5 to E15.5). However, as the ECs start to express arterial markers (E17.5), endoglin expression starts to decline in these arterial ECs, whereas in ECs of veins and capillaries, endoglin expression increases during the active phase of coronary vasculature development. Once the vasculature development is almost complete (P21), a decline in endoglin expression was observed in venous and capillaries ECs. In adult mice (14wks), the lowest amount of endoglin expression was observed in ECs, however, at this stage the expression of endoglin was still almost double in the venous and capillaries ECs compared to the arterial ECs.

Consistent with previous publications, quiescent arterial ECs in this study were observed to express low level of endoglin expression (215, 216). However, coronary veins expressed similar levels of endoglin as the surrounding capillaries. It is not clear why quiescent ECs of veins express higher levels of endoglin compared to arterial ECs. In the study by Laake *et al.* (216),

---

it was observed that mice heterozygous for endoglin expression showed reduced angiogenesis in the peri-infarct region of the heart. This reduced angiogenic response could be due to lack of endoglin not in all ECs but specifically due to loss of endoglin in venous ECs. During coronary vasculature development, the majority of coronary ECs arise from the sinus venosus ECs [(43, 44) and (discussed in section 1.3.2)], so potentially during an injury due to MI, coronary veins initiate the developmental like process again. Evidence from a recent publication by Dubé *et al.* (260), support this hypothesis. During development, the sinus venosus is a transient structure, however in adults, the coronary sinus veins act as the similar source. Using pulse-chase genetic lineage tracing in *Pdgf<sup>Cre-ERT2</sup>; Rosa26R<sup>eYFP</sup>* mice, Dubé *et al.* (260) showed, after a MI the heart structure changes to developing hyper-trabeculated state and the new vessels originate from coronary sinus and endocardium (260).

To test this hypothesis, it might be useful to study the angiogenic remodelling after a MI in mice lacking endoglin in venous ECs. To knockdown endoglin in venous ECs, a cre-loxP system would be a best approach but unfortunately a quiescent venous ECs specific Cre (e.g. driven by the EphB4 promoter) is not yet available for adult mice (261). Furthermore, it might also be useful to observe if other organs also display a similar endoglin expression pattern i.e. lower in arteries than in veins. For instance, in the study by Mahmoud *et al.* (141), endoglin expression was observed in the endothelium of the pulmonary veins and venules of adult mice. In contrast, endoglin expression was only observed in the ECs of arterioles but not in the ECs of pulmonary arteries (141).

### **3.3.2. Endoglin in Cardiac Mesenchymal Cells**

During embryonic development (E13.5 to E17.5), mesenchymal cells were also observed to express endoglin, previously shown in valvular mesenchymal cells (128, 239, 240), but here for the first time in EPDCs. Both valvular mesenchymal cells and presumed EPDCs expressed significantly lower levels of endoglin compared to endocardium and sub-epicardial endothelium (Figure 3.17). Consistent with their known dynamics, as initial epicardial cells undergoing EMT to generate mesenchymal cells at E13.5, that later differentiated into vSMCs or fibroblasts, these presumed EPDCs were only observed from E13.5 to E17.5 with the highest numbers present at E15.5 (Figure 3.10). However, in future studies it would be beneficial to confirm these cells as EPDCs by staining heart sections with a EPDCs specific markers potentially WT1 and RALDH2 (262).

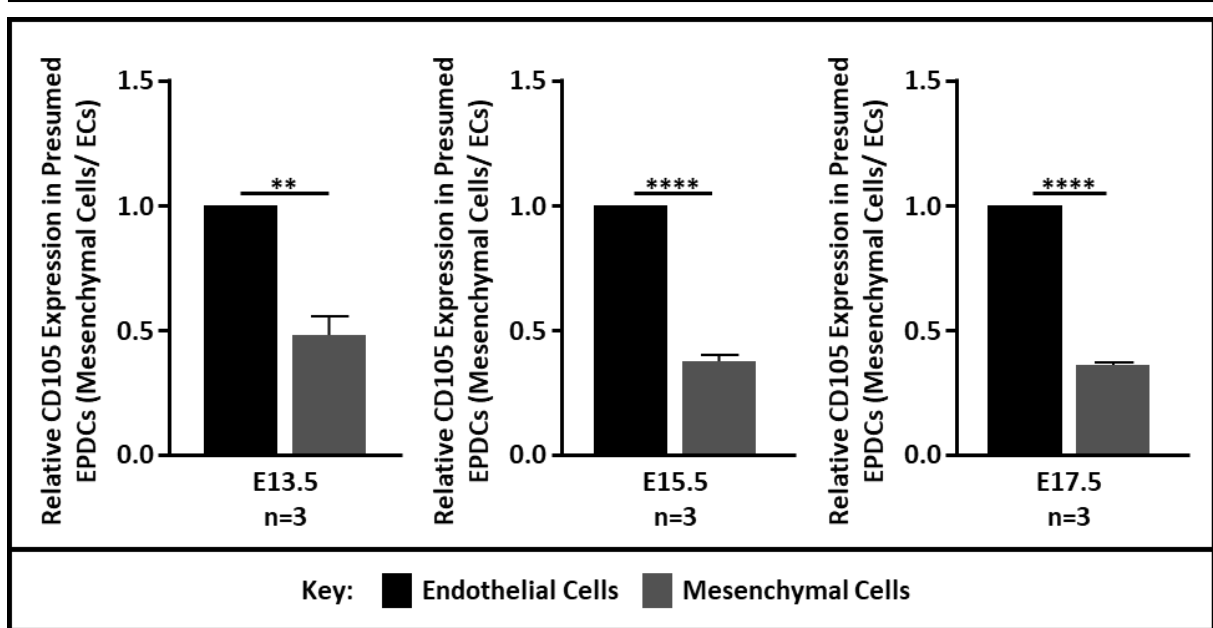


**Figure 3.17: Endoglin is strongly expressed in the coronary ECs compare to a weaker expression in the mesenchymal cells.** Endoglin is highly expressed in the coronary endothelium of E13.5, E15.5 & E17.5 developing hearts. In comparison to ECs, a significantly weaker endoglin expression was observed in the presumed EPDCs at respective ages (*E13.5: 0.480±0.072, n=3, p = 0.0019; E15.5: 0.373±0.0267, n=3, p = <0.0001 and E17.5: 0.357±0.0145, n=3, p = <0.0001*). Data shown as mean±SEM and analysed using two tailed unpaired t-test (\*\*  $p < 0.01$  and \*\*\*\*  $p < 0.0001$ ).

In conclusion, this chapter provides a comprehensive description of endoglin expression in developing and adult heart. Endoglin expression in presumed EPDCs suggests it may have a functional role which is the subject of the next chapter.

---

**Chapter 4. Role of Endoglin and  
TGF $\beta$ R2 in Epicardial Derived Cells during  
Heart Development**

---

## 4.1. Introduction

In the previous chapter, I analysed the relative expression of endoglin in three cell types during heart development: endocardial ECs, vascular ECs and mesenchymal cells, including presumed EPDCs. In this chapter, I investigate the role of endoglin and TGF $\beta$ R2 in EPDCs during development of the coronary vessels.

As described in section 1.3.1, the epicardium is the outer layer of the heart and by E10.5 whole heart is covered by epicardial cells (53). The epicardium is not in direct contact with the myocardium but separated by sub-epicardial space filled with ECM which is rapidly populated by EPDCs derived via EMT of epicardial cells (46). These EPDCs then start to invade the myocardium around E12.0 (54) and differentiate, primarily into vSMCs and fibroblasts (54, 70-75) with minor contribution towards ECs (43, 44, 73, 78, 79).

### 4.1.1. Endoglin and TGF $\beta$ Signalling in EMT

The role of some of the TGF $\beta$  ligands & their receptors have been studied in the epicardium using different Cre-loxP mouse lines [discussed in section 1.5.2 and summarised in Table 1.2]. TGF $\beta$  signalling is important during EMT of epicardial cells (60, 62, 68). For instance, epicardial cells fail to undergo TGF $\beta$  induced EMT *in vitro* after epicardial specific knockdown of *Alk5* (16). However, the role of the type 2 receptor (*Tgfr2*) and endoglin in epicardial cells has not yet been evaluated *in vivo*.

Sridurongrit *et al.* (60) showed that epicardial specific *Alk5* knockout (*Alk5-KO<sup>epi</sup>*) using the *Gata5-Cre* led to impaired myocardial growth due to defective SMCs support of the coronary vessels (60). They also observed that the epicardium was not attached properly over the myocardium and there were increased numbers of capillaries in the myocardium in *Alk5-KO<sup>epi</sup>* mutants compared to controls during late embryonic cardiac development (E17.5 and E18.0) potentially due to lack of larger muscularised vessels. *In vitro* analysis also showed that the EPDCs EMT process was disturbed in *Alk5-KO<sup>epi</sup>* mutants (60). During the signalling process ALK5 binds specifically with TGF $\beta$ R2 (263, 264). Therefore, knockdown of TGF $\beta$ R2 in epicardial cells could potentially results in a phenotype similar to *Alk5-KO<sup>epi</sup>* mutants. I tested this hypothesis in this study by using *Wt1<sup>Cre-ERT2</sup>* mouse line to knockout *Tgfr2* specifically in epicardial cells and EPDCs.

The TGF $\beta$  co-receptors type 3, endoglin were also shown to be necessary during the process of EMT in AV cushions. In chicks, endoglin protein and mRNA expression is present in the

---

endothelium (stage 16) and AV canal mesenchymal cells (stage 17) and OFT cushions (242). In mouse, expression of endoglin has been reported in the endothelium and AV cushions at E12.5 (137, 161). Analysis of E10.5 heart after global deletion of endoglin in mice showed hypocellular cardiac cushions (127, 128, 161). However, detailed analysis of these embryos was not possible as embryos die by mid-gestation.

*In vitro* studies using chick AV explants showed blocking endoglin with siRNA led to reduction in EMT markers including RhoA, slug and  $\beta$ -catenin as well as reduction in proliferative markers such as cyclin B2 and Id1. They also reported a significant reduction number of mesenchymal cells in AV explants (242). In the same study, a similar phenotype was observed in AV explants treated with siRNA and ALK5 specific inhibitor. This study further indicates that endoglin interacts with ALK5 to promote EMT as well as mesenchymal cell proliferation (242).

In another study by Nomura-Kitabayashi *et al.* (239), the role of endoglin in AV mesenchymal cells was studied *in vivo* in mice using chimeric endoglin knockout mice. They show that in chimeric endoglin knockout mice, very few endoglin negative endocardial cell underwent EMT and migrated into AV cushions at E10.5 compared to WT embryos. They further confirmed this role endoglin *in vitro* using AV canal explant culture on hydrated collagen gel (239) and showed reduced number of mesenchymal cells in endoglin null AV canal explants (63). They suggested that endoglin is potentially required to initiate EMT as the endoglin null endocardial cell interaction with surrounding cells was hindered (239). Furthermore, qPCR analysis of endoglin null hearts tissue showed significantly reduced levels of EMT promoter gene *Snai1* (239). *Snai1* is a transcription factor required for EMT (Figure 1.10) activated by TGF $\beta$  mediated signalling, so it is possible endoglin promotes EMT by promoting *Snai1* expression in EPDCs.

As seen in chapter 3, mesenchymal cells present in the myocardium express endoglin (Section 3.2.3, Figure 3.10) and are presumed to be epicardial in origin (EPDCs) for two reasons. Firstly, the location of these cells is similar to that of EPDCs (73, 265). Secondly, *in vitro* studies showed that human adult epicardial cells express endoglin in culture after EMT (64).

In the study by Bax *et al.* (64), cultured adult EPDCs after EMT attain a spindle like structure (similar to SMCs) and 73% were observed to express endoglin (64). Bax *et al.* (64) also showed the absence of endoglin led to a significant increase in epicardial markers ( $\beta$ -catenin, E-cadherin and VCAM-1) but did not block TGF $\beta$  mediated EMT. In this study, they suggested that endoglin is not directly involved during the EMT process but might play a role later in the mesenchymal cells or during EPDCs differentiation to cardiac cell types (64).

To date, no study has examined the expression and functional role of endoglin in EPDCs *in vivo*, which is the goal of this part of the current study. Considering the importance of endoglin in mesenchymal cell, migration proliferation and differentiation (64, 239, 242), it is possible similar process would be affected in the absence of endoglin in EPDCs *in vivo* (discussed in section 1.3.1.2). To study this,  $Wt1^{Cre-ERT2}$  was used in combination with endoglin floxed mice ( $Eng^{fl/fl}$ ) (266) to allow specific depletion of endoglin in  $Wt1^{Cre-ERT2}$  epicardial cells and EPDCs along with  $Rosa26^{eYFP}$  reporter mice (267) for lineage tracing.

## 4.2. Results

### 4.2.1. $Wt1^{Cre-ERT2}$ Optimisation and Lineage Tracing

To investigate the role of endoglin and  $Tgfb\beta 2$  in EPDCs during cardiac development *in vivo* the epicardial specific Cre transgenic mouse line  $Wt1^{Cre-ERT2}$  was used (81). The  $Wt1^{Cre-ERT2}$  is a widely used as an epicardial specific inducible Cre mouse line. To activate Cre-ERT2, tamoxifen is injected at specific a dose and time point. Zhou and Pu (253), also suggested that different reporter line could affect the recombination efficiency of  $Wt1^{Cre-ERT2}$  (Table 4.1). To ensure the  $Wt1^{Cre-ERT2}$  mice line was as effective as possible in activating Cre and could be used to target epicardial cells and their derivative EPDCs I first optimised Cre activation for  $Wt1^{Cre-ERT2}$  mouse line using a  $Rosa26^{eYFP}$  reporter mouse line both in C57Bl/6 background mice.

**Table 4.1: Combinations of  $Wt1^{Cre-ERT2}$  with different Cre-Activated Rosa26 Reporters from different genetic background [adapted from (253)]**

Reporter	Observations	Pitfalls
$Rosa26^{Lz-Orkin}$	Inefficient Cre recombination after tamoxifen injection.	Low labelling efficiency.
$Rosa26^{Lz-Soriano}$	Moderately efficient Cre recombination with one dose of tamoxifen between E9.5-E11.5.	Endothelial labelling if induced Tam treatment performed at E14.5 or P4. Late gestational Tam toxicity and failure to yield live pups.
$Rosa26^{mTmG}$	Moderately efficient Cre recombination with one dose of tamoxifen between E9.5-E11.5.	Endothelial labelling if induced Tam treatment performed at E14.5 or P4. Late gestational Tam toxicity and failure to yield live pups.

#### 4.2.1.1. $Wt1^{Cre-ERT2}$ Optimisation

The  $Wt1^{Cre-ERT2}$  mouse line has been extensively studied and when Cre is activated with tamoxifen between E9.5 to E11.5, the activation is specific to the epicardium as most of the  $Wt1$  expressing cells are located in the proepicardium and epicardium but not in the myocardium (81, 253). Therefore, to test the  $Wt1^{Cre-ERT2}$  activation labelling efficiency and reproducibility,  $Wt1^{Cre-ERT2}$  was activated in three different ways in pregnant females using 1mg tamoxifen (tam) dose per injection (Figure 4.1). The three groups were: (i) two subcutaneous

(subcut) tamoxifen injections on E9.5 and E10.5; (ii) three subcut tamoxifen injections from E9.5 to E11.5 and (iii) three intra-peritoneal (IP) tamoxifen injections from E9.5 to E11.5.

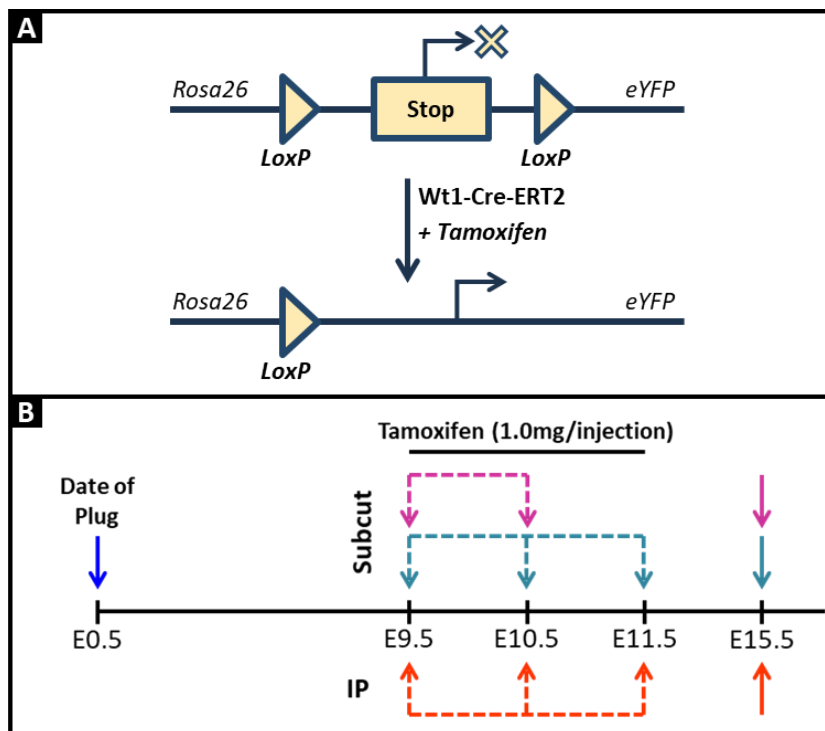


**Figure 4.1: Analysis of  $Wt1^{Cre-ERT2}$  activity using  $Rosa26^{eYFP}$  reporter.** (A) To test different doses and sites of tamoxifen injections to activate  $Wt1^{Cre-ERT2}$ , a male mouse with heterozygous expression of  $Wt1^{Cre-ERT2/+}$  and homozygous expression of  $Rosa26^{eYFP/eYFP}$  was crossed with a  $Rosa26^{eYFP/eYFP}$  female mouse. In the presence of tamoxifen Cre-ERT2 is activated and removes a stop sequence which in turn leads to expression of eYFP in all  $Wt1$  positive cells and their daughter cells. (B)  $Wt1^{Cre-ERT2}$  is activated by tamoxifen injection in three different strategies: (i) two subcut injection at E9.5 & E10.5 (pink arrows); (ii) three subcut injections from E9.5 to E11.5 (light blue arrows) and (iii) three IP injections from E9.5 to E11.5 (orange arrows). The embryos were harvested from all three different groups are E15.5 stage of development.

The embryos from all three groups were harvested at E15.5 stage of development, fixed in 4% PFA, embedded in paraffin (section 2.2.1) and sectioned into sister sections (section 2.4.1). These sections were then stained using anti-GFP antibody to detect eYFP protein following IHC-DAB protocol (Section 2.5.2) and imaged using bright-field setting on M2 axio-imager (section 2.10.2). A minimum of three embryos from the same litter were stained for each group to test intra-litter variability and 5 sections per embryo were imaged. The quantification of data was done using the event function of Zen 2012 software. Analysis of low power tiled images of whole hearts showed strong expression of eYFP in epicardial cells of all three groups (Figure 4.2, black arrows).

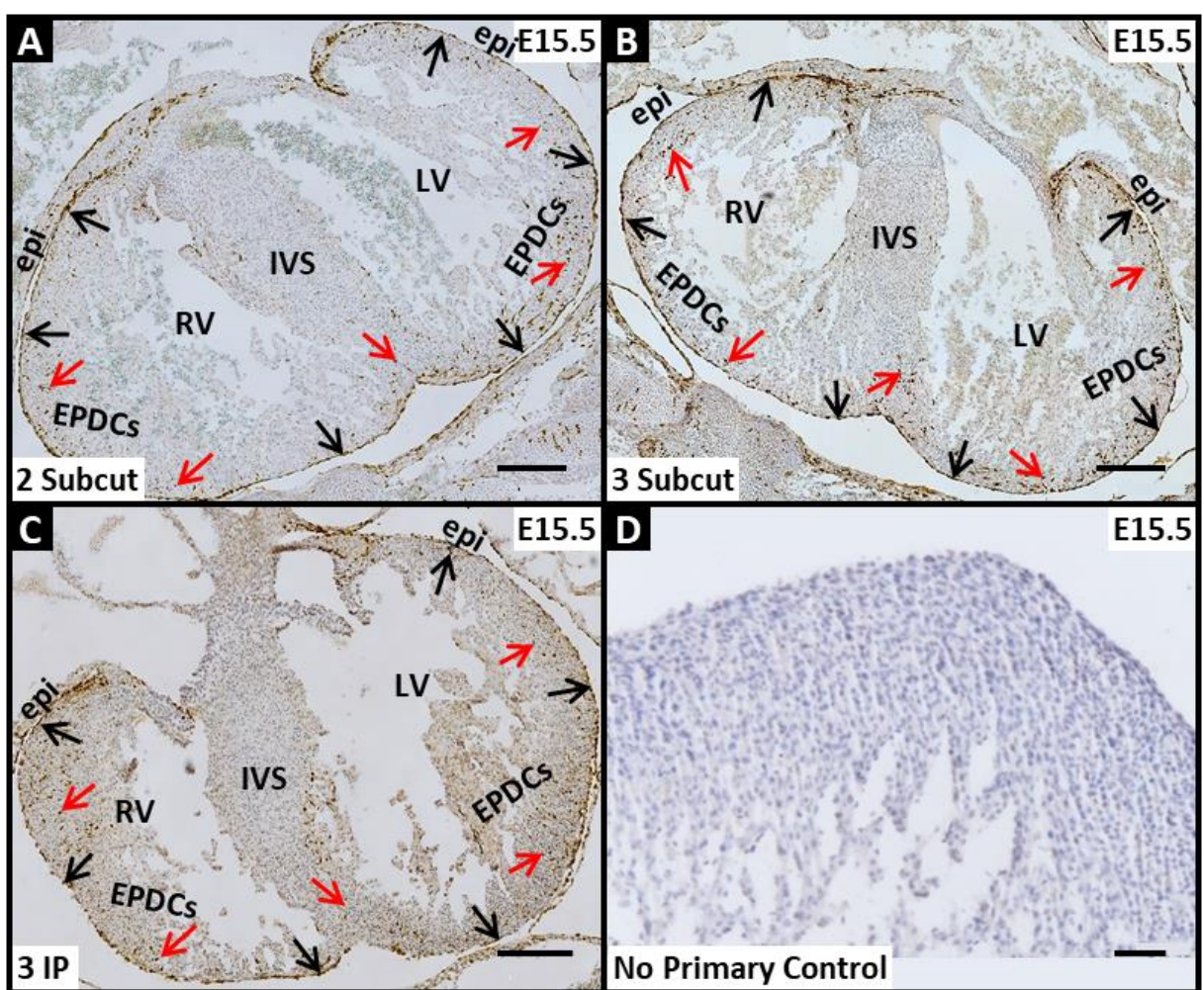
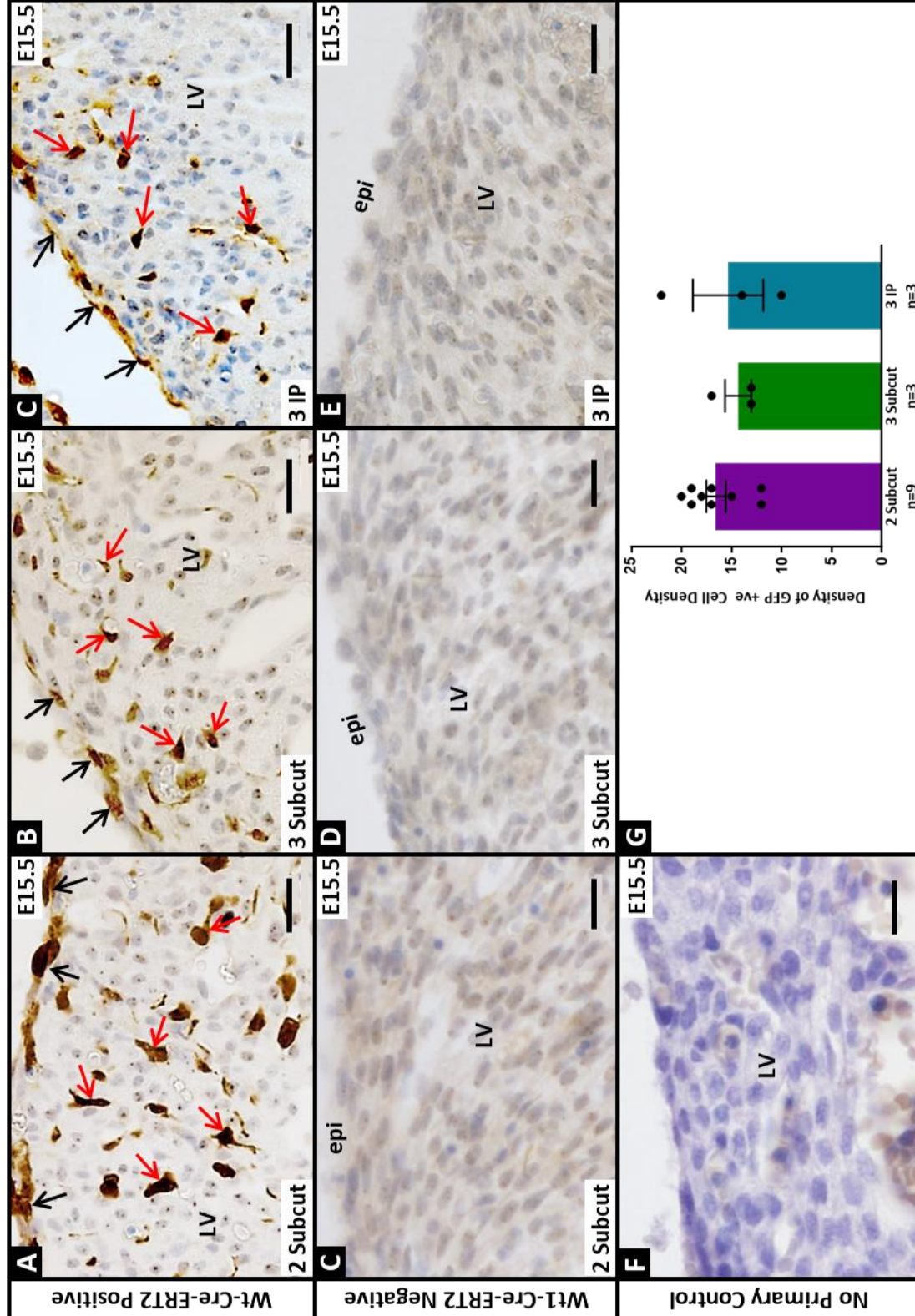


**Figure 4.2: Strong eYFP expression was observed in the epicardium and in the EPDCs after activation of  $Wt1^{Cre-ERT2}$ .** IHC-DAB tiled images of E15.5 hearts stained with anti-GFP antibody to detect eYFP protein (brown). Activation of  $Wt1^{Cre-ERT2}$  via (A) 2 Subcut (E9.5 and E10.5, n=9), (B) 3 Subcut (E9.5 to E11.5, n=3) and (C) 3IP (E9.5 to E11.5, n=3) tamoxifen injections (1mg/injection) led to similar levels of expression of eYFP in epicardial (black arrows) and EPDCs (red arrows) in three groups. (D) No primary antibody staining control. Abbreviations: epi – epicardium; EPDCs – Epicardially Derived Cells; IP – Intraperitoneal; IVS - Interventricular Septum; LV - Left Ventricle; RV - Right Ventricle and Subcut – Subcutaneous. Scale Bar: A to C = 200 $\mu$ m and D = 50 $\mu$ m.

Next, the number of GFP labelled EDPCs (eYFP<sup>+ve</sup> EPDCs) were compared between the three groups. Quantification of higher power images of the free ventricle walls (RV and LV) showed a similar density of eYFP<sup>+ve</sup> EPDCs in all three groups (Figure 4.3E).

**Figure 4.3:  $Wt1^{Cre-ERT2}$  activation to detect EPDCs in the hearts of E15.5  $Wt1^{Cre-ERT2}; Rosa26^{eYFP/eYFP}$  embryos.** IHC-DAB staining on  $Wt1^{Cre-ERT2}$  positive and  $Wt1^{Cre-ERT2}$  negative E15.5 hearts stained with anti-GFP antibody to detect eYFP (brown) protein. Activation of  $Wt1^{Cre-ERT2}$  by (A) 2 Subcut (E9.5-E10.5, n=9), (B) 3 Subcut (E9.5-11.5, n=3) and (C) 3 IP (E9.5-E11.5, n=3) tamoxifen injections (dose = 1mg/ injection) led to strong eYFP expression in both epicardium (black arrows) and EPDCs (red arrows) at E15.5. (D-F) No eYFP expression was seen in littermate  $Wt1^{Cre-ERT2}$  negative embryos. (G) No primary antibody staining control. (H) Quantification showed similar density of  $GFP^{+ve}$  epicardial cells per FOV in all three groups (2 Subcut:  $16.56 \pm 0.988$ , n=9; 3 Subcut:  $14.33 \pm 1.333$ , n=3 and 3 IP:  $15.33 \pm 3.528$ , n=3). Data shown as mean  $\pm$  SEM and analysed using one-way ANOVA. Abbreviations: EPDCs – Epicardially Derived Cells; IP – Intraperitoneal; LV – Left Ventricle and Subcut – Subcutaneous. Scale bar: A to



To compare all three groups, the density of eYFP<sup>+</sup> EPDCs was calculated per FOV from higher power images. The eYFP<sup>+</sup> EPDCs density was calculated from four FOV per section (Boxed regions 1, 3, 4 & 6, Figure 4.4) and three sections with four chamber view were analysed from each heart. Each section analysed were at least 50µm apart to avoid duplicate cell counting.

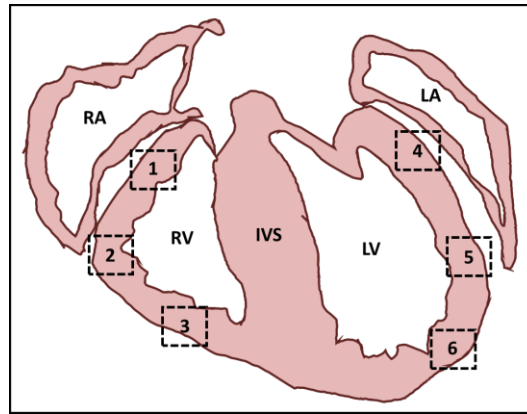


**Figure 4.4: Cartoon image of transverse section of an embryonic heart section.** For quantification, higher power images were taken from free wall of RV and LV around the dotted white boxed region. *Abbreviation: RA – Right Atria; RV – Right Ventricle; LA – Left Atria; LV – Left Ventricle and IVS – Inter Ventricular Septum.*

The quantification showed similar density of eYFP<sup>+</sup> EPDCs per FOV in all three groups (Figure 4.3 and summarised in Table 4.2). Thus, activation of *Wt1*<sup>Cre-ERT2</sup> using any of three strategies leads to a similar number of YFP labelled epicardially derived cells. During this study, I also analysed *Wt1*<sup>Cre-ERT2</sup> negative embryos for each group (n=3/ group) to ensure the *Wt1*<sup>Cre-ERT2</sup> specificity. Analysis of *Wt1*<sup>Cre-ERT2</sup> negative embryos showed no eYFP expression in any cell types (Figure 4.3, C-E), confirming the no *Wt1*<sup>Cre-ERT2</sup> activity in the absence of cre.

**Table 4.2: The activation of *Wt1*<sup>Cre-ERT2</sup> using three different tamoxifen regimes (2 Subcut, 3 Subcut & 3 IP) showed a similar density of eYFP positive EPDCs at E15.5.**

	2 Subcut Tam on E9.5 & E10.5	3 Subcut Tam from E9.5 to E11.5	3 IP Tam from E9.5 to E11.5
N	9	3	3
No. of Litters	3	1	1
Total No. of eYFP <sup>+</sup> EPDCs per FOV	27 ± 2	27 ± 3	29 ± 3
Total No. of Nucleated Intra-myocardial Cells per FOV	165 ± 5	183 ± 9	199 ± 25
Proportion of eYFP <sup>+</sup> EPDCs per myocardial cell	16% ± 1%	15% ± 1%	16% ± 4%
Total No. of eYFP <sup>+</sup> Epicardial Cells per FOV	60 ± 4	Detailed Analysis not performed	Detailed Analysis not performed
Total No. Nucleated Epicardial Cells per FOV	79 ± 4		
Proportion of Epicardial Cells that are eYFP <sup>+</sup>	75% ± 2%		
Heart Development	Normal	VSD in 2 out of 6 hearts (1 cre <sup>+</sup> & 1 cre <sup>-</sup> )	Normal
<i>The above analysis was performed on 4 FOV per section and 3 sections were analysed per heart.</i>			

---

Moving forwards, the ‘2-subcut’ injection method for Cre activation was chosen for following reasons: (i) all three groups showed similar eYFP labelling efficiency (Table 4.2); (ii) IP injections risk injection of tamoxifen directly into the uterus; (iii) higher doses of tamoxifen can cause developmental defects due tamoxifen toxicity (268, 269). In the current study, VSD was observed in 2 out of 6 hearts (1 cre<sup>+ve</sup> and 1 cre<sup>-ve</sup>) from the 3 subcut tam injection group (Table 4.2), which was potentially due to tamoxifen toxicity. In contrast, no developmental defects were observed in the other two groups.

To ensure the 2 subcut method led to efficient epicardial labelling a quantitative analysis was performed. The percentage epicardial labelling efficiency was calculated by counting total number of epicardial cells and eYFP<sup>+ve</sup> epicardial cells (identified as cells displaying thin morphology on the surface of the heart). The analysis showed an average of 75% of epicardial cells were eYFP<sup>+ve</sup> after 2 subcut tam injections (Table 4.2). This is moderately high efficiency and has been considered sufficient for most fate mapping studies (253).

#### **4.2.1.2. *Wt1*<sup>Cre-ERT2</sup>: Lineage Tracing**

As mentioned in Section 1.3.1.2, epicardial cells significantly contribute to smooth muscle and fibroblasts cell population in the developing heart via EMT of EPDCs (54, 70-75) but only a minor contribution towards coronary ECs (43, 44, 73, 78, 79) and cardiomyocytes (78, 80, 81). Before addressing the role of endoglin in EPDCs, I first established the EPDCs contribution towards these different cell types (SMCs, fibroblasts, ECs and cardiomyocytes) at E17.5 using lineage tracing and my optimised protocol to activate *Wt1*<sup>Cre-ERT2</sup>.

Three *Wt1*<sup>Cre-ERT2</sup>; *Rosa26*<sup>eYFP</sup> positive embryonic hearts were analysed at E17.5 from two different litters. The E17.5 embryonic hearts were fixed in 0.2% PFA, embedded in OCT (section 2.2.2) and sectioned into sister sections (section 2.4.2). The sections were then subjected to optimised double immunofluorescence staining described in section 2.5.4 using the antibodies shown in Table 4.3 and imaged using fluorescence setting in M2 axio-imager microscope. Two different anti-GFP antibodies (to detect eYFP protein) were used during the current study due to compatibility issues with the SMCs and fibroblasts marker. The images were taken from six different regions of free ventricle walls (Figure 4.4), from five different sections (50µm apart) per embryo and from three embryos.

**Table 4.3: Antibodies used to for lineage tracing of EPDCs after activation of  $Wt1^{Cre-ERT2}$  using the optimised protocol. Antibodies details are summarised in Table 2.8.**

Antibody	Target protein	Raised In	Specificity within Heart
Anti-GFP	GFP	Chicken/ Rabbit	YFP Positive EPDCs
Anti-CD31	PECAM1	Rat	ECs & Endocardium (244)
Anti-SM22 $\alpha$	TAGLN	Rabbit	vSMCs (246-248) & Mesenchymal Cells (249)
Anti-Vimentin	Fibroblasts	Chicken	Fibroblasts and Mesenchymal Cells (270)
Anti-MF20	Cardiomyocytes	Mouse	Cardiomyocytes (271-274)
Anti $\alpha$ -Actinin	Cardiomyocytes	Mouse	Cardiomyocytes (275)

To analyse the contribution of EPDCs towards different cardiac cells, co-localisation between anti-GFP and cell specific markers were analysed. The immunofluorescence analysis showed differentiation of eYFP<sup>+</sup> EPDCs into vSMCs (Figure 4.5, A-C, white arrows), fibroblasts ((Figure 4.5, E-G, white arrows) and ECs ((Figure 4.5, I-K, white arrows) as expected (section 1.3.1.2). At E17.5, a few low Sm22 $\alpha$  expressing mesenchymal cells were also observed (Figure 4.5, A-C, yellow arrows). During this study, to verify the contribution of epicardial cells towards cardiomyocytes, heart sections were stained with two different cardiomyocyte markers, MF20 ((Figure 4.5, M-O) and  $\alpha$ -Actinin (data not shown). However, none of the cardiomyocytes were observed to be from  $Wt1^{+ve}$  epicardial origins.

I next calculated percentage contribution of eYFP<sup>+</sup> EPDCs towards these cardiac cell types (Table 4.4). As expected, the majority of EPDCs were observed to differentiate into vSMCs (17%  $\pm$ 1.15) or fibroblasts (22%  $\pm$ 2.33). While, 6%  $\pm$ 1.33 of EPDCs differentiated into EC (3% of total ECs). This data is consistent with previous publications showing majority of vSMCs and fibroblasts arise from epicardial cells (54, 70-75) while only a minor amount differentiate into ECs (43, 44, 73, 78, 79). In contrast to the previous studies (78, 80, 81), no contribution towards cardiomyocytes was observed. At E17.5, 38%  $\pm$ 2.40 EPDCs appeared to be undifferentiated according to the marker panel used (Table 4.3). These undifferentiated EPDCs are predicted to eventually differentiate into cardiac cell types (vSMCs, fibroblasts or ECs) as the heart development continues into post-natal life. This percentage contribution of EPDCs towards different lineages (Table 4.4) was next used as the baseline to determine whether this differentiation process is affected after epicardial specific *endoglin* or *Tgfbr2* knockdown.

**Figure 4.5:  $Wt1^{Cre-ERT2}$  lineage tracing using the optimised activation protocol.** E17.5 hearts stained with anti-GFP antibody (green) and cell specific markers (red) to detect either SMCs (anti-SM22 $\alpha$ ), fibroblasts (anti-vimentin), ECs (anti-CD31) or cardiomyocytes (MF20).

The eYFP positive EPDCs arising from the  $Wt1^{Cre-ERT2}$  positive epicardial cells were observed to differentiate into (A-C) vSMCs (white arrows, n=3), (E-G) fibroblasts (white arrows, n=3) and (I-K) ECs (white arrows, n=3). (M-O) During this study, none of cardiomyocytes originate from eYFP positive EPDCs. At E17.5, a few single eYFP positive cells with weak SM22 $\alpha$  expression (A-C, yellow arrows) were also observed. These are possibly undifferentiated mesenchymal cells. (D,H,L,P) No primary staining controls. Abbreviations: ECs – Endothelial Cells; EPDCs – Epicardially Derived Cells and vSMCs – Vascular smooth muscle cells. Scale bars: A-P – 20 $\mu$ m.

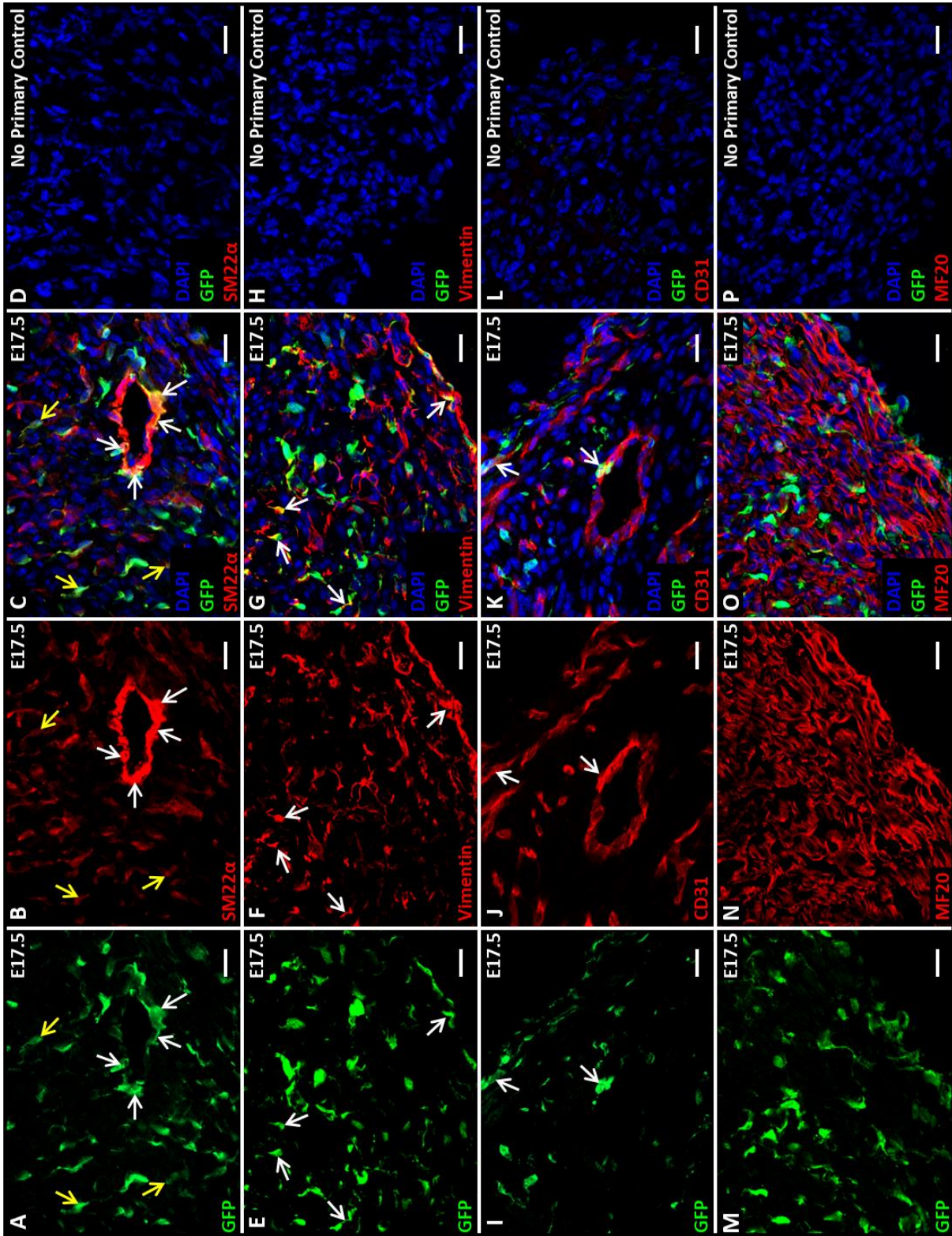


**Table 4.4: EPDCs differentiation into Cardiac Cell Types at E17.5**

Cell Type	Percentage of EPDCs Differentiating to Cardiac Cell Types
vSMCs	17% ± 1.15
Mesenchymal Cells (SM22 $\alpha$ )	17% ± 2.03
Fibroblasts	22% ± 2.33
ECs	6% ± 1.33
Cardiomyocytes	0% ± 0
Undifferentiated EPDCs	38% ± 2.40

#### 4.2.2. Expression of Endoglin in EPDCs *in vivo*

To knockout endoglin in epicardial cells the  $Eng^{fl/fl}; Wt1^{Cre-ERT2}; Rosa26^{eYFP}$  mouse line was used (Figure 4.6B) and  $Wt1^{Cre-ERT2}$  was activated using the optimised protocol (2 subcut tam injections at E9.5-E10.5). Embryos were harvested at E15.5 for analysis as most of the endoglin expressing presumed EPDCs were observed at this stage of development (Figure 3.11).

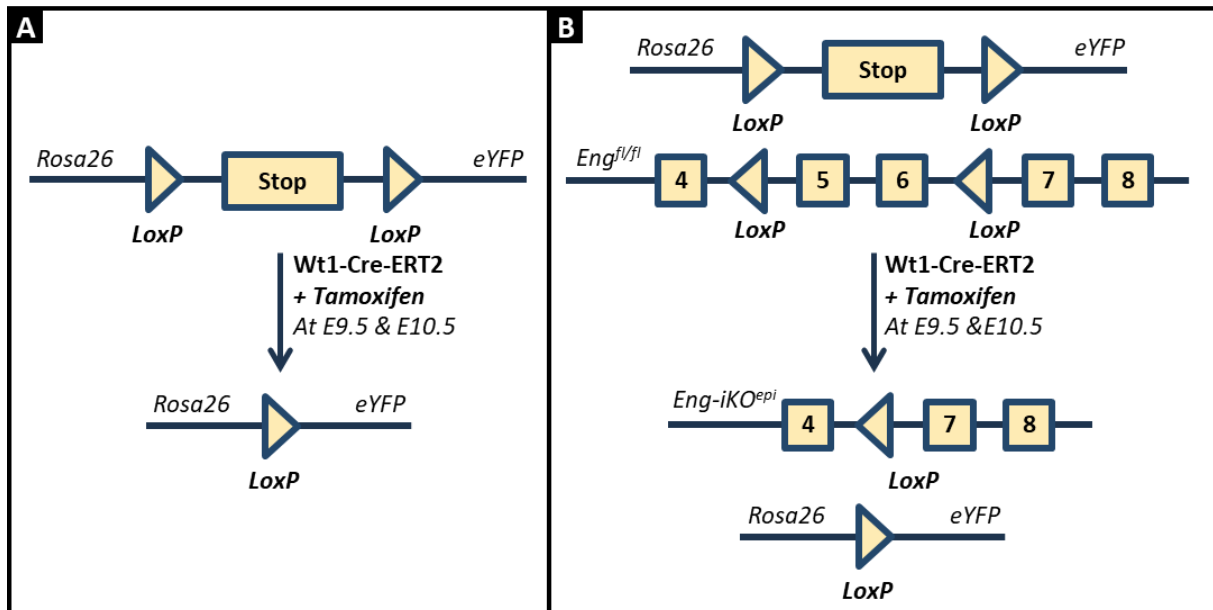


**Figure 4.6: Mouse lines used to study and knockdown the expression of endoglin in epicardium and EPDCs *in vivo*.** (A) To verify the expression of endoglin in EPDCs *in vivo*, embryos were harvested at E15.5 using the  $Wt1^{Cre-ERT2/+}; Rosa26^{eYFP/eYFP}$  mouse line. (B) To knockout endoglin gene in  $Wt1^{+ve}$  cells,  $Eng^{fl/fl}; Wt1^{Cre-ERT2/+}; Rosa26^{eYFP/eYFP}$  mouse line was used. In both lines a Cre-negative female was mated with a Cre-positive male to avoid possible effects of Cre activation on the pregnant mother, and limit Cre activity to the developing embryos.  $Wt1^{Cre-ERT2}$  was activated by injecting tamoxifen at E9.5 and E10.5 via subcut route (in scruff) and embryos were harvested at E15.5.

The E15.5 embryonic hearts were fixed in 0.2% PFA, embedded in OCT, sectioned into sister sections and stained using double immunofluorescence protocol with rat anti-CD105 and chicken anti-GFP antibodies. In each immunofluorescence experiment, the control ( $Wt1^{Cre-ERT2/+}; Rosa26^{eYFP/eYFP}$ ) and epicardial-specific inducible endoglin knockout ( $Eng^{fl/fl}; Wt1^{Cre-$

$ERT2^{+/+}; Rosa26^{eYFP/eYFP}$ , Eng-iKO<sup>epi</sup>) hearts were stained simultaneously and were compared with each other. Once stained, images were taken from free RV & LV wall per section (1-6 boxed region, Figure 4.4) from 5 sections imaged per embryo and 3 embryos were analysed per group. To validate the expression of endoglin in EPDCs *in vivo*, z-stack imaging was performed using fluorescence setting on M2 axio-imager microscope with an apotome at x63 magnification. The z-stack imaging allows confirmation of the expression of a marker in a cell in all three planes (X-Y, X-Z and Y-Z, Figure 4.7A). This helps to verify that expression of both makers (GFP and CD105) are expressed by same cell and not by two different cells either stacked on top of each other or next to each other (Figure 4.7B). To remove any observer bias during quantification, data was blinded prior to analysis.

The z-stack image analysis on control embryos ( $Wt1^{Cre-ERT2^{+/+}}; Rosa26^{eYFP/eYFP}$ ) at E15.5 confirmed that EPDCs do express endoglin *in vivo* (Figure 4.8) consistent with *in vitro* study (64). However, not all EPDCs were observed to express endoglin *in vivo*. In contrast to Bax *et al.* (64), who reported 73% EPDCs *in vitro* expressed endoglin, only an average of 13%  $\pm 2$  EPDCs were observed to express endoglin (n=3 hearts, n=114  $\pm 8.327$  EPDCs per heart) *in vivo*. In agreement with Bax *et al.* (64), endoglin expression was only observed in the EPDCs and not in the epicardial cells.

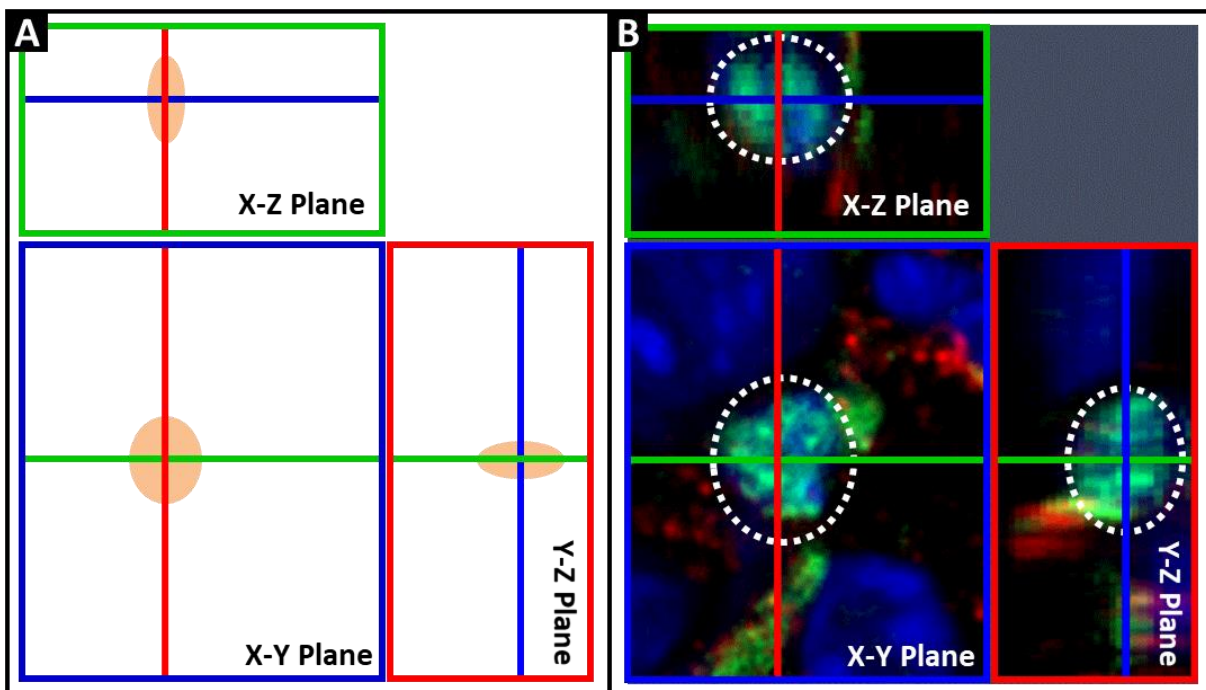


**Figure 4.7: A cartoon and an example image of a z-stack. (A)** A cartoon of a z-stack showing a cell (cream circle) in the 2D plane (X-Y) and the in the 3D plane, X-Z and Y-Z. **(B)** Example of eYFP<sup>+ve</sup> EPDCs (green) showing expression of eYFP in all three planes X-Y, X-Z and Y-Z planes thus confirming the expression of eYFP in one single EPDCs and not two adjacent cells. This process was repeated for 728 endoglin expressing EPDCs from 6 embryos. *Abbreviation: EPDCs – Epicardially Derived Cells.*

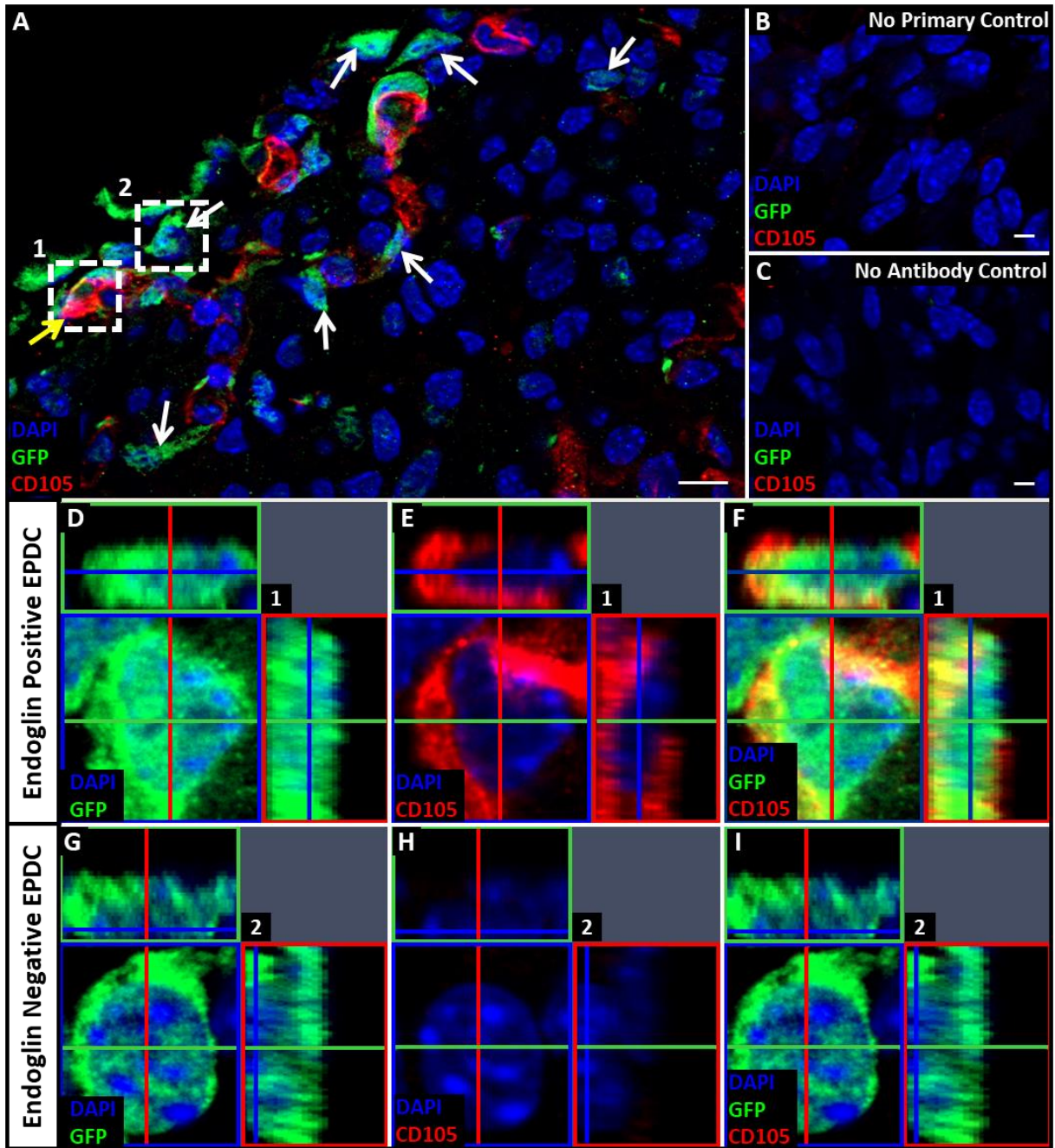


**Figure 4.8: EPDCs express endoglin *in vivo*.** Immunofluorescent stained section of E15.5 *Wt1<sup>Cre-ERT2/+</sup>; Rosa26<sup>eYFP/eYFP</sup>* mouse heart stained with chicken anti-GFP antibody (green) to mark EPDCs and rat anti-CD105 antibody (red) to detect endoglin positive cells. Counter stained with DAPI to detect nuclei. **(A)** High power (x63) image of endoglin & eYFP positive EPDCs (yellow arrow) and endoglin negative eYFP positive EPDCs (white arrows,  $n=3$ ). **(D-F)** Split channel z-stack image of an EPDC positive for endoglin (A, white box 1). **(G-I)** Split channel z-stack image of an EPDC negative for endoglin (A, white box 2). **(B)** No primary and **(C)** no antibody staining control. *Abbreviation: EPDCs – Epicardially Derived Cells.* Scale Bars: A to C – 10 $\mu$ m.

Next, I studied the effect of endoglin knockdown in EPDCs. To study this, embryos were harvested at E15.5 stage of development from *Eng<sup>fl/fl</sup>; Wt1<sup>Cre-ERT2/+</sup>; Rosa26<sup>eYFP/eYFP</sup>* mice. The external morphology and shape of both control (Figure 4.9 A-B, n=3) and *Eng-iKO<sup>epi</sup>* mutant (Figure 4.9 C-D, n=3) hearts was similar. However, analysis of E15.5 coronal sectioned hearts stained with chicken anti-GFP and rat anti-CD105 antibodies showed a reduced number of EPDCs in *Eng-iKO<sup>epi</sup>* mutants compared to control embryo hearts (Figure 4.9 E-F). The quantification using the event function of Zen 2012 software showed a 28% reduction in EPDCs number in *Eng-iKO<sup>epi</sup>* mutants compared to control embryos (Figure 4.9G). A summary of quantification is shown in Table 4.5.

**Table 4.5: Data summary of *in vivo* expression of endoglin in EPDCs of E15.5 control and *Eng-iKO<sup>epi</sup>* mutant embryos.**

	Control EPDCs	<i>Eng-iKO<sup>epi</sup></i> EPDCs	Percentage Cell Reduction in <i>Eng-iKO<sup>epi</sup></i>	<i>P value</i>
No. of hearts	3	3	n/a	n/a
Total No. of eYFP+ve EPDCs ± SEM per FOV	29 ± 2	21 ± 2	28%	0.0249
Total No. of eYFP+ve Eng+ve EPDCs ± SEM per FOV	4 ± 0.3	2 ± 0.3	50%	0.0474
Percentage of Eng+ve EPDCs ± SEM per FOV	13% ± 2	11% ± 1	15%	0.3232
Total No. of Nucleated myocardial cells ± SEM per FOV	145 ± 2	142 ± 4	2%	0.5899
Percentage of EPDCs ± SEM per myocardial cell	20% ± 1	15% ± 1	25%	0.0197
Percentage of eYFP+ve Eng+ve EPDCs ± SEM per myocardial cell	3% ± 0.2	2% ± 0.1	33%	0.0133

Next, a 50% reduction in the number of double positive CD105<sup>+ve</sup>; eYFP<sup>+ve</sup> EPDCs was observed in *Eng-iKO<sup>epi</sup>* embryos compared to controls (Figure 4.9H). The most likely reasons for only ~50% (and not 100%) endoglin knockdown in *Eng-iKO<sup>epi</sup>* could be due to incomplete Cre-LoxP recombination of the floxed Endoglin allele. However, even this partial knockdown did affect the number of EPDCs. Therefore, the effect of epicardial specific knockdown on EPDCs contribution to coronary vessels was investigated.

As controls and *Eng-iKO<sup>epi</sup>* mutant hearts were collected from different mouse litters, hind limbs from the embryos were collected to confirm the similar stage of development (Figure 4.10). Hind limbs from both control and *Eng-iKO<sup>epi</sup>* were observed to be at a similar stage of development within and between litters. The hind limb morphology was also cross referenced with the E15.5 phenotype described in ‘the atlas of mouse development’ (250).

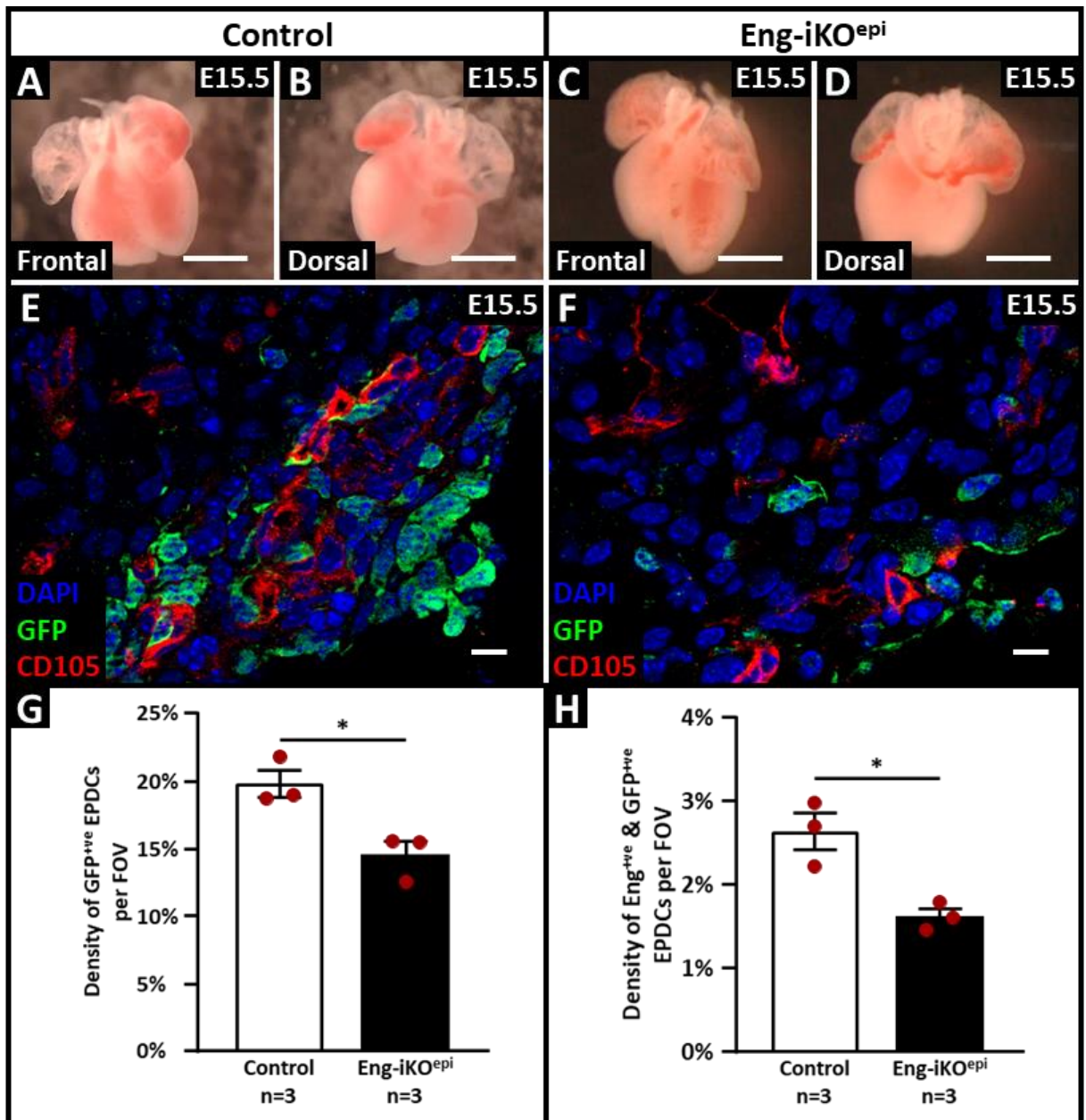


**Figure 4.9: Endoglin knockout in the EPDCs led to a significantly reduced number of EPDCs in *Eng-iKO<sup>epi</sup>* mutants compared to age matched controls.** Normally developed frontal and dorsal view of E15.5 (A-B) control ( $n=3$ ) and (C-D) *Eng-iKO<sup>epi</sup>* mutant ( $n=3$ ) embryonic hearts. E15.5 (E) control and (F) *Eng-iKO<sup>epi</sup>* heart sections stained with chicken anti-GFP antibody (green), rat anti-CD105 (red) and DAPI (blue) showing reduced number of EPDCs (white arrows) in *Eng-iKO<sup>epi</sup>* mutant compared to age matched control hearts. (G) Endoglin knockout led to significant reduction in density of EPDCs in *Eng-iKO<sup>epi</sup>* mutant per FOV ( $14.54 \pm 0.989$ ,  $n=3$ ) compared to controls ( $19.81 \pm 0.994$ ,  $n=3$ ,  $p = 0.0197$ ) embryonic hearts. (H) Significantly reduced density of  $Eng^{+ve}$  EPDCs were observed in *Eng-iKO<sup>epi</sup>* mutant per FOV ( $1.623 \pm 0.097$ ,  $n=3$ ) compared to age matched controls ( $2.636 \pm 0.221$ ,  $n=3$ ,  $p = 0.0137$ ) embryonic hearts. Data shown as mean  $\pm$  SEM and analysed using two tailed unpaired *t*-test (\*  $p < 0.05$ ). EPDCs – Epicardially Derived Cells. Scale Bars: A-D – 1mm; E-F – 10 $\mu$ m.

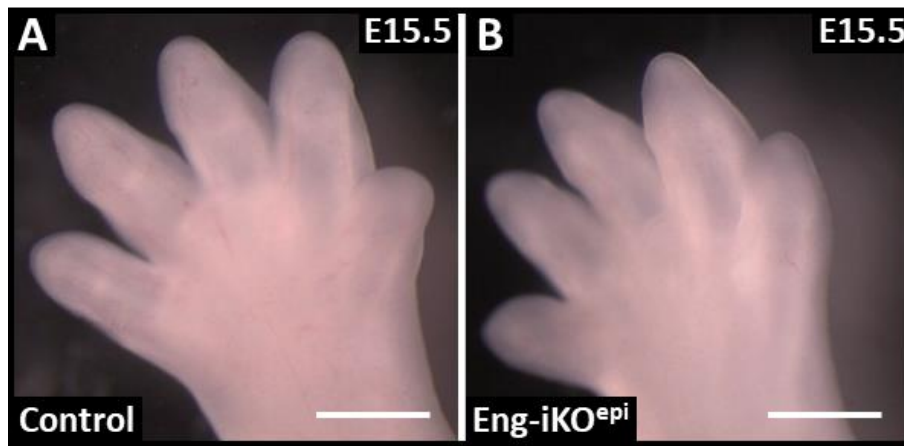


**Figure 4.10: Staging control and *Eng-iKO<sup>epi</sup>* mutant embryos using hind limb development.** To confirm the developmental age of embryos from both mouse lines (*Wt1<sup>Cre-ERT2/+</sup>; Rosa26<sup>eYFP/eYFP</sup>* and *Eng<sup>fl/fl</sup>; Wt1<sup>Cre-ERT2/+</sup>; Rosa26<sup>eYFP/eYFP</sup>*) hind limbs were collected and compared. The hind limbs of both (A) control and (B) *Eng-iKO<sup>epi</sup>* were observed to be at a similar stage of development. Scale bar: A-B – 1mm.

### 4.2.3. Effect of Epicardial Specific Endoglin Knockdown on Coronary Vessel Development

As reported in numerous publications (43, 44, 78, 79) and observed during this study (Figure 4.5), EPDCs contribute towards ECs, vSMCs and fibroblasts of the developing heart. The reduction in the number of EPDCs due to lack of endoglin could lead to vasculature related defects which in turn could have a detrimental effect on development of the myocardium. Therefore, to analyse if the epicardial specific knockdown of endoglin causes any coronary vasculature defects, embryos were collected at E17.5 from *Eng<sup>fl/fl</sup>; Wt1<sup>Cre-ERT2/+</sup>; Rosa26<sup>eYFP/eYFP</sup>* mice. Littermate embryos without *Wt1<sup>Cre-ERT2/+</sup>* were used as controls. The E17.5 stage of development was selected for two reasons: (i) it allows analysis of the coronary vasculature at a late stage of embryogenesis and (ii) as the pregnant mice were injected with tamoxifen to activate Cre which inhibits labour, by harvesting embryos at E17.5 any labour induced complications were avoided.

The freshly dissected E17.5 embryonic hearts were imaged (section 2.10.1), fixed in 4% PFA at 4°C O/N and then embedded in paraffin wax (section 2.2.1). The embryos were next sectioned into sister sections (section 2.4.1) and stained using the optimised double immunofluorescence protocol (section 2.5.3). During this staining due to incompatibility between rat anti-CD31 antibody and the embedding protocol, isolectin B4 (lectin) was used as the endothelial marker alongside Sm22 $\alpha$  to mark vSMCs. Once stained, images were taken at x10 and x40 magnification using the fluorescence setting on M2 axio-imager microscope. A minimum three sections were analysed per embryo and around 3 to 5 images were taken from the free RV & LV wall.

The external morphology of the E17.5 heart was observed to be similar in both control (n=5) and Eng-iKO<sup>epi</sup> mutants (n=6; Figure 4.11, A&B). Next the whole heart width was calculated using the line function of Zen 2012 software, which was also observed to be similar between the two groups (Figure 4.11C).

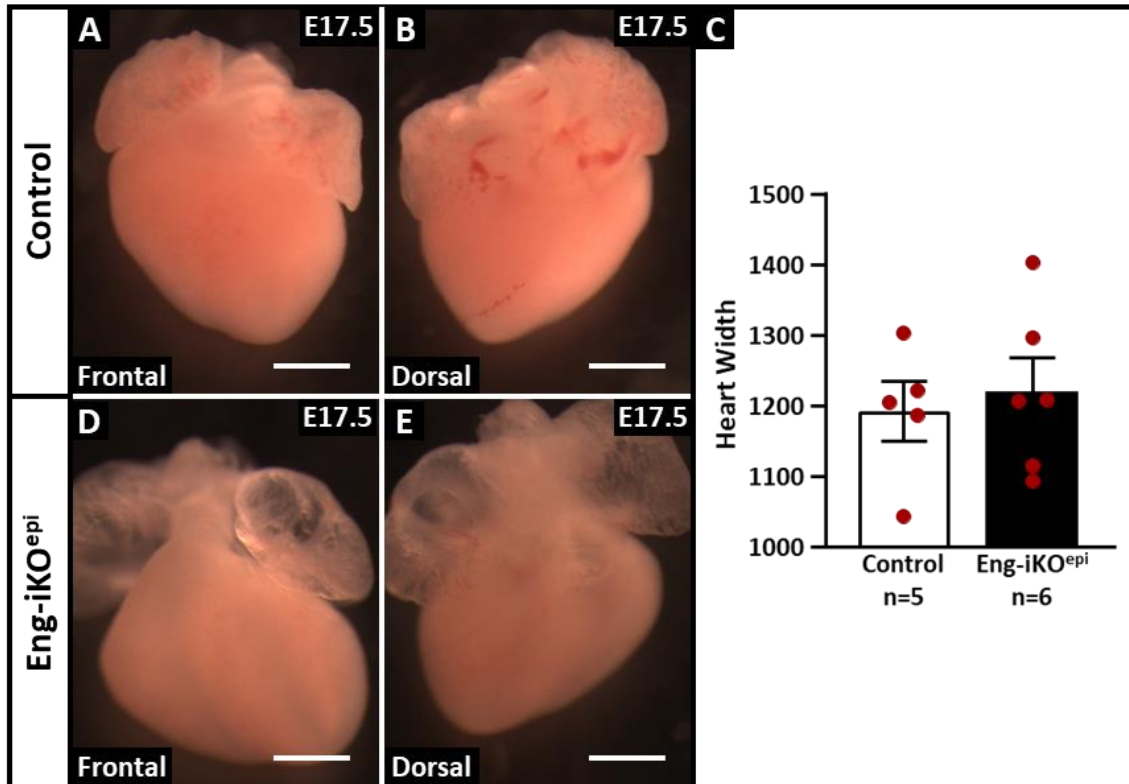


**Figure 4.11: Normal heart morphology of control and Eng-iKO<sup>epi</sup> mutant embryos at E17.5.** Normal frontal & dorsal view of E17.5 (A) control (*Eng*<sup>fl/fl</sup>; *Rosa26*<sup>eYFP</sup>, n=5) and (B) Eng-iKO<sup>epi</sup> (*Eng*<sup>fl/fl</sup>; *Wt1*<sup>Cre-ERT2</sup>; *Rosa26*<sup>eYFP</sup>, n=6) embryonic hearts. (C) There was no difference between the width of control (1192±42.20, n=5) and Eng-iKO<sup>epi</sup> (1220±47.26, n=6; *p* = 0.6741) embryonic hearts. Data shown as mean±SEM and analysed using two tailed unpaired *t*-test. Scale Bars: A-B & D,E – 1mm.

Next, the myocardium width was calculated following the method described by MacDonald *et al.* (276). Briefly, to measure myocardial width x10 tiled images of coronal heart sections were selected (middle of the heart). Three sets of measurements were taken from each of the six sites from free RV and LV wall (1-6 boxed region, Figure 4.4; 3x6 measurements in total per heart section). The average of these measurements was then normalised dividing it by the heart width of each section (276). This process was repeated for a minimum of 5 sections per heart. The control (n=3) and Eng-iKO<sup>epi</sup> mutant (n=3) hearts displayed similar morphological structure (Figure 4.12, A&E) and myocardial width analyses showed no difference between the two groups (Figure 4.12L, *p* value = 0.4362).

To analyse the effect of reduced number of EPDCs on development of coronary vessels in E17.5 hearts, 3 to 5 images from each ventricle free wall were taken at x40 magnification from immunofluorescence stained hearts (section 2.10.2). To compare ECs density in the myocardium, the threshold function of ImageJ software was used to calculate lectin stained

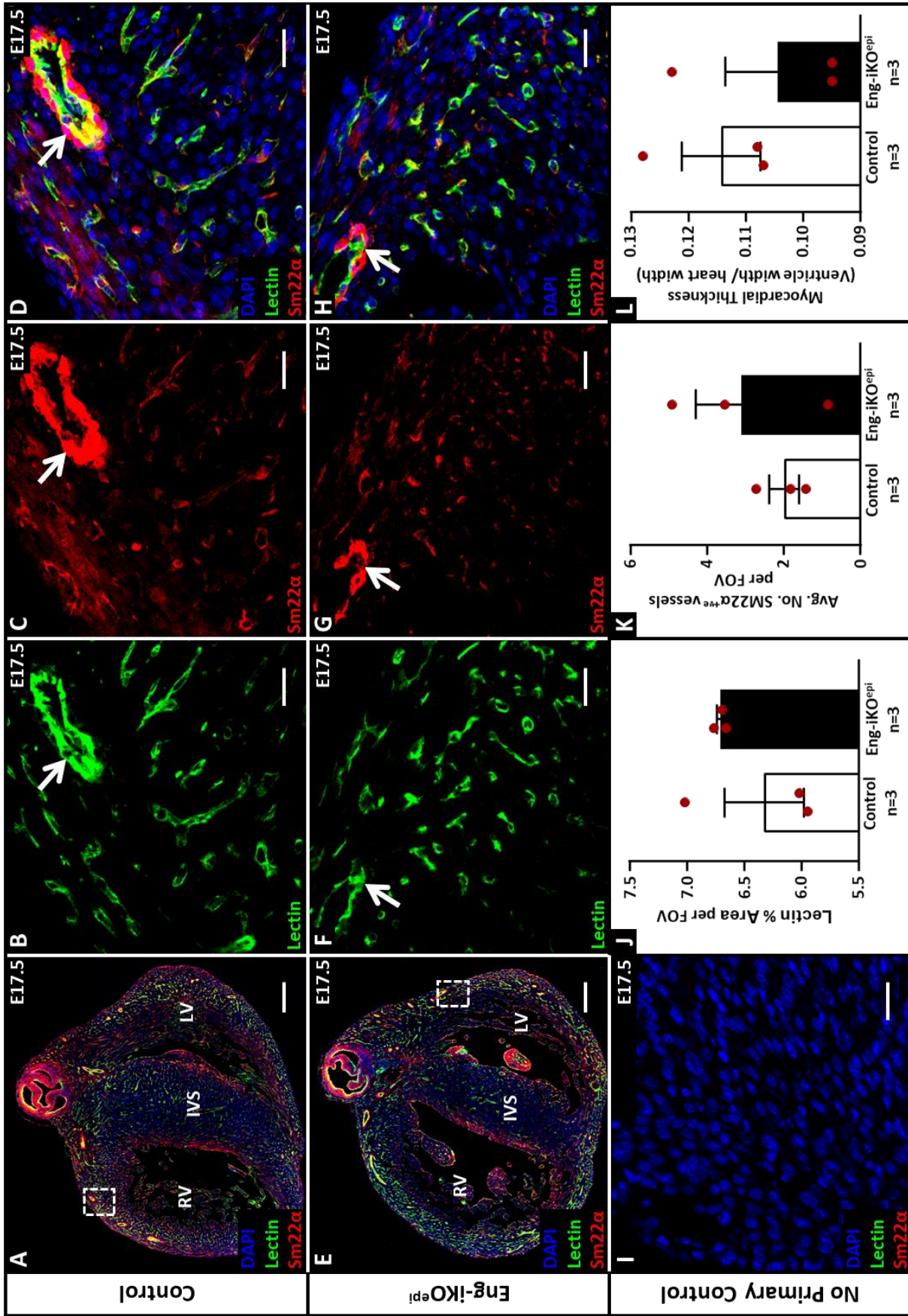
---

percentage area. While to compare the number of (Sm22 $\alpha$  positive) muscularised vessels in control and Eng-iKO<sup>epi</sup> embryo hearts, manual counting was performed on vessels (identified by a distinct lectin<sup>+ve</sup> endothelium layer) using the event function of Zen 2012 software.

The analysis of isolectin B4 staining showed no difference in the density of isolectin B4 staining in myocardial tissue of control (n=3) and Eng-iKO<sup>epi</sup> mutant (n=3) embryonic hearts (Figure 4.12, B,F,J). This was expected as only 6% of EPDCs were observed to differentiate into ECs and this contributed only 3% of total ECs (Table 4.4). The number of muscularised vessels were also observed to be similar in both wax embedded control (n=3) and Eng-iKO<sup>epi</sup> mutant (n=3) embryonic hearts (Figure 4.12, white arrows).

After thorough analysis of the above data, it was concluded that EPDCs do express endoglin *in vivo* and knockdown of endoglin using Wt1<sup>Cre-ERT2</sup> did lead to significant reduction in the number of EPDCs but it did not lead any detectable structural or vasculature related defects in E17.5 Eng-iKO<sup>epi</sup> mutant hearts.

**Figure 4.12: specific endoglin knockdown did not lead to vasculature or structural defects.** Coronal sections of E17.5 hearts stained using Isolectin B4 (Lectin, Green) to mark ECs and rabbit anti-SM22 $\alpha$  antibody (Red) to mark vSMCs. Counterstained with DAPI to mark nuclei. Tiled image of an E17.5 (A) control ( $n=3$ ) and (E) Eng-iKO<sup>epi</sup> mutant ( $n=3$ ) hearts, showing no structural differences between the two groups. Split channel higher power images of (B-D) control and (F-H) Eng-iKO<sup>epi</sup> mutant hearts showing no vasculature related defects between the two groups. (I) No primary staining control. (J) Quantification of percentage lectin stained area showed no significant difference between control ( $6.329\pm 0.348$ ,  $n=3$ ) and Eng-iKO<sup>epi</sup> mutant ( $6.684\pm 0.010$ ,  $n=3$ ;  $p = 0.3655$ ) hearts. (K) Quantification of number of muscularised vessels per FOV showed no difference between controls ( $1.993\pm 0.389$ ,  $n=3$ ) and Eng-iKO<sup>epi</sup> mutants ( $3.105\pm 1.197$ ,  $n=3$ ;  $p = 0.4265$ ) hearts. (L) No difference in the myocardial width was observed between control ( $0.114\pm 0.007$ ,  $n=3$ ) and Eng-iKO<sup>epi</sup> mutant ( $0.104\pm 0.009$ ,  $n=3$ ;  $p = 0.4362$ ) hearts. *Data shown as mean $\pm$ SEM and analysed using two tailed unpaired t-test. Abbreviations: ECs – Endothelial Cells; IVS – Interventricular Septum; LA – Left Atria; LV – Left Ventricle; RA – Right Atria; RV – Right Ventricle and vSMCs – Vascular smooth muscle cells. Scale Bars: A&E – 200 $\mu$ m and B-D & F-I = 20 $\mu$ m*



#### 4.2.4. Effect of Epicardial Specific *Tgfb2* Knockdown on Coronary Vessels Development

To further investigate the role of TGF $\beta$  signalling in EPDC differentiation and especially in light of data showing an important role for ALK5 [i.e. TGF $\beta$ R1, (60)], I analysed the role of epicardial specific *Tgfb2* knockdown (*Tgfb2-iKO<sup>epi</sup>*) using *Tgfb2<sup>fl/fl</sup>*; *Wt1<sup>Cre-ERT2/+</sup>*; *Rosa26<sup>eYFP/eYFP</sup>* mice. *Wt1<sup>Cre-ERT2</sup>* was activated by two subcut tam injections at E9.5 & E10.5 (Figure 4.13) and embryos were harvested at E17.5 for structural & vasculature analysis.

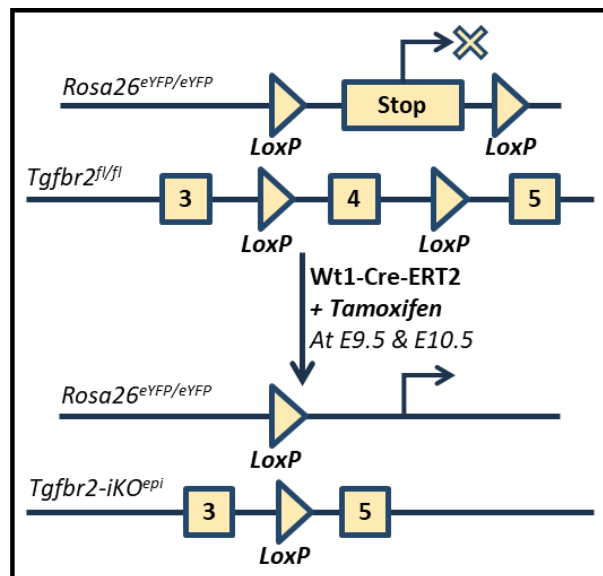


**Figure 4.13: Epicardial Specific *Tgfb2* knockout using *Wt1<sup>Cre-ERT2</sup>* mouse line.** To knockout *Tgfb2* gene in *Wt1<sup>+ve</sup>* cells, *Tgfb2<sup>fl/fl</sup>*; *Wt1<sup>Cre-ERT2</sup>*; *Rosa26<sup>eYFP/eYFP</sup>* mouse line was used. During experiment, a Cre-negative female was mated with a Cre-positive male to avoid possible effects of Cre activation on the pregnant mother, and limit Cre activity to the developing embryos. *Wt1<sup>Cre-ERT2</sup>* was activated by injecting tamoxifen at E9.5 and E10.5 via subcut route (in scruff) and embryos were harvested at E17.5.

*Tgfb2* is ubiquitously expressed (277-281) but due to lack of a suitable antibody (host lab data), during this study confirmation of *Tgfb2* knockdown in epicardial cells and EPDCs was done using genomic PCR. DNA was extracted from heart sections of *Tgfb2-iKO<sup>epi</sup>* mutants (*Tgfb2<sup>fl/fl</sup>*; *Wt1<sup>Cre-ERT2</sup>*; *Rosa26<sup>YFP/YFP</sup>*) and litter-mate controls (*Tgfb2<sup>fl/fl</sup>*; *Rosa26<sup>YFP/YFP</sup>*) using the protocol described in section 2.3.2. The concentration of extracted DNA from each sample was measured using nanodrop and summarised in Table 4.6.

**Table 4.6: Concentrations of DNA in *Tgfb2-iKO<sup>epi</sup>* and littermate control embryonic heart sections.**

ID	Avg. DNA Conc. (ng/ $\mu$ l)	DNA Volume ( $\mu$ l)	Final DNA Conc. (ng)
1	39.33	5.10	200.60
2	17.04	9.20	156.79
3	15.95	9.20	146.69
4	32.24	6.20	199.90
5	81.47	2.50	203.66
6	45.97	4.40	202.25
7	13.93	9.20	128.16

ID	Avg. DNA Conc. (ng/μl)	DNA Volume (μl)	Final DNA Conc. (ng)
8	21.14	9.20	194.47
9	26.82	7.50	201.13
10	27.12	7.40	200.65

Next, PCR was performed using Cre, *Tgfb2-iKO<sup>epi</sup>* and Myo primers (Table 2.4; Figure 4.14A). Following activation of *Wt1<sup>Cre-ERT2</sup>* by tamoxifen, exon 4 is removed from the *Tgfb2<sup>fl/fl</sup>* gene leading to a frameshift mutation (Figure 4.14, B&C). This recombination was confirmed in *Tgfb2-iKO<sup>epi</sup>* embryos using P3b and P5b primers (Figure 4.14D, ~450bp). Details of DNA concentrations for each sample are summarised in Figure 4.14.

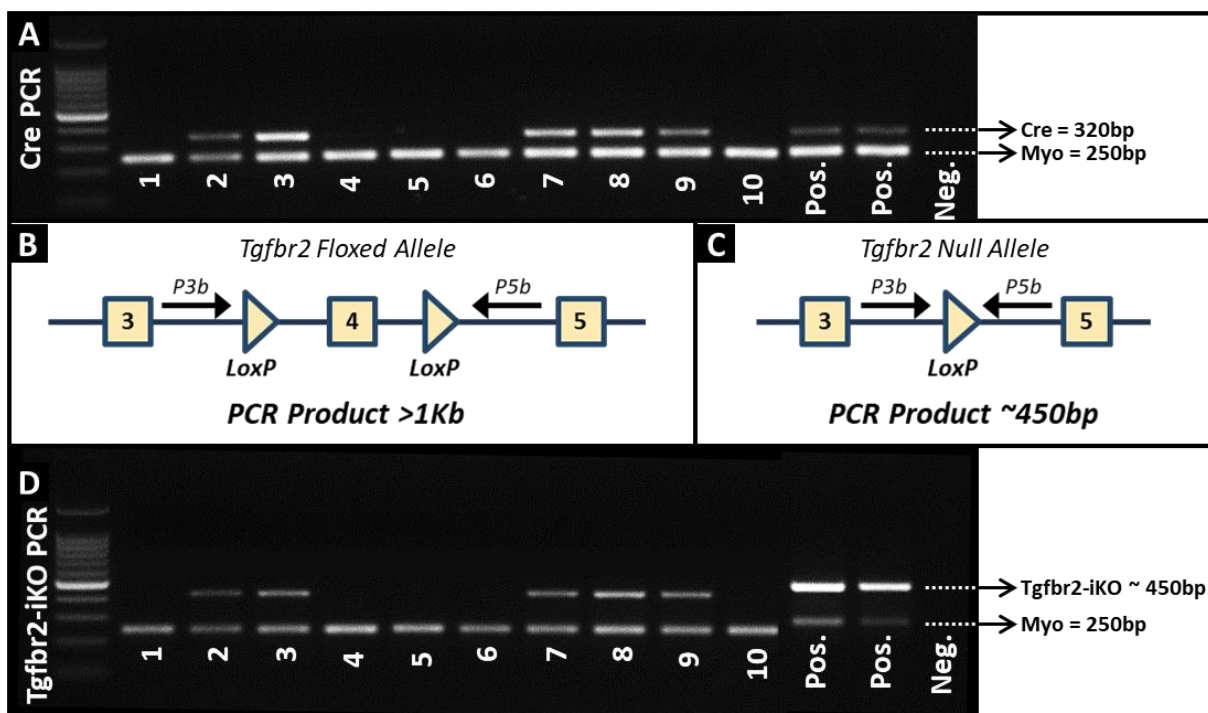


**Figure 4.14: Confirmation of the presence of *Tgfb2-iKO<sup>epi</sup>* recombined gene in epicardial and epicardially derived cells from tissue sections.** (A) To detect the presence of *Wt1-Cre* gene, Cre PCR was performed using cre forward and cre reverse primers. To confirm the presence of template DNA in the samples myo gene is used as a control. To detect myo gene, myo forward and myo reverse primers were used. (B) Schematic of a floxed *Tgfb2* allele showing the location of P3b and P5b primers. In a WT mice the PCR product is >1Kb so could not be amplified. (C) However, in the presence of an active cre causes a frameshift mutation so exon 5 is located immediately after exon 3. This genetic mutation can be confirmed by using P3b forward primer and P5b reverse primer (PCR product ~450bp). (D) The recombined *Tgfb2* gene was detected in all *Cre<sup>+ve</sup>* samples confirming Cre activity while no bands were detected in Cre negative as expected. Myo provided a positive control to show sufficient genomic DNA template was present to support a PCR reaction.

To analyse the effect of epicardial specific *Tgfb2* knockdown on cardiac and coronary development freshly dissected E17.5 hearts were imaged (section 2.10.1) and measured using the line function of Zen 2012 software but showed no difference between control (n=5) and *Tgfb2-iKO<sup>epi</sup>* mutants (n=5; Figure 4.15).

To investigate vasculature related defects in *Tgfb2-iKO<sup>epi</sup>* mutants, OCT embedded E17.5 *Tgfb2-iKO<sup>epi</sup>* mutants and littermate control hearts were sectioned into sister sections and

subjected to double immunofluorescence staining using rat anti-CD31 and rabbit anti-Sm22 $\alpha$  antibodies. The sections were then imaged at x10 and x40 magnification using fluorescence setting on M2 axioimager microscope. Three sections were images per heart and 6 images were taken from free RV & LV wall per section (Figure 4.4).

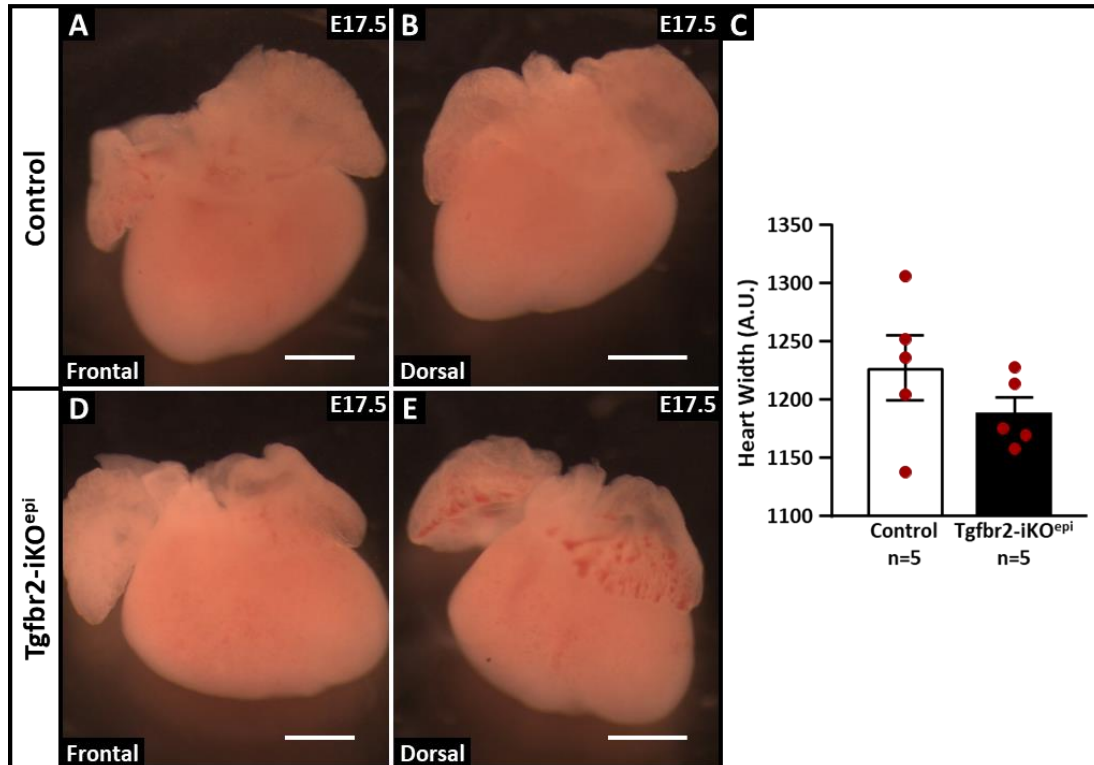
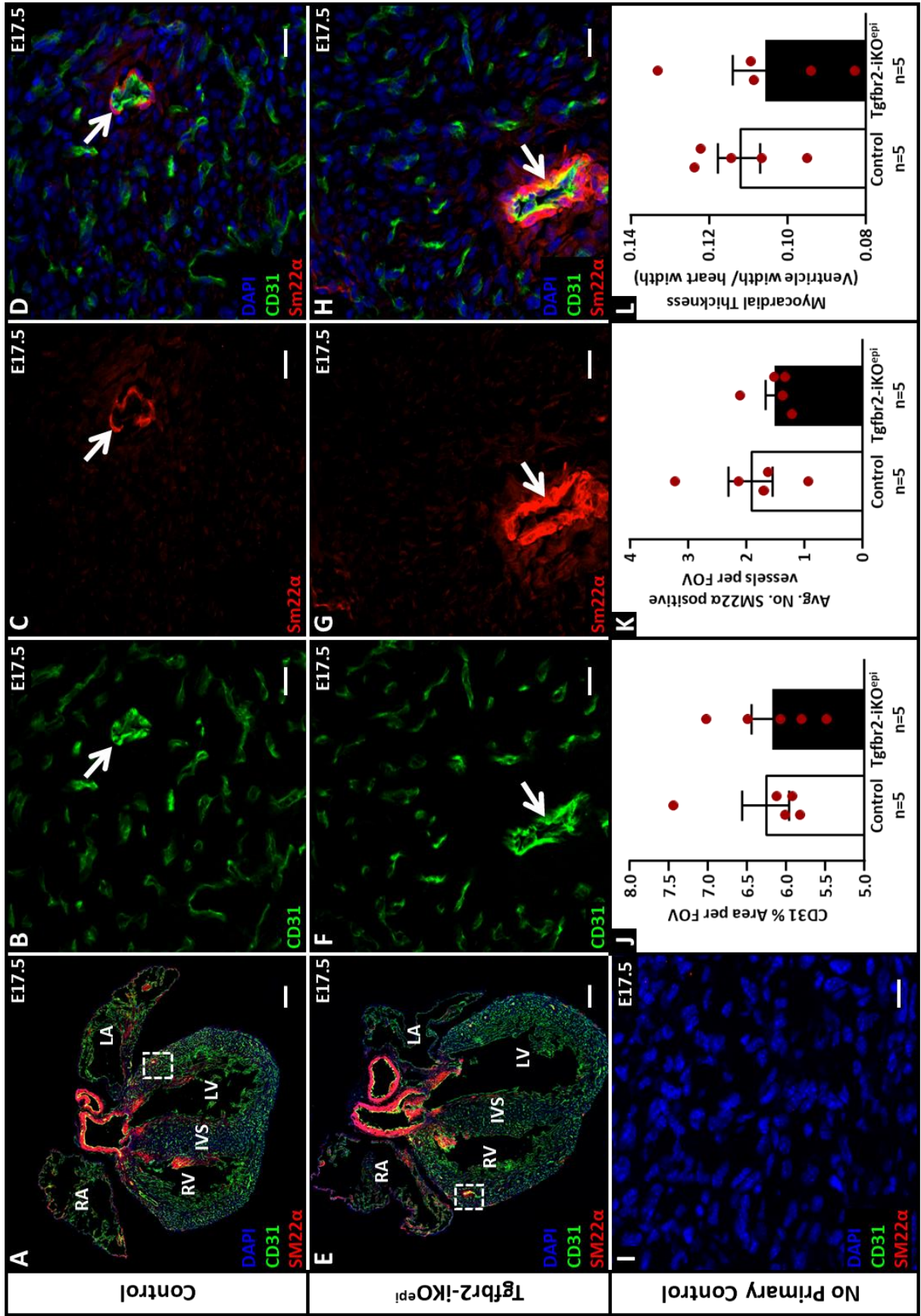


**Figure 4.15: Epicardial Specific *Tgfb2* knockout using *Wt1*<sup>Cre-ERT2</sup> did not have any effect on development of the mouse heart.** The external morphology of E17.5 embryonic hearts was similar in both controls (A-B) and *Tgfb2-iKO*<sup>epi</sup> (D-E) embryos (n=5/ group). (C) Quantification using Zen 2012 showed no difference between the myocardial width of control ( $1227.0 \pm 27.81$ , n=5) and *Tgfb2-iKO*<sup>epi</sup> mutant ( $1189.0 \pm 13.43$ , n=5,  $p = 0.2476$ ) embryonic hearts. Data shown as mean  $\pm$  SEM and analysed using two tailed unpaired t-test (\*  $p < 0.05$ ). Scale Bars: A-B & D-E – 1mm.

In whole view images of control (n=5) and *Tgfb2-iKO*<sup>epi</sup> mutant (n=5) embryonic hearts no gross developmental heart defects or changes in myocardial width measurements were observed (Figure 4.16). I next analysed the vasculature of control and *Tgfb2-iKO*<sup>epi</sup> mutant embryonic hearts in x40 magnification images. The quantification of CD31 staining using threshold function of ImageJ software showed a similar percentage area stained in both controls (n=5) and *Tgfb2-iKO*<sup>epi</sup> mutant (n=5) hearts (Figure 4.16, B,F,J). The manual counting of Sm22 $\alpha$  positive muscularised vessels using event function of Zen 2012 software also showed no difference between controls (n=5) and *Tgfb2-iKO*<sup>epi</sup> mutant (n=5) hearts (Figure 4.16, white arrows).

The analysis of the above data clearly showed that knockdown of *Tgfb2* in epicardial and epicardially derived cells using *Wt1*<sup>Cre-ERT2</sup> does not lead to any clear developmental (structural or vascular) related defects in E17.5 embryonic hearts.

**Figure 4.16: Epicardial specific *Tgfb2* knockdown did not lead to any vasculature related defects.** Coronal sections of E17.5 hearts stained using rat anti-CD31 (green, ECs), rabbit anti-SM22 $\alpha$  (red, vSMCs) and counterstained with DAPI (blue, nuclei). Tiled image of a normally developed (A) control and (E) *Tgfb2-iKO<sup>epi</sup>* mutant E17.5 hearts. Split channel higher power images of (B-D) control and (F-H) *Tgfb2-iKO<sup>epi</sup>* mutant hearts showing similar vasculature in both groups. (I) No primary staining control. (J) Quantification of percentage CD31 stained area showed no significant difference between control ( $6.266 \pm 0.298$ ,  $n=5$ ) and *Tgfb2-iKO<sup>epi</sup>* mutant ( $6.176 \pm 0.270$ ,  $n=5$ ;  $p = 0.8284$ ) embryonic hearts. (K) No difference in the quantification of number of muscularised vessels was observed between control ( $1.922 \pm 0.3794$ ,  $n=5$ ) and *Tgfb2-iKO<sup>epi</sup>* mutant ( $1.508 \pm 0.1556$ ,  $n=5$ ;  $p = 0.3422$ ) embryonic hearts. (L) Quantification showing similar myocardial width between control ( $0.112 \pm 0.0053$ ,  $n=5$ ) and *Tgfb2-iKO<sup>epi</sup>* mutant ( $0.106 \pm 0.0085$ ,  $n=5$ ;  $p = 0.5157$ ) embryonic hearts. Data shown as mean  $\pm$  SEM and analysed using two tailed unpaired *t*-test (\*  $p < 0.05$ ). Abbreviations: E – Embryo Age; RA – Right Atria; RV – ECs – Endothelial Cells; IVS – Interventricular Septum; LA – Left Atria; LV – Left Ventricle; RA – Right Ventricle; RV – Right Ventricle and vSMCs – Vascular smooth muscle cells. Scale Bars: A&E = 200 $\mu$ m and B-D & F-I = 20 $\mu$ m.



---

### 4.3. Discussion

The aim of this study was to understand the importance of *endoglin* and *Tgfb $\beta$ 2* in epicardium and epicardially derived cells *in vivo* during coronary development. To this end,  $Wt1^{Cre-ERT2}$  was used to knockdown these genes in epicardial and epicardially derived cells.

#### 4.3.1. Specificity of $Wt1-Cre^{ERT2}$

There is some debate regarding the specificity of  $Wt1-Cre$ . Theoretically, in order to use cre-loxP technology to accurately trace cell fate, the promoter that drives the cre recombinase should only be expressed in the precursor cell population but not in the descendent cell population. In case of endogenously active *Wt1-Cre* mouse line, expression of  $Wt1$  is reported not only in the epicardial cells but EPDCs as well and in the ECs (82). Therefore, inducible  $Wt1^{Cre-ERT2}$  mouse line (used during this study) is preferred over *Wt1-Cre* mouse line. Furthermore, it is suggested that the recombination efficiency can be influenced by multiple tamoxifen doses, route of tamoxifen delivery and genetic background (outbred or inbred) of mice (253). There are also slight concerns regarding recombination efficiency of  $Wt1^{Cre-ERT2}$  (82, 253).

Zhou and Pu (253) showed that activation of  $Wt1^{Cre-ERT2}$  between E9.5 to E11.5, is quite specific to epicardium. They activated  $Wt1^{Cre-ERT2}$  by a single tamoxifen injection at E10.5 (2.5 to 3.75mg) via gavage route has showed a moderately high efficiency (70.2 $\pm$ 10.4%) labelled epicardial cells (81, 253). This efficiency was said to be enough for lineage tracing the fate of epicardial and epicardially derived cells. Higher Cre activation could be achieved by increasing the tamoxifen dose or multiple tamoxifen injections but too much tamoxifen can also lead to embryonic lethality or congenital defects due to tamoxifen toxicity (253). They also showed that gavage route is preferable to IP injections as it has lower risk of tamoxifen toxicity. Furthermore, they also observed rare GFP<sup>+ve</sup> ECs when  $Wt1^{Cre-ERT2}$  was activated at E10.5 but suggested these to be epicardially derived ECs (253).

Therefore, during the current study, I first optimised the dose and site of tamoxifen injection to activate  $WT1^{Cre-ERT2}$  and showed that 2 subcut tam injection at E9.5 and E10.5 gave reproducible moderately high (~75%)  $WT1^{Cre-ERT2}$  recombination, similar to Zhou and colleagues [ $\sim$ 70%, section 4.2.1.1, (78, 253)].

Using lineage tracing I showed that the majority of EPDCs differentiated into vSMCs and fibroblasts (Figure 4.5 and Table 4.4) consistent with the previous studies (54, 78, 253, 282).

---

Around 3% of ECs were observed to have an epicardial origin (Figure 4.5 and Table 4.4), consistent with the work suggesting minor epicardial cells towards ECs population of the heart (43, 44, 79, 253). However, in contrast to previous studies (78, 80, 81) no epicardially originating cardiomyocytes were observed during this study (Figure 4.5 and Table 4.4).

Compared to previous studies where only qualitative analysis is performed, I show the exact percentage contribution of  $Wt1^{Cre-ERT2}$  positive cells into different cardiac cell types. However, using this Cre line ~25% of epicardium remains unlabelled consistent with previous publication (253) therefore, the percentage analysis is likely to be an underestimate of epicardial contribution towards the cardiac cell types. Another limitation of the work described in this chapter is the microscope used was epi-fluorescence microscope with apotome. Apotome does help to remove out of focus light however imaging with confocal would give superior resolution to cell specific signal.

### 4.3.2. Role of Endoglin in EPDCs

TGF $\beta$  pathway has been shown to be vital during EMT and knockdown of any of its ligands or receptors have detrimental effects [discussed in 4.1.1, (60, 62, 68)]. One of the main objectives of this study was to study the expression of endoglin in EPDCs *in vivo*. Using z-stack imaged E15.5 embryonic hearts sections from  $Wt1^{Cre-ERT2/+}; Rosa26^{eYFP/eYFP}$  mice I confirmed that EPDCs do express endoglin *in vivo* (Figure 4.8). However, in contrast to the 73% of EPDCs expressing endoglin *in vitro* (64) only 13% EPDCs were observed to express endoglin *in vivo* (Figure 4.9). Knockdown of endoglin in these EPDCs using the  $Eng^{fl/fl}; Wt1^{Cre-ERT2/+}; Rosa26^{eYFP/eYFP}$  mouse line, led to a significant reduction (28%) in total number of eYFP<sup>+ve</sup> EPDCs in Eng-iKO<sup>epi</sup> mutants compared to age matched controls (Figure 4.9). However, this reduction in EPDCs number did not affect the cardiac development. Furthermore, no difference in the vasculature was observed between E17.5 Eng-iKO<sup>epi</sup> mutant and littermate control hearts (Figure 4.12). The lack of defect in ECs density is expected as only 3% of ECs arise from EPDCs however no effect on the muscularised vessels number and heart was surprising considering a 28% reduction in EPDCs number. This could potentially be due to only a partial (~50%) endoglin knockdown in EPDCs.

It is still possible that this reduction in eYFP<sup>+ve</sup> EPDCs number (Figure 4.9) could cause a subtle effect on the vasculature and the myocardium postnatally. To analyse this, embryos would need to be fostered and analysed at later stages of development potentially around P10 or end of heart development around P21.

---

An additional approach would be to analyse the effect of endoglin depletion on gene expression in EPDCs. Using a laser dissection microscope or cell sorting, eYFP<sup>+ve</sup> cells could be collected and subjected to qPCR to analyse the effect of endoglin knockdown on EMT associated genes, such as those studied in AV explant studies (242) for example RhoA,  $\beta$ -catenin or Fibulin-2. Another factor to consider for any future studies would be to check percentage endoglin knockdown in each embryo/ pup. As tam would have been given to a pregnant female and not all embryos would have received it in even proportions, this could have an impact on the phenotype. This could either be done by western blot on protein lysates extracted from GFP<sup>+ve</sup> EPDCs or by analysing endoglin mRNA using qPCR.

It would also be useful to analyse whether the cause of reduced EPDCs number I observed in endoglin mutants was due to lack of proliferation or increased apoptosis of Eng<sup>-ve</sup> EPDCs using pHH3 and an apoptosis marker such as caspase 3/ Ki67.

During the current study, due to tissue constraints caused by poor mating, it was not possible to look at the effect of epicardial specific endoglin knockdown on the EPDC-derived cardiac fibroblast population. This would be useful to address in a future study. However, major issue with fibroblasts is lack of single cell specific marker potentially due to the multiple origin/ functional roles (283). In this study, I used anti-vimentin to mark fibroblasts but in future studies it might be wise to use an additional fibroblast marker such as anti-FSP1.

### **4.3.3. Role of TGF $\beta$ 2 in Epicardium and EPDCs**

During EMT TGF $\beta$ 1 is a major driver of the process and signals through a receptor complex of TGF $\beta$ 2 and ALK5 (Figure 1.17). Loss of ALK5 in epicardial cells (*Alk5-KO<sup>epi</sup>*) leads to: (i) defective myocardial development; (ii) problems with vSMCs recruitment; (iii) improper attachment of epicardium; (iv) increased capillary density and (v) EPDCs failed to undergo EMT (60). Similar defects were expected from *Tgfbr-iKO<sup>epi</sup>* mutants. To study this, *Tgfbr-iKO<sup>epi</sup>* mutant and litter-mate control embryos were harvested at E17.5 stage of development.

However, in contrast to *Alk5-KO<sup>epi</sup>* mutants, the analysis of E17.5 *Tgfbr-iKO<sup>epi</sup>* mutant and littermate control hearts did not display any defects in morphology Figure 4.15 and Figure 4.16). Furthermore, no differences in the vasculature of *Tgfbr-iKO<sup>epi</sup>* mutant and littermate controls were observed both EC density and number of muscularised vessels appeared normal (Figure 4.16).

---

This lack of phenotype in E17.5 *Tgfbr-iKO<sup>epi</sup>* mutants could be due multiple reasons. For instance, in the study by Sridurongrit *et al.* (60), constitutively active *Gata5-Cre* was used to knockdown *Alk5* in epicardial cells compared to *Wt1<sup>Cre-ERT2</sup>* used in the current study to knockout *Tgfbr2*. The *Gata5-cre* is activated in epicardium around 9.25 while *Wt1<sup>Cre-ERT</sup>* was activated at E9.5 in this study. *Gata5-Cre* is also shown to be expressed not only in the epicardium but in the myocardium as well (284). Therefore, loss of *Alk5* in myocardium as well as epicardium could lead to loss of signalling required for EMT to form EPDCs, reduced or no production of ECM formation which could affect vessels development. The reduced number of mature vessels may also explain the myocardium related defects.

Another reason for lack of a phenotype in *Tgfbr-iKO<sup>epi</sup>* mutants could be that TGFβR2 has a level of redundancy (285). Dudas *et al.* (285) showed that knockdown of *Alk5* in neural crest cells led to severe craniofacial defects in contrast to neural crest specific *Tgfbr2* knockdown (286). They speculated that the role of ALK5 role during craniofacial development is non-redundant compared to TGFβR2 and that ALK5 can be activated combining with some other type 2 receptor of the TGFβ family if TGFβR2 is not available (285).

In conclusion, the current study demonstrated that knockdown of endoglin led to reduction in total number of EPDCs in *Eng-iKO<sup>epi</sup>* mutants at E15.5 but does not cause any structural or vasculature related defects in E17.5 *Eng-iKO<sup>epi</sup>* mutants. Similarly, knockdown of *Tgfbr2* in epicardial and epicardially derived cells did cause any structural or vasculature related defects at E17.5. The TGFβ signalling pathway in EPDCs could have a negligible dependence on endoglin and continue to signal in the absence of TGFβR2 (Figure 4.17), explaining the lack of a detectable coronary vessel phenotype in the absence of each of these genes. To confirm the effect on TGFβ signalling, further *in vivo* studies using a TGFβ signalling reporter line (SBE-luc mice) would need to be carried out. The SBE-luc mice are transgenic mice in which expression of luciferase is promoted when SMAD2/3 signalling cascade is activated (287). This mouse line in combination with *Wt1<sup>Cre-ERT2</sup>* and *Eng<sup>fl/fl</sup>* or *Tgfbr2<sup>fl/fl</sup>* mouse line would allow evaluation of the functional role of these receptors (in terms of SMAD2/3 signalling *in vivo*) in epicardial and epicardially derived cells.

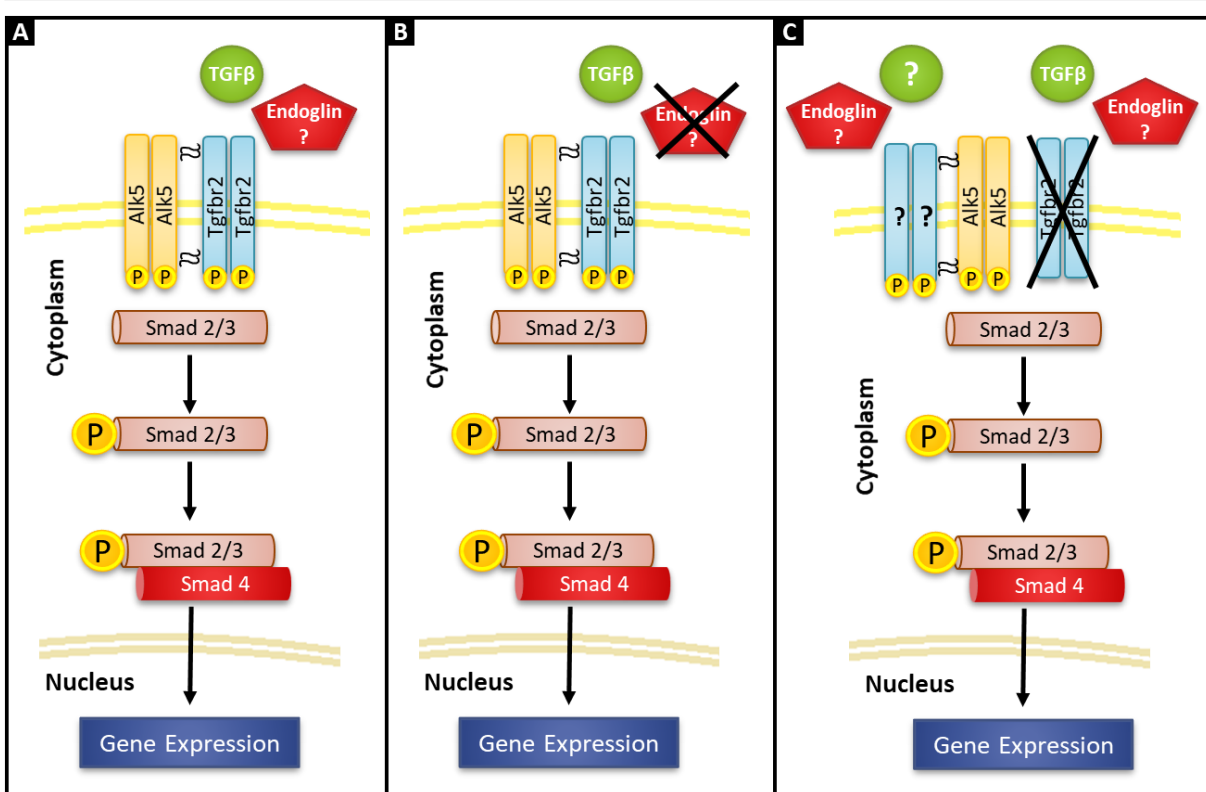


**Figure 4.17: Summary of TGF $\beta$  signalling in EPDCs in the presence and absence of Endoglin or TGF $\beta$ R2.** (A) Normal TGF $\beta$  signalling in EPDCs in the presence of endoglin and TGF $\beta$ R2. Endoglin potentially promotes TGF $\beta$  signalling through the ALK5/TGF $\beta$ R2 receptor complex. ALK5 phosphorylates SMAD2/3 which then combines with SMAD4 and moves to the nucleus to activate gene expression related to proliferation and differentiation of EPDCs. (B) My results showed that knockdown of endoglin in EPDCs potentially affects the epicardial EMT, reduced proliferation or increased apoptosis of EPDCs post EMT but it did not cause any problems with EPDCs differentiation. (C) Analysis of the current results showed that knockdown of TGF $\beta$ R2 in EPDCs did not lead to any defects, potentially due to activation of ALK5 via a different type 2 receptor. It is unclear from the current data whether endoglin plays an important role in this pathway in EPDCs.

---

**Chapter 5. Role of Endoglin in  
Endothelial Cells during Development and  
in Adult Life**

---

## 5.1. Introduction

To address the role of endoglin in endothelial cells I have taken three different approaches. First, in the heart, ECs start to express endoglin from early development of new vessels (chapter 3), but its function in coronary endothelial cells during heart development has not yet been investigated and forms the first part of this chapter.

Second, endothelial endoglin is also essential to maintain vessel calibre and integrity (section 1.5.1). Mutations in the endoglin gene lead to HHT1, which is associated with AVMs (section 1.6, see also Figure 1.21) (178). The mouse models of HHT1 generated in my host laboratory showed AVM formation in the developing neonatal retina when endoglin is depleted from the ECs (188). This phenotype is thought to be due to an imbalance between the pro-angiogenic factors in the developing retina and BMP9 pro-quiescent signalling, such that in the absence of endoglin excess angiogenesis occurs and vessels enlarge to generate AVMs. In the second part of this chapter, I used the neonatal retinal model to test whether additional BMP9 can over-ride this signalling defect (in the absence of endoglin) to rescue the AVM phenotype. In addition, I investigated whether loss of endoglin in veins (but not arteries) leads to AVM formation.

Finally, little is known about the role of endoglin in quiescent vessels in adult life. Therefore, in this chapter I address the role of endoglin in quiescent vessels in the adult vasculature.

### 5.1.1. Endoglin in Coronary Vessel Development

Studies to investigate the effect of endoglin knockdown in ECs during the different waves of coronary vessel angiogenesis during heart development (Figure 1.15) have not been possible to date because global knockout of endoglin is embryonic lethal at E10.5 (137, 161, 288). Furthermore, even using a conditional endothelial specific Cre line (*VE-Cad*<sup>Cre-ERT2</sup>) with Cre activation at later stages of development (E11.5 to E13.5), the analysis of the role of endoglin in coronary vessel development was prohibited due to rapid foetal lethality at E13.5 and E14.5 (Figure 5.1, unpublished data, Arthur Lab). This is likely because loss of endothelial endoglin in the foetus leads to similar defects in the placental vasculature seen following loss of ALK1 signalling (289).

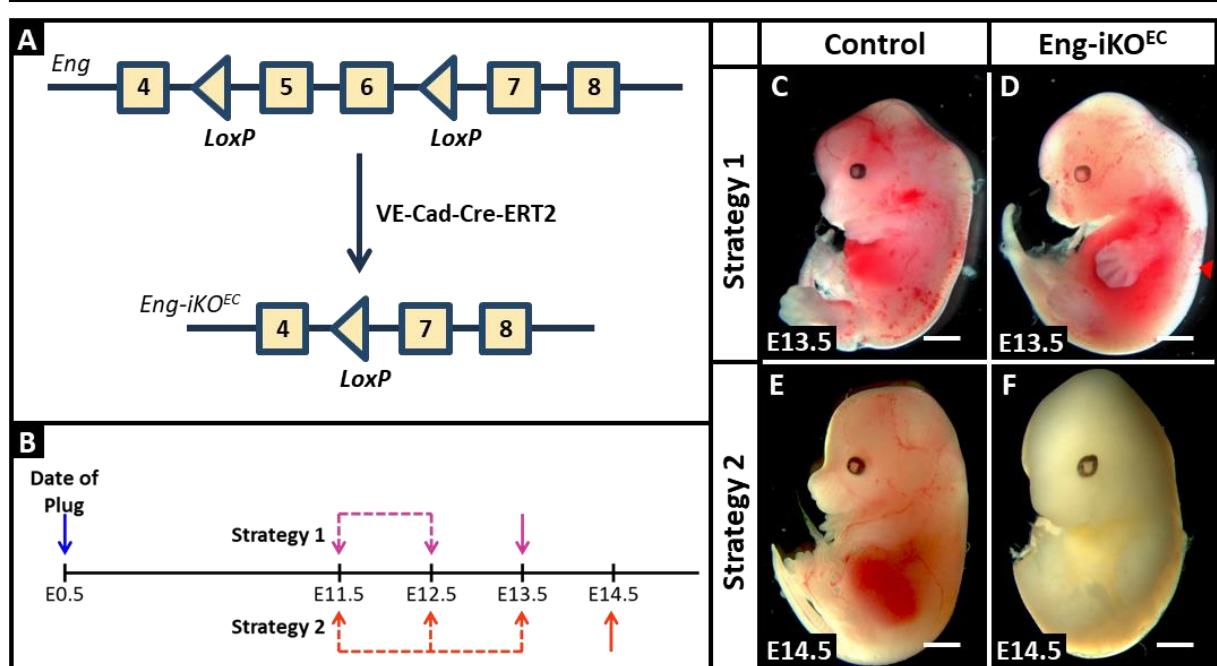


**Figure 5.1: Depletion of *Endoglin* using *VE-Cad*<sup>Cre-ERT2</sup> even at later stages led to rapid embryonic lethality (unpublished data, Arthur Lab).** (A) To knockdown *Endoglin* in endothelial cells (ECs), *Eng*<sup>fl/fl</sup> mice were used. In the presence of an active Cre, the first *LoxP* site and exon 5 are removed leading to formation of a truncated endoglin protein. During this study, *VE-Cad*<sup>Cre-ERT2</sup> was used to knockdown *Endoglin* in ECs. (B) In this study, *VE-Cad*<sup>Cre-ERT2</sup> is activated either by 2 (Strategy 1, pink arrows) or 3 (Strategy 2, orange arrows) IP injections of tamoxifen (dose: 1mg/injection) and embryos were harvested at E13.5 or E14.5 respectively. Whole view images of normally developed E13.5 (C) and E14.5 (E) control embryos. While knockdown *Endoglin* led to rapid lethality of embryos at E13.5 (D, in strategy 1) and E14.5 (F, in strategy 2). Scale bars: C-F = 1mm.

To address this limitation in this project, a new arterial specific Cre, *Dll4in3*<sup>Cre-ERT2</sup> (with low expression in the placenta) was used to study the role of endoglin in coronary arterial ECs during foetal development (in collaboration with Sarah de Val, University of Oxford). Endogenous *Dll4* is highly expressed in various arterial endothelium including aorta, yolk sac arteries, and coronary arteries during development (290, 291).

To generate this *Dll4in3*<sup>Cre-ERT2</sup> Cre line, initially an in silico search of the *Dll4* gene showed that the third intron of *Dll4* (*Dll4in3*) contained a highly conserved enhancer sequence (233). This sequence was cloned upstream of a LacZ reporter gene and used to generate a reporter mouse to evaluate *Dll4in3* expression prior to generating a Cre line. *Dll4* enhancer expression was observed in dorsal aorta in E9.0 and E15.0 embryos. At E15.0, the expression of *Dll4in3* only occurs in a small subset of placental vessels, minimising the impact of the corresponding Cre line on the placental vasculature. The expression of the enhancer is also seen in coronary arteries at P6 (233). This *Dll4* enhancer sequence (*Dll4in3*) was cloned upstream of Cre-ERT2 (de Val, unpublished work) and inserted into the mouse genome to produce the transgenic *Dll4in3*<sup>Cre-ERT2</sup> mouse which was then imported to our mouse facility (Figure 5.2). The expression pattern of *Dll4in3*<sup>Cre-ERT2</sup> was first established using the *Rosa26*<sup>eYFP</sup> reporter mouse (230).

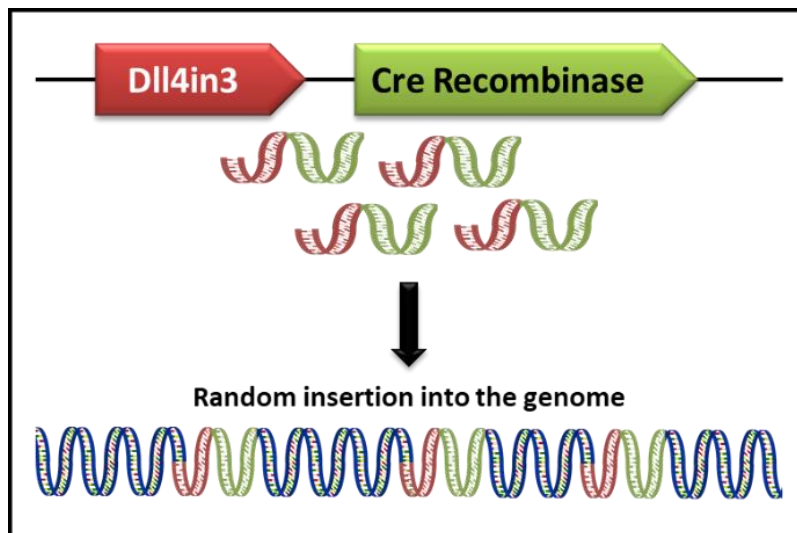


**Figure 5.2:** *Dll4in3<sup>Cre-ERT2</sup>* cloned sequence and its insertion into mouse genome. A 937bp fragment of a highly conserved enhancer of *Dll4* gene (*Dll4in3*) is cloned upstream of the Cre-ERT2 Recombinase gene. This sequence is then randomly inserted into a mouse genome to form a transgenic mouse line.

The next aim of this study was to use this novel *Dll4in3<sup>Cre-ERT2</sup>* line to understand the role of endoglin during early development of coronary arteries. I hypothesised that lack of endoglin in arteries would lead to reduced proliferation of arterial ECs and delayed or lack of mature vessels. This was addressed in the results section 5.2.1 below.

### 5.1.2. Endoglin and the Developing Retinal Vasculature

The reason for formation of AVMs in HHT patients is not clear but preclinical models show that endothelial knockdown of endoglin alone does not result in formation of AVMs. An additional angiogenic stimulus is required (182, 188, 292). This indicates that endothelial endoglin is required for normal angiogenesis. As discussed in the section 1.5.1, endoglin has high affinity towards BMP9 and BMP10 ligands (130, 134) and promotes signalling via ALK1 receptor in ECs (Figure 5.3A). Furthermore, antibody mediated deletion of BMP9 and BMP10 via a trans-mammary route led to formation of AVMs in P6 neonate retinas (293). This along with previous studies strongly suggest that the AVM phenotype observed in neonatal retinas of HHT1 (endoglin-deficient) mice was potentially due to lack of BMP9/10 mediated signalling (Figure 5.3B). I therefore hypothesised that treatment with active BMP9 would prevent the formation of AVMs in Eng-iKO neonatal retinas by bypassing the role of endoglin to activate ALK1 signalling (Figure 5.3C). To address this hypothesis, the effect of intra-ocular (IO) BMP9 treatment on retinal AVM formation was tested in HHT1 mice and is addressed in results section 5.2.4.

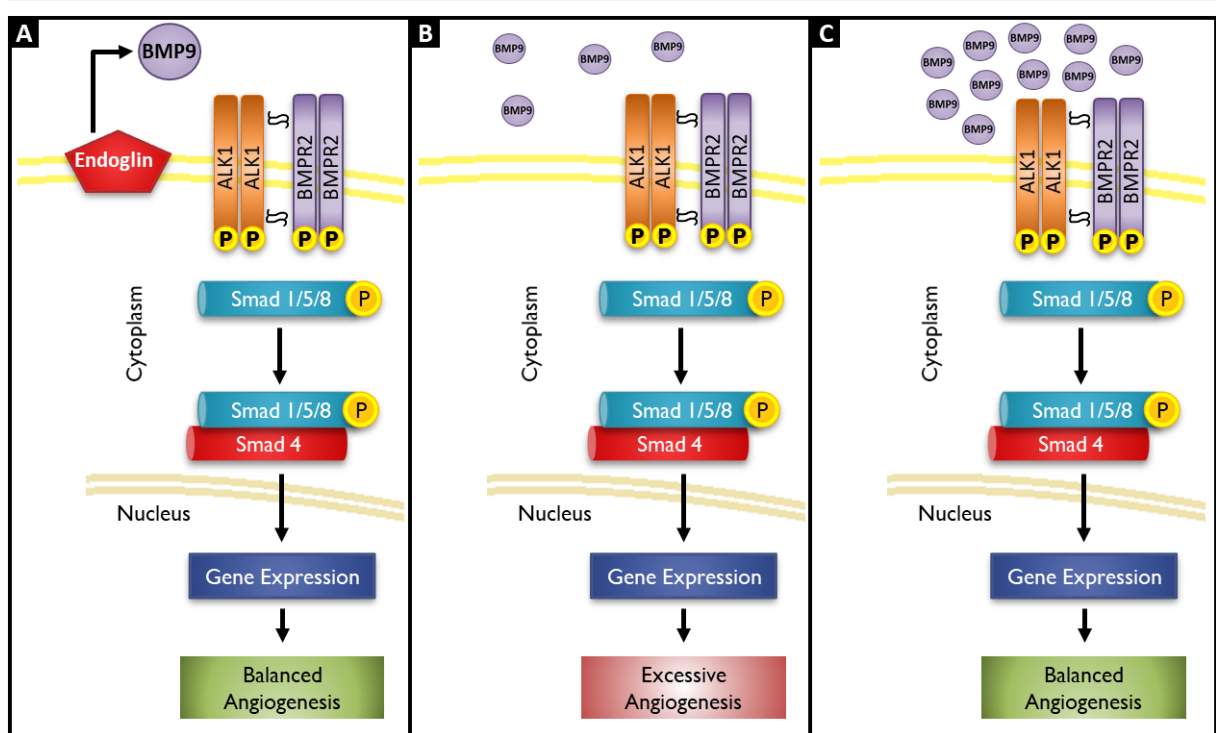


**Figure 5.3: BMP9 mediated signalling in ECs via ALK1 and endoglin mediated signalling.** (A) In normal/control retinas, during the angiogenesis process, endoglin promotes BMP9 ligand recruitment/binding to the BMPR2 which then combine with ALK1 type 1 receptor to induce ECs proliferation via SMAD mediated signalling. (B) However, in *Eng-iKO<sup>EC</sup>* retinas ALK1 mediated signalling is inhibited leading to imbalanced angiogenesis. (C) I hypothesise, that in the presence of abundant active BMP9 ligands, ALK1 mediated signalling is promoted leading to ECs proliferation.

In a recent study by Jin *et al.* (294), they showed that arteries are the origin for AVM formation. They showed that in the absence of endoglin, arterioles enlarge and over time expand to merge with veins to form AVMs (294). In this chapter, I analysed the effect of endoglin knockdown specifically in venous and capillary ECs on AVM formation, using a venous ECs specific *Apj<sup>Cre-ER</sup>* mouse line (44). The expression of the apelin receptor *Apj* has been shown in venous ECs during embryonic development (43, 44). I hypothesised that endoglin knockdown only in venous ECs would either prevent or delay AVM formation and address this in results section 5.2.5.

### 5.1.3. Endoglin and Quiescent Adult Vasculature

Finally, in my host laboratory, knockdown of endoglin in quiescent adult ECs (*Eng-iKO<sup>qEC</sup>*) in mice has been shown to lead to HOHF (Figure 5.4). In HOHF, heart failure is coupled with increased cardiac output and this pathology occurs due to reduced vascular resistance which could be due to anaemia, vasodilation or formation of AVMs (295-297).

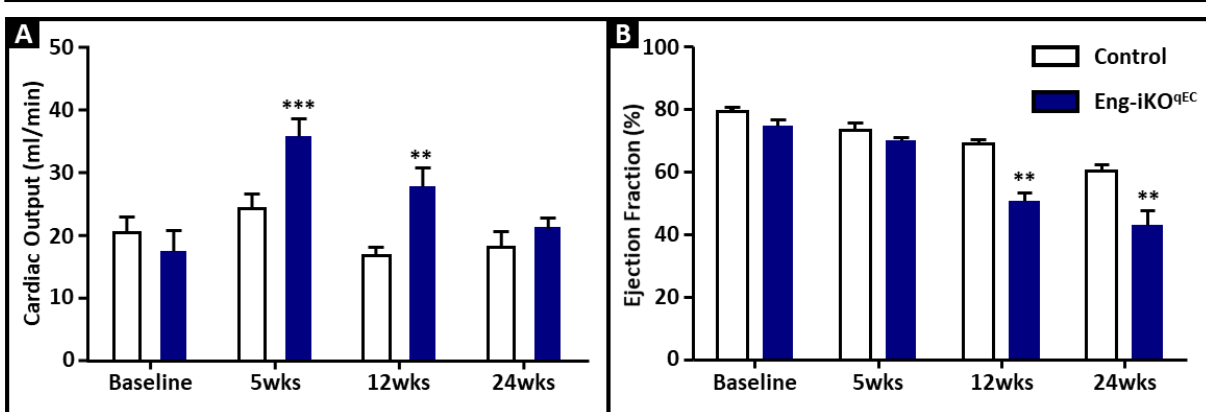


**Figure 5.4: Knockdown of *Endoglin* in ECs lead to High Output Heart Failure.** Magnetic resonance imaging showed increased cardiac output (A) and reduced ejection fraction (B) in *Eng-iKO<sup>qEC</sup>* mice (data courtesy Dr. Simon Tual-Chalot).

Aortic telemetry analysis showed reduced aortic pressure in Eng-iKO<sup>qEC</sup> mice whilst cardiac conductance catheter analysis showed decreased end systolic LV blood pressure, indicating reduced systemic vascular resistance (unpublished data, Arthur Lab). Further experiments to analyse the cause of HOHF phenotype showed normal haemoglobin levels and normal dilation of aorta in Eng-iKO<sup>qEC</sup> mice, eliminating anaemia and vascular tone as the cause of HOHF (unpublished data, Arthur Lab). I therefore hypothesised that the reduced vascular resistance leading to HOHF in Eng-iKO<sup>qEC</sup> mice could be due to AVMs in the systemic circulation. In this chapter (section 5.2.6) I sought to address this question using microbeads to detect arteriovenous shunting.

## 5.2. Results

### 5.2.1 Optimisation of *Dll4in3<sup>Cre-ERT2</sup>* activation

*Dll4in3<sup>Cre-ERT2</sup>* is a new arterial specific Cre mouse line. To determine an optimal dose of tamoxifen to activate Cre-ERT2, *Dll4in3<sup>Cre-ERT2</sup>* mice were crossed with Rosa26<sup>eYFP</sup> reporter mice (230) so that expression of eYFP protein could be used to track all Dll4in3-Cre positive cells and their descendants (Figure 5.5A).

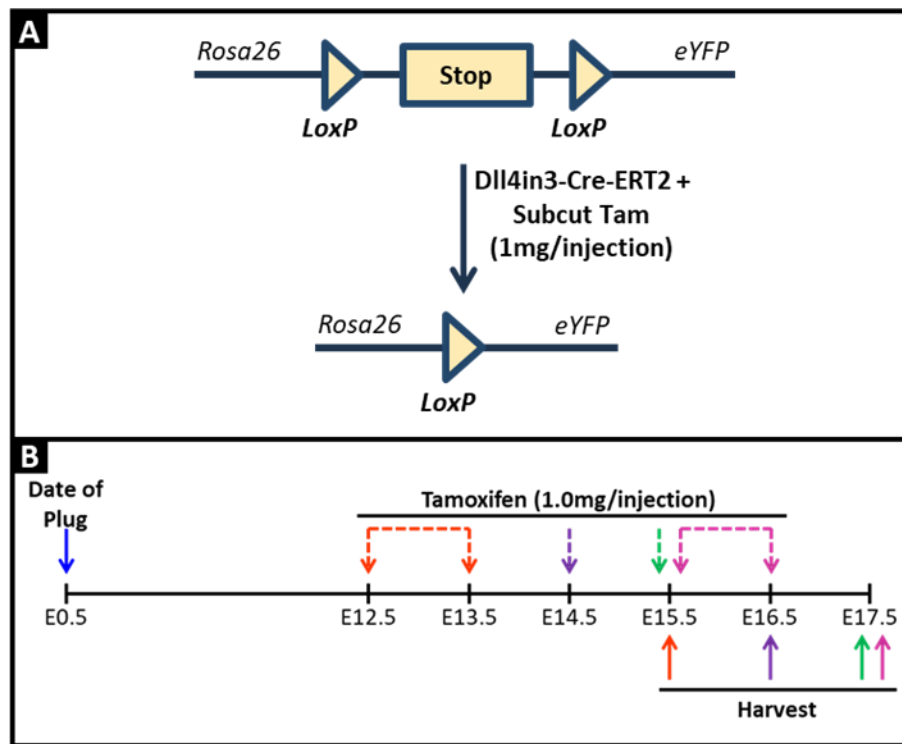


**Figure 5.5: Optimisation of  $Dll4in3^{Cre-ERT2}$  activation.** (A) Cre mediated deletion of stop sequence from the *eYFP* gene in Rosa26 floxed stop eYFP reporter mice leads to expression of eYFP protein in all *Dll4in3*-Cre positive cells. (B) Experiment design used to activate  $Dll4in3^{Cre-ERT2}$  using 1mg tamoxifen/injection (subcut) at different time points. Each dotted coloured arrow represents a different time points used to activate the Cre-ERT2 while the same colour continuous arrow represents the day embryos were harvested.

As the development of coronary vessels begins around E11.5 from the sinus venous (43, 44), the arterial markers are probably not yet expressed, I first activated  $Dll4in3^{Cre-ERT2}$  by two tamoxifen injections at E12.5 and E13.5 (orange arrows, Figure 5.5B). The embryos were harvested at E15.5 and embedded in paraffin wax (protocol described in section 2.4.1). Next, to visualise eYFP expression, embryos were sectioned and stained with rabbit anti-GFP antibody following the IHC-DAB staining protocol (section 2.5.2). The analysis of eYFP stained images showed very few eYFP positive coronary arteries in the myocardium (Black arrow, Figure 5.6A) but strong expression was observed in the aortic endothelium (red arrows, Figure 5.6F) and right coronary artery (yellow arrow, Figure 5.6F).

To analyse if later activation of  $Dll4in3^{Cre-ERT2}$  would yield better labelling of coronary arteries,  $Dll4in3^{Cre-ERT2}$  was activated by injecting tamoxifen at (i) E14.5, (ii) E15.5 and (iii) E15.5 & E16.5 (Figure 5.5B). The embryos were harvested at E16.5 or E17.5 and were embedded in paraffin wax, sectioned and stained with rabbit anti-GFP antibody as before. In all three scenarios, very few coronary arteries expressed eYFP protein (black arrows, Figure 5.6, B-D). However, positive expression of *Dll4in3-Cre* was observed in the pulmonary artery (blue arrows, Figure 5.6 G&H) and in aorta (red arrows, Figure 5.6I). As *Dll4in3-Cre* was only expressed in a few coronary arteries, further studies using this mouse line were discontinued.

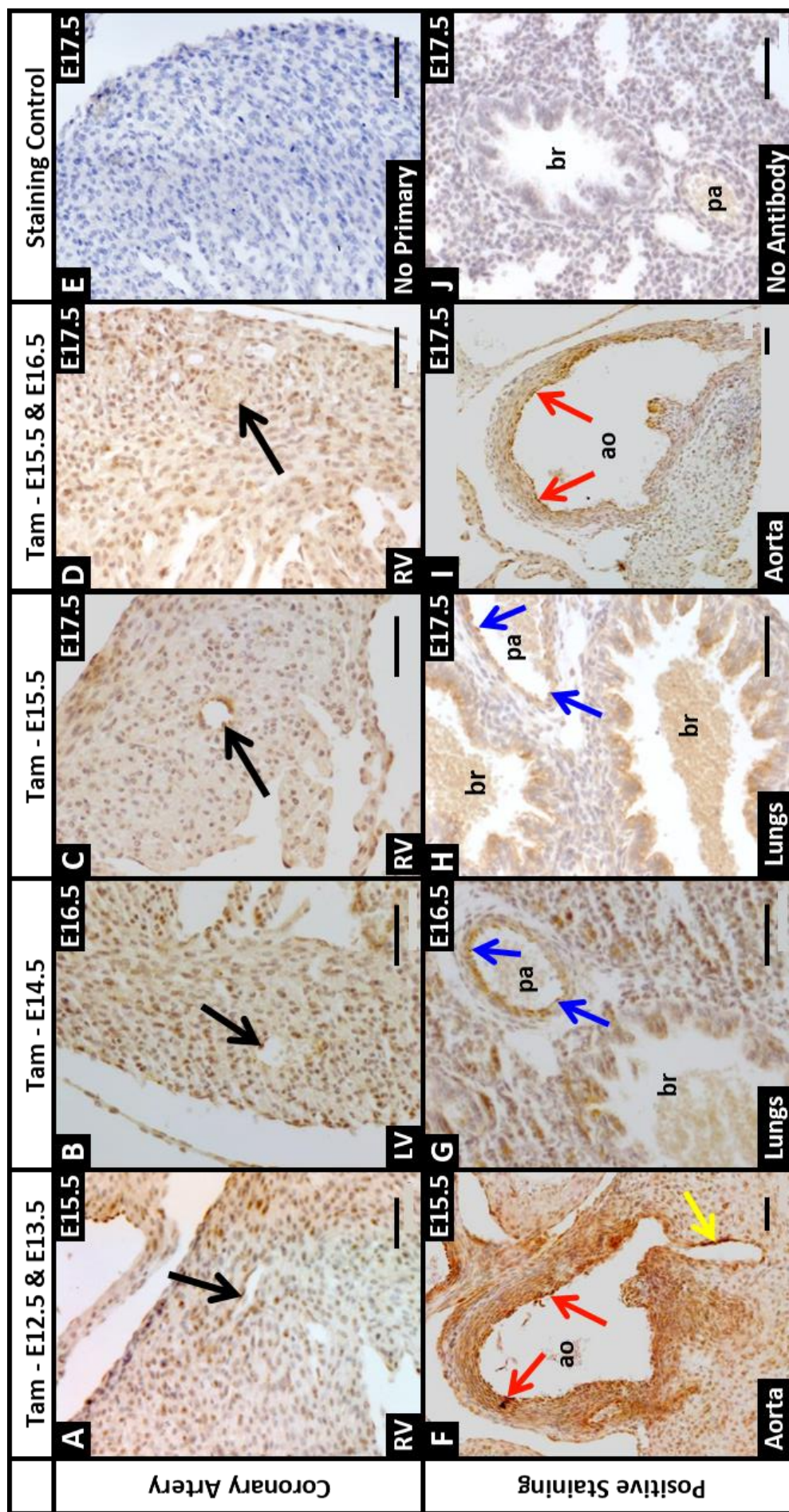


**Figure 5.6: *Dll4in3<sup>Cre-ERT2</sup>* activation and analysis at different time points in heart development.** IHC-DAB stained heart with anti-GFP antibody to detect eYFP protein (brown) and counterstained with haematoxylin to mark the nuclei (purple). Activation of *Dll4in3<sup>Cre-ERT2</sup>* via subcutaneous tamoxifen injection (1mg/injection) at (A) E12.5 & E13.5 ( $n=2$ ); (B) E14.5 ( $n=2$ ); (C) E15.5 & E16.5 ( $n=2$ ) and (D) E15.5 & E16.5 ( $n=2$ ) did not show strong labelling of coronary arteries (black arrows A-D). However, high expression was observed in the aorta (red arrows, F&I), base of right coronary artery (yellow arrow, F) and pulmonary artery (blue arrows, G&H). (E) No primary and (J) no antibody staining controls. Scale bars: A-J = 50µm. Abbreviation: RV - Right ventricle; LV - Left ventricle; ao - Aorta; br - Bronchioles and pa - Pulmonary Artery.

---

## 5.2.2 Effect of Endothelial Specific Endoglin Knockdown on Coronary Vessel Development in the Foetal and Neonatal Heart

In this section, the role of endoglin in ECs during the third wave of coronary vessel development (Figure 1.15) was analysed using the *Eng<sup>fl/fl</sup>; VE-Cad<sup>Cre-ERT2</sup>* mouse (Figure 5.7). The expression of *VE-Cad<sup>Cre-ERT2</sup>* was first mapped using *Rosa26<sup>eYFP</sup>* reporter mice (230) using a previously optimised protocol (i.e. subcut 0.5mg tamoxifen injection at P2 and P4; Figure 5.7). Following this, pup hearts were harvest at P7, fixed in 1% PFA, embedded in OCT, sectioned and stained with rat anti-CD31 to detect ECs and chicken anti-GFP antibody to detect eYFP protein expression.

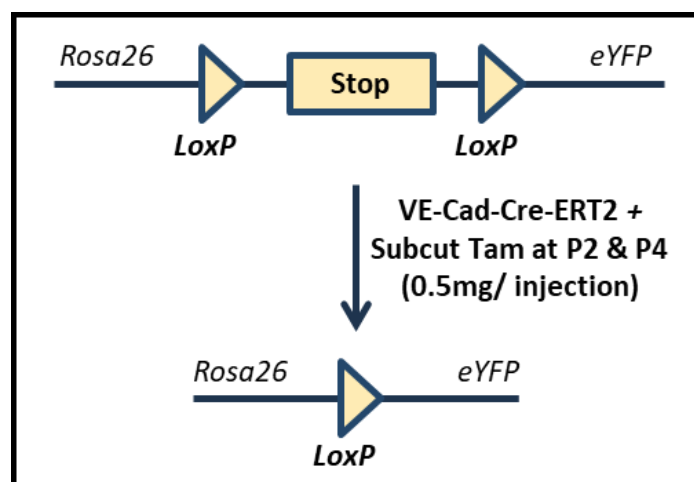


**Figure 5.7: Mapping the expression pattern of *VE-Cad<sup>Cre-ERT2</sup>* in neonate mouse hearts using *Rosa26<sup>eYFP</sup>* reporter mice.** Activation of *VE-Cad<sup>Cre-ERT2</sup>* by Subcut tamoxifen injection (0.5mg/injection) at P2 and P4 leads to deletion of stop sequence from the *eYFP* gene, leading to expression of eYFP in all VE-Cad-Cre positive cells and daughter cells, hence confirms activation of Cre-ERT2.

Overview images of stained P7 hearts showed strong expression of eYFP in coronary vessels (Figure 5.9, A-C). Qualitative analysis of x20 magnification images showed eYFP expression in coronary arteries, coronary veins and many capillaries (Figure 5.9, E-G). However, a few capillaries were observed to be negative for eYFP expression interspersed throughout the myocardium (white arrows, Figure 5.9, E-G). These VE-Cad-Cre negative capillaries could possibly be lymphatic vessels. However, this would need confirmation by staining with a lymphatic vessels marker such as LYVE1 (298).

As the majority of coronary vessel ECs expressed eYFP, showing efficient Cre activation endoglin was next depleted in these cells using the *Eng<sup>fl/fl</sup>* mouse (Figure 5.8). To knockdown endoglin in ECs, tamoxifen (0.5mg/injection) was injected on day P2 and P4 as before. On day P7, pups were weighed and humanely killed by cervical dislocation. The beating pup hearts were harvested following the protocol describe in section 2.1.3. The freshly dissected hearts were weighed and imaged using MZ6 Leica microscope. Next, hearts were fixed in 1% PFA,

embedded in OCT, coronally sectioned into sister sections and subjected to double immunofluorescence staining to analyse the vasculature.

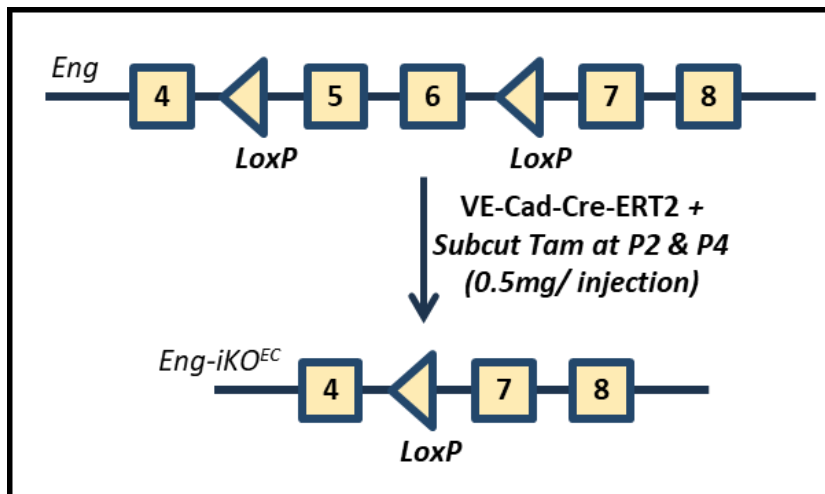


**Figure 5.8: Endothelial specific *Endoglin* knockdown using *Eng<sup>fl/fl</sup>*; *VE-Cad<sup>Cre-ERT2</sup>* mouse line.** In *Eng<sup>fl/fl</sup>* mouse line, exon 5 and 6 of *Endoglin* gene are flanked by *LoxP* sequences. In the presence of an active Cre, *LoxP* site along with exon 5 and 6 are removed from the gene leading to formation of truncated endoglin protein. In the current experiment, *VE-Cad<sup>Cre-ERT2</sup>* was used to knockdown endoglin in all *VE-Cad<sup>Cre-ERT2</sup>* positive cells. To activate Cre-ERT2, tamoxifen was injected via subcut route on day P2 and P4 (dose: 0.5mg/ injection).

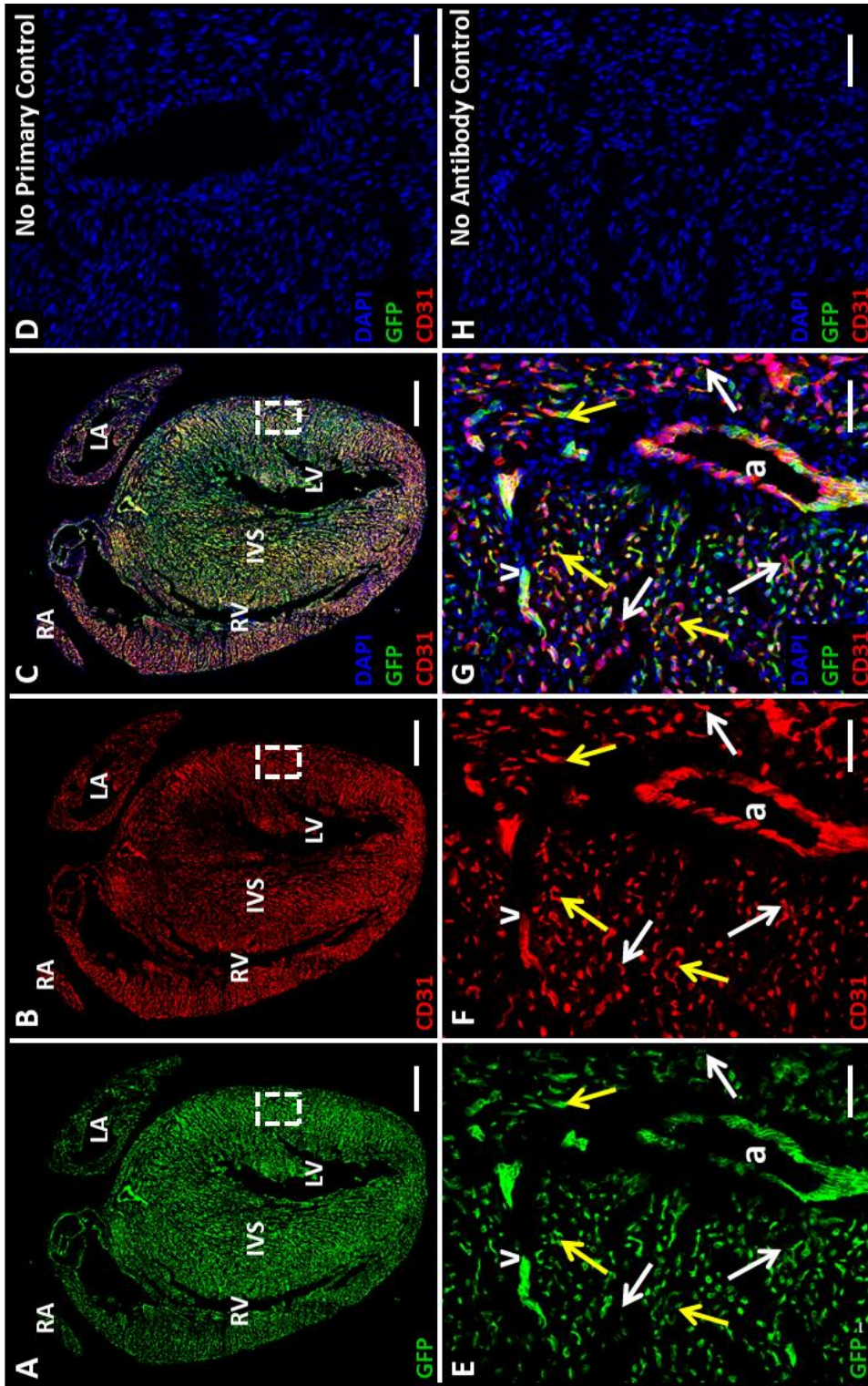


**Figure 5.9: Activation of *VE-Cad*<sup>Cre-ERT2</sup> at P2 & P4 showed strong expression of eYFP in coronary endothelium of P7 hearts.** P7 heart sections stained with chicken anti-GFP (green) and rat anti-CD31 (red) antibodies and counterstained with DAPI to mark nuclei (blue). (A-C) Split channel tiled images of a P7 heart showed *VE-Cad*<sup>Cre-ERT2</sup> expressing coronary vessels throughout the myocardium. (E-G) Split channel images (dotted box, A to C) of P7 heart showed eYFP expression in arteries (a), veins (v) and most of the capillaries (yellow arrow). A few capillaries were observed to be eYFP negative (white arrows). These were randomly distributed throughout the myocardium (n=2). (D) No primary and (H) no antibody staining control. Abbreviation: a – Artery; IVS – Interventricular Septum; LA – Left Atria; LV – Left Ventricle; RA – Right Atria; RV – Right Ventricle and v – Vein. Scale Bars: A-C = 1mm & D-H = 50µm.

The body weight (both male and female pups) of control (n=38) and Eng-iKO<sup>EC</sup> (n=28) mice were similar (Figure 5.10C). However, the size and weight of Eng-iKO<sup>EC</sup> hearts was significantly higher than controls. This difference was maintained when heart weight was normalised to body weight showing a 61% increase in heart size compared to controls (Figure 5.10D). This shows that loss of endothelial endoglin led to heart enlargement potentially due to cardiac hypertrophy or dilation.

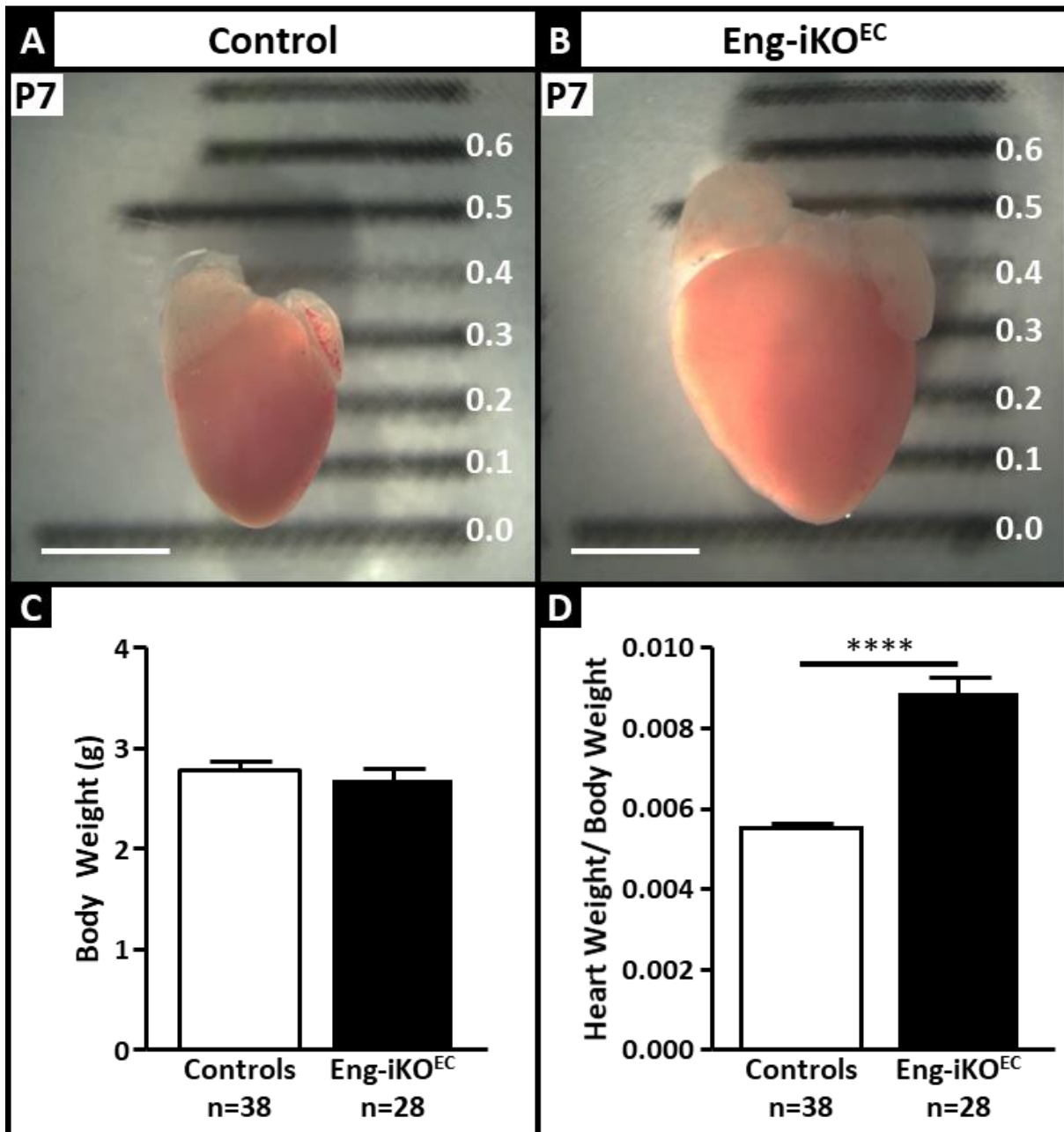


**Figure 5.10: Endothelial specific *Endoglin* knockdown using *VE-Cad*<sup>Cre-ERT2</sup> led to development of enlarged hearts in P7 *Eng-iKO<sup>EC</sup>* mice compared to controls.** Whole-view images of (A) a control and (B) an enlarged *Eng-iKO<sup>EC</sup>* heart. (C) The body weight of both controls ( $2.774 \pm 0.097$ ,  $n=38$ ) and *Eng-iKO<sup>EC</sup>* ( $2.686 \pm 0.115$ ,  $n=28$ ;  $p = 0.5601$ ) mice was observed to be similar. (D) In contrast, heart weight (normalised to body weight) of *Eng-iKO<sup>EC</sup>* ( $0.0089 \pm 0.0004$ ,  $n=28$ ) mice was significantly higher compared to controls ( $0.0055 \pm 0.0001$ ,  $n=38$ ;  $p = < 0.0001$ ). Data shown as mean  $\pm$  SEM and analysed using two tailed unpaired t-test (\*\*\*\*  $p < 0.0001$ ). Scale bar A&B = 2mm.

---

I next analysed the effect of endothelial endoglin knockdown on coronary vascular development. To study this, coronal sister sections of the above P7 control (n=3) and Eng-iKO<sup>EC</sup> (n=3) hearts were stained using immunofluorescence staining with rat anti-CD105, rabbit anti-Sm22 $\alpha$  and goat anti-podocalyxin (EC marker). Once stained, 3 to 4 images (x20 magnification) were taken from the free ventricular wall (RV and LV) as described in Figure 5.11. Endoglin knockdown efficiency and vascular density were calculated by quantification of percentage stained area of CD105 and podocalyxin staining using the threshold function of ImageJ software. In addition, to compare the effect of endothelial specific endoglin knockdown on the density of muscularised vessels (Sm22 $\alpha$  positive), manual counting was performed following the method described in Chapter 4 (section 4.2.3) using the event function of Zen 2012 software.

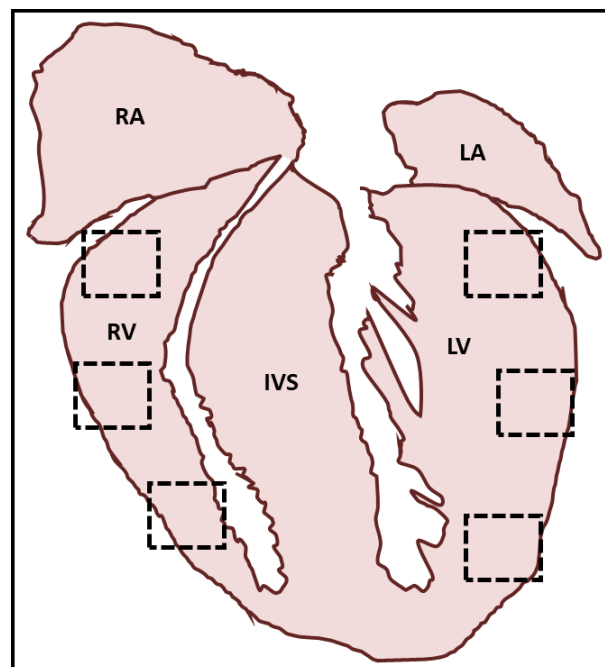
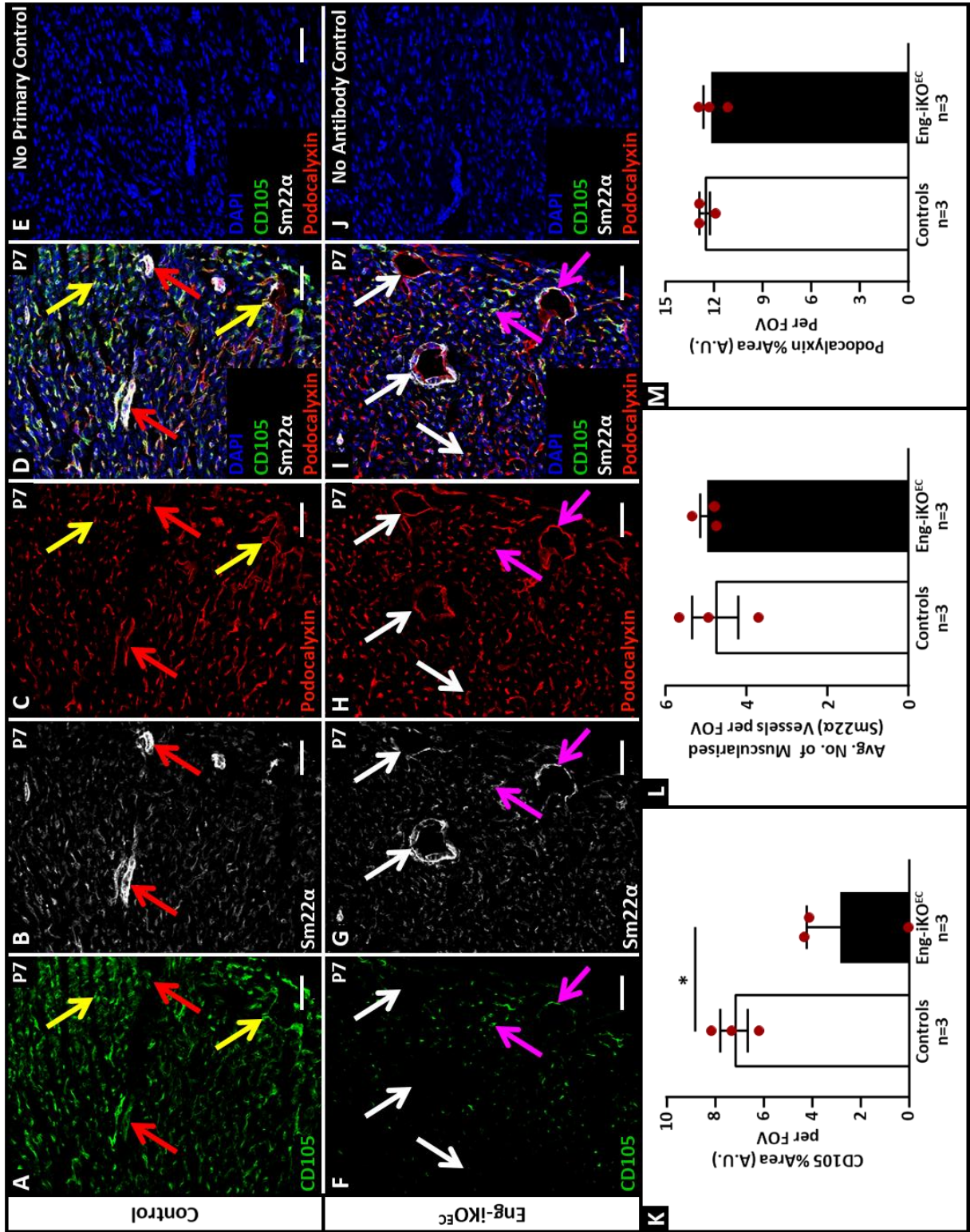


**Figure 5.11: Cartoon image of coronal P7 heart section.** For quantification, higher power images were taken from free RV and LV wall around the dotted black boxed region. Abbreviation: RA – Right Atria; RV – Right Ventricle; LA – Left Atria; LV – Left Ventricle; IVS – Inter Ventricular Septum.

Image analysis showed expression of endoglin in large (red arrows, Figure 5.12A) and small vessels (yellow arrows, Figure 5.12A) in controls. The quantification of percentage stained CD105 area showed a significant endoglin knockdown (~61%) in Eng-iKO<sup>EC</sup> hearts compared with controls (Figure 5.12K). However, number of muscularised vessels (Figure 5.12L) and podocalyxin staining density (Figure 5.12M) per FOV was similar in Eng-iKO<sup>EC</sup> hearts compared to controls suggesting that endoglin knockdown did not lead to any obvious coronary vascular defects

**Figure 5.12: Lack of Endoglin in ECs did not lead to any coronary vasculature related defects in P7 Eng-iKO<sup>EC</sup> hearts.** Immunofluorescence stained P7 coronal heart sections, stained with rat anti-CD105 (green), rabbit anti-Sm22 $\alpha$  (white, to mark SMCs), goat anti-podocalyxin (red, to mark ECs) antibodies and counterstained with DAPI (blue). **(A-D)** Split channel x20 magnification images of a control P7 heart showed expression of endoglin in capillaries (yellow arrows) and muscularised vessels (red arrows). **(F-I)** Split channel images of an Eng-iKO<sup>EC</sup> P7 heart showed patchy endoglin knockdown. Complete endoglin knockdown was observed in most of the capillaries and muscularised vessels (white arrows) while a few vessels were observed to express endoglin (pink arrows). No difference in the **(G)** Sm22 $\alpha$  and **(H)** podocalyxin staining was observed with Eng-iKO<sup>EC</sup> compared to control **(B&C)**. **(E)** No primary and **(J)** no antibody staining controls. **(K)** Quantification showed significantly reduced percentage CD105 stained area in Eng-iKO<sup>EC</sup> ( $2.832 \pm 1.399$ ,  $n=3$ ) compared to control ( $7.228 \pm 0.571$ ,  $n=3$ ,  $p = 0.0437$ ) hearts. **(L)** No statistical difference was observed in the average number of muscularised vessels per FOV in controls ( $4.780 \pm 0.569$ ,  $n=3$ ) and Eng-iKO<sup>EC</sup> ( $4.967 \pm 0.192$ ,  $n=3$ ;  $p = 0.7716$ ) hearts. **(M)** Similarly, no statistical difference in the endothelial cells (ECs) density was observed between controls ( $12.16 \pm 0.5147$ ,  $n=3$ ;  $p = 0.5209$ ) hearts. Data shown as mean  $\pm$  SEM and analysed using two tailed unpaired *t*-test (\*  $p < 0.05$ ). Scale bar A-J = 50 $\mu$ m.



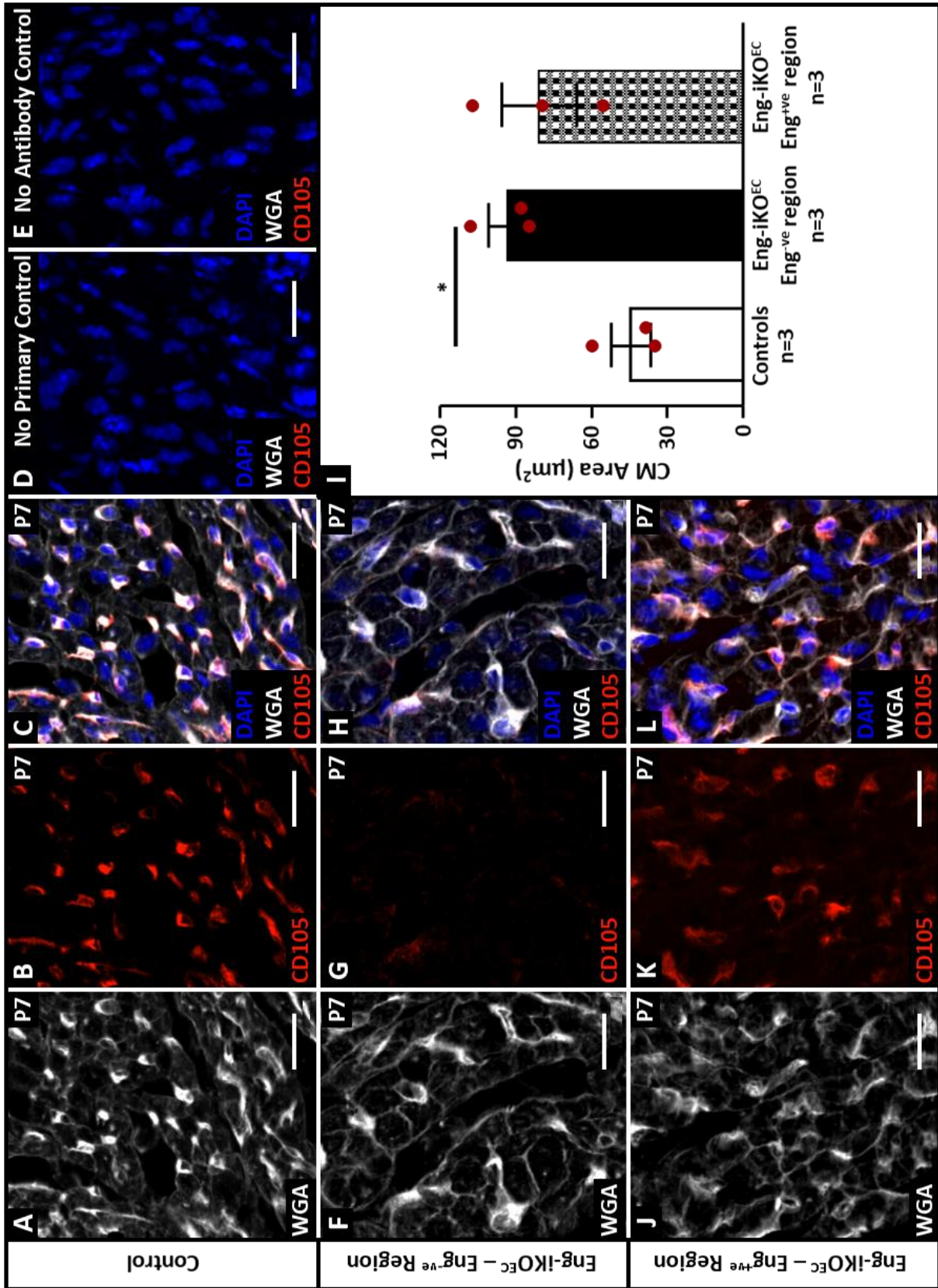
---

Next, the cardiac structure was analysed, coronal heart sections of P7 control (n=3) and Eng-iKO<sup>EC</sup> (n=3) mice were stained with fluorescein labelled wheat germ agglutinin (WGA) and rat anti-CD105 antibody to investigate CM hypertrophy. Once stained, three images were taken from free RV and LV region of the heart (boxed region, Figure 5.11) using fluorescence setting on M2 axio-imager at x40 magnification. These images were taken from a minimum of three sections per heart and each of these sections was at least 100µm apart to avoid duplicate imaging of same cell.

Analysis of CD105 staining showed ~40% endoglin knockdown in 2 out 3 Eng-iKO<sup>EC</sup> hearts and over 90% knockdown in the third heart. In order to evaluate whether there were differences between the myocardial regions with and without endoglin expression in Eng-iKO<sup>EC</sup> hearts, a mosaic analysis was performed: CM cell area was measured in Eng-ve areas and compared with Eng+ve regions within the same heart using spline contour function of Zen 2012 software. The analysis showed a significant increase in the area of CM in the Eng-ve region of Eng-iKO<sup>EC</sup> mice (Figure 5.13 F-H) compared to controls (Figure 5.13 A-C, *p value* = 0.050). The area of CM in the Eng+ve region of Eng-iKO<sup>EC</sup> mice was similar to area of CM in the Eng-ve region (Figure 5.13, J-L, *p value* =0.999). These CM in the Eng+ve region of Eng-iKO<sup>EC</sup> mice also showed a trend to be bigger than control CM (*p value* = 0.154).

---

**Figure 5.13: Endothelial specific *Endoglin* knockdown led to cardiomyocyte hypertrophy in P7 *Eng-iKO<sup>EC</sup>* hearts compared to controls.** Immunofluorescence stained P7 hearts with fluorescein labelled wheat germ agglutinin (WGA, white) and rat anti-CD105 antibody (red). Counterstained with DAPI to mark nuclei (blue). Split channel high-power image of a (A-C) control and (F-H, J-L) *Eng-iKO<sup>EC</sup>* hearts showed an increased cardiomyocyte (CM) area in *Eng-iKO<sup>EC</sup>* compared to controls. (D) No primary and (E) no antibody staining controls. (I) Quantification showed significantly increased area of CMs in the complete *Eng*-ve region of *Eng-iKO<sup>EC</sup>* mutants ( $93.56 \pm 7.251$ ,  $n=3$ ) compared to controls ( $44.51 \pm 7.819$ ,  $n=3$ ;  $p = 0.050$ ). The area of CM in *Eng*+ve region of *Eng-iKO<sup>EC</sup>* mutant hearts ( $80.73 \pm 14.85$ ,  $n=3$ ) was similar to *Eng*-ve region CMs ( $p > 0.999$ ). These CMs in *Eng*+ve region of *Eng-iKO<sup>EC</sup>* mutant hearts also showed a non-significant trend to be bigger than control CMs ( $p = 0.154$ ). Data shown as mean $\pm$ SEM and analysed using one-way Anova (\*  $p < 0.05$ ). Scale bar A-H & J-L = 20 $\mu$ m.



---

Total heart width of Eng-iKO<sup>EC</sup> heart sections (using x10 tiled images mid-coronal sections in 4 chamber view, Figure 5.14B) was observed to be significantly higher than control hearts (Figure 5.14A). I next analysed if these enlarged hearts had any difference in wall thickness by measuring width of free ventricular walls from a minimum of 3 sections per heart. There was a non-significant trend towards slightly reduced ventricular wall thickness of both right (~8%) and left (~16%) free walls in Eng-iKO<sup>EC</sup> hearts compared to controls (Figure 5.14F). This suggests that these hearts have eccentric cardiac hypertrophy with enlarged ventricle chambers. Eccentric cardiomyopathy is characterised by occurrence of increased chamber volume in response to chronic volume overload without a significant change in myocardial wall thickness (299).

As no coronary vasculature related defects were observed, the cause of this enlarged cardiac phenotype could be due to a systemic vasculature defect, potentially due to reduced vascular resistance due to formation of AVMs in the systemic vasculature. As a previous study in my host laboratory using the same mouse line showed formation of AVMs in the neonatal retina of Eng-iKO<sup>EC</sup> mice (188) I repeated this analysis in a small group of neonates. The postnatal retina model provides a powerful tool to study pathological angiogenesis during vascular development *in vivo*. In the first week after birth, the retinal vasculature expands towards the periphery of the retina and by P8 the entire surface of retina is covered with a 2D primary vascular plexus with an alternating pattern of arteries and veins (easily distinguished as arteries are thinner than veins, and capillaries are less dense around arteries) providing a valuable structure to study vascular development *in vivo* (300, 301).

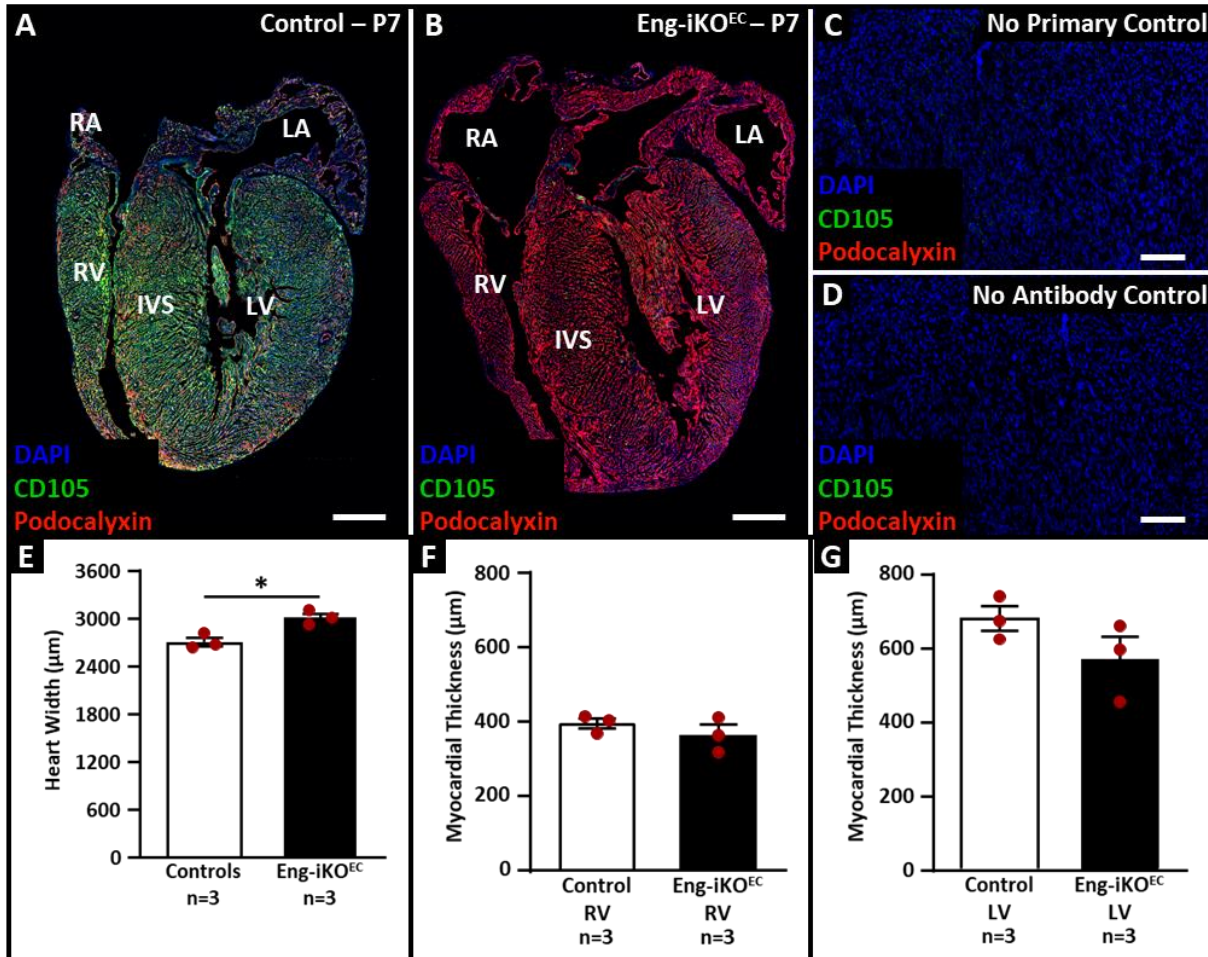


**Figure 5.14: Endothelial specific *Endoglin* knockdown led to an enlarged heart.** Immunofluorescence stained P7 coronal heart sections, stained with rat anti-CD105 (green) and goat anti-podocalyxin (red, to detect ECs) antibodies. Counterstained with DAPI to mark nuclei (blue). Tiled overview images of (B) an Eng-iKO<sup>EC</sup> heart showing an enlarged and slightly dilated ventricles compared to littermate (A) control hearts. (C) No primary and (D) no antibody staining controls. (E) Quantification showed that overall the Eng-iKO<sup>EC</sup> hearts were significantly wider ( $3015.00 \pm 49.10$ ,  $n=3$ ) compared to controls ( $2709.00 \pm 55.21$ ,  $n=3$ ;  $p = 0.0144$ ). (F) The myocardial width analysis of RV and LV free wall showed a similar width between Eng-iKO<sup>EC</sup> (RV:  $365.20 \pm 27.44$ ,  $n=3$  and LV:  $571.30 \pm 59.99$ ,  $n=3$ ) and control (RV:  $396.60 \pm 13.67$ ,  $n=3$ ;  $p = 0.3641$  and LV:  $681.30 \pm 33.88$ ;  $n=3$ ;  $p = 0.1856$ ) hearts. Data shown as mean  $\pm$  SEM and analysed using two tailed unpaired *t*-test (\*  $p < 0.05$ ). Abbreviation: RA – Right Atria; RV – Right Ventricle; LA – Left Atria; LV – Left Ventricle; IVS – Inter Ventricular Septum. Scale bar: A-B = 1mm & C-D = 100 $\mu$ m.

---

### 5.2.3 Effect of Endothelial Specific Endoglin Knockdown on the Neonatal Retinal Vasculature

To investigate the presence of retinal AVMs in P7 mice, control and Eng-iKO<sup>EC</sup> retinas were harvested according to the protocol described in section 2.1.3. These retinas were then stained using rat anti-CD105 antibody and isolectin GS-IB4 (to mark ECs) using the wholemount immunofluorescence staining protocol described in section 2.5.5. Next, whole-view retinal images were taken using M2 axio-imager microscope. To measure vascular progression, the ratio of length of each retina petal (Figure 15.5, grey line) and expanding vasculature (Figure 15.5, yellow line) was calculated from the centre of the retina using the line function of Zen 2012 software (Figure 5.15).

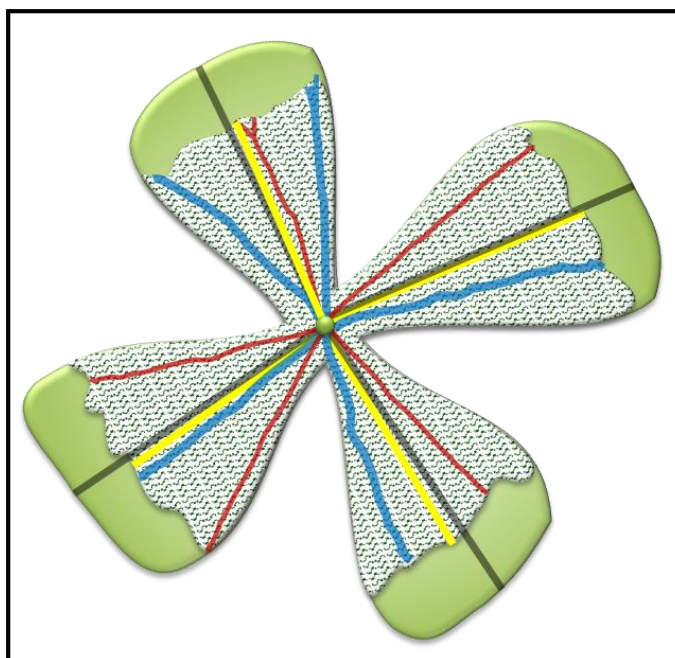


**Figure 5.15: Cartoon of neonate retina showing vasculature structure and progression.** The development of the retinal vasculature begins at the centre of the retina with alternating pattern between arteries (red) and veins (veins). The vasculature progression was measured by calculating a ratio of expanding vasculature length (yellow line) over the radius of the retina (black line).

The vasculature in control retinas (n=6) showed the typical pattern of alternating arteries and veins (Figure 5.16, A-F) with normal progression of the vascular plexus towards the retinal periphery (red & blue arrows, Figure 5.16, A-F). In contrast, AVMs were observed in 67% (4/6) of P7 Eng-iKO<sup>EC</sup> retinas (yellow arrows, Figure 5.16, G-L) with an average of 3 AVMs per retina. In addition there was delayed vascular progression (blue & red arrows, Figure 5.16, G-L) and hypervascularisation (white arrows, Figure 5.16, G-L) of the retinal plexus; consistent with previously published data (188).

Furthermore, and as previously observed in the current study, the hearts of all the P7 Eng-iKO<sup>EC</sup> (n=28) mice were enlarged compared to controls (n=38). As mentioned before, retinas were

---

selected to analyse the systemic vasculature because of the unique vasculature development in 2D format (300). However, it does not mean that AVMs are only expected in the retinas. AVMs can form in other organs such as brain, lungs and liver, and the retina merely serves as a representative tissue. For example, deletion of endothelial endoglin in neonates showed AVMs in brain as well as in retinas (294). However, this would need further confirmation by analysing other organs such as brain, liver and gut using different imaging techniques for instance latex injection in LV.

In conclusion, the current study shows a novel cardiac phenotype in Eng-iKO<sup>EC</sup> neonates that could be due to the presence of systemic AVMs, such as those seen in the retinas, leading to reduced vascular resistance. If AVMs could be prevented by using a therapeutic intervention and this could also rescue the cardiac phenotype, this would help to confirm the cause of the cardiac pathology and could potentially be developed in future work to treat HHT patients.

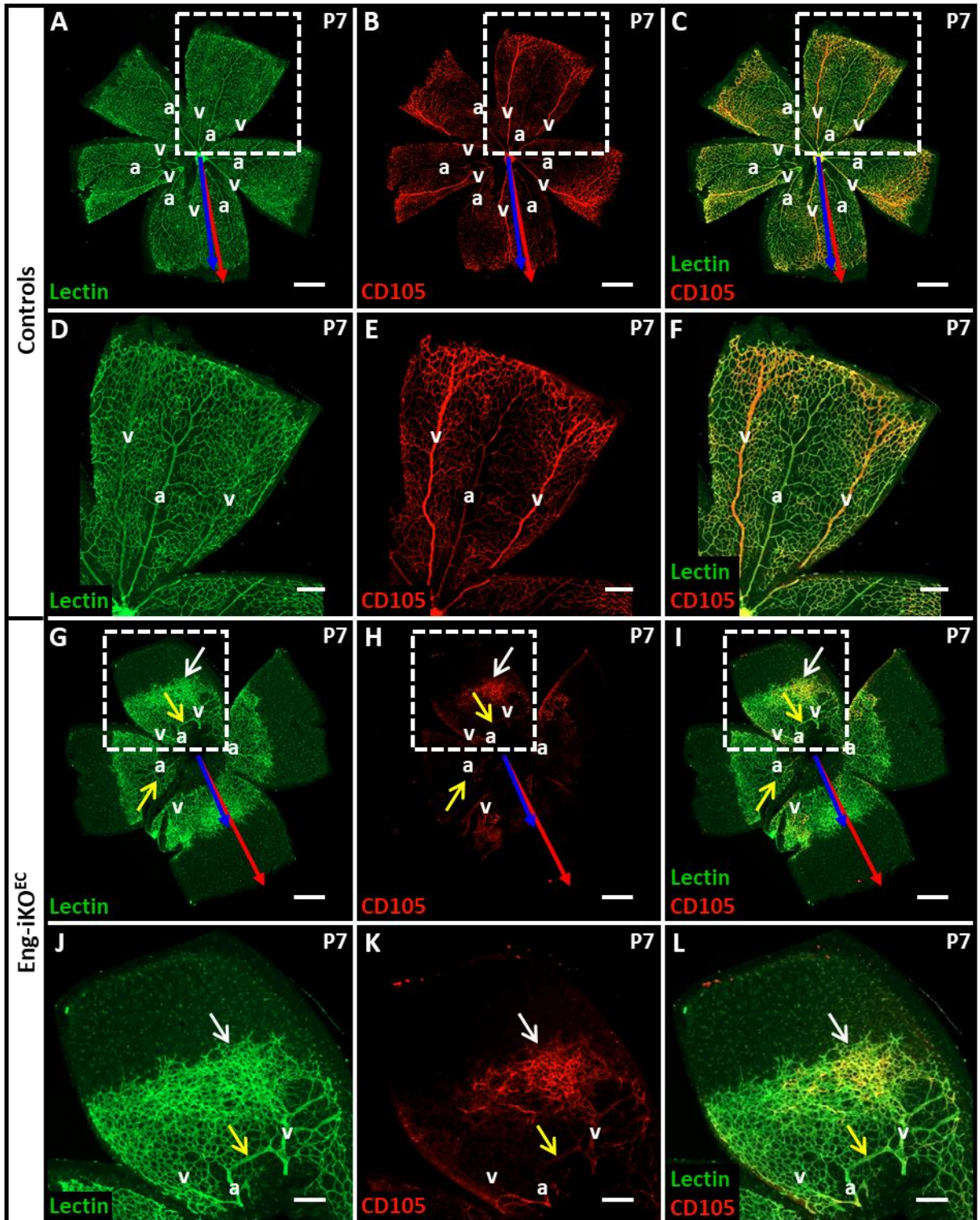


**Figure 5.16: Endothelial specific *Endoglin* knockdown led to development of AVMs in P7 *Eng-iKO<sup>EC</sup>* retinas.** Immunofluorescence stained P7 retinas with isolectin GS-IB4 (green, to mark ECs) and rat anti-CD105 antibody (red). Split channel (A-C) overview and (D-F) digital zoomed (white box) images of control of retina showed normally developed retina vasculature with alternate arteries and vein pattern as well as normal retina vasculature progression (red & blue arrows). Split channel (G-I) overview and (J-L) digitally zoomed (white box) images of an *Eng-iKO<sup>EC</sup>* retina showed presence of AVMs (yellow arrows), hypervascularisation (white arrows) and delayed retina vasculature progression (red & blue arrows). *Abbreviations: a – artery; AVMs – Arteriovenous malformations and v – vein.* Scale Bar: A-C & G-I = 500 $\mu$ m and D-F & J-L = 200 $\mu$ m.

---

## 5.2.4 To investigate the effect of exogenous BMP9 treatment on AVM formation in Eng-iKO<sup>EC</sup> mice – A Pilot Study

As discussed in section 5.1.2, absence of BMP9/10 signalling led to formation of AVMs in retinas (192, 293). During the signalling cascade, BMP9/10 signals via endoglin and ALK1 pathway (Figure 5.3). Therefore, in this section, I investigated whether exogenous BMP9 treatment could be used to reduce retinal AVM development in *Eng*<sup>fl/fl</sup>; *VE-Cad*<sup>Cre-ERT2</sup> mice. The *VE-Cad*<sup>Cre-ERT2</sup> was activated by tamoxifen injection at P2 and P4 via subcut route (Figure 5.8). Following this, active BMP9 ligand (3µl of 1.5mg/ml, right eye) and 3µl PBS (left eye) was injected via IO route on day P4 or P5 following the protocol described in section 2.6. Retinas were harvested on day P7, stained with isolectin GS-IB4 and imaged using the M2 axio-imager to detect AVMs.

The P7 retinas treated with IO injection of either BMP9 or PBS at P4 showed very poor morphology (data not shown) potentially due to the injury caused by the needle (27G). This hindered any data analysis on this group. While for IO injection at P5, the retinal vascular morphology was slightly better. To study the effect of BMP9 treatment, several parameters were analysed including retina vasculature progression, width of veins and AVMs following the methods described by Mahmoud *et al.* (188). Briefly, the vein width was calculated by taking 5 measurements along the vein (red lines, Figure 5.16C) using the line function of Zen 2012 software. Two to six veins were analysed per retina. The vein width was then normalised to controls within each litter. Similarly, to calculate AVM width, 3 measurements were taken (red lines, Figure 5.16E) from all the AVMs in the Eng-iKO<sup>EC</sup> retinas.

Analysis of P7 retinas showed a slight delay in the vascular progression at baseline (untreated) Eng-iKO<sup>EC</sup> mice compared to controls (Figure 5.17B). A similar result was observed in groups with IO injection of BMP9 and PBS (Figure 5.17B). The veins in the baseline Eng-iKO<sup>EC</sup> retinas were also observed to be wider compared to controls, consistent with previous work (188). However, after treatment with BMP9 the venous vessels diameter was still observed to be wider compared to controls (Figure 5.17D). Surprisingly, an increase in the number of AVMs (~2.8 fold in PBS treated and ~3.5 fold in BMP9 treated) and width of AVMs (~1.8 fold in PBS treated and ~2.0 fold in BMP9 treated) was observed in IO injected Eng-iKO<sup>EC</sup> compared to untreated Eng-iKO<sup>EC</sup> mice (Figure 5.17). This dramatic increase in the number of AVMs even in the PBS injected group suggests that the injection itself might have acted as a second trigger (186-190) which led to an enhanced angiogenic stimulus. This could be masking any potential rescue by BMP9.

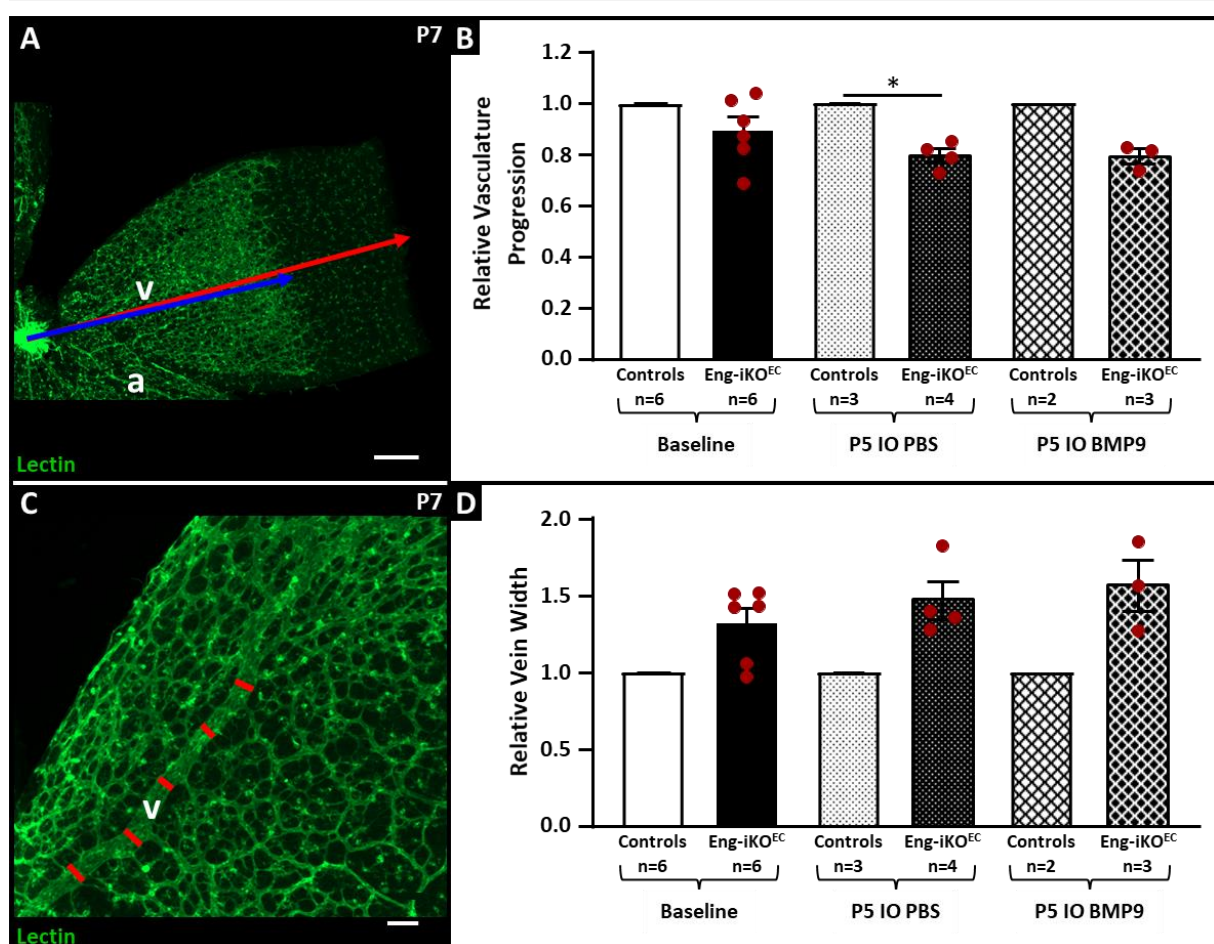
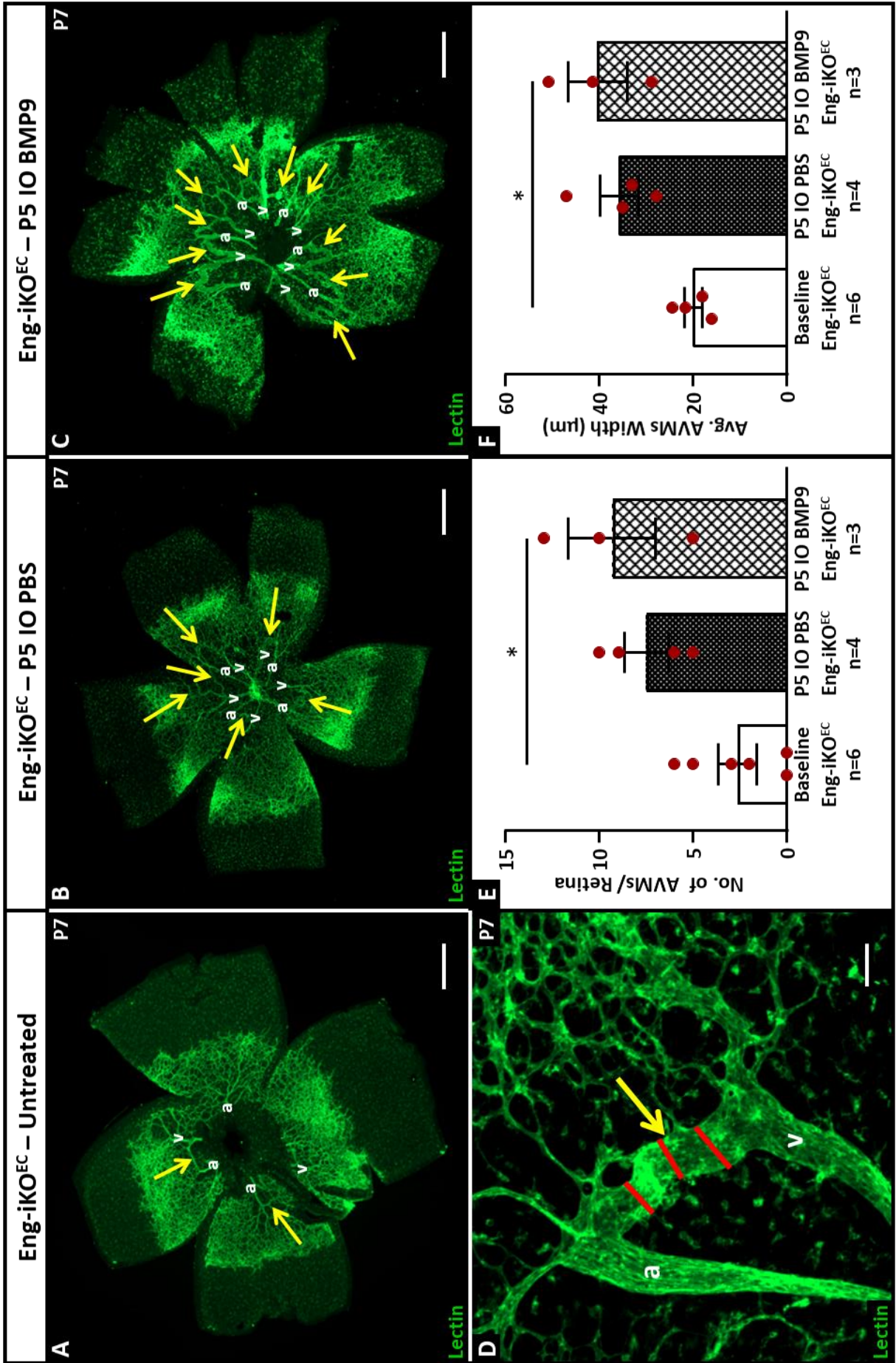


**Figure 5.17: Intraocular exogenous treatment of BMP9 did not rescue the AVMs phenotype in P7 Eng-iKO<sup>EC</sup>.** Immunofluorescence stained P7 retinas with isolectin GS-IB4 (Lectin, green). (A) Example of an Eng-iKO<sup>EC</sup> mice retina petal, showing relative progression of retinal vasculature (red arrow) towards the retina periphery (blue arrow). The control retinas from the two litters used in this analysis appeared to be at a different stage in retinal vascular development suggesting they were slightly different ages (+/- half a day). Therefore, vascular progression and vein width from Eng-iKO<sup>EC</sup> retinas were normalised to their litter mate controls. (B) Quantification showing a delayed relative vasculature progression (Eng-iKO<sup>EC</sup> over controls) in all baseline (untreated,  $0.8948 \pm 0.053$ ,  $n=6$ ;  $p = 0.3484$ ), PBS ( $0.7970 \pm 0.027$ ,  $n=4$ ;  $p = 0.0294$ ) and BMP9 ( $0.7933 \pm 0.030$ ,  $n=3$ ) treated Eng-iKO<sup>EC</sup> retinas compared to respective control retinas (baseline  $n=6$ ; IO P5 PBS,  $n=3$  and P5 IO BMP9,  $n=2$ ). (C) Example of a retina vein showing approximate sites of measurements to calculate vein width (red lines). (D) Quantification showed a non-significant trend towards wider veins in retinas of baseline (untreated,  $1.318 \pm 0.098$ ,  $n=6$ ;  $p = 0.1375$ ), PBS injected ( $1.466 \pm 0.123$ ,  $n=4$ ;  $p = 0.0687$ ) and BMP9 treated Eng-iKO<sup>EC</sup> retinas ( $1.562 \pm 0.168$ ,  $n=3$ ) compared to respective littermate control retinas (baseline  $n=6$ ; IO P5 PBS  $n=3$  and P5 IO BMP9  $n=2$ ). Data shown as mean  $\pm$  SEM and analysed using two-way ANOVA (\*  $p < 0.05$ ). Abbreviations: a – artery AVMs – Arteriovenous malformations and v – vein. Scale bars: A = 200  $\mu$ m & C = 50  $\mu$ m.

**Figure 5.18: Intraocular injection of PBS and BMP9 at P5 exacerbates the AVMs phenotype in P7 Eng-iKO<sup>EC</sup> mice.** Immunofluorescence stained whole-view images of (A) Eng-iKO<sup>EC</sup> – untreated (baseline); (B) Eng-iKO<sup>EC</sup> – P5 IO PBS; and (C) Eng-iKO<sup>EC</sup> – P5 IO BMP9 P7 retinas stained with isolectin GS-IB4 (green) showing AVMs connections (yellow arrow). (D) Digitally zoomed image of an AVM in Eng-iKO<sup>EC</sup> mice (yellow arrow) with approximate sites used to calculate AVM width (red lines). (E) Quantification showed a significant increase in the number of AVMs per retina in Eng-iKO<sup>EC</sup> mice with BMP9 ( $9.33 \pm 2.33$ ,  $n=3$ ;  $p = 0.0235$ ) compared to baseline Eng-iKO<sup>EC</sup> mice ( $2.67 \pm 1.0$ ,  $n=6$ ). While a non-significant increase was observed in IO injected PBS ( $7.50 \pm 1.19$ ,  $n=4$ ;  $p = 0.0754$ ) compared to baseline Eng-iKO<sup>EC</sup> retinas. (F) The AVMs width comparison between two groups showed a similar trend. Significantly wider AVMs were observed in BMP9 treated Eng-iKO<sup>EC</sup> retinas ( $40.40 \pm 6.34$ ,  $n=3$ ;  $p = 0.0269$ ) compared to baseline Eng-iKO<sup>EC</sup> mice ( $20.12 \pm 1.87$ ,  $n=4$ ). While a non-significant increase in AVMs width was observed in PBS injected retinas ( $35.80 \pm 4.05$ ,  $n=4$ ;  $p = 0.0633$ ) compared to baseline Eng-iKO<sup>EC</sup> mice. Data shown as mean  $\pm$  SEM and analysed using one-way ANOVA (\*  $p < 0.05$ ). Abbreviations: a – artery; AVMs – Arteriovenous malformations and v – vein. Scale Bar: A-C = 500 $\mu$ m & 50 $\mu$ m.



---

### 5.2.5 Effect of Venous Endothelial Specific Endoglin Knockdown on AVM formation in Neonates using *Apj*<sup>Cre-ER</sup>

The study by Jin *et al.* (294) showed that AVMs potentially originate from arteries following loss of endothelial endoglin. However, endoglin expression is greater in veins than arteries and there is a significant increase in vein width in Eng-iKO<sup>EC</sup> retinas, pointing to a venous role for endoglin. Therefore, in this section, I analysed the role of endoglin in venous ECs using *Apj*<sup>Cre-ER</sup>.

In retinas, the expression of *Apj* is reported as early as P3 (301, 302) however, the earliest *Apj*<sup>Cre-ER</sup> expression has only been shown in the sinus venosus of E9.5 hearts (44). Therefore, the first aim of the current study was to establish the venous specificity of *Apj*<sup>Cre-ER</sup> in neonatal retinas. To investigate this, *Apj*<sup>Cre-ER</sup> was activated at different time-points by injecting tamoxifen (0.5–0.6mg per injection) via subcut route (Figure 5.19A). To report the *Apj*<sup>Cre-ER</sup> activity, *Rosa26*<sup>mTmG</sup> reporter mice were used. The *Rosa26*<sup>mTmG</sup> is a dual Cre reporter, which in the absence of an active Cre leads to expression of red fluorescence (mT) in a cell while in the presence of an active Cre, the polyadenylation (pA) sequence is removed and expression of eGFP (mG) is observed in all Cre positive cells and their daughter cells [(235), (Figure 5.19B)]. To test *Apj*<sup>Cre-ER</sup> activity after activation via injection of tamoxifen at different time points (Figure 5.19A), neonatal hearts and retinas were harvested on day P8 following protocols described in section 2.1.3. Next, dissected retinas images were taken and then retinas were flattened following the protocol described in section 2.10.2 and stored at -20°C until required. Harvested hearts were imaged (section 2.10.1), fixed in 1% PFA, embedded in OCT and stored at -80°C until required.

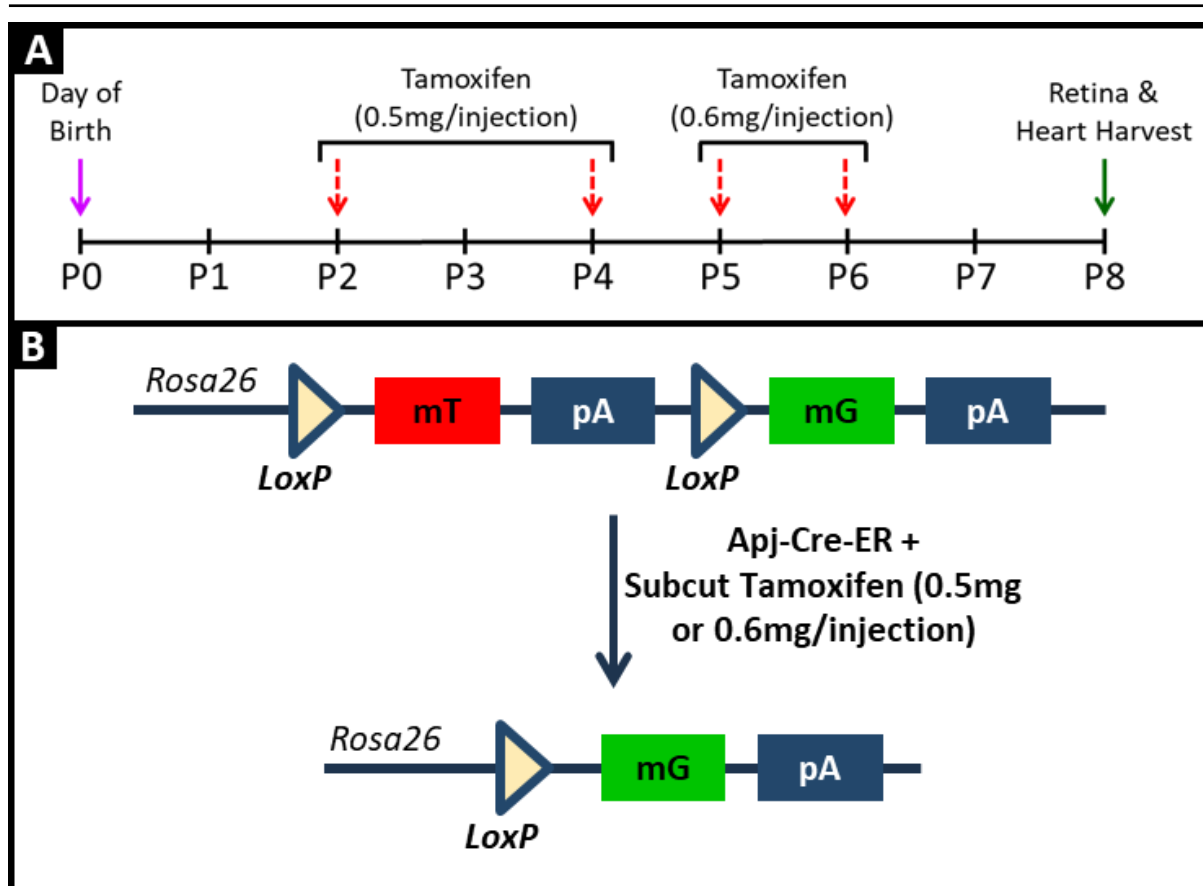


**Figure 5.19: Optimisation of  $Apj^{Cre-ER}$  activation using  $Rosa26^{mTmG}$  reporter mice.** (A) Experiment design showing different time-points used (red arrows) to activate  $Apj^{Cre-ER}$  by subcut tamoxifen injection [0.5mg (P2 & P4) or 0.6mg (P5 & P6) per injection]. From all the different groups, retinas and hearts were harvested at P8 (green arrow). (B) Activation of Cre was reported using  $Rosa26^{mTmG}$ , a dual fluorescence reporter mouse. In the absence of Cre, cells express a red fluorescence (membrane tomato, mT), while in the presence active  $Apj^{Cre-ER}$  (after tamoxifen injection) the polyadenylation (pA) sequence is removed leading to expression of eGFP (mG) in all  $Apj^{Cre-ER}$  positive and daughter cells.

The activation of  $Apj^{Cre-ER}$  at P2 led to expression of eYFP in all the vessels (arteries, veins and capillaries) of P8 retinas (Figure 5.20A-C). This was expected as at P2 arterial and venous differentiation has not yet occurred, therefore  $Apj$ -Cre expression is not yet specific to veins. Furthermore, this result also suggests that the primitive capillary plexus at P2 expresses  $Apj$ -Cre. Similarly, tamoxifen activation of  $Apj^{Cre-ER}$  at P4 showed strong expression of  $Apj^{Cre-ER}$  in all veins and capillaries (Figure 5.20D-F). However, there was reduced arterial expression of  $Apj^{Cre-ER}$  as observed by low eGFP expression at the base of the arteries (white arrows, Figure 5.20D-F) suggesting arterial differentiation potentially begins by P4. Activation of  $Apj^{Cre-ER}$  at late P5 (Figure 5.20G-I) and P6 (Figure 5.20J-L), led to eGFP expression only in veins and capillaries while arteries retained expression of red fluorescence (Figure 5.20G-L). This established appropriate timings of  $Apj^{Cre-ERT2}$  activation (late P5 onwards) for venous specific endoglin depletion and is consistent with the lack of arterial expression of  $Apj$  protein observed in the P5 retinas in previous studies (301, 302).

---

Next, venous specific  $Apj^{Cre-ER}$  expression was analysed in P8 hearts harvested from  $Apj^{Cre-ER}; Rosa26^{mT/mG}$  mouse line after injection at P6. Hearts were sectioned and subjected to immunofluorescence staining using chicken anti-GFP and rat anti-CD31 antibodies. The sections were then imaged using fluorescence setting on M2 axio-imager microscope. To identify arteries and veins following criteria were used. A coronary vessel was presumed to be a vein if: (i) the vessels was present in the sub-epicardial region and (ii) lacking a thick SMCs coat (identified by presence of nuclei in centric circles around the endothelial cells, Figure 5.21, pink arrows). In contrast, a vessel was presumed as an artery if it was present in deeper in the myocardium and had an evident thick SMC layer (recognised by concentric DAPI only staining).

Analysis of x20 images showed GFP expression (Apj-Cre positive and/ or daughter cells) in the coronary veins of P8 post-natal hearts as observed by anti-GFP staining (Figure 5.21, B,E,H) while presumed coronary arteries were negative for GFP expression (Figure 5.21, C,F,I) indicating venous specificity for Apj-Cre. However, a uniform mosaic pattern of GFP expression was observed in capillaries, although the majority of capillaries were GFP+ve (yellow arrows, Figure 5.21). The Apj-Cre negative capillaries could be lymphatic vessels, but this remains to be confirmed.

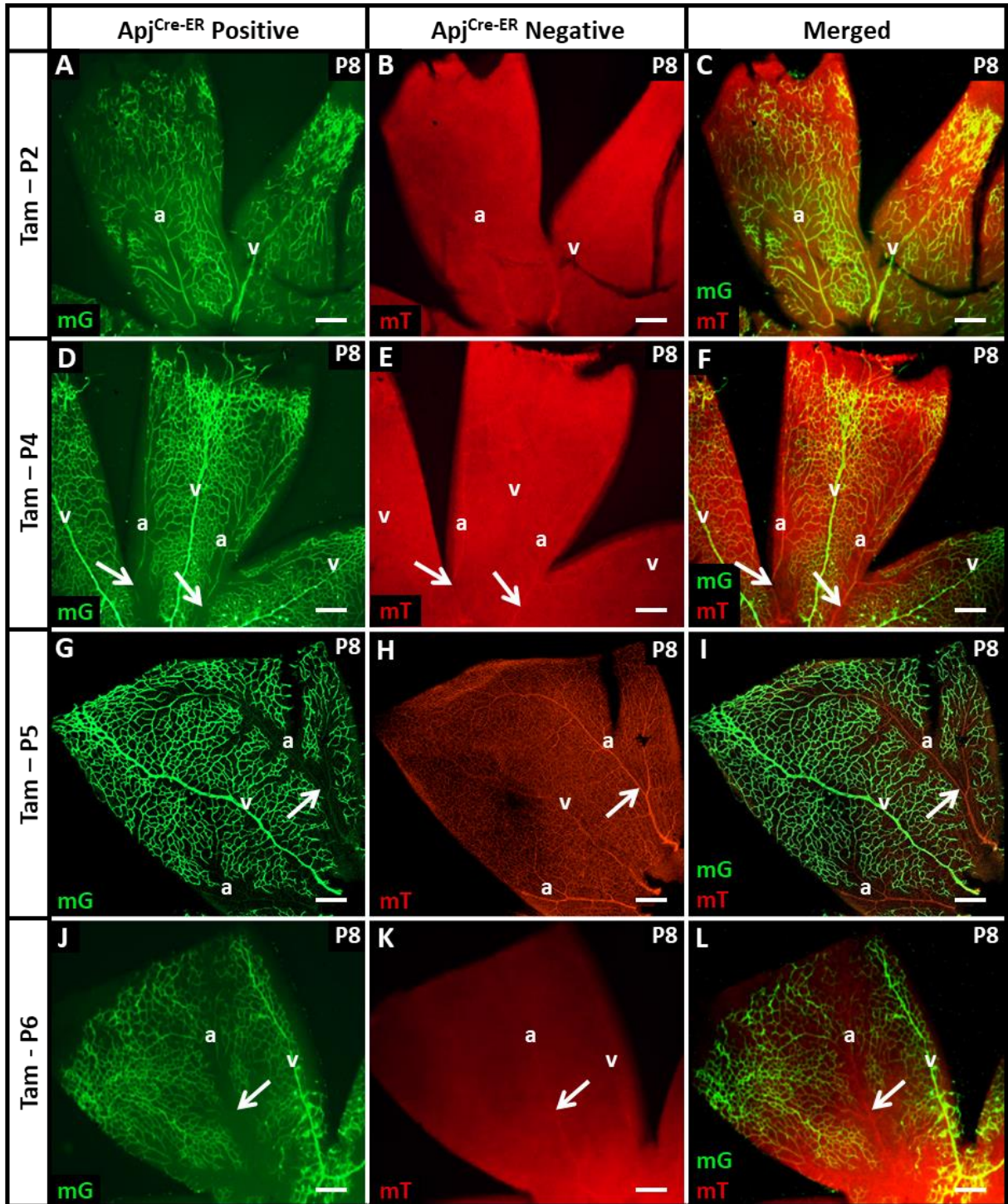


**Figure 5.20: Activation of  $Apj^{Cre-ER}$  by tamoxifen injection at P5 or P6 showed GFP expression in veins and capillaries of P8 retinas.** Expression of enhanced GFP (mG, green) indicates Cre activity in the blood vessels of the retina and expression of red fluorescence (mT) indicates the absence of active Cre. In retinas, vasculature is developed in a unique format with arteries and veins developing in alternate pattern (Figure 5.15). **(A-C)**  $Apj^{Cre-ER}$  activation by subcut tamoxifen (0.5mg/injection) injection on P2 ( $n=1$ ) leads to expression on eGFP in all arteries, veins and capillaries. **(D-F)** Activation of  $Apj^{Cre-ER}$  at P4 ( $n=1$ ) showed expression of eGFP in all veins, capillaries and in most of the arteries except for near the centre of the retina (white arrows). In contrast, activation of  $Apj^{Cre-ER}$  at **(G-I)** late P5 ( $n=4$ ) and **(J-L)** late P6 ( $n=3$ ) showed the expression of eGFP in veins and capillaries while red fluorescence was observed in the arteries (white arrows). *Abbreviations: a – arteries; v – veins; mT – membrane Tomato; mG – membrane enhanced GFP. Scale bar, A to L = 200 $\mu$ m.*

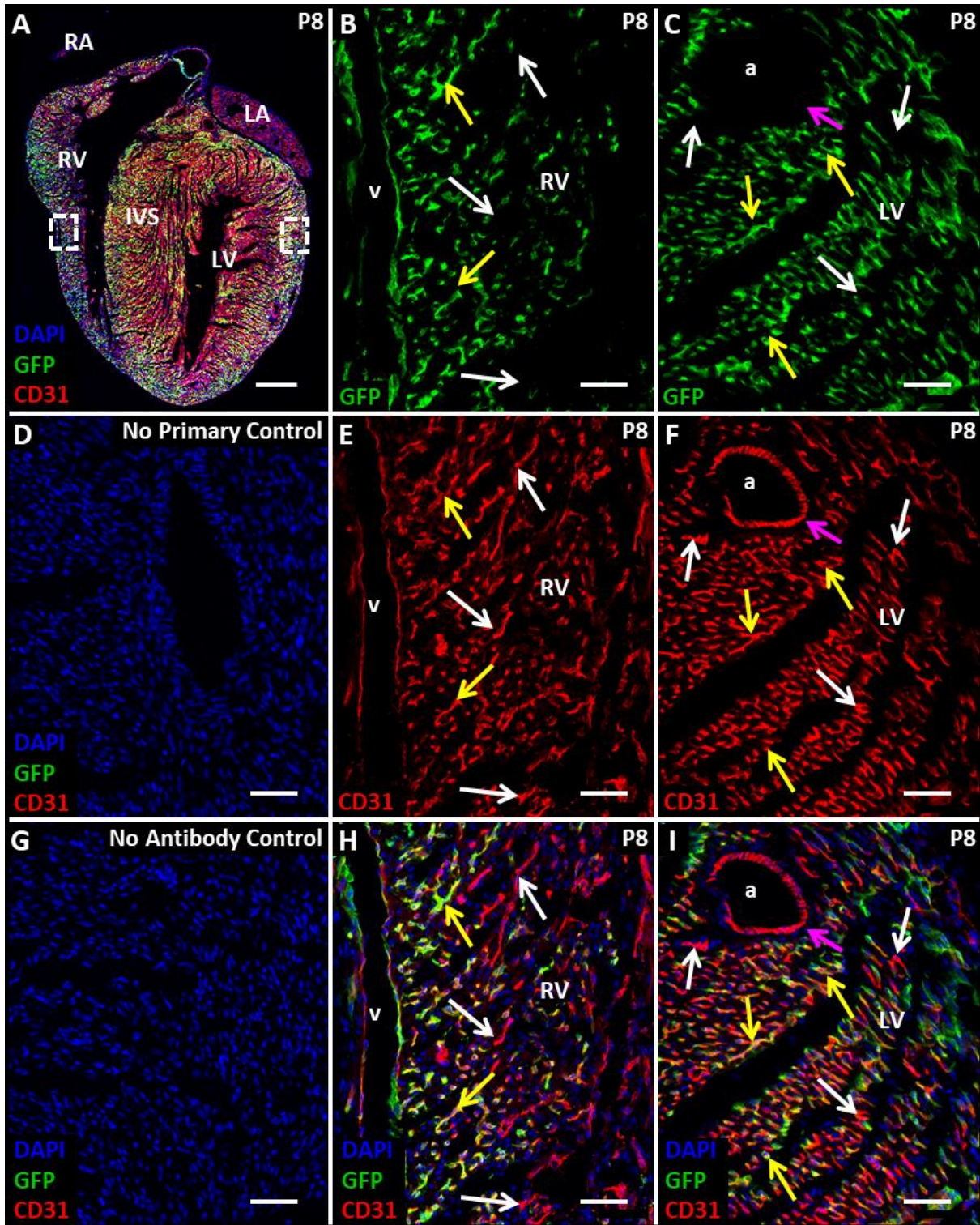


**Figure 5.21: Activation of  $Apj^{Cre-ER}$  at P6 by tamoxifen leads to GFP reporter expression in coronary veins and capillaries but not arteries of P8 hearts.** Immunofluorescence stained P8 heart with chicken anti-GFP (green), rat anti-CD31 (red) antibodies and counterstained with DAPI to mark nuclei (blue). (A) Overview image of a P8  $Apj^{Cre-ER}$  heart showed expression of GFP in coronary vasculature. Qualitative analysis on high power split channel images of (B,E,H) RV and (C,F,I) LV free wall showed expression of GFP in a coronary vein (v) and majority of the capillaries (yellow arrows, n=2). While coronary artery (a, pink arrows) and a few capillaries (white arrows) were observed to be negative for GFP expression (n=2). (D) No primary and (G) no antibody staining controls. Abbreviations: RA – Right Atria; RV – Right Ventricle; LA – Left Atria; LV – Left Ventricle; IVS – Interventricular Septum. Scale bar: A – 1mm; B-I - 50 $\mu$ m.

The next question was to address the effect of endoglin depletion in the veins and venous derived capillaries. To maximise endoglin depletion two tamoxifen injections were used to activate *Apj<sup>Cre-ER</sup>*: late afternoon on day P5 (0.6mg subcut) and 24h later at P6 (0.6mg; Figure 5.22A). These timings are much later than the work described earlier in this chapter when *VE-Cad<sup>Cre-ERT2</sup>* was activated by tamoxifen injection at P2 and P4 (Figure 5.8). In order to use *VE-Cad<sup>Cre-ERT2</sup>* retinas as a comparator (i.e. endoglin knockdown in all ECs) *VE-Cad<sup>Cre-ERT2</sup>* was activated using the same protocol (subcut tamoxifen on late P5 and P6, 0.6mg/day, Figure 5.22B). Hearts and retinas were then harvested from both mouse lines at two time points (P8 and P11) to compare the effect of total EC (*Eng-iKO<sup>EC</sup>*) and venous EC (*Eng-iKO<sup>V</sup>*) endoglin knockdown on cardiac hypertrophy and retinal vascular development.

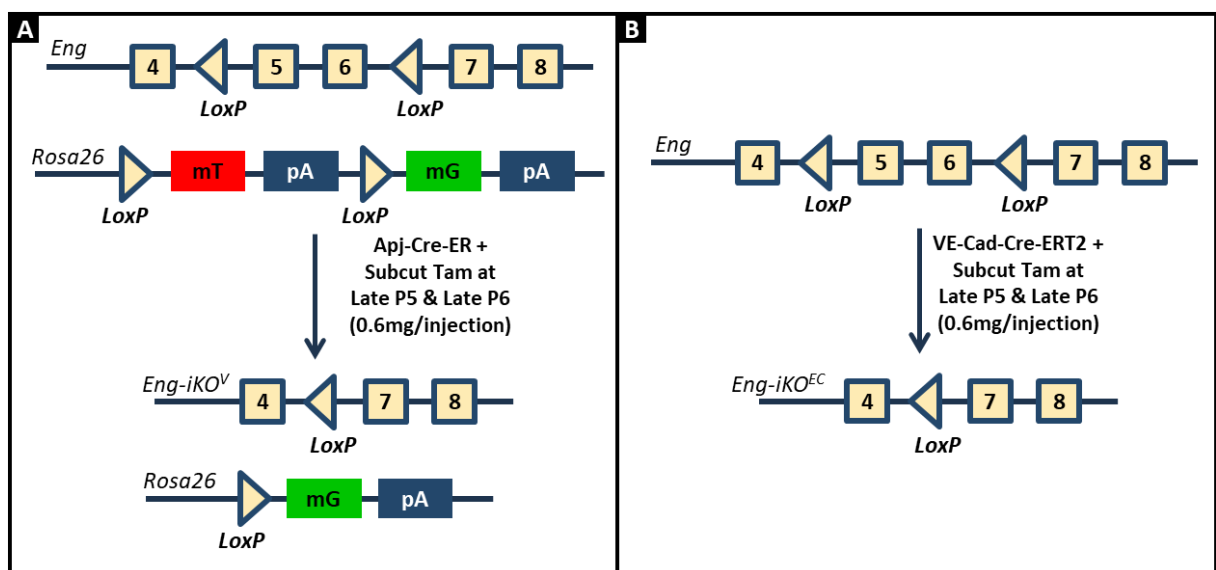
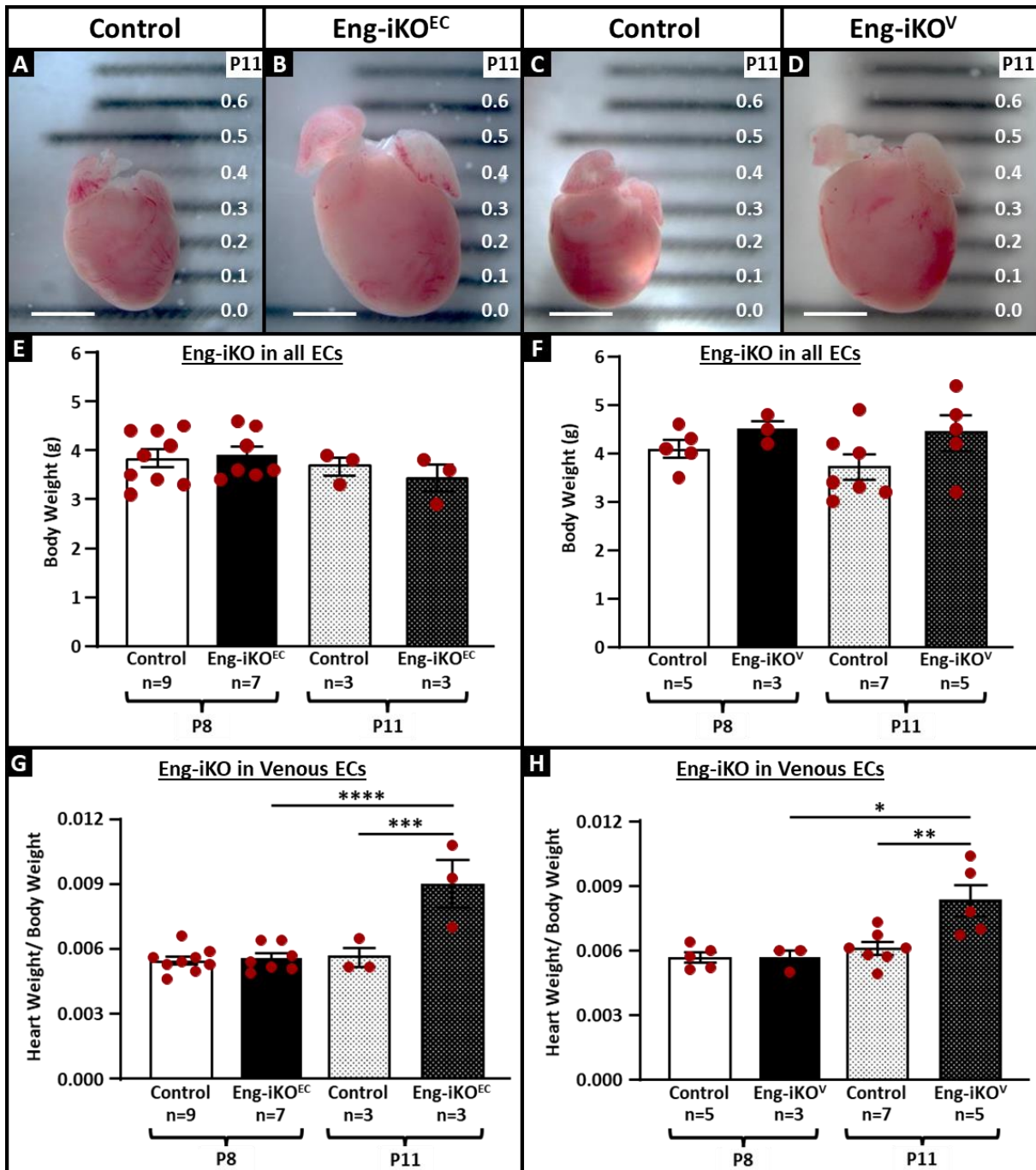


**Figure 5.22: Mouse models used to study the effect of venous ECs specific *Endoglin* knockdown.** (A) Activation of *Apj<sup>Cre-ER</sup>* by subcut tamoxifen injection on late P5 and P6 (dose: 0.6mg/ injection) leads to knockdown of *Endoglin* and expression of eGFP in all *Apj-Cre* positive cells. (B) To compare the effect of venous specific *Endoglin* knockdown using *Apj<sup>Cre-ER</sup>* vs. *Endoglin* knockdown in all ECs using *VE-Cad<sup>Cre-ERT2</sup>* on AVMs formation, *VE-Cad<sup>Cre-ERT2</sup>* was also activated by subcut tamoxifen injection at late P5 and P6 (dose: 0.6mg/ injection). This leads to knockdown of endoglin in all *VE-Cad-Cre* positive cells.

The body weight of all pups (*Cre*-negative controls, *Eng-iKO<sup>EC</sup>* and *Eng-iKO<sup>V</sup>*) was similar at P8 as well as at P11 (Figure 5.23 E&F). The heart weight of *Eng-iKO<sup>EC</sup>* pups showed no difference at P8 but did increase significantly (~52%) at P11, compared to controls (Figure 5.23). A similar cardiac phenotype was observed in the *Eng-iKO<sup>V</sup>* pups with no difference in heart weight at P8 and ~57% increase in heart at P11 compared to controls (Figure 5.23).



To analyse if the above cardiac phenotype was due to AVMs in the systemic vasculature as observed earlier (Figure 5.16), P8 and P11 retinas from both Eng-iKO<sup>EC</sup> and Eng-iKO<sup>V</sup> were analysed for presence of AVMs along with their respective controls. At P8, whole view tiled images retinas were taken. However, from P8 onwards the expansion of retina vasculature progresses deeper into the retina leading to two parallel interconnected vascular planes by P11 [(Figure 5.24), (300)]. Therefore, to investigate primary and secondary plexus of P11 retinas, z-stack images of the primary and secondary plexus were taken at x20 using M2 axio-imager microscope. Once imaged, in-depth coding was applied to colour code different layer of tissue according to its depth from the focus point. This enables each layer of retina vasculature to be observed in 2D plane.

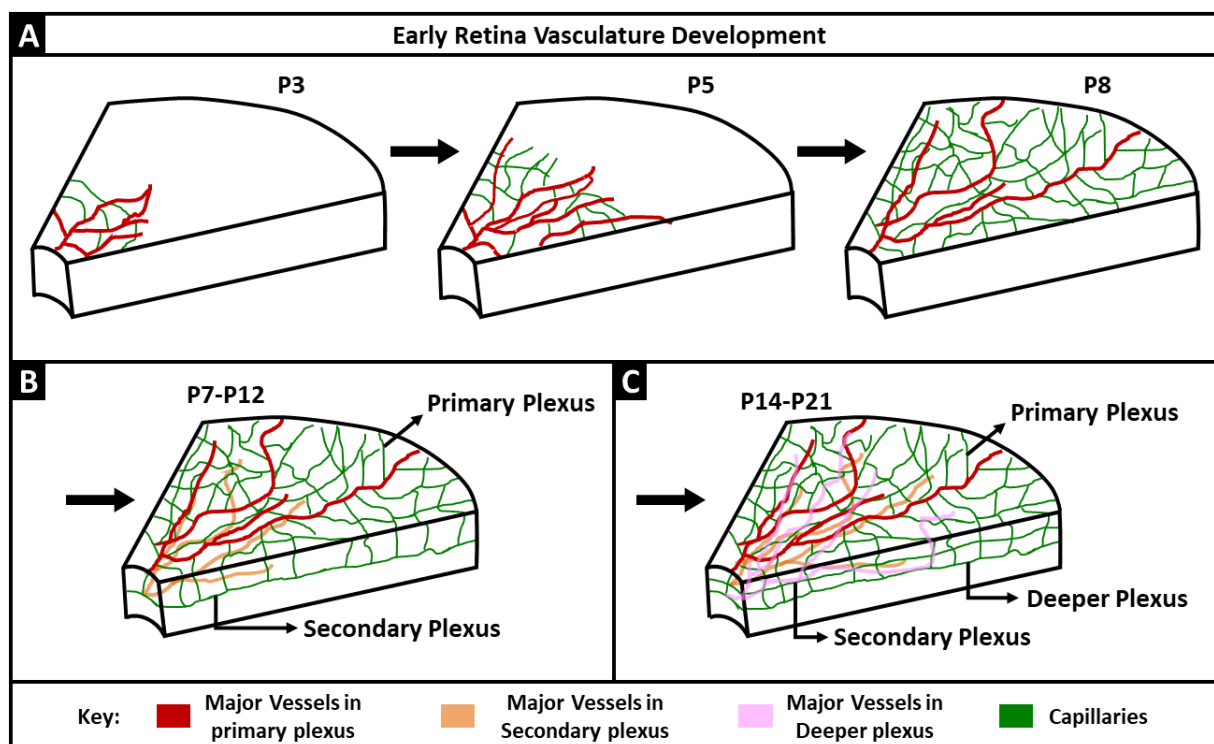


**Figure 5.24: Cartoon of retina vasculature development in mice [adapted from (300, 303)].** New born mice retinas are avascular. (A) In the first week of retina vasculature development, the vascular plexus starts to migrate from the middle of the retina (P3) and progress towards the periphery of the retina (P5). By P8, the whole surface of the retina is covered by primary vascular plexus. (B) In the next week of retina development, the vessels start to develop in 3D plane with the formation of deeper plexus or secondary plexus by P12. (C) Finally, in the third week of post-natal development deeper plexus are formed to form mature three-layered retina vasculature.

The control retinas from both lines at P8 and P11 showed normally developing retina vasculature expressing higher levels of endoglin in veins compared to arteries (Figure 5.25 A-D & I-L). The Eng-iKO<sup>EC</sup> retinas showed successful endoglin knockdown in arteries, veins and capillaries as well as occurrence of retinal AVMs in both P8 (Figure 5.25 E-F, white arrows) and P11 (Figure 5.25 G-H, white arrows) retinas. The in-depth coding images analysis of P11 retinas showed that the AVMs observed in both Eng-iKO<sup>EC</sup> and Eng-iKO<sup>V</sup> retinas (Figure 5.26) were formed in both primary and secondary plexus layers of the retinas (white arrows, Figure

---

5.25C-F). This shows despite delayed or venous EC specific endoglin knockdown, AVMs still persist to form in both primary and secondary plexus layer.

In Eng-iKO<sup>V</sup> retinas, consistent with the expression of Apj<sup>Cre-ER</sup> observed earlier (Figure 5.20 G-L), *endoglin* knockdown was only observed in the veins and capillaries but not in the arteries of P8 and P11 retinas (Figure 5.25 M-P). However, in contrast to P8 Eng-iKO<sup>EC</sup> retinas, only a mild AVM phenotype was observed in P8 Eng-iKO<sup>V</sup> retinas (Figure 5.25 M-N, white arrows). While at P11, AVMs were observed in Eng-iKO<sup>V</sup> retinas (Figure 5.25 O-P, white arrows) similar to the Eng-iKO<sup>EC</sup> retinas. Again, these AVMs in Eng-iKO<sup>V</sup> retinas were also observed in the primary and secondary plexus layer however, it does not rule out smaller AVMs in between primary and secondary plexus (Figure 5.24, B&C).

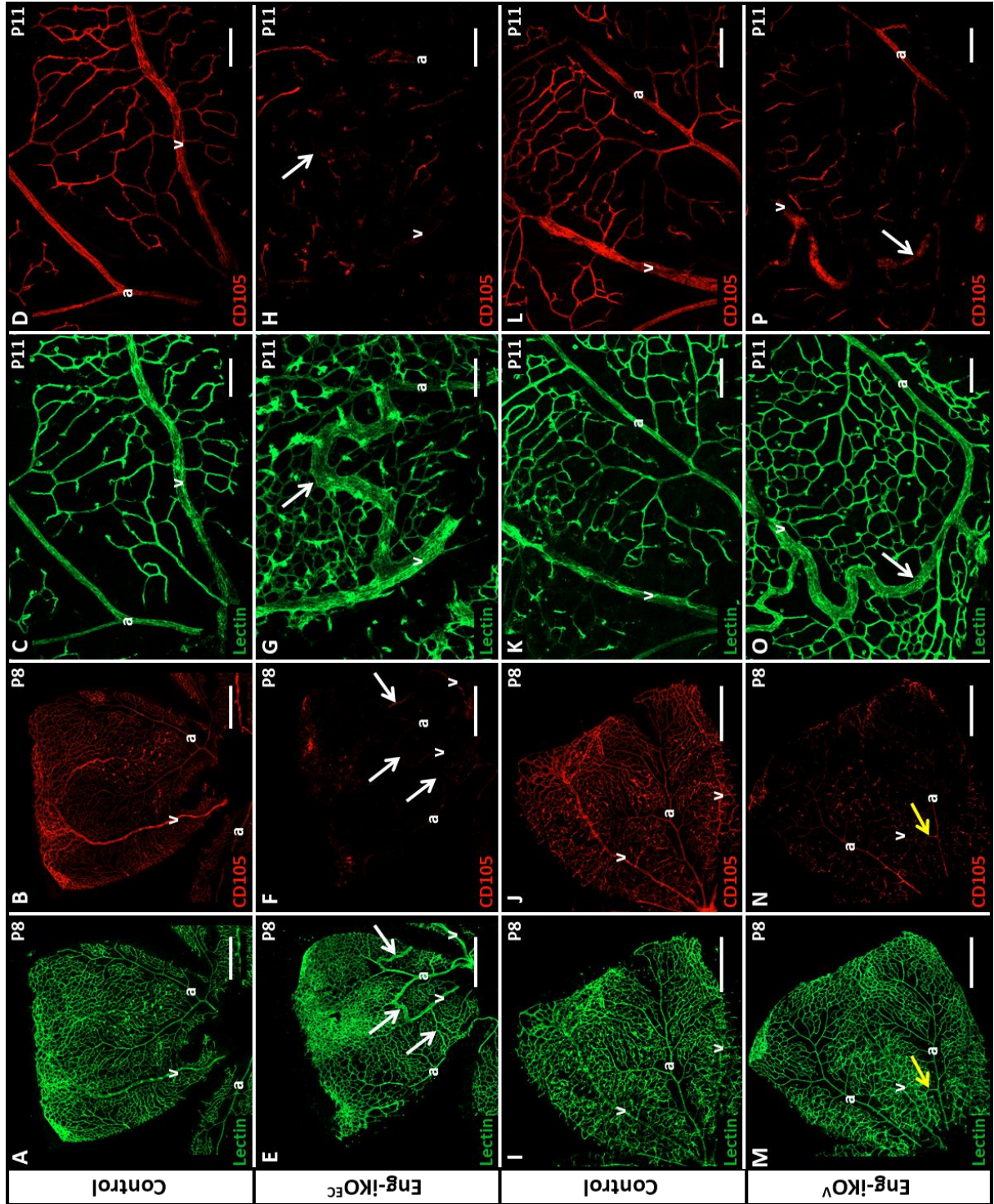


**Figure 5.25: Endoglin knockdown using *VE-Cad<sup>Cre-ERT2</sup>* and *Apj<sup>Cre-ER</sup>* led to formation of AVMs in P8 and P11 retinas.** Immunofluorescence stained P8 & P11 retinas with isolectin GS-IB4 (green) and rat anti-CD105 antibody (red). Split channel images of controls showed normally developing retina vasculature at (A-B, I-J) P8 and (C-D, K-L) P11 with baseline endoglin expression in arteries (a), veins (v) and adjacent capillaries. (E-H) Split channel images of Eng-iKO<sup>EC</sup> retinas showed endoglin knockdown in all vessels with AVMs (white arrows) in both P8 (E-F) and P11 (G-H) retinas. (M-P) Split channel images of Eng-iKO<sup>V</sup> retinas showing endoglin knockdown in veins and capillaries but not in arteries. However, in contrast to P8 Eng-iKO<sup>EC</sup> retinas, thinner AVM (white arrows) phenotype was observed in P8 Eng-iKO<sup>V</sup> retinas (M-N) but by P11 (O-P), wider AVMs (white arrows) were observed in Eng-iKO<sup>V</sup> retinas. Abbreviations: a – artery; AVMs – Arteriovenous malformations and v – vein. Scale bar: A-B, E-F, I-J, M-N = 200μm and C-D, G-H, K-L, O-P = 100μm.

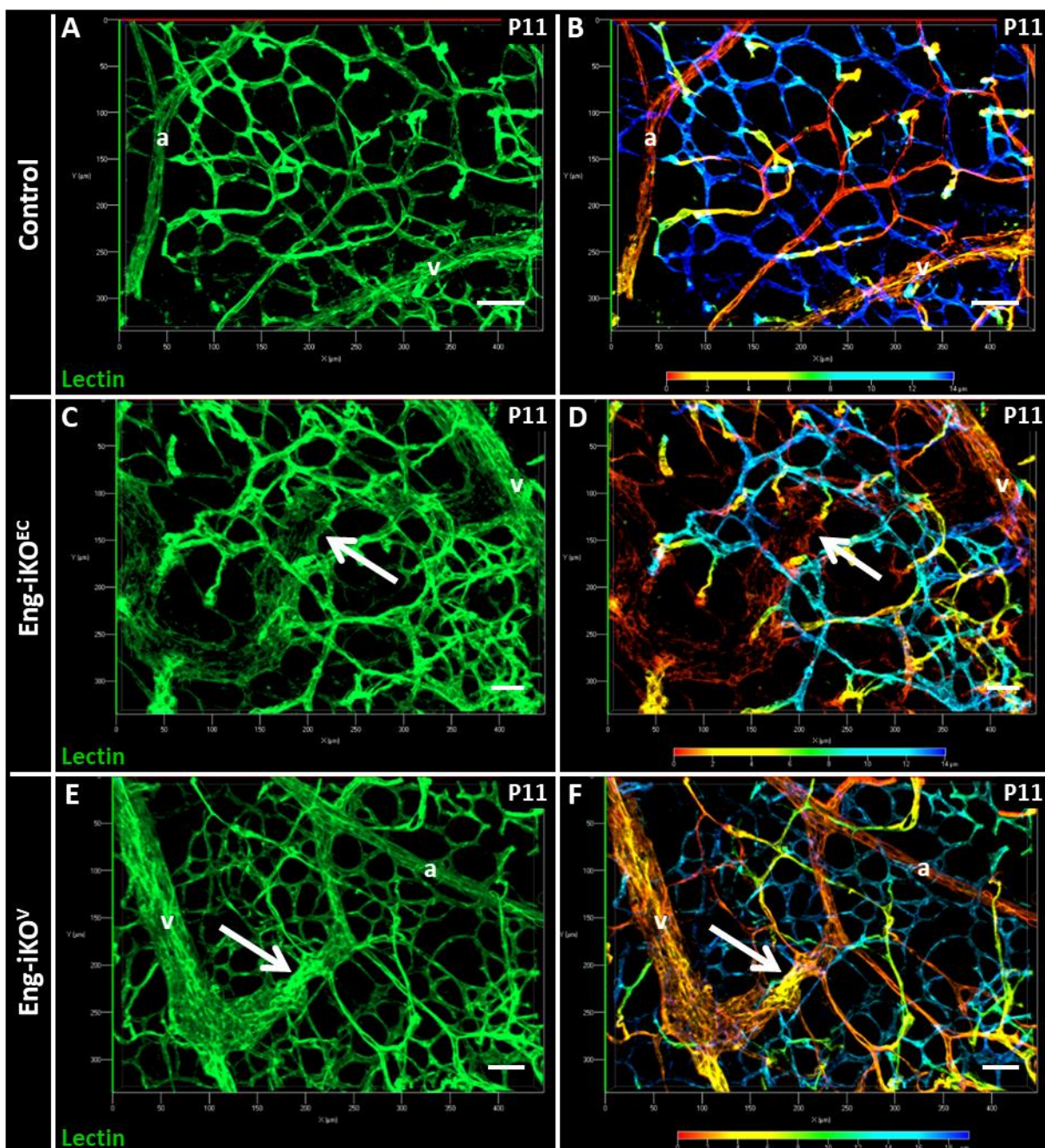


**Figure 5.26: In-depth coding showed the AVMs observed in P11 *Eng-iKO<sup>EC</sup>* and *Eng-iKO<sup>V</sup>* retinas had developed in the primary plexus. (A) Isolectin GS-IB4 stained and (B) in-depth coding image of a control retina showing normal retina vasculature with major vessels formed in the primary plexus layer (first layer, reddish orange) interconnected through capillaries (green/yellow) with an extensive vascular network forming in the second layer (blue). Images of *Eng-iKO<sup>EC</sup>* (C-D) and *Eng-iKO<sup>V</sup>* (E-F) showing forming of AVMs (white arrows) in the primary plexus layer (red/orange). Abbreviations: a – artery; AVMs – Arteriovenous malformations and v – veins. Scale bars: A-F = 50μm.**

By P8 as expected (300, 303), the retinal vasculature has reached the periphery of the retina in all controls (Figure 5.25, A&I) and endoglin knockout pups (Figure 5.25, E&M). The analysis of vein width showed a significant increase in the vein width of both P8 (~11%) and P11 (~45%) *Eng-iKO<sup>EC</sup>* veins compared to their respective controls (Figure 5.27I). This was consistent with the results observed earlier using the standard endoglin knockout strategy (Figure 5.10D). A similar phenotype was observed in the *Eng-iKO<sup>V</sup>* mice: in P8 retinas, veins were ~14% wider

while by P11 veins were ~53% wider compared to their respective controls (Figure 5.27J). During this analysis, only the veins in the primary plexus were analysed.

No statistically significant difference was observed between the number of AVMs per retina in Eng-iKO<sup>EC</sup> and Eng-iKO<sup>V</sup> retinas at either P8 or P11 (Figure 5.27K). However, the probability of AVM formation was much higher in P8 Eng-iKO<sup>EC</sup> retinas (~57%) compared to Eng-iKO<sup>V</sup> (~33%) retinas. In contrast, at P11 this ratio was reversed as all Eng-iKO<sup>V</sup> retinas (7/7) had AVMs while only 4 out of 6 Eng-iKO<sup>EC</sup> retinas had AVMs.

At P8, no statistical difference was observed between Eng-iKO<sup>EC</sup> and Eng-iKO<sup>V</sup> AVMs width, although there was a trend towards wider AVMs in Eng-iKO<sup>EC</sup> (Figure 5.24L). But by P11 this difference was lost due to growth of AVMs in P11 Eng-iKO<sup>V</sup> retinas, such that they were significantly wider than P8 Eng-iKO<sup>V</sup> retinas (Figure 5.24L).

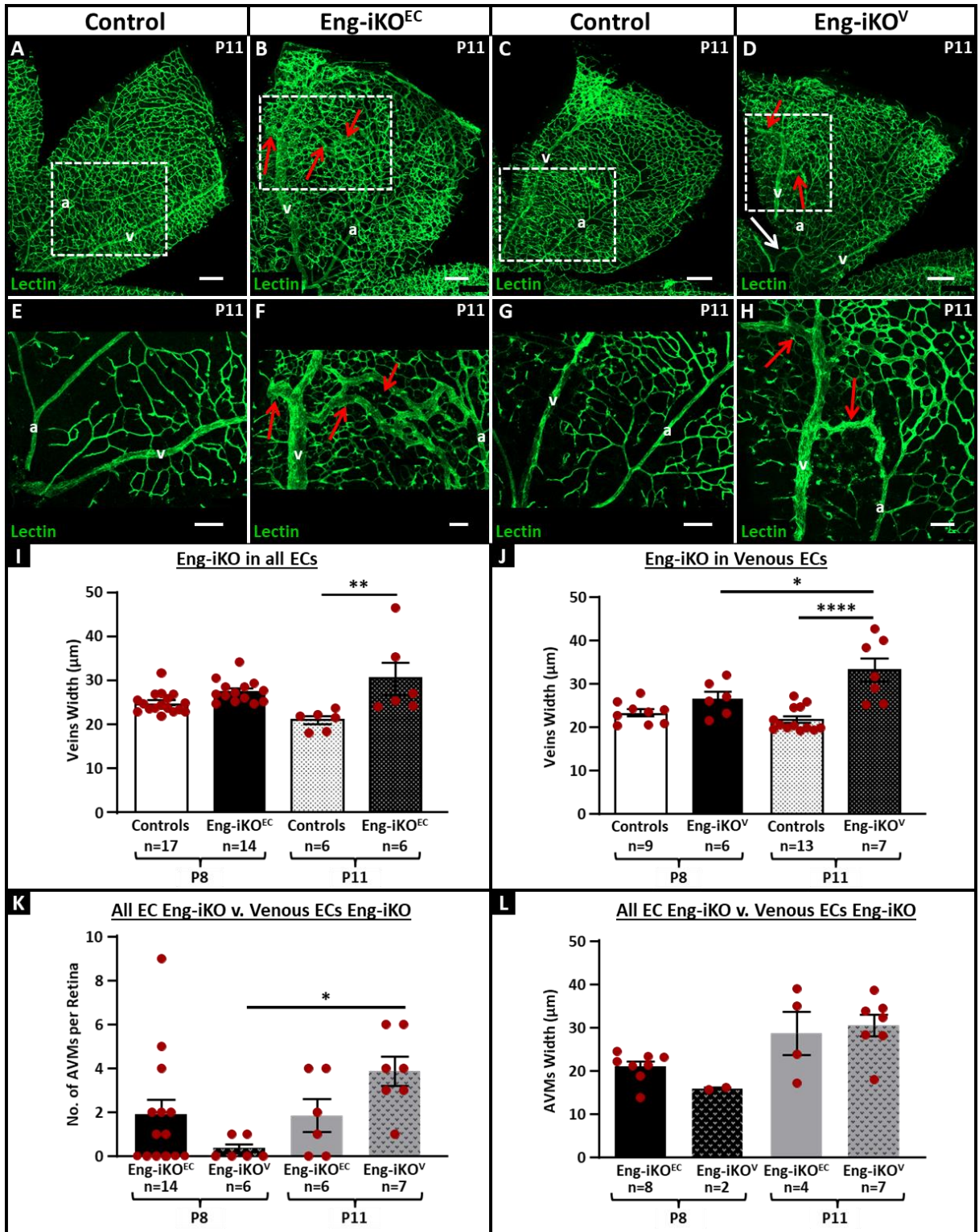
A summary of these results compared with early deletion of endoglin in all EC using VE-Cad<sup>Cre-ERT2</sup> (activated at P2 and P4) are shown in Table 5.1. This shows that, lack of endothelial endoglin (in all ECs) in the first week of neonatal life leads to development of enlarged hearts (Figure 5.10 and Figure 5.23) and AVMs (Figure 5.16 and Figure 5.25) in retinas, and likely also in other organs. The same phenotype was observed after venous ECs specific endoglin knockdown (Figure 5.23 and Figure 5.25). This suggests that endoglin in veins plays a crucial role in normal vascular development.

**Table 5.1: Data summary of heart and retinal phenotype in pups with endoglin knockout in all ECs (Eng-iKO<sup>EC</sup>) and venous & capillary ECs (Eng-iKO<sup>V</sup>)**

Age at time of Cre activation	P2 & P4	P5 & P6			
Genotype	Eng-iKO <sup>EC</sup>	Eng-iKO <sup>EC</sup>		Eng-iKO <sup>V</sup>	
Age at time of analysis	P7	P8	P11	P8	P11
No. of Retinas analysed	6	14	6	6	7
Avg. No. of AVMs per Retina ±SEM	3.0±1.0	2.0±0.7	2.0±0.7	0.3±0.2	3.4±0.7
Probability of AVMs incidence per retina	67%	57%	67%	33%	100%
Avg. AVMs Width (in µm) ±SEM	20.12±3.75	21.01±1.19	28.68±5.02	15.88±0.18	30.47±2.51
Avg. Veins Width (in µm) ±SEM	32.93±3.36	27.58±0.70	30.46±3.67	26.61±1.62	33.18±2.72
Percentage increase in vein width compared to controls	21%	11%	45%	14%	53%
Heart weight/body weight	0.0089±0.0003	0.0056±0.0002	0.0090±0.0011	0.0057±0.0003	0.0083±0.0007

---

**Figure 5.27: *Endoglin* knockdown using *VE-Cad*<sup>Cre-ERT2</sup> and *Apj*<sup>Cre-ER</sup> leads to development of wider veins and AVMs in P8 and P11 retinas.** Immunofluorescence stained P11 retinas with isolectin GS-IB4 (green) showing normal retina vasculature in controls (**A,C,E,G**). In contrast, wider veins (v) and AVMs (red arrows) were observed in Eng-iKO<sup>EC</sup> (**B,F**) and Eng-iKO<sup>V</sup> (**D,H**) retinas. (**I**) Quantification showed similar width of veins in P8 Eng-iKO<sup>EC</sup> retinas ( $27.58 \pm 0.697$ ,  $n=14$ ) compared to P8 controls (P8:  $24.91 \pm 0.574$ ,  $n=17$ ;  $p = 0.4093$ ). However, by P11 the veins were observed to be significantly in Eng-iKO<sup>EC</sup> retinas ( $30.46 \pm 3.668$ ,  $n=6$ ) compared to P11 controls (P11:  $20.98 \pm 0.912$ ,  $n=6$ ;  $p = 0.0010$ ). (**J**) Vein width quantification of Eng-iKO<sup>V</sup> retinas also showed a similar pattern with no difference in the vein width of P8 controls ( $23.31 \pm 0.843$ ,  $n=9$ ) and Eng-iKO<sup>V</sup> ( $26.61 \pm 0.616$ ,  $n=6$ ;  $p = 0.8475$ ) retinas while, a significant increase in vein width was observed in P11 Eng-iKO<sup>V</sup> retinas ( $33.18 \pm 2.720$ ,  $n=7$ ) compared to P11 controls ( $21.71 \pm 0.770$ ,  $n=13$ ;  $p = < 0.0001$ ). The vein width analysis also showed the presence of significantly wider veins in P11 Eng-iKO<sup>V</sup> compared to P8 Eng-iKO<sup>V</sup> retinas ( $p = 0.0466$ ). (**K**) The average number of AVMs per retina in P8 Eng-iKO<sup>EC</sup> ( $1.857 \pm 0.695$ ,  $n=14$ ) was almost double that in Eng-iKO<sup>V</sup> ( $0.333 \pm 0.211$ ,  $n=6$ ;  $p = 0.8577$ ). The average number of AVMs were still observed to be similar to in P11 Eng-iKO<sup>EC</sup> retinas ( $1.833 \pm 0.749$ ,  $n=6$ ) while, in contrast a significant increase in number of AVMs were observed in P11 Eng-iKO<sup>V</sup> ( $3.375 \pm 0.755$ ,  $n=8$ ;  $p = 0.0288$ ) retinas. (**L**) Quantification of AVMs width analysis showed a trend towards wider AVMs in P8 Eng-iKO<sup>EC</sup> retinas ( $21.01 \pm 1.191$ ,  $n=8$ ) compared to P8 Eng-iKO<sup>V</sup> AVMs ( $15.87 \pm 0.182$ ,  $n=2$ ) retinas. By P11, no difference in the retina AVMs width was observed between Eng-iKO<sup>EC</sup> ( $28.68 \pm 5.016$ ,  $n=4$ ) and Eng-iKO<sup>V</sup> ( $30.47 \pm 2.512$ ,  $n=7$ ;  $p > 0.9999$ ) retinas. Data shown as mean  $\pm$  SEM and analysed using one-way ANOVA (\*  $p < 0.05$ ; \*\*  $p < 0.01$  and \*\*\*\*  $p < 0.0001$ ). Abbreviations: a – artery; v – vein. Scale bar: A-D = 200 $\mu$ m and E-H = 100 $\mu$ m.



## 5.2.6 Effect of Endoglin Knockdown in Adult Quiescent Endothelial Cells using VE-Cad<sup>Cre-ERT2</sup>

As mentioned above, endoglin knockdown in adult quiescent ECs leads to development of HOHF (Figure 5.4) due to reduced vascular resistance potentially caused by formation of AV shunts in the pulmonary or systemic vasculature (unpublished data, Arthur Lab). To investigate this, 10-12week old adult mice from *Eng*<sup>fl/fl</sup>; *VE-Cad*<sup>Cre-ERT2</sup> mouse line were treated with 2mg tamoxifen per day (IP) for 5 consecutive days (Figure 5.28) to deplete endoglin in quiescent ECs (*Eng*-iKO<sup>qEC</sup>). To control for any tamoxifen related effects from these analyses, control (*Eng*<sup>fl/fl</sup>) mice were also treated with tamoxifen following the same protocol. The organs from *Eng*-iKO<sup>qEC</sup> and control mice were harvested 5wks after the first tamoxifen injection for all experiments.

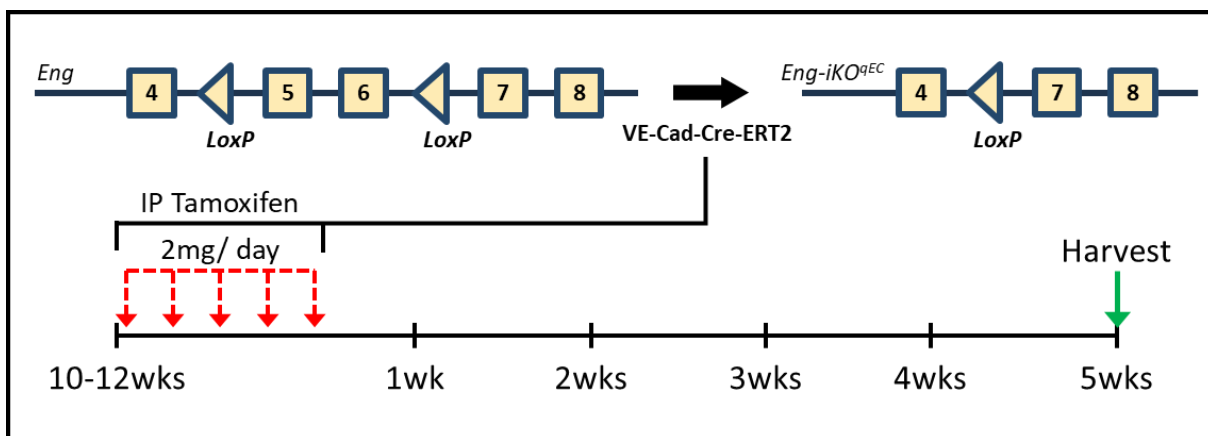
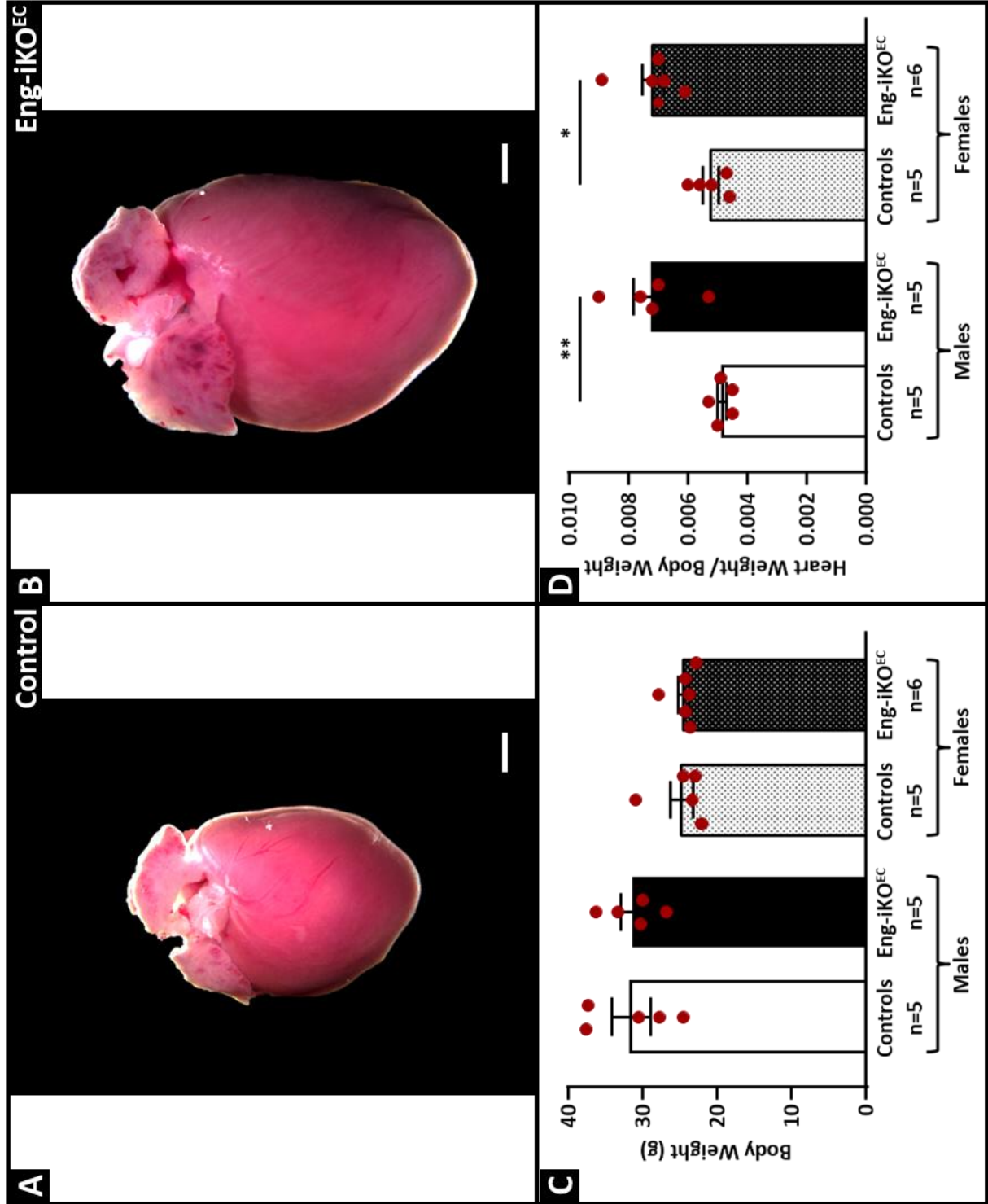


**Figure 5.28: Endoglin knockout in adult quiescent ECs using *VE-Cad*<sup>Cre-ERT2</sup>.** In adult mice to knockout endoglin, *VE-Cad*<sup>Cre-ERT2</sup> was activated by IP injections of tamoxifen (dose: 2mg/injection) for 5 consecutive days. To analyse the effect of endoglin knockdown, organs were harvested 5wks after the first tamoxifen injection.

Knockdown of endothelial endoglin in adult mice led to development of enlarged hearts (Figure 5.29A&B). This phenotype was observed in both male and female *Eng*-iKO<sup>qEC</sup> mice. Analysis of heart weight showed significantly enlarged male (~47%) and female (~34%) hearts of *Eng*-iKO<sup>qEC</sup> mice compare to their respective controls. This difference was maintained when heart weight was normalised to body weight (Figure 5.29D). This phenotype was similar to the neonatal study above (Figure 5.10).



---

I analysed the expression and knockdown of endoglin in arteries, veins and capillaries of lungs, liver and heart in Eng-iKO<sup>qEC</sup> mice to establish the model. To perform this analysis, organs harvested from both Eng-iKO<sup>qEC</sup> and control mice, were fixed in 1% PFA, embedded in OCT and sectioned in sister sections. These sections were then stained with rat anti-CD31 and goat anti-CD105 antibodies and imaged at x40 magnification using fluorescence setting on M2 axio-imager. Individual cell staining intensity was measured using spline counter function of Zen 2012 software (Figure 3.5). The identification of arteries and veins in these organs was performed by using morphological characteristics described in Figure 5.30.

In control mice showed strongest endoglin expression in coronary veins, pulmonary arteries, pulmonary veins and liver central veins (Figure 5.31, C,E,G&K), while lower expression was observed in coronary arteries and liver portal veins (Figure 5.31, A &M). The lowest endoglin expression in control mice was observed in hepatic arteries (Figure 5.31I, white arrow).

In Eng-iKO<sup>qEC</sup>, varying levels of endoglin knockdown was observed in all vessels. A significant reduction in endoglin expression was observed in coronary veins, pulmonary arteries, pulmonary veins and liver central (Figure 5.31, D,F,H&L). While a non-significant reduction in endoglin expression was observed in coronary arteries and portal veins (Figure 5.31, B&N). In hepatic arteries, no apparent reduction in endoglin expression was observed in Eng-iKO<sup>qEC</sup> mice compared to controls (Figure 5.31J, white arrow).

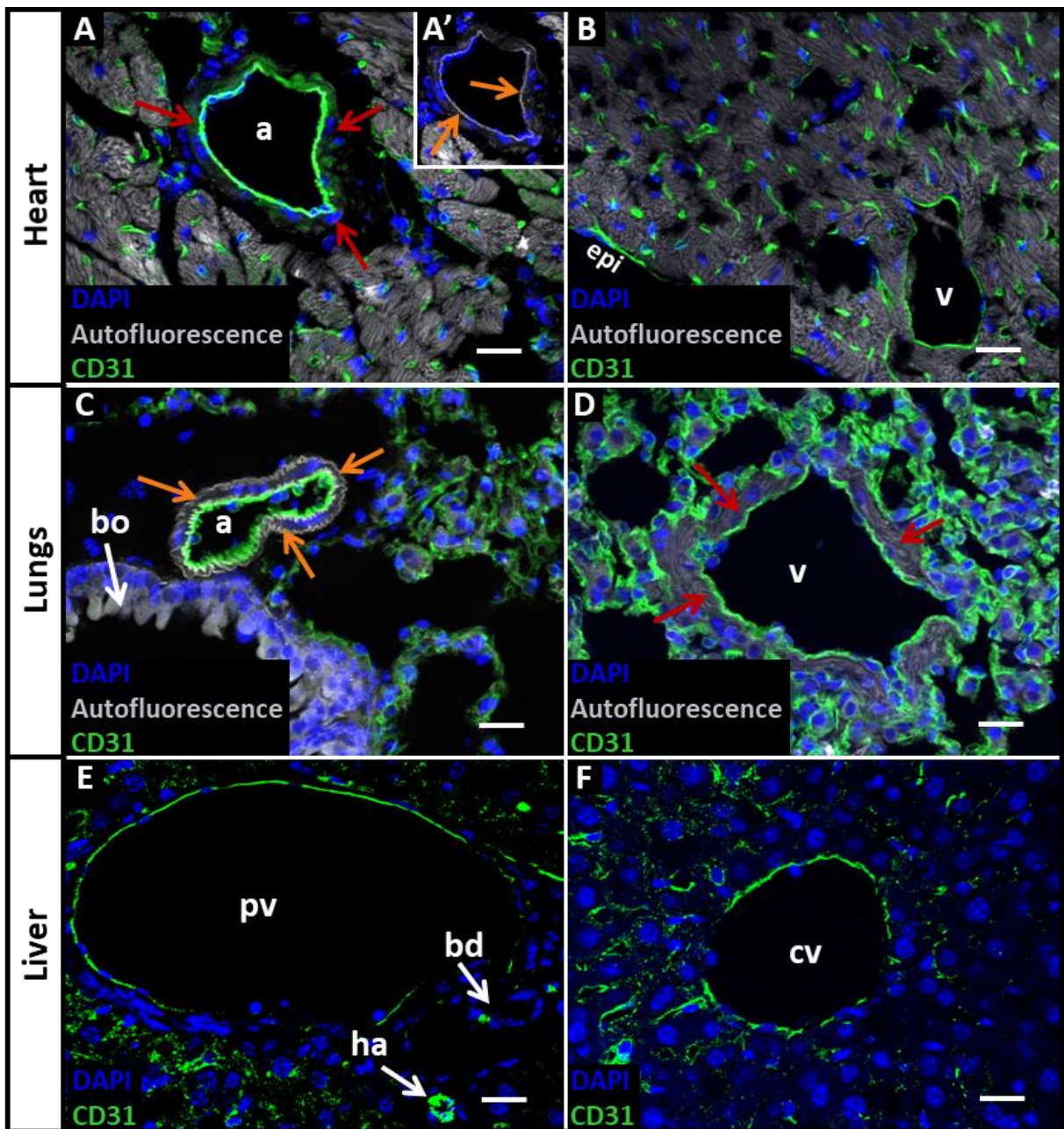
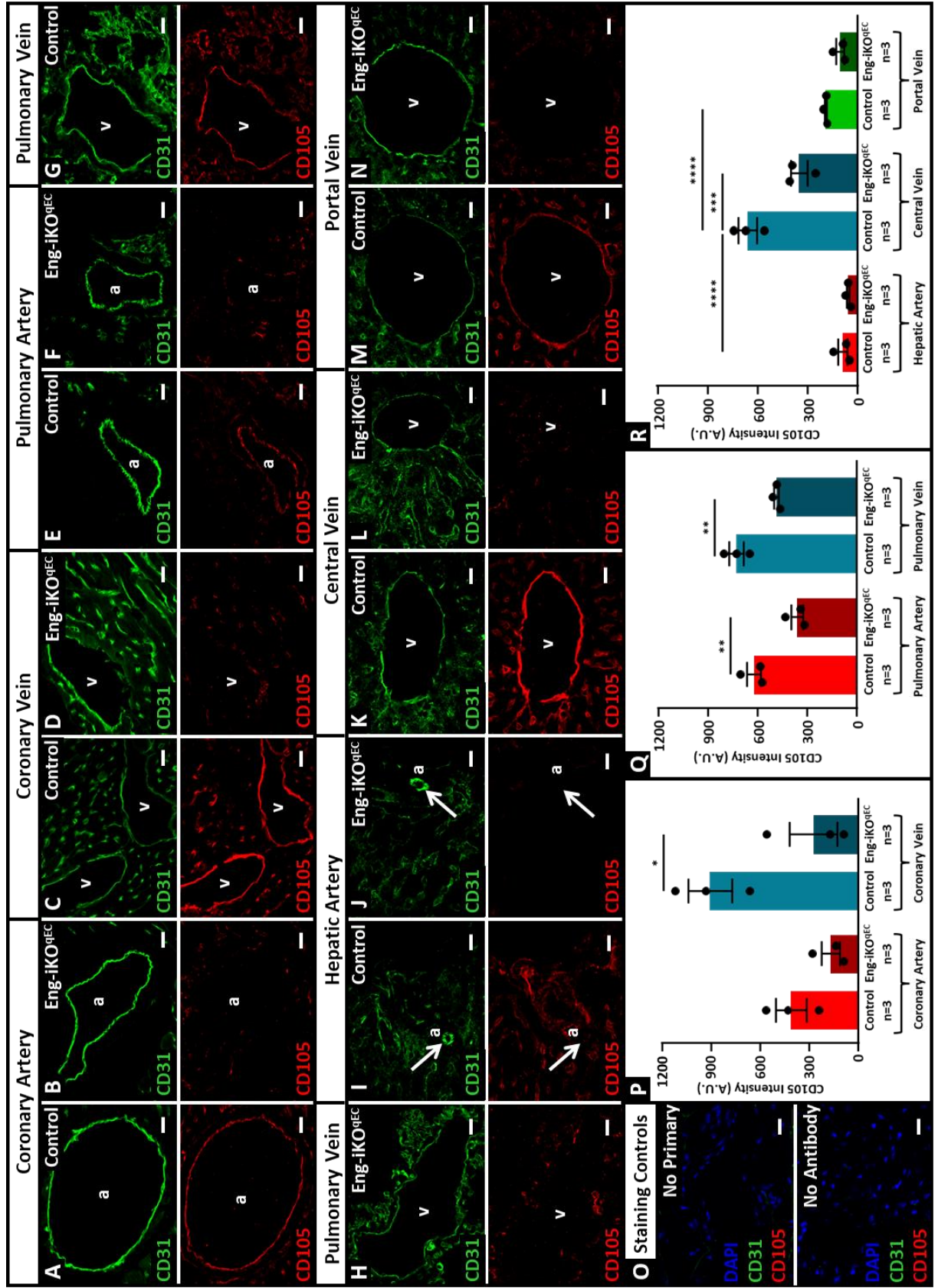


**Figure 5.30: Morphological characteristic used to identify arteries and veins in heart, lungs and liver.** In the heart, (A) a vessel was presumed to be a coronary artery if it was present in the mid-myocardium, showed a presence of elastin auto-fluorescence (A' inset, orange arrows) and thick SMCs layer [recognised by presence of concentric nuclei round the vessels (red arrows)]. (B) In contrast, a vessel was presumed to be a coronary vein, if it was present in the sub-epicardial space, lack elastin and obvious SMCs layer. In the lungs, (C) a vessel was identified as pulmonary arteries if it was present next to a bronchioles (bo) and presence of elastin auto-fluorescence (orange arrows). (D) However, if a vessel was present away from bronchioles, showed presence of SMCs [recognised by presence of concentric nuclei round the vessels and auto-fluorescence (red arrows)] and was devoid of elastin, it was presumed to be a pulmonary vein. In the liver, (E) hepatic artery (ha) was present in a trio with bile duct (negative for CD31) and portal vein (pv). (F) While central vein (cv) was located away from the trio showed in E. Abbreviations: a – artery; v – vein; bo – bronchioles; pv – pulmonary vein; ha – hepatic artery; bd – bile duct and cv – central vein. Scale bar: A-F = 20 $\mu$ m.

**Figure 5.31: Different levels of Endoglin knockdown was observed in the arteries and veins of heart, lungs and liver using VE-Cad<sup>Cre-ERT2</sup>.** Immunofluorescence stained sections of control and Eng-iKO<sup>qEC</sup> heart, lungs and liver stained with rat anti-CD31 (green), goat anti-CD105 (red) antibodies and counterstained with DAPI (blue). Split channel images of control coronary veins (C), pulmonary arteries (E), pulmonary veins (G) and central vein (K) showed strong endoglin expression. While weaker endoglin expression was observed in the coronary arteries (A), and portal vein (M) with weakest expression in hepatic artery (I, white arrow). In Eng-iKO<sup>qEC</sup> mice, 5 wks after tamoxifen treatment varying levels of endoglin knockdown was observed in coronary (B,D), pulmonary (F,H) and hepatic (J,L,N) vessels. (O) No primary and no antibody staining controls. (P) Quantification showed non-significantly high endoglin expression in control coronary veins (907.90±132.50, n=3) compared to control coronary arteries (411.60±94.19, n=3; p = 0.0869). In Eng-iKO<sup>qEC</sup> mice, a partial endoglin knockdown was observed in coronary arteries (170.00±57.59, n=3; p = >0.9999) while a significant reduction in endoglin expression was observed in Eng-iKO<sup>qEC</sup> coronary veins (275.30±145.80, n=3; p = 0.0250) compared to their respective controls. (Q) Endoglin intensity analysis showed similar levels of endoglin expression in control pulmonary arteries (623.1±42.23, n=3) and veins (729.3±45.24, n=3; p = 0.4300). In Eng-iKO<sup>qEC</sup>, a significant reduction in endoglin expression was observed in both pulmonary arteries (363.00±35.36, n=3; p = 0.0057) and pulmonary veins (487.20±12.82, n=3; p = 0.0089) compared to respective controls. (R) Quantification showed significantly high levels of endoglin expression in central veins (658.50±53.82, n=3) compared to both hepatic arteries (85.15±28.63, n=3; p <0.0001) and portal veins (188.80±6.46, n=3; p <0.0001). The endoglin expression analysis also showed slightly reduced levels of endoglin in hepatic arteries compared to portal veins (p = 0.7564) in control mice. In Eng-iKO<sup>qEC</sup> mice, a significant reduction in endoglin expression was observed in central veins (349.5±49.09, n=3) compared to control central veins (p = 0.0004). The endoglin expression in Eng-iKO<sup>qEC</sup> hepatic arteries (53.69±9.175; p >0.9999) and portal veins (103.6±22.76, n=3; p >0.9999) was observed to be similar to their respective controls. Data shown as mean±SEM and analysed using two-way ANOVA (\*\*\*\* p < 0.0001 and \*\*\*\*\* p < 0.0001). Abbreviations: a – arteries; v – veins. Scale bar: A-O – 20µm



Next, to analyse if heart enlargement is associated with CM hypertrophy, the above control and Eng-iKO<sup>qEC</sup> hearts sections stained with WGA to measure CM area. The CM area was measured using Zen 2012 software from only transversely cut CMs of both Eng-iKO<sup>qEC</sup> and controls. This analysis showed a significantly higher CM area of both right (~47%) and left (~79%) ventricle CM of Eng-iKO<sup>qEC</sup> compared to their respective controls (Figure 5.26G). This result confirms CM hypertrophy following endothelial endoglin depletion and indicated the continued importance of endoglin expression even in quiescent ECs.

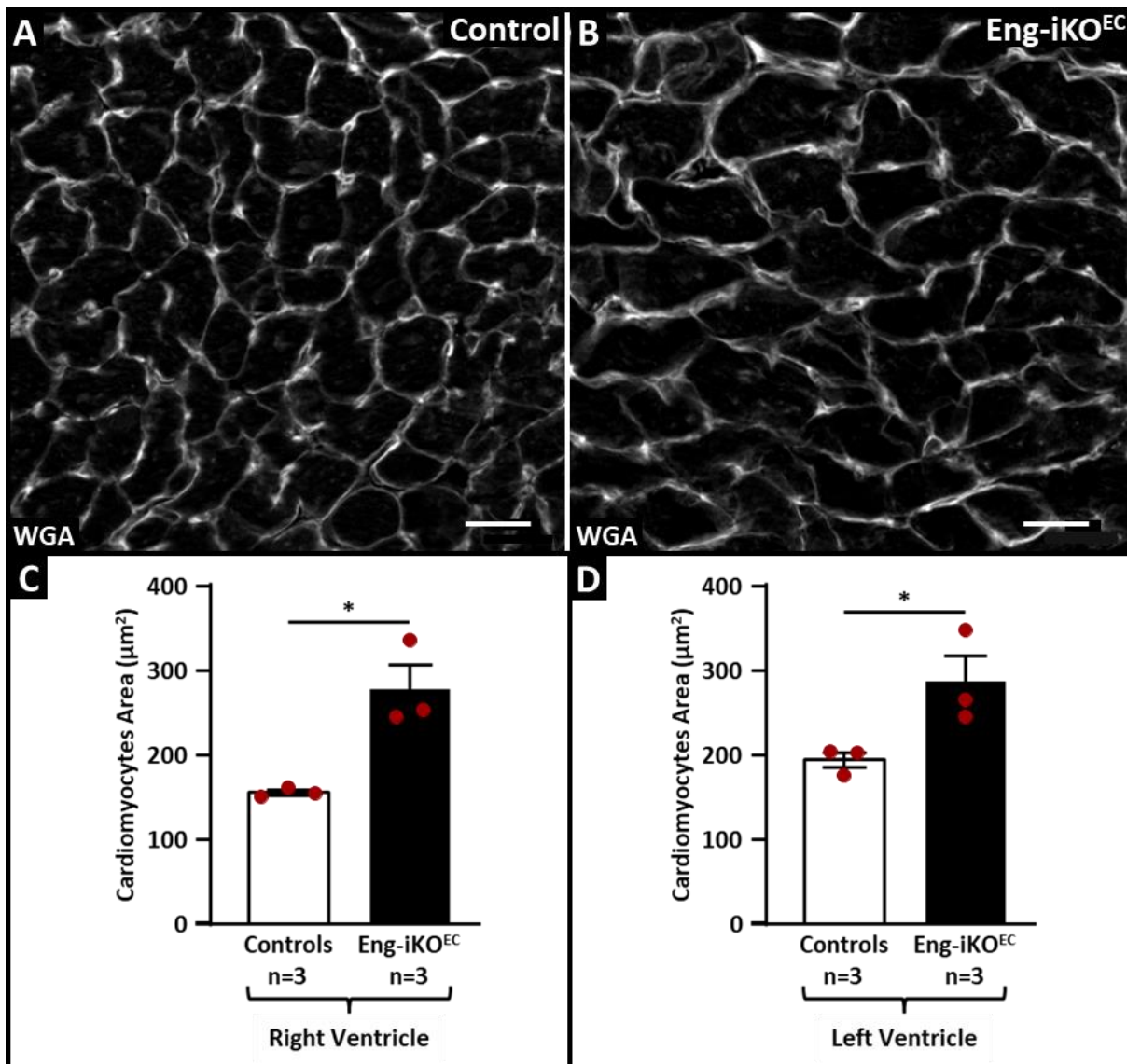


**Figure 5.32: Depletion of Endoglin in adult quiescent ECs using *VE-Cad<sup>Cre-ERT2</sup>* leads to cardiac hypertrophy.** WGA stained (white) control (A) and Eng-iKO<sup>qEC</sup> (B) mice transverse heart sections showing cardiomyocyte (CM) hypertrophy in Eng-iKO<sup>qEC</sup> mice. (C) Quantification of WGA staining showed significantly increased area of Eng-iKO<sup>qEC</sup> CM in RV ( $285.9 \pm 31.34$ ,  $n=3$ ;  $p = 0.0137$ ) and LV ( $277.6 \pm 29.02$ ,  $n=3$ ;  $p = 0.0477$ ) compared to respective controls (RV:  $194.0 \pm 8.90$ ,  $n=3$ ; LV:  $155.1 \pm 3.14$ ,  $n=3$ ). Data shown as mean  $\pm$  SEM and analysed using two tailed unpaired *t*-test (\*  $p < 0.05$ ). Scale bar: A-B – 20 $\mu\text{m}$  (Data collected and analysed in collaboration with Dr. Simon Tual-Chalot).

### 5.2.6.1 Effect of Endoglin knockdown in Adult ECs on AVM formation

As seen during the neonatal study, this cardiac phenotype could be due to AVMs in the systemic vasculature (Figure 5.16) These AVMs can occur in any part of the body, however HHT1 patients are more prone to AVMs in lungs and brain [(section 1.6), (182)]. To detect arteriovenous shunts (AVS), Eng-iKO<sup>qEC</sup> (Figure 5.28) and control mice were injected with fluorescently labelled microspheres. To detect pulmonary AVMs, 15 $\mu\text{m}^3$  microspheres (red beads) were injected into the venous circulation (Figure 5.33, red arrow) as these are readily trapped in the pulmonary capillaries (141). While to analyse the presence of AV shunts in the systemic circulation beads were injected into the left ventricle, also larger (45 $\mu\text{m}^3$ ) green fluorescent microspheres (green beads, Figure 5.33, green arrow) were used as smaller beads passed through natural endogenous AV shunts even in control mice, such as those between hepatic artery and portal veins (304).

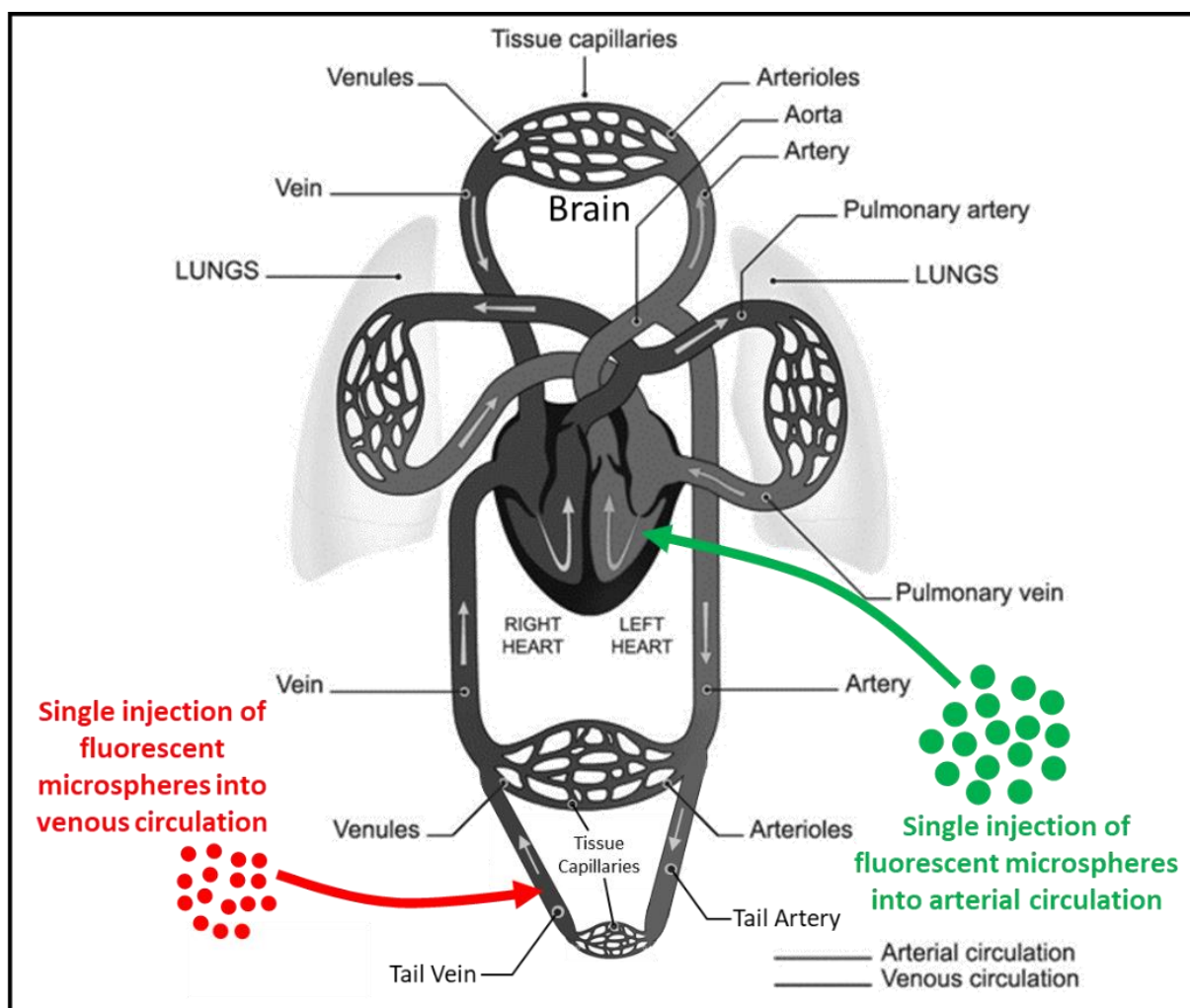


**Figure 5.33: Injection of fluorescently labelled microsphere to investigate the presence of AVMs in pulmonary or systemic circulation [adapted from (305)].** To investigate presence of AVMs in lungs, 15 $\mu\text{m}^3$  red fluorescent microspheres were injected via tail vein and to study the presence of AVMs in systemic vasculature, 45 $\mu\text{m}^3$  green fluorescent microspheres were injected in the left ventricle.

To check that the red  $15\mu\text{m}^3$  beads were consistently trapped in the lungs in control mice,  $200\mu\text{l}$  of  $10^6$  beads per ml was injected via tail vein in three control female mice. The organs were harvested and prepared following the protocol described in section 2.7.3 and imaged using filter set 31 on M2 axio-imager microscope. The red beads were efficiently trapped in the lungs (Figure 5.34A) with no beads in the brain, liver and kidneys of control female mice ( $n=3$ ) (Figure 5.34, F-H). The examination of left lung slices showed even distribution of beads throughout the left lung lobe (Figure 5.34, B-E). In Eng-iKO<sup>qEC</sup> female mice ( $n=6$ ), a similar phenotype was observed with all the red beads trapped in the lungs (Figure 5.34I), with an even distribution in lungs slices (Figure 5.34, J-M). Similarly, no beads were observed in the other organs of Eng-iKO<sup>qEC</sup> mice (Figure 5.34, N-P). A summary of this data is showed in Table 5.2. Together, this current data confirms that lack of endothelial endoglin did not cause any vascular shunting of greater than  $15\mu\text{m}$  diameter in lungs.

**Table 5.2: Results summary of tail vein injection of  $2 \times 10^5$  ( $200\mu\text{l}$ )  $15\mu\text{m}^3$  red fluorescently labelled microspheres in control and Eng-iKO<sup>qEC</sup> female mice**

No.	Genotype	Gender	Beads				
			Brain	Liver	Lungs	Left Lung Slices	Kidneys
1	Control	F	No	No	Yes *****	Even Distribution	No
2	Control	F	No	No	Yes *****	Even Distribution	No
3	Control	F	No	No	Yes *****	Even Distribution	No
1	Eng-iKO <sup>qEC</sup>	F	No	No	Yes *****	Even Distribution	No
2	Eng-iKO <sup>qEC</sup>	F	No	No	Yes *****	Even Distribution	No
3	Eng-iKO <sup>qEC</sup>	F	No	No	Yes *****	Even Distribution	No
4	Eng-iKO <sup>qEC</sup>	F	No	No	Yes *****	Even Distribution	No
5	Eng-iKO <sup>qEC</sup>	F	No	No	Yes *****	Even Distribution	No
6	Eng-iKO <sup>qEC</sup>	F	No	No	Yes *****	Even Distribution	No
<b>Key: * – lowest beads density; ***** – highest beads density</b>							

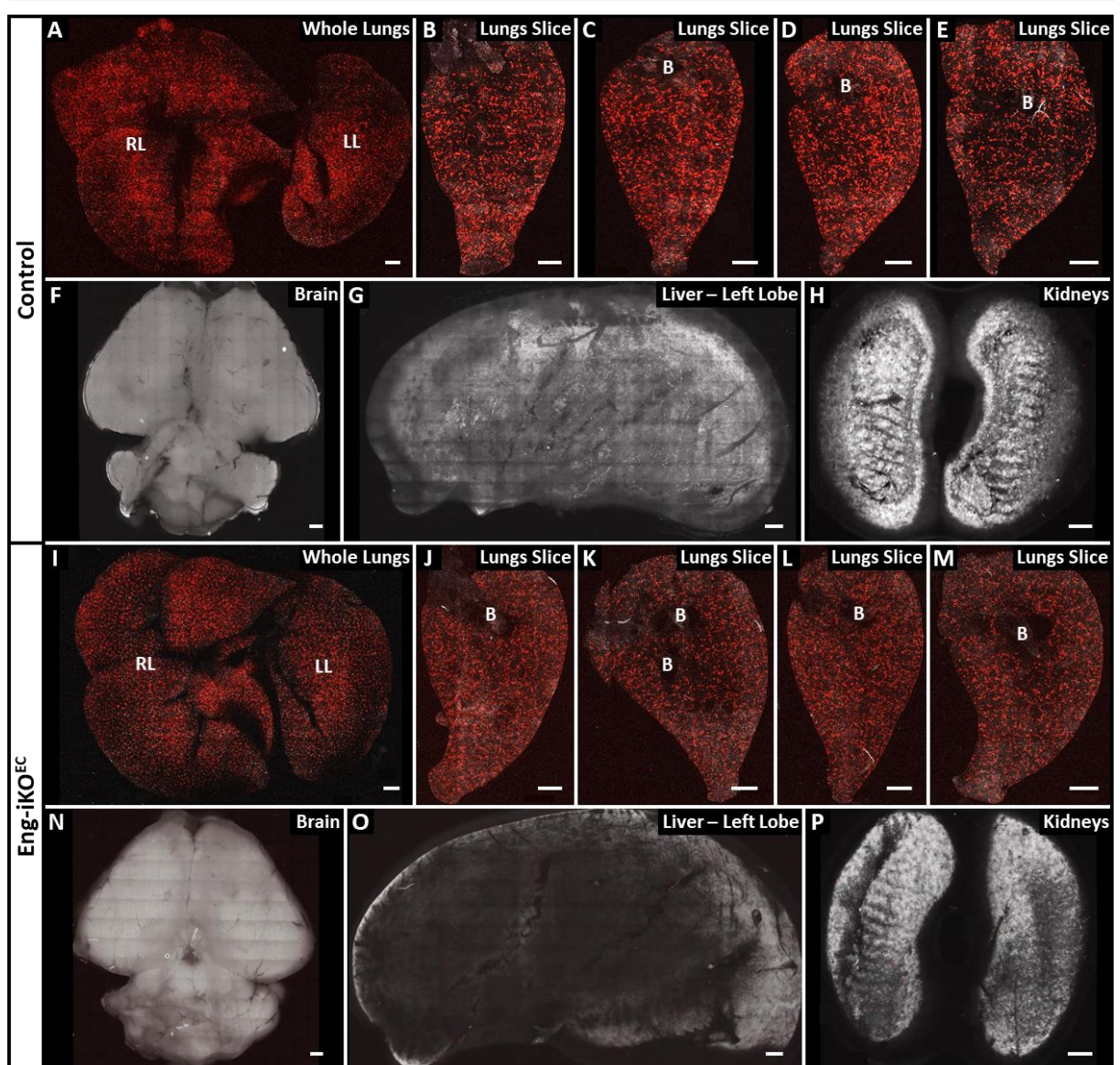


**Figure 5.34: Knockdown of *Endoglin* in quiescent ECs using *VE-Cad*<sup>Cre-ERT2</sup> did not lead to formation of AVMs in the lungs.** 15 $\mu$ m<sup>3</sup> red fluorescence beads injected via the tail vein were efficiently trapped in the lungs [whole view lungs (A,L) and transverse 100 $\mu$ m thick slices of left lungs (B-E, J-M) of both controls and Eng-iKO<sup>qEC</sup> mice. No beads were observed in the brain (F,N), liver (G,O) and kidneys (H,P) of control and Eng-iKO<sup>qEC</sup> mice. Abbreviations: RL – right lung; LL – left lung; B – bronchioles. Scale bar: A-P = 1mm.

To detect AVMs in the systemic circulation, various volumes of (50 to 300 $\mu$ l) 45 $\mu$ m<sup>3</sup> green beads (5 x 10<sup>5</sup>/ml) were injected via LV and allowed to circulate for one minute under terminal anaesthesia following the protocol described in section 2.7.2. In all cases very few beads reached the lung in control females, but large numbers of beads reached the lung in control males. Male mice are larger than female mice so the shunting of 45 $\mu$ m<sup>3</sup> beads from the arterial to the venous side in control males could potentially be due to larger vessels in males compared to females. However, this would need further analysis to confirm.

A volume of 100 $\mu$ l containing 5.5x10<sup>4</sup> green beads injected via LV was selected for testing in a larger group (n=8) control female mice. The organs and lungs slices were prepared as before (section 2.7.3) and imaged using filter set 10 on M2 axio-imager microscope. Results showed

---

a fairly consistent pattern of green beads entrapment in brain, liver, kidneys and intestine. A high number of beads were trapped in major vessels of brain (Figure 5.35A), liver (Figure 5.35B, white arrows) and arteries in intestine (Figure 5.35D) with an even spread throughout both kidneys (Figure 5.35C). Only one control liver was observed with a lower number of beads in all organs suggesting failure in the injection (Control 7, Table 5.3). In the lungs of all the control mice, only a small number of green beads were observed (Figure 5.35, E&F, yellow arrows). These could potentially have reached the lungs due to presence of natural endogenous shunts in the liver (304).

Repeating the experiment in Eng-iKO<sup>qEC</sup> mice (n=7), gave a similar pattern of green beads trapped in brain (Figure 5.35G), kidneys (Figure 5.35I) and intestine (Figure 5.35J). In contrast, green beads were observed in the vessels present in the periphery of the liver (red arrows, Figure 5.35H) and a significantly increased number of beads reached the lungs (Figure 5.35, K&L and Figure 5.35M) indicating presence of AV shunts greater than 45µm diameter in the systemic circulation. To compare the number of beads reaching lungs in controls and Eng-iKO<sup>qEC</sup> mice, total number of beads were counted using event function of Zen 2012 software from the tiled images of all left lung slices. The quantification using unpaired t-test showed a 98% increase in the number of beads reaching the left lung of Eng-iKO<sup>qEC</sup> female mice compared to controls (Figure 5.35M, *p value* = 0.0023). A summary of this data is shown in Table 5.3.

**Table 5.3: Results summary of 45µm<sup>3</sup> green fluorescently labelled microspheres (5.5x10<sup>4</sup>) entrapment in organs of female controls and Eng-iKO<sup>qEC</sup> mice injected via left ventricle.**

No.	Genotype	Gender	Presence of Beads				
			Brain	Liver	Kidneys	Lungs	Left Lung Slices
1	Control	F	Yes ****	Yes ****	Yes ****	Yes *	21
2	Control	F	Yes ****	Yes ****	Yes ***	Yes *	5
3	Control	F	Yes ****	Yes ****	Yes ***	Yes *	20
4	Control	F	Yes ****	Yes ****	Yes ***	Yes *	20
5	Control	F	Yes ****	Yes ****	Yes *****	Yes *	36
6	Control	F	Yes ****	Yes ****	Yes ***	Yes **	135
7	Control	F	Yes ***	No	Yes **	Yes *	5
8	Control	F	Yes ****	Yes ***	Yes **	Yes *	19
1	Eng-iKO <sup>qEC</sup>	F	Yes ****	Yes *	Yes ***	Yes ****	1416
2	Eng-iKO <sup>qEC</sup>	F	Yes ****	Yes ***	Yes ****	Yes ****	1322
3	Eng-iKO <sup>qEC</sup>	F	Yes ****	Yes ***	Yes ***	Yes *****	6553
4	Eng-iKO <sup>qEC</sup>	F	Yes ****	Yes ***	Yes ***	Yes ****	2694
5	Eng-iKO <sup>qEC</sup>	F	Yes **	Yes *	Yes **	Yes ****	2333
6	Eng-iKO <sup>qEC</sup>	F	Yes **	Yes *	Yes **	Yes ***	905
7	Eng-iKO <sup>qEC</sup>	F	Yes ****	Yes ***	Yes ****	Yes ***	2698

**Key: \* – lowest beads density; \*\*\*\*\* – highest beads density**

In conclusion, the analysis of red beads showed that endoglin knockdown in quiescent ECs does not lead to any pulmonary vascular abnormalities (Figure 5.34 and Table 5.2). In contrast, green beads injected into the systemic circulation via LV readily reach the lungs in Eng-iKO<sup>qEC</sup> female mice (Figure 5.35 and Table 5.3) demonstrating the presence of arteriovenous shunts in the systemic circulation of (Figure 5.31). However, further experiments potentially using microfil and microCT would be required to locate these AVMs.

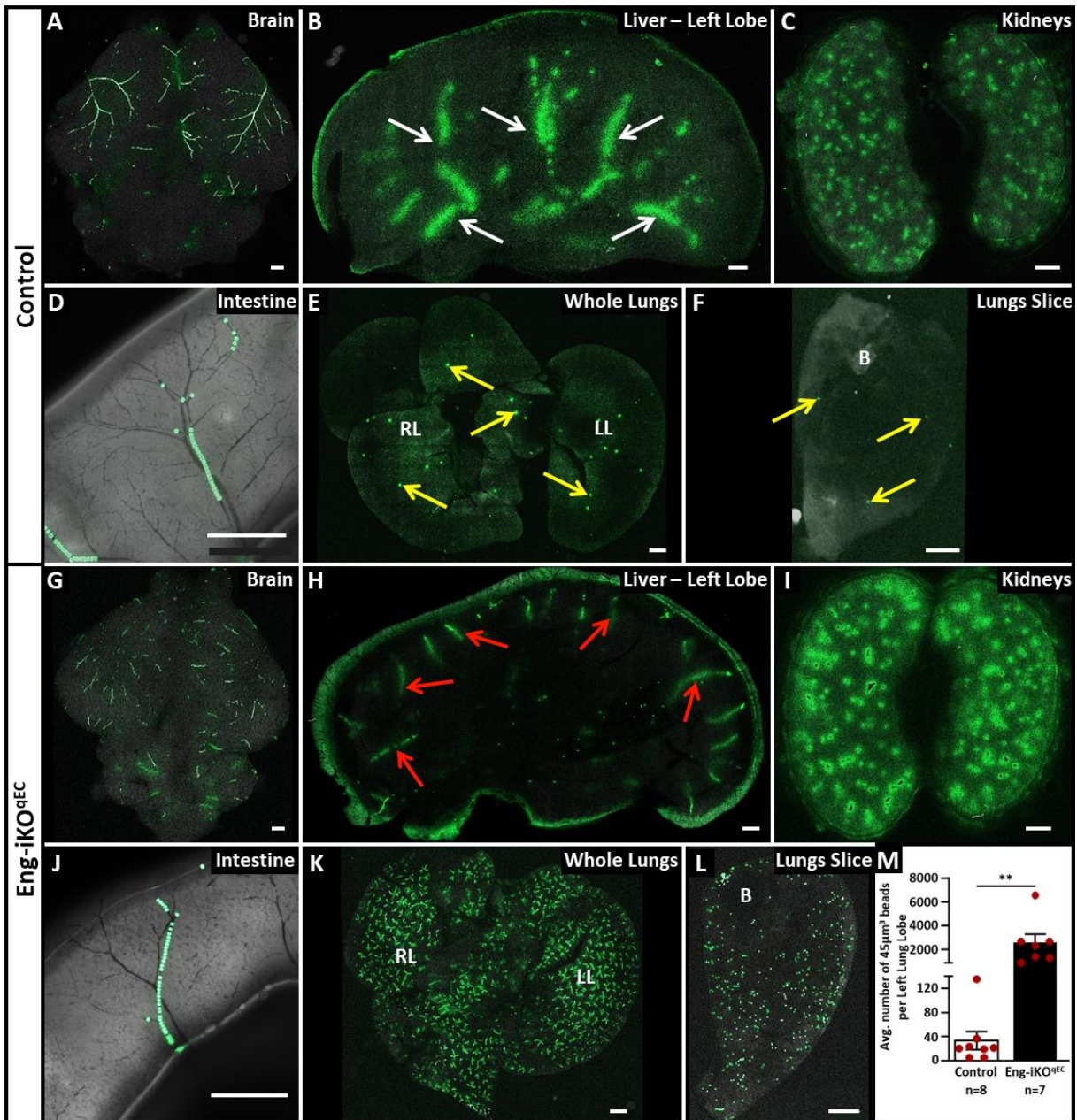


**Figure 5.35: Knockdown of *Endoglin* in quiescent ECs using *VE-Cad*<sup>Cre-ERT2</sup> cause systemic vasculature related abnormalities.** Most of the 45μm<sup>3</sup> green fluorescence beads injected via the left ventricle were observed to be trapped in the brain (A), liver (B), kidneys (C) and intestine (D) of control mice. While a few beads were observed to reach the lungs [yellow arrows; whole view (E) & transverse 100μm thick slice of left lung (F)] of control mice. In contrast, numerous beads were observed in Eng-iKO<sup>qEC</sup> mice lungs [whole view (K) & transverse 100μm thick slice of left lung (L)]. The pattern of beads in brain (G), kidneys (I) and intestine (J) of Eng-iKO<sup>qEC</sup> mice was observed to be similar to controls. However, in liver the beads were observed near the periphery (red arrows, H) while in controls these trapped in the middle (white arrows, B). (M) Quantification showed significantly higher number of 45μm<sup>3</sup> green beads trapped in Eng-iKO<sup>qEC</sup> mice (2560.00±717.40, n=7;  $p = 0.0023$ ) compared to control (33.00±14.99, n=8) mice. Data shown as mean±SEM and analysed using two tailed unpaired *t*-test (\*\*  $p < 0.01$ ). Abbreviations: RL – right lung; LL – left lung; B – bronchioles. Scale bar: A-L= 1mm.

---

## 5.3. Discussion

### 5.3.1 Endoglin in coronary ECs during cardiac development

#### 5.3.1.1 Endoglin in ECs during embryonic heart development

To investigate the role of endoglin in ECs of the developing coronary vessels, a new inducible arterial ECs specific Cre (*Dll4in3<sup>Cre-ERT2</sup>*) mouse model was used. This part of the work would provide further insights into the development of coronary vessels which in turn could be utilised to design better treatment strategies for patients with coronary vasculature related defects.

Unfortunately, activation of *Dll4in3<sup>Cre-ERT2</sup>* at different time-points did not label many coronary arteries in developing embryos (Figure 5.6). This could be potentially due to following reasons: (i) poor Cre recombinase efficiency, (ii) long gap between the *loxP* sites (306-308), (iii) lack of stability or efficiency of the small enhancer sequence (*Dll4in3-Cre-ERT2*) (309) or else (iv) depending on the location of enhancer sequence in the genome, it could also be affected by chromatin condensation. This poor Cre recombination postnatally due to long gap in between *loxP* sites is unlikely as the same reporter is widely used including in this thesis (chapter 4 & 5). In a publication by Turlo *et al.* (310), a similar issue was observed with poor  $\beta 1$  integrin knockdown using *Sm22 $\alpha$ <sup>Cre-ER</sup>* in one mouse strain. It was observed that the knockdown was unsuccessful due to the presence of a Cre recombinase episomal product (small circular DNA product formed from the excised sequence) in slowly proliferating cells (310). It is possible that arterial ECs proliferate at a slower rate compared to venous ECs, to analyse this, embryo sections would need to be stained with a proliferation, arterial and venous markers such as pHH3, Jagged1 and Endomucin respectively. To analyse the presence of the episomal product, qPCR was used in the study by Turlo *et al.* (310) by custom designed primer sequences against: (i) recombined *loxP* sites; (ii) unrecombined sequence and (iii) another set against the excised DNA sequence (episomal product). In the presence of successful recombination, there would be minimal amount of product in latter two. However, in this study, due to these disappointing results no further experiments were performed using this mouse line.

#### 5.3.1.2 Endoglin in ECs during postnatal heart development

I next investigated the role of endothelial endoglin during the third phase of coronary development in the first week of postnatal life (122). Activation of *VE-Cad<sup>Cre-ERT2</sup>* on day P2 and P4 showed knockdown of endoglin in all cardiac blood vessels except for a few capillaries (Figure 5.9) and development of enlarged hearts by P7 (Figure 5.10) along with CM hypertrophy (Figure 5.13) and enlarged ventricle chambers (Figure 5.14). It is possible that

---

these mice develop eccentric cardiomyopathy caused by chronic overload due to systemic vasculature defects (discussed below). However, no abnormalities were observed in the coronary vasculature of Eng-iKO<sup>EC</sup> mice at P7 (Figure 5.12). It is possible that there could be still some subtle defects which are not visible in the 2D imaging plane of heart tissue sections. To analyse this, 3D reconstruction would need to be performed on serially sectioned heart tissue.

Another possible reason for the lack of observed coronary vascular defects could be that the development (third wave) of vessels in the trabeculae starts earlier than reported by Tian *et al.* (122), potentially intra-embryonically. In a future study, it might be beneficial to activate VE-Cad<sup>Cre-ERT2</sup> immediately after birth (P0 and P1) to investigate the effect of endoglin knockdown on coronary vasculature. Mahmoud *et al.* (188) reported that endoglin knockdown in ECs led to increased EC proliferation. Therefore, it would also be informative in future studies to analyse the effect on endothelial cell proliferation using markers such as pHH3 or BrdU and apoptosis using Caspase 3. Furthermore, it might also be useful to isolate coronary ECs from controls and Eng-iKO<sup>EC</sup> mice; and check the levels of phosphorylated smad1/5/8 and smad2/3 as well as proteins including Pai1, Id1, and PDGF using techniques such as western blots or qPCR or both. This will help to reveal which proteins are affected downstream of TGF $\beta$ /BMP9 signalling pathway in heart.

In the current model, AVMs were suspected as causal for the eccentric cardiac hypertrophy phenotype as loss of endothelial endoglin leads to AVMs in neonatal retinas of Eng-iKO<sup>EC</sup> mice (188) and I confirmed this phenotype in P7 Eng-iKO<sup>EC</sup> mice (Figure 5.16). These mice could also be developing HOHF similar to that observed in Eng-iKO<sup>EC</sup> adult mice (Figure 5.4). However, further experiments to study cardiac function would be required to calculate cardiac output and ejection fraction of control and Eng-iKO<sup>EC</sup> neonatal mice.

Another parameter to check would be cardiac fibrosis, a common histological parameter observed in multiple heart diseases (311). To analyse this, the heart sections would need to be stained with masson trichrome or Sirius Red, which would allow quantification of cardiac fibrosis. It might also be beneficial to analyse the impact of endoglin knockdown on angiogenic factors which could be downstream of TGF $\beta$ /BMP signalling. To analyse this, an angiogenesis antibody array kit (e.g. from R&D systems, cat. no. ARY015) with various angiogenic factors could be used with lysates of whole organs or if possible, with isolated ECs from AVMs prone organs such as lungs, liver and brain from control and Eng-iKO<sup>EC</sup> mice. This would aid in showing possible angiogenic factors which could be working downstream of TGF $\beta$ /BMP

---

signalling. The selected factors then further quantified either using qPCR or western blots and could generate new therapeutic targets in patients with vascular related illness/ disorders.

### 5.3.2 BMP9 mediated rescue of AVM phenotype

The standard treatment for severe AVMs is embolization, performed under general anaesthesia to block the vessels while most of the small AVMs are generally left untreated (194, 195). However, these embolized vessels could reopen again in future (194). Therefore, delivery of a pharmaceutical molecule could definitely aid in development of better treatment strategy. During the current study, I tested the effect on AVMs formation after exogenous BMP9 treatment *in vivo*.

During the TGF $\beta$ /BMP signalling, endoglin is required to help to bind the BMP9/10 ligand to BMPR2 (130, 134). Therefore, in the absence of endoglin, availability of ligands BMP9/10 would be reduced which could potentially cause AVMs in retinas along with delayed vascular progression and wider veins [(188) Figure 5.16]. However, IO injection of BMP9 on day P4 or P5 in Eng-iKO<sup>EC</sup> mice did not rescue the AVMs phenotype in P7 Eng-iKO<sup>EC</sup> retinas (Figure 5.16) but the IO injection itself exacerbated the AVM phenotype (Figure 5.18). This was potentially because a 27G needle was used to inject BMP9 and PBS which led to a severe injury in the eyes such that many retinas had very poor morphology. In a study by Hombrebueno *et al.* (312), they showed IO injection of normal saline in 3 months led to upregulation of multiple inflammatory genes including *VEGF*. It is possible in the current study, IO injection led to increased *Vegf* expression providing the angiogenic stimuli leading to an aggravated phenotype (Figure 5.18). In any future studies it might be beneficial to use a smaller gauge potentially 33G Hamilton syringe. This might provide better morphology potentially due to reduced injury

If IO injection still does not work due to morphological issue; systemic delivery (IP injection) could be tested however, much higher doses of BMP9 would be needed. Long *et al.* (313) using immunoprecipitation and immunoblotting showed that BMP9 signals via canonical signalling pathway in combination with BMPR2 *in vitro* and prevents tumour necrosis factor  $\alpha$  (TNF $\alpha$ ) induced ECs apoptosis. Mutations in BMPR2 are shown to be associated with pulmonary arterial hypertension (PAH) (314, 315). Long *et al.* (313), also showed that 6 month old *Bmpr2*<sup>+/<sup>R899X</sup></sup> mice develop PAH as observed by increased right ventricular systolic pressure (RVSP) and enhanced muscularisation of pulmonary arteries. Interestingly, treatment of these mice with exogenous BMP9 by IP injection (75ng dose daily for 4wks) reversed these PAH symptoms by reducing in RVSP to WT levels as well as reduction in the enhanced vascular muscularisation phenotype (313). If the HHT phenotype is due to lack of BMP9/10 signalling

---

(192, 293), it is possible similar treatment with BMP9 would also reduce the AVM phenotype in HHT1 mice to generate a protective response (i.e. prevent AVM formation). Further studies would be required to determine if BMP9 could also revert established AVMs.

### 5.3.3 Origin of AVMs: Arterial, Venous or Both

AVMs are abnormal direct connections between arteries and veins (Figure 1.21). However, the origin of these AVMs is still unclear. Jin *et al.* (294), suggested that AVMs originate from arteries. However, I analysed the effect of endoglin knockdown in venous ECs and capillaries on AVMs formation. The activation of *Apj*<sup>Cre-ER</sup> using tamoxifen at P5 was the earliest time-point that allowed specific activation in veins and capillaries of the retinas (Figure 5.20).

Mirroring these Cre activation times (P5 & P6) in the VE-Cad<sup>Cre-ERT2</sup> mouse model generated AVMs and enlarged veins in P8 and P11 Eng-iKO<sup>EC</sup> retinas (Figure 5.25). The probability of AVM formation in Eng-iKO<sup>EC</sup> retinas was ~67% after Cre activation at P2&P4 (similar to that observed by in Mahmoud *et al.* (188)). Later depletion of endothelial endoglin (at P5&P6), a comparable incidence of retinas with AVMs was observed (~57% at P8 and ~67% at P11). Furthermore, these AVMs as well as additional AVMs likely present in the systemic circulation also led to development of enlarged heart in P11 mice (Figure 5.23B). This strongly suggests that endothelial endoglin is required for normal cardiovascular development. I next compared these results with venous ECs specific endoglin knockdown using *Apj*<sup>Cre-ER</sup>. Interestingly, a similar phenotype was observed in both P8 and P11 hearts (Figure 5.23) and retinas (Figure 5.25). However, in the current preliminary study slight differences were observed in the P8 phenotype of Eng-iKO<sup>V</sup> compared to Eng-iKO<sup>EC</sup> retinas. The AVMs formation probability was considerably lower in P8 Eng-iKO<sup>V</sup> retinas (~33%) compared to P8 Eng-iKO<sup>EC</sup> retinas (~57%). The AVMs in the Eng-iKO<sup>V</sup> were also ~24% thinner compared to Eng-iKO<sup>EC</sup> mice. If confirmed in larger numbers of mice this finding suggests that AVMs in Eng-iKO<sup>EC</sup> develop earlier than in Eng-iKO<sup>V</sup> mice and enlarge over time potentially due to increased EC proliferation and blood flow through the AV connection (188, 316).

To test any difference in EC proliferation, P8 and P11 retinas from both mouse lines would need to be first injected then stained with BrdU. Furthermore, the effect of venous ECs specific endoglin knockdown could also be studied on vessel muscularisation in retinas (using  $\alpha$ SMA antibody). As reduced BMP9/10 signalling could be causing this effect it might be useful to compare the angiogenic factor profile in retina ECs from VE-Cad<sup>Cre-ERT2</sup>, venous and arterial ECs from *Apj*<sup>Cre-ER</sup> mice using an angiogenesis antibody protein array. The ECs from P8 control and Eng-iKO<sup>EC</sup> retinas could be extracted using Dynabeads conjugated with anti-PECAM1

---

antibodies (317). However, to isolate venous ECs from littermate control and Eng-iKO<sup>V</sup> P8 retinas, Dynabeads would need to be used with antibodies such as anti-apj [located on cell surface (318)] or anti-endomucin. An alternative approach would be to isolate ECs from Eng-iKO<sup>V</sup> (and controls) using FACS, as *Apj*<sup>Cre-ER</sup>*Rosa26*<sup>mT/mG</sup> mice express eGFP in all Cre-recombined cells. These ECs could then be subjected to angiogenesis antibody array kit to discover any common angiogenic factors potentially crucial for formation of AVMs, which could then be quantified either using western blots or qPCR.

In conclusion, this study shows a clear HHT1 phenotype in a novel mouse line. More importantly, this study indicates the importance of endoglin in veins and capillaries for maintaining vascular homeostasis.

### 5.3.4 Endoglin in Vascular Maintenance in Adult Mice

HOHF is a rare complication in HHT patients and in most cases is associated with liver AVMs (170-172). HOHF could also be caused due to anaemia or vasodilation or loss of systemic vascular resistance (295-297). Lack of endoglin in quiescent endothelial cells using VE-Cad<sup>Cre-ERT2</sup> consistently led to development of HOHF (Figure 5.4). In my host laboratory, analysis of aortic pressure showed that loss of endothelial endoglin led to reduced systemic vascular resistance. This reduced vascular resistance was not due to anaemia as Eng-iKO<sup>qEC</sup> mice had normal haematocrit. Another cause of HOHF could be AV shunts in the pulmonary and systemic circulation. I therefore analysed Eng-iKO<sup>qEC</sup> mice to study the presence of AVMs.

In Eng-iKO<sup>qEC</sup> mice, 5wks after first tamoxifen injection, enlarged hearts (Figure 5.29) were observed with CM hypotrophy (Figure 5.32) similar to neonate phenotype (Figure 5.10 and Figure 5.13). In addition, strong endoglin expression was observed in coronary veins, pulmonary veins, central veins and pulmonary arteries compared to arterial ECs coronary, hepatic arteries and portal veins (Figure 5.31). This was a novel discovery, potentially suggesting that ECs of these vessel proliferate at higher rate as during angiogenic phase, proliferating ECs express strong levels of endoglin (144). In Eng-iKO<sup>qEC</sup> mice, a varying level of endoglin knockdown was observed all the vessels except hepatic arteries (Figure 5.31). As mentioned above, this poor recombination could be linked with low proliferating cells (310). This hypothesis would need to be verified either by staining for proliferative marker pHH3 on sister sections of the above mice or harvesting fresh organs from BrdU injected mice and then stain for BrdU.

---

The analysis of pulmonary AVMs using  $15\mu\text{m}^3$  red fluorescent beads injected via tail vein showed normal pulmonary vasculature in control and Eng-iKO<sup>qEC</sup> with all the red beads trapped only in the lungs (Figure 5.34). In addition to this, oxygen saturation analysis in Eng-iKO<sup>qEC</sup> mice showed no difference in comparison to controls (unpublished data, Arthur Lab). Taking this data together confirmed lack of pulmonary AVMs in Eng-iKO<sup>qEC</sup> mice. This is contrast with 33% risk of pulmonary AVMs in HHT1 patients (319). This difference could be potentially due to lack of a second angiogenic stimulus (e.g. lung infection) or somatic mutations which potentially lead to formation of pulmonary AVMs in patients (187-190).

Analysis of the systemic circulation using  $45\mu\text{m}^3$  green fluorescent beads injected via LV showed a significantly higher number of green beads in Eng-iKO<sup>qEC</sup> lungs compared to controls (Figure 5.35, E,K&M). This indicated the presence of AVMs or enlarged AV connections in the systemic circulation. The distribution pattern of green beads was similar in brain, kidneys and intestine of control and Eng-iKO<sup>qEC</sup> mice (Figure 5.31). However, in liver the beads were observed in the central hepatic vasculature in control while in Eng-iKO<sup>qEC</sup> mice, beads were trapped in the periphery of the liver (Figure 5.31B&H). Further analysis in the Arthur laboratory using beads showed a 50:50 occurrence of central or peripheral location of beads in the liver in both controls and Eng-iKO<sup>qEC</sup> mice. This could be due to variation in the size of endogenous shunts between hepatic artery and portal vein (304). Further work using latex (which when injected into the aorta is normally retained in the arterial side of the circulation unless AV shunts are present) showed consistent large AVMs in the pubis symphysis region of Eng-iKO<sup>qEC</sup> mice (Figure 5.36). This finding confirmed the initial hypothesis that reduced vascular resistance was caused by AVMs in the systemic circulation leading to HOHF.

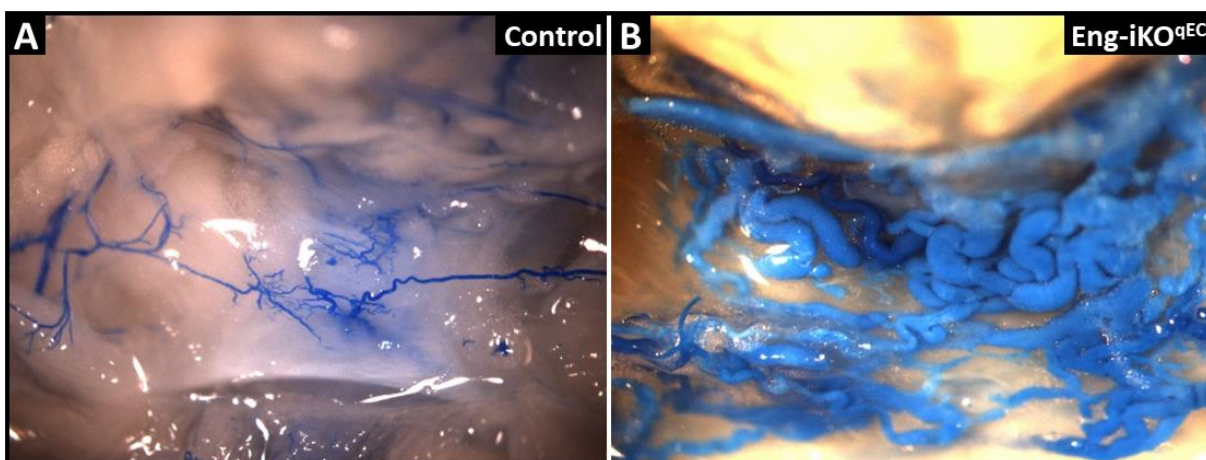


**Figure 5.36: Endothelial *Endoglin* knockdown in adult ECs leads to development of AVMs in pubis symphysis.** (A) Image of pubic symphysis region of control (n=11) showed normally developed vasculature visualised using injection of latex (blue) via aorta. (B) Image of Eng-iKO<sup>qEC</sup> pubic symphysis showed enlarged vessels and AVMs (n=9). *Data courtesy of Dr. Simon Tual-Chalot.*

---

This work showed that continued expression of endoglin in ECs is crucial for maintaining normal adult vasculature. However, the mechanism behind this is still unknown. In a recent publication by Jin *et al.* (294), it was observed that neonate mice lacking endothelial endoglin develop AVMs in brain and retina. They also observed high level of Vegfa expression in the brain lysates from Eng-iKO mice potentially induced due to hypoxia (294). Furthermore, *in vivo* inhibition of VEGFR2 or PI3K (a downstream target of VEGF induced signalling) led to reduction in expansion of these AVMs (294). In addition to this, HHT patients also have increased VEGF levels in their serum/plasma (320, 321). Therefore, VEGF signalling could be playing an important role in the current cardiac and AVMs phenotype. Furthermore, during the current study *in vivo* inhibition of VEGF signalling via treatment with anti-VEGFR2 antibody (DC101, 1wk after first tamoxifen injection) showed normal vessel development in the pubic symphysis region of Eng-iKO<sup>qEC</sup> mice that partially rectified the cardiac phenotype (unpublished data, Arthur lab).

In light of this new evidence from the adult and neonatal mice studies, it is possible endoglin not only promotes EC proliferation during angiogenesis but also helps to maintain ECs in quiescent state by influencing VEGF signalling. The expression of both endoglin (144) and VEGF (13, 14, 16, 107) is reported in proliferating ECs and both are upregulated during hypoxia (216, 217, 322-325). Perhaps, in proliferating ECs, hypoxia promote expression of endoglin which then stimulate Vegf signalling pathway via BMP9/ALK1 mediated signalling cascade (Figure 5.37A). When the hypoxic trigger is lifted, these ECs enter a quiescent/ vessels maturation phase. It is widely known that the endoglin keeps a balance between ALK1 and ALK5 pathway (123) so potentially, endoglin supresses VEGF signalling pathway via ALK5 mediated pathway (Figure 5.37B). However, in the absence of endoglin, this balance is disturbed leading to enhanced VEGF signalling leading to increased EC proliferation and AVMs (Figure 5.37C).

To test this hypothesis, primary endothelial cells could be used from *Eng<sup>fl/fl</sup>; Rosa26<sup>Cre-ERT2</sup>* mice. Half of the cells would be subjected to endoglin knockdown using 4-hydroxy tamoxifen and seeded to a desired cell density. Cells from both groups (control and Eng-iKO<sup>u</sup>), would be cultured in either hypoxic or normoxic conditions. At the end of incubation time, one hypoxic batch of cells would be returned to normoxia to simulate an *in vivo* scenario. Once cells from all three batches are collected, they would need to be analysed for levels of signalling proteins involved in BMP9 (e.g. endoglin, Smad1/5/8, pSmad1/5/8, Sma2/3, pSmad2/3, ID1 and Pai-1) and VEGF (e.g. Vegfa, Vegfr1, Vegfr2, pI3K and pERK) signalling using either qPCR, western blots or both.

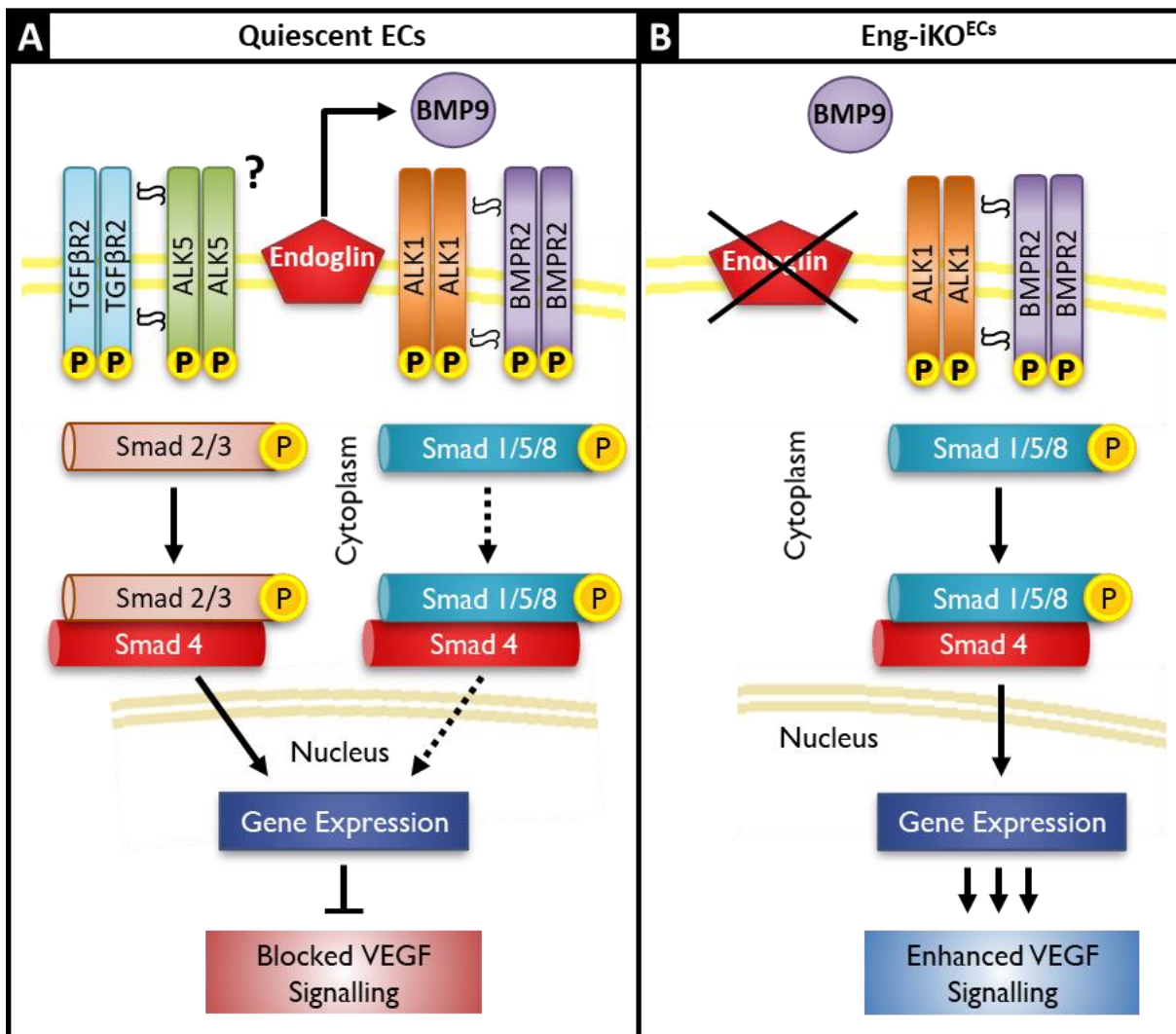


**Figure 5.37: Summary of TGFβ/BMP9 signalling in quiescent endothelial cells in the presence and absence of endoglin.** (A) In quiescent ECs, endoglin potentially suppresses VEGF signalling probably indirectly via ALK5 pathway. (B) However, in the absence of endoglin, this balance is disturbed leading to enhanced VEGF signalling which in turn cause hyper-proliferation leading to vascular abnormalities such as AVMs.

In conclusion, at the end of this study, the role of endoglin in coronary vasculature development is still elusive and would need a better genetic tool to study it during embryogenesis. However, this study did highlight various novel aspects of endoglin in ECs. In neonatal proliferating ECs, loss of endoglin not only leads to the formation of AVMs (188) but also cause an enlarged heart in *Eng-iKO*<sup>EC</sup> mice. This phenotype occurs after complete loss of endoglin using *VE-Cad*<sup>Cre-ERT2</sup>, as well as in the venous and capillary ECs specific endoglin knockdown using *Apj*<sup>Cre-ER</sup>. This strongly indicates that even a partial imbalance of endoglin is detrimental for vascular development. Furthermore, similar phenotype occurs in adult quiescent ECs which shows that continuous endoglin expression is still crucial in quiescent ECs for maintenance of normal vasculature.

---

**Chapter 6. Role of Endoglin in CDC  
Promoted Angiogenesis in Post-MI Hearts**

---

## **6.1. Introduction**

In this chapter I describe my investigations of the role of endoglin in cardiac stem cells used in pro-angiogenic cell therapy following myocardial infarction (MI). As described in section 1.7, a normal healthy heart has a high energy demand and to keep with energy demand every CM is in the close vicinity of a capillary (45, 46). Blockage of a coronary artery leads to MI (201) and severity of MI depends on the coronary artery involved. The CM death post-MI is inevitable and to reduce CM loss, acute MI patients are subjected to PPCI also known as angioplasty to restore the blood supply to the affected region (203). Occurrence of MI results in a cascade of cellular responses to initiate heart repair in three phases: (i) inflammatory, (ii) proliferative and (iii) maturation (Figure 1.20). The process of angiogenesis occurs during the second phase while arteriogenesis occurs during the third phase. These two processes are critical for cardiac healing but are generally insufficient at the endogenous level to protect the CM death (218).

During angiogenesis, endoglin promotes BMP9 signalling via the ALK1 pathway (Figure 1.17) and following MI, increased endoglin expression is observed in the infarcted region (216, 217). Furthermore, following MI in mice with heterozygous deletion of endoglin there was reduced angiogenesis along with significant reduction in stroke volume, cardiac index and ejection fraction compared to control mice (216). To improve cardiac healing post-MI various stem cells are being exploited and promising results are observed using CDCs (discussed in section 1.7.2).

### **6.1.1. Cardiospheres Derived cells in Therapeutic Angiogenesis Post-MI**

CDCs are a mixed population of cells generated from cultured heart tissue biopsies and express various cell specific markers including mesenchymal markers (Eng/CD105) and stem cell markers (c-kit1, SCA-1) (326). Various studies have tested CDCs for their regenerative potential for heart repair post-MI [reviewed in (220)]. The beneficial effects of CDCs are primarily derived via a paracrine mechanism (Figure 1.22). Injection of CDCs in post-MI hearts showed beneficial effects including improved heart function and reduction in scar size 3 weeks after MI (225, 327). In the current study I analysed the importance of endoglin expression in the beneficial paracrine effect of CDCs.

### 6.1.2. Role of Endoglin in CDCs: Pilot study

In my host laboratory, CDCs were cultured from heart biopsies taken from *Eng<sup>fl/fl</sup>; Rosa<sup>Cre-ERT2</sup>; CAG-GFP* mice (150) following the protocol described in Section 2.8 (Figure 6.1). CDCs cultured from this line allows depletion of endoglin in all cardiac cells in the presence of 4 hydroxy tamoxifen (4-OH tam).

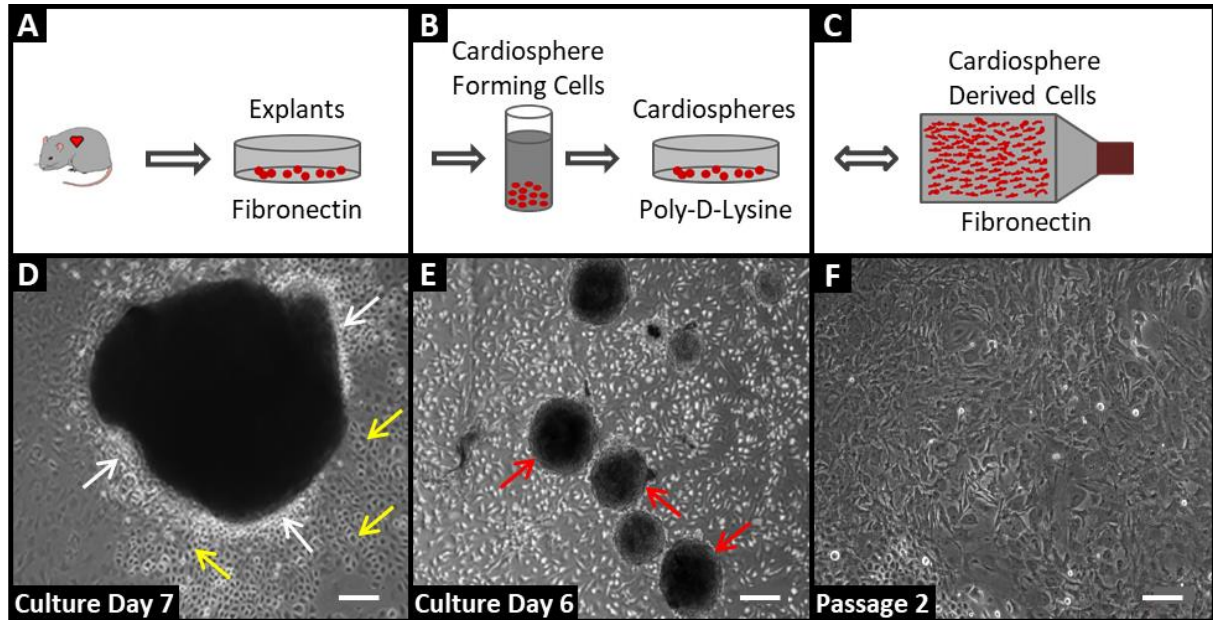


**Figure 6.1: Derivation of murine CDCs [Images courtesy of Dr. Rachael Redgrave].** (A-C) Schematic showing stages of CDC culture. Briefly, heart tissue from *Eng<sup>fl/fl</sup>; Rosa26<sup>Cre-ERT2</sup>* neonatal mice is cut into small explants and plated onto fibronectin. Explant outgrowth cells (A,D) are cultured for approximately 2 weeks and consist of a layer of stromal-like cells (yellow arrows) over which small, phase-bright cells (white arrows) grow. (B,E) All cells are harvested and re-plated onto poly-d-lysine in a growth factor rich media. Over 1-week cells begin to aggregate and form spherical clusters or cardiospheres (E, red arrows). (C) Loosely adherent cardiospheres are then re-plated onto fibronectin-coated flasks and expanded as a monolayer of cardiospheres-derived cells (F). Scale bars B-F = 100 $\mu$ m.

My colleague Dr Rachael. Redgrave showed using flow cytometry that over 70% CDCs express CD105 (Figure 6.2A) with a few CDCs express CD45 consistent with their non-haematopoietic origins. To confirm endoglin knockdown in *Eng*-iKO CDCs, cells with and without tamoxifen treatment at P1 were seeded in chamber slides and stained with rat anti-CD105 antibody (Figure 6.2C-E). Quantification showed that, 93% $\pm$ 3 of control CDCs express endoglin while 23% $\pm$ 5 *Eng*-iKO CDCs express endoglin (data analysed by Dr. Rachael Redgrave). In other words, 96hrs treatment with 4-OH tam led to a 75% endoglin knockdown in CDCs at P2.

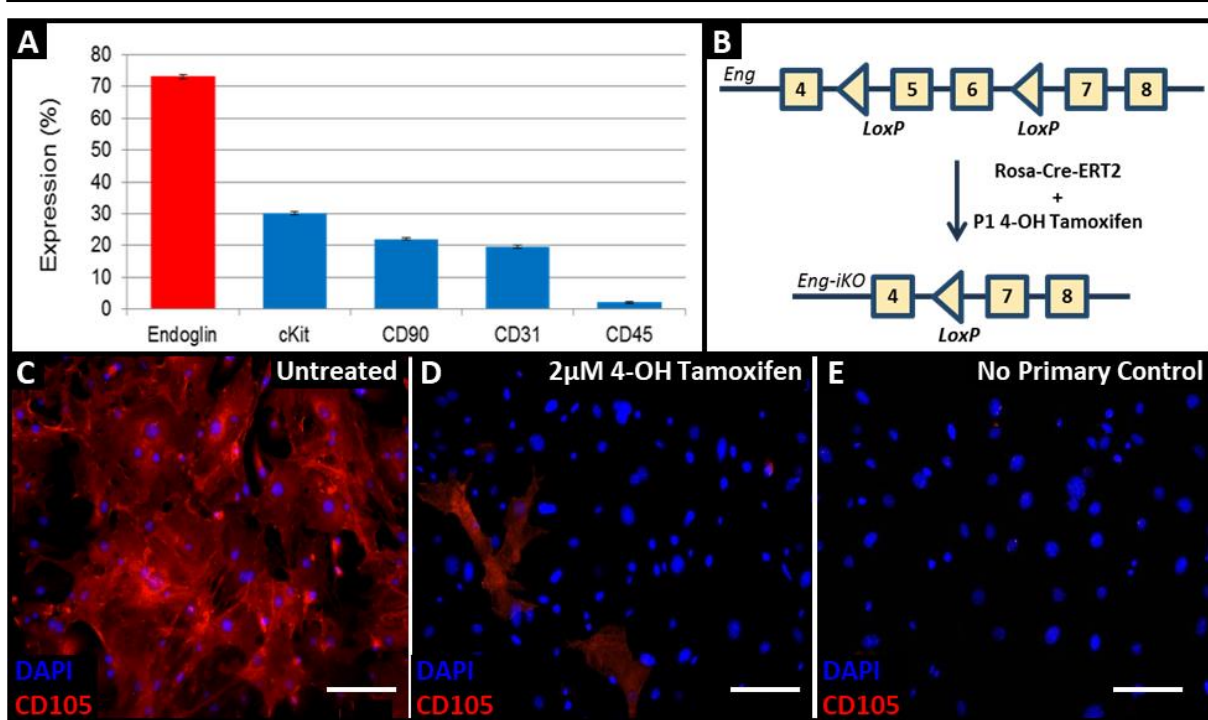


**Figure 6.2: Characterisation of endoglin expression in CDCs and knock-down [Images & data courtesy of Dr. Rachael Redgrave].** (A) Over 70% of CDCs express endoglin, as shown by representative FACS analysis. (B) To induce *Endoglin* knockdown in vitro, CDCs are treated with 2µM of 4-hydroxy tamoxifen for 4 days to activate Rosa26-Cre-ERT2. Representative anti-CD105 immuno-fluorescence images of (C) control CDCs (no tamoxifen) showed high expression of endoglin (red), whereas (D) Eng-iKO CDCs (tamoxifen-treated) showed a marked reduction in endoglin levels. Nuclei are stained with DAPI. (E) No primary staining control. Scale bars: C-E = 50µm.

To investigate whether endoglin is required for the pro-angiogenic properties of CDCs I performed experiments that built on pilot data (Figure 6.3) gathered in my host laboratory. This preliminary work, from Dr Redgrave’s PhD thesis, used CDCs from a small number of mice (n=2-4) and the results suggested that knockout of endoglin in CDCs prior to intra-myocardial injection post-MI led to reduced angiogenesis at 4 weeks post-MI compared to CDCs without endoglin knockout (328).

The purpose of my study was firstly, to expand this pilot study MI and sham groups. Therefore, group sizes were calculated based on identifying a difference in vessel density at a significance of  $p \leq 0.05$  with 80% power using UBC online tool (329) and minitab software. Following the power calculations, the groups ‘n’ numbers were increased as follows: (i) MI+PBS from n=4 to n=8; (ii) MI+CDC-Ctl from n=4 to n=8 and (iii) MI+CDC-Eng-iKO from n=4 to n=7. The sham group were increased to a minimum of 3. The second aim of my study to investigate the effect of endoglin knockdown in CDCs on the maturation and stabilisation of the new blood vessels.

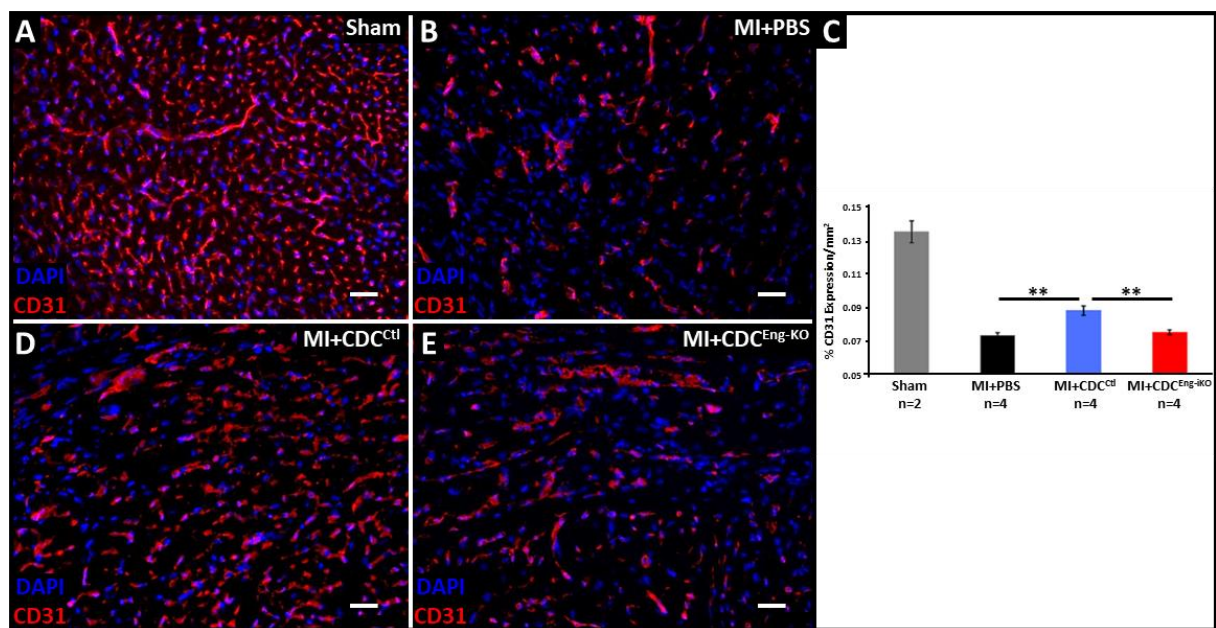


**Figure 6.3: Effect of endoglin knockout on CDC mediated heart repair, pilot data results [Image courtesy of Dr. Racheal Redgrave (328)].** Incidence of MI (B) lead to reduction in the density of vessels in the infarcted zone compared to Sham hearts (A). Transplantation of WT CDCs lead to increased angiogenic response in infarcted zone (D). However, this pro-angiogenic response of CDCs was lost after depletion of endoglin (E). (C) Quantification showed a significant increase in angiogenesis in the infarcted zone after transplantation of Control CDCs ( $0.088 \pm 0.003$ ,  $n=4$ ) in post-MI hearts compared to MI+PBS ( $0.073 \pm 0.002$ ,  $n=4$ ;  $p < 0.0010$ ) and MI+CDC-Eng-iKO ( $0.075 \pm 0.001$ ,  $n=4$ ;  $p < 0.001$ ) group. Abbreviations: CDC – Cardiospheres Derived Cells; Eng-KO – Endoglin knockout; PBS – Phosphate Buffer Saline; MI – Myocardial Infarction and WT – Wild Type. Data analysed using one-way ANOVA (\*\*  $p < 0.01$ ). Scale bar: A,B,D,E = 50  $\mu\text{m}$ .

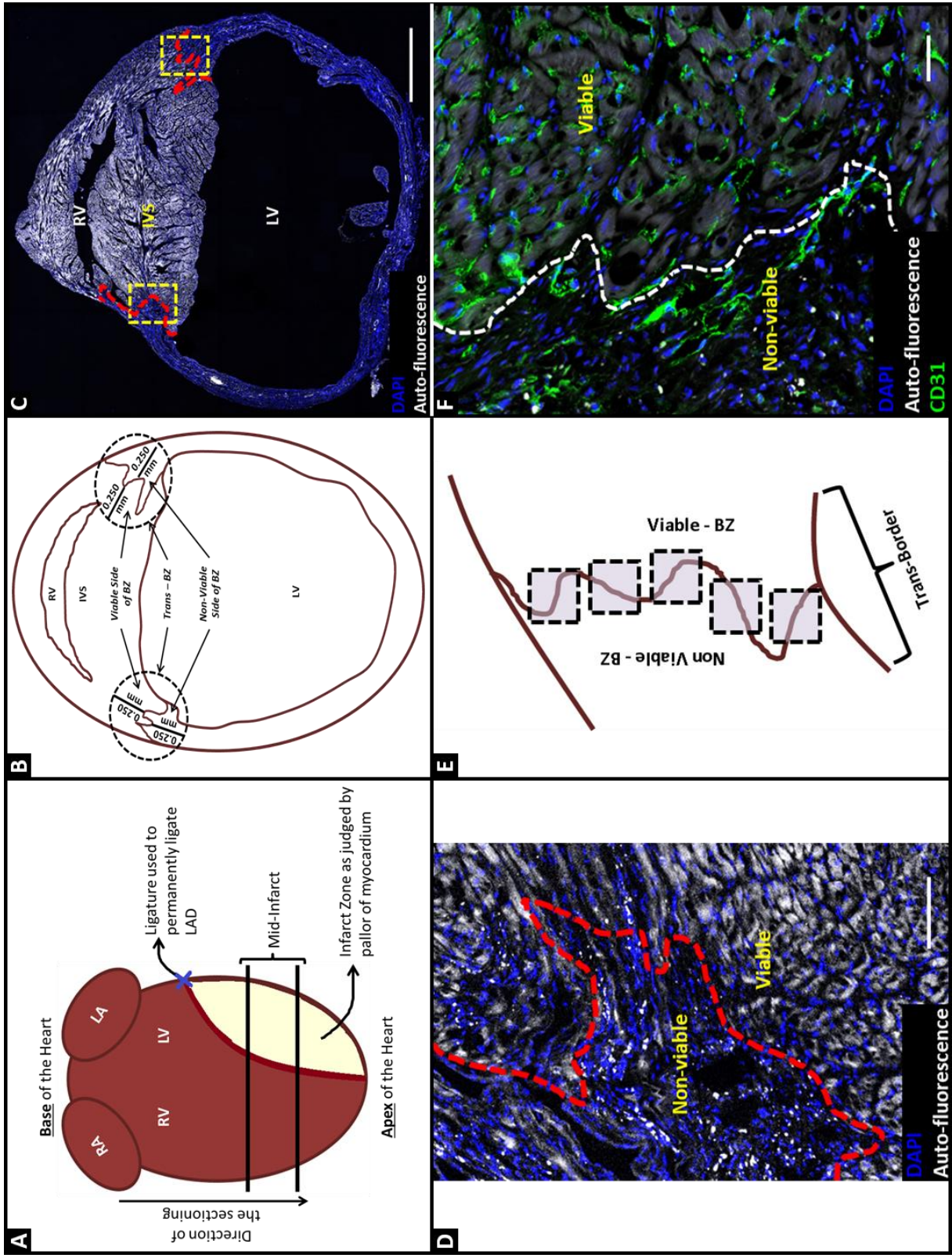
## 6.2. Results

### 6.2.1. Experimental setup and optimisation of CD31 quantification

In order to expand the pilot study group sizes, approximately 12-weeks old C57Bl/6 male mice were given MI by permanent ligation of the LAD. Following MI, two intra-myocardial injection of either PBS or control or Eng-iKO CDCs [ $(5 \times 10^5 \text{ cells}/10 \mu\text{L})$ , prepared by Dr. Darroch Hall during surgeries] was administered by Dr. Rachael Redgrave. The chest was then closed, and mice were allowed to recover. For sham mice, the same surgery was performed without a coronary ligation and without any intra-myocardial injections. After 4 weeks, mice from all four groups were humanely killed and hearts were fixed in 0.2% PFA. These hearts were then embedded in OCT and transversely cut into sister sections (Figure 6.4, A&B). The sections were then subjected to immunofluorescent staining and in each immunofluorescence experiment, heart sections from all groups were included to reduce variability due to different staining batches.

---

**Figure 6.4: Experimental Design: Immuno-fluorescent Staining.** (A) Cartoon of a typical post-MI heart showing site of LAD coronary artery ligation (blue cross) and infarcted zone (pale area). At 4 weeks following surgery hearts were processed as described in Section 2.2.2 and sectioned in the transverse orientation in the direction indicated (A). Sections collected from the mid-infarct region (indicated by horizontal black lines in cartoon) were used for immunofluorescent staining. (B) Cartoon of transverse section of a 4 weeks Post-MI Heart with dotted circles represent trans-border zone region; composed of 0.25mm of viable and 0.25mm non-viable side of border zone. (C) Tiled image of a representative transverse section of a 4 weeks post-MI heart showing dilated LV and thin LV free wall. (D) Optical zoom of the yellow square in (C) of trans-border zone showing viable and non-viable regions identified by CM auto-fluorescence (white). Red dotted line represents approximate position of the infarct border. (E) Depending upon the width of the trans-border zone, up to 8 images of CD31 staining were taken using an x20 objective across the infarct zone (red line) from 5 different sections from the mid-infarct region of infarcted hearts. CD31 area/vessel density was analysed using ImageJ software. (F) Example of an image showing CD31 positive vessels (green) in the viable and non-viable side of the trans-border zone. Abbreviations: BZ – border zone; IVS – Interventricular septum; LA – Left Atria; LV – left ventricle; RA – Right Atria and RV – Right Ventricle. Scale bars: C = 1000 $\mu$ m; D = 100 $\mu$ m and F = 50 $\mu$ m.



To quantify vessel density and maturation in post-MI hearts, images were taken from the infarct border zone of the mid-infarct region (Figure 6.4A). By definition, the infarct border is the region of the heart where infarcted myocardium meets the viable myocardium (Figure 6.4, C&D) recognised by auto-fluorescent CM. The trans-border region used for this analysis was approximately 0.25mm on either side of the infarct border (Figure 6.4B).

For quantification, 5 sections from the mid-infarct region were selected from MI mice (Figure 6.4A) and imaged at x20 magnification using a M2 axio-imager microscope. To minimise imaging of the same vessels, each of the five sections selected were at least 200µm apart. In the case of the sham mice, 8 images were taken from a similar region of heart (free LV wall). To quantify vessel density (by CD31 staining), the same white and black balance was set for each of the x20 images. These images were then converted into tiff format to quantify vessel density by measuring the percentage of CD31 positive stained area using the threshold function of ImageJ software. This process was repeated for all images taken from the 5 different heart sections per heart. Furthermore, to remove observer bias, data was blinded prior to quantification and data analysed by two independent observers (Esha Singh and Dr. Rachael Redgrave).

## 6.2.2. Pro-angiogenic effect of CDCs is Endoglin Dependent

The transverse sections of 4-weeks post-MI hearts were stained with rat anti-CD31 antibody. Table 6.1, shows the average vessel density calculated using ImageJ function for each heart, from all four groups (Sham (n=3), MI+PBS (n=4), MI+ CDCs-Ctl (n=4), and MI+CDCs-Eng-iKO (n=3)).

**Table 6.1: Summary of ImageJ area analysis of CD31 stained heart sections 4 weeks post-MI and cell delivery.** Images were taken along the trans-border zone region (mid-ventricle) of MI hearts at x20 and in similar region of Sham hearts (in arbitrary units). Each cell of the table represents an individual mouse heart and is an average of at least 26 images. Grey coloured cells represent the pilot data from Dr Redgrave and white cells represent the hearts analysed as part of this thesis.

	SHAM	MI +PBS	MI + CDC-Ctl	MI + CDC-Eng-iKO
CD31 Area (A.U.)	128858.93	74897.07	98407.07	77504.05
	114915.41	66911.68	89356.37	63493.55
	123863.18	64039.52	79256.82	64390.78
	112354.05	53506.87	63995.71	60438.52
	119420.80	62009.60	79509.13	86889.46
		57739.70	94724.89	78939.00
		57680.38	79111.33	62989.58
		59119.14	93797.31	
Average ± SEM	119882.47 ±2983.00	61988.00 ±2360.00	84769.83 ±4029.00	70663.56 ±3881.00

---

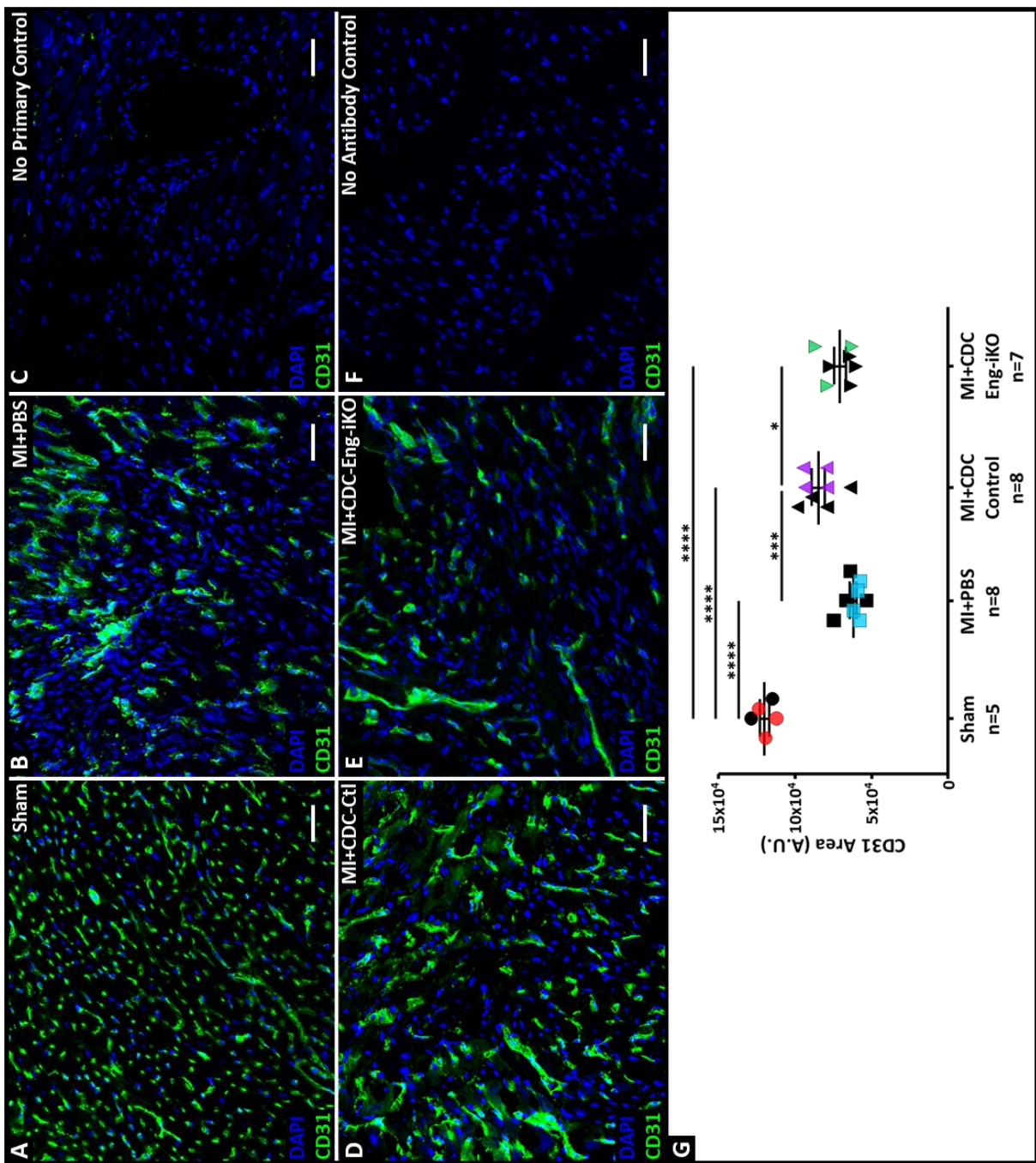
Quantification of the CD31 staining on the new hearts showed similar results to those from the pilot experiment (Figure 6.3). A significant reduction in vessel density was observed at the trans-border zone region of all the MI group hearts (Figure 6.5, B,D&E) compared to sham hearts (Figure 6.5A). However, transplantation of control CDCs post MI led to a significant increase in the vessel density of these heart (Figure 6.5D) compared to PBS injected group (Figure 6.5B). This pro-angiogenic effect of CDCs was lost upon depletion of endoglin as shown by reduced angiogenesis in MI+CDC-Eng-iKO group (Figure 6.5E).

As the results from the current study and pilot study were similar (Table 6.1), both data sets were combined and are shown in the form of scatter plot in Figure 6.5G with pilot data coloured in black and current data in different colours according to group type. Quantification analysis of the merged data showed a decrease in CD31 vessel area in all groups compared to sham. These decreases were 48% in 'MI+PBS', 29% in 'MI+CDC-Ctl' and 41% in 'MI+CDC-Eng-iKO'. Comparing the MI groups with one another, transplantation of control CDCs led to a 37% increase in vessel density compared to MI+PBS group, whilst transplantation of Eng-iKO CDCs only led to a 14% increase in vessel density compared to MI+PBS group. Taken together this data shows that, intra-myocardial injection of CDCs led to a significant increase in the CD31 vessel density in the ischemic border-zone. This effect of CDCs was endoglin dependent.

### **6.2.3. Endoglin Promotes Vessel Maturation in the Infarct Border Zone**

Many studies have shown that endoglin promotes recruitment of vSMCs, which are required for vessel maturation (129, 330-333). As the pro-angiogenic effect of CDCs in 4-weeks post-MI hearts was endoglin dependent, the effect of control and Eng-iKO CDCs on vessel maturation was examined. Sister sections from the mid-infarct region of all the MI hearts (Figure 6.4A) and similar regions from sham hearts were stained with anti-CD31 and anti- $\alpha$ SMA antibodies. Images were taken as described earlier in section 6.2.1.

I first analysed the vascular remodelling in the infarcted zone of MI hearts. As a result of MI, blood vessels are damaged, therefore to cope with the increased energy demand viable vessels dilate and eventually muscularised during the scar maturation phase to form collateral vessels (Figure 1.22). These vessels are formed in response to stress induced by MI (334). Analysis of the low power tiled images from all MI groups showed a thin left ventricle 4 weeks after MI (Figure 6.6, B-D) compared to healthy compact myocardium in sham hearts (Figure 6.6A). Digitally zoomed images of infarcted zone of MI hearts (Figure 6.6, F-H & J-L) revealed presence of large muscularised vessels suggestive of vascular remodelling and arterialisation.



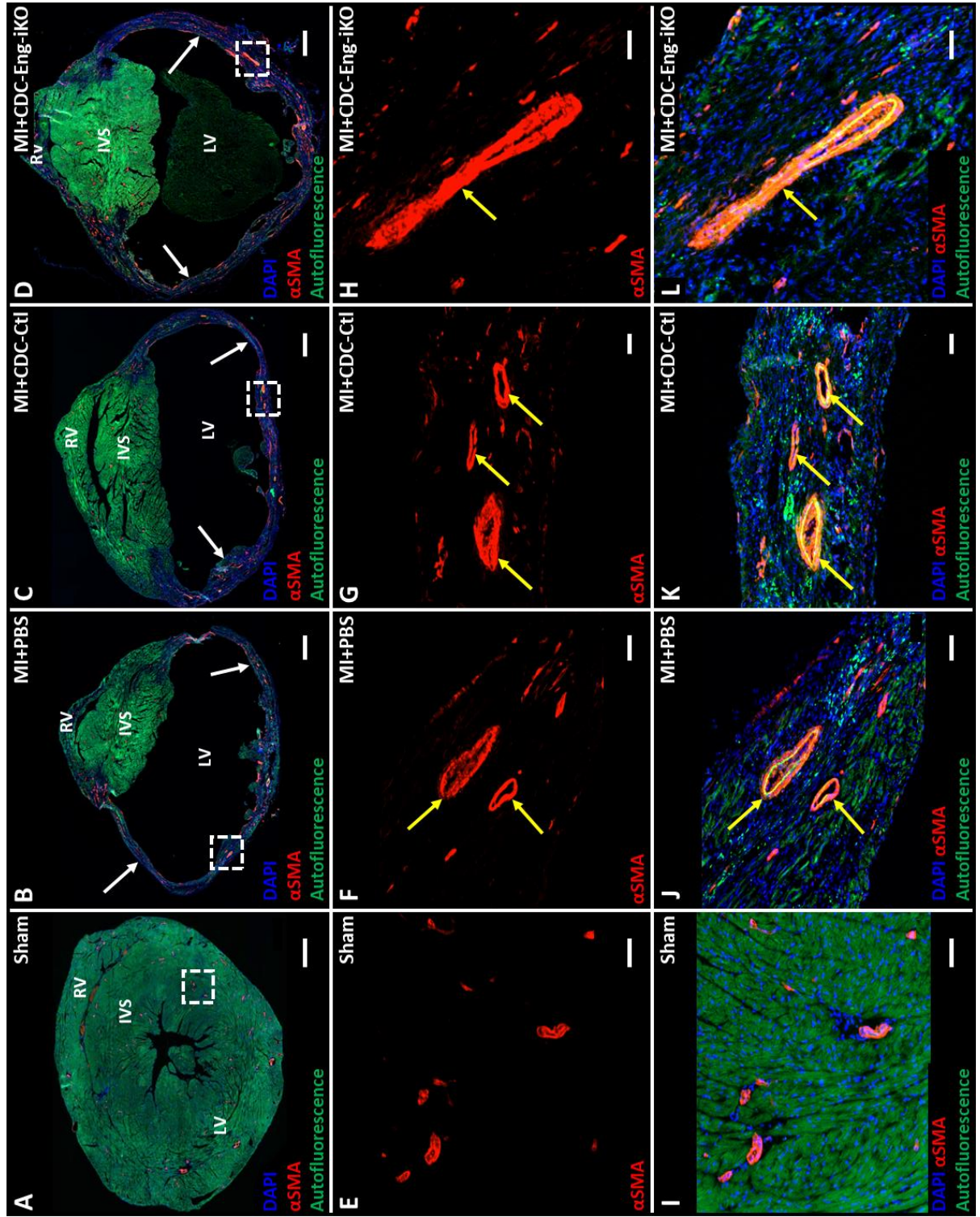


**Figure 6.6: Major vascular and ventricular remodelling was observed in all 4-weeks post-MI hearts.** Sham and MI heart transverse sections stained with anti- $\alpha$ SMA antibody to mark SMCs (red) and counter stained with DAPI to mark nuclei (blue). During imaging, the images were also taken in filter set 10 to capture viable cardiomyocyte autofluorescence (green). (A) Overview image of a sham hearts showing viable myocardium and only a minor number of vessels were muscularised. (E,I) Split channel, digitally zoomed image (white box, A) showing normally occurring muscularised vessels in sham heart. (B-D) While in the infarcted region (white arrows) of post-MI hearts from all three groups (MI+PBS; MI+CDC-Ctl and MI+CDC-Eng-iKO) showed the presence of large muscularised vessels (yellow arrows). No such vessels were observed in the viable region of the myocardium (green region). (F-H, J-L) Split channel digitally zoomed image (white box, B-D) of infarcted region of MI hearts showing with highly muscularised vessels. Abbreviation: RV – Right Ventricle; IVS – Interventricular Septum; LV – Left Ventricle; MI – Myocardial Infarction and CDC – Cardiosphere Derived Cells. Scale Bars: A-D = 500 $\mu$ m and E-L = 50 $\mu$ m.

---

To analyse the role of CDCs on vessel muscularisation at the border zone, x20 magnification images were taken across the trans-border zone region (Figure 6.4, C-F) of the MI hearts and similar region in sham hearts. Visual inspection showed a high number of large vessels in the transborder zone region of all MI group hearts that were covered with a thick layer of  $\alpha$ SMA positive vSMCs (Figure 6.7B-D, white boxes). In contrast, there were very few large muscularised vessels in the sham hearts (Figure 6.7A, white arrows). This was confirmed by manual counting on x20 images using event function of Zen 2012. During manual counting, each vessel identity was also confirmed by the presence of CD31 staining of the vascular endothelium.

Using the manual counting method, the average numbers of vessels per FOV from 5 different heart sections were compared across the four different groups. As before, analysis was blinded to treatment to remove observer bias. This analysis showed a high number of muscularised vessels in the transborder zone region of MI mice (Figure 6.8 B-D & F-H, white arrows) compared to sham hearts (Figure 6.8 A&E, white arrows). In MI hearts, the transborder region is populated with large muscularised vessels (Figure 6.7B-D) while in sham hearts, muscularised vessels distribute evenly across the heart (Figure 6.7A) and were not enriched in the equivalent region.

Visual inspection of the MI hearts, suggested that most muscularised vessels occurred at the border zone of the 'MI+CDC-Ctl' group (Figure 6.8 C&G) compared to 'MI+PBS' (Figure 6.8 B&F) and 'MI+CDC-Eng-iKO' hearts (Figure 6.8 D&H), which were similar to each other.

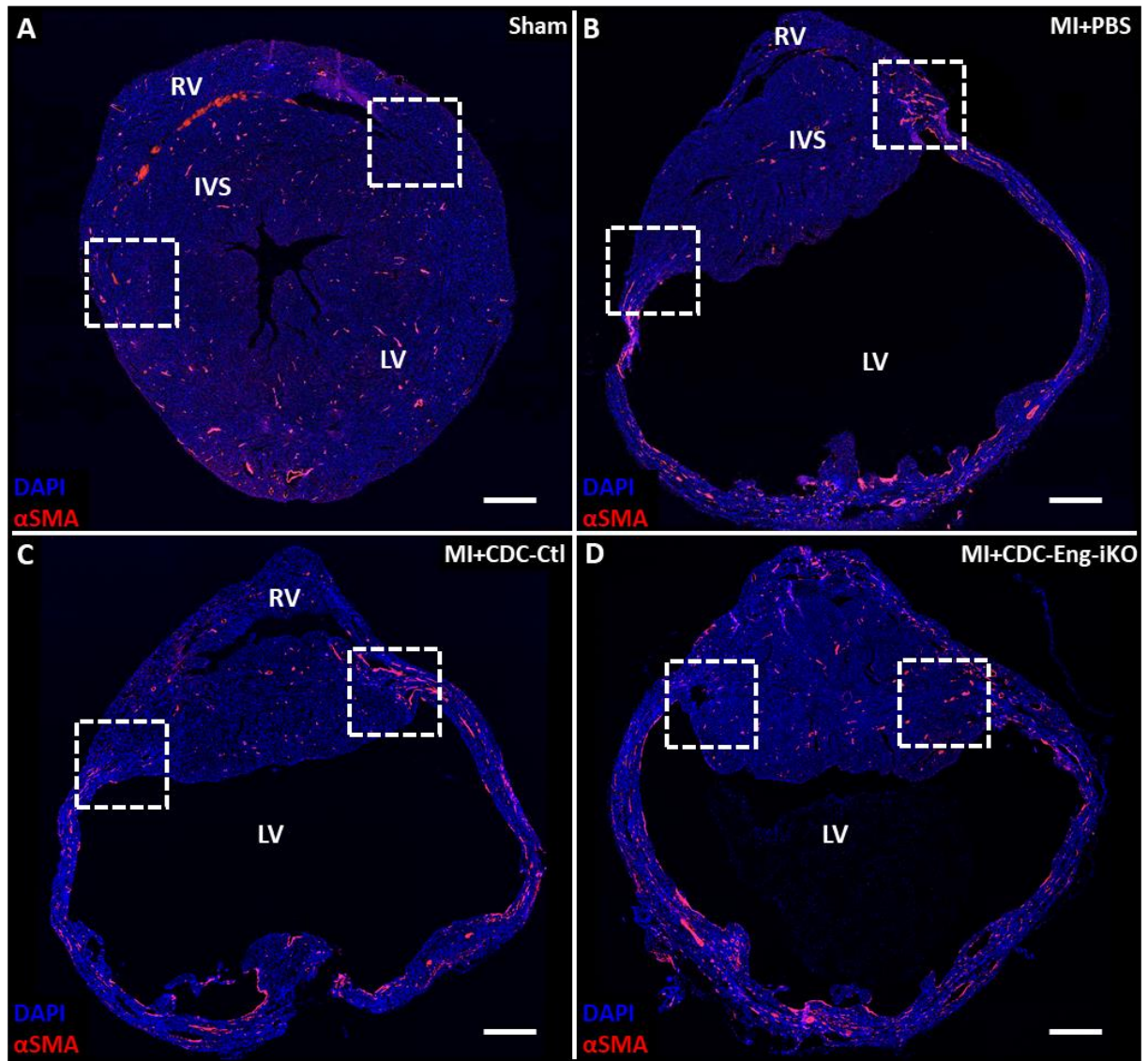
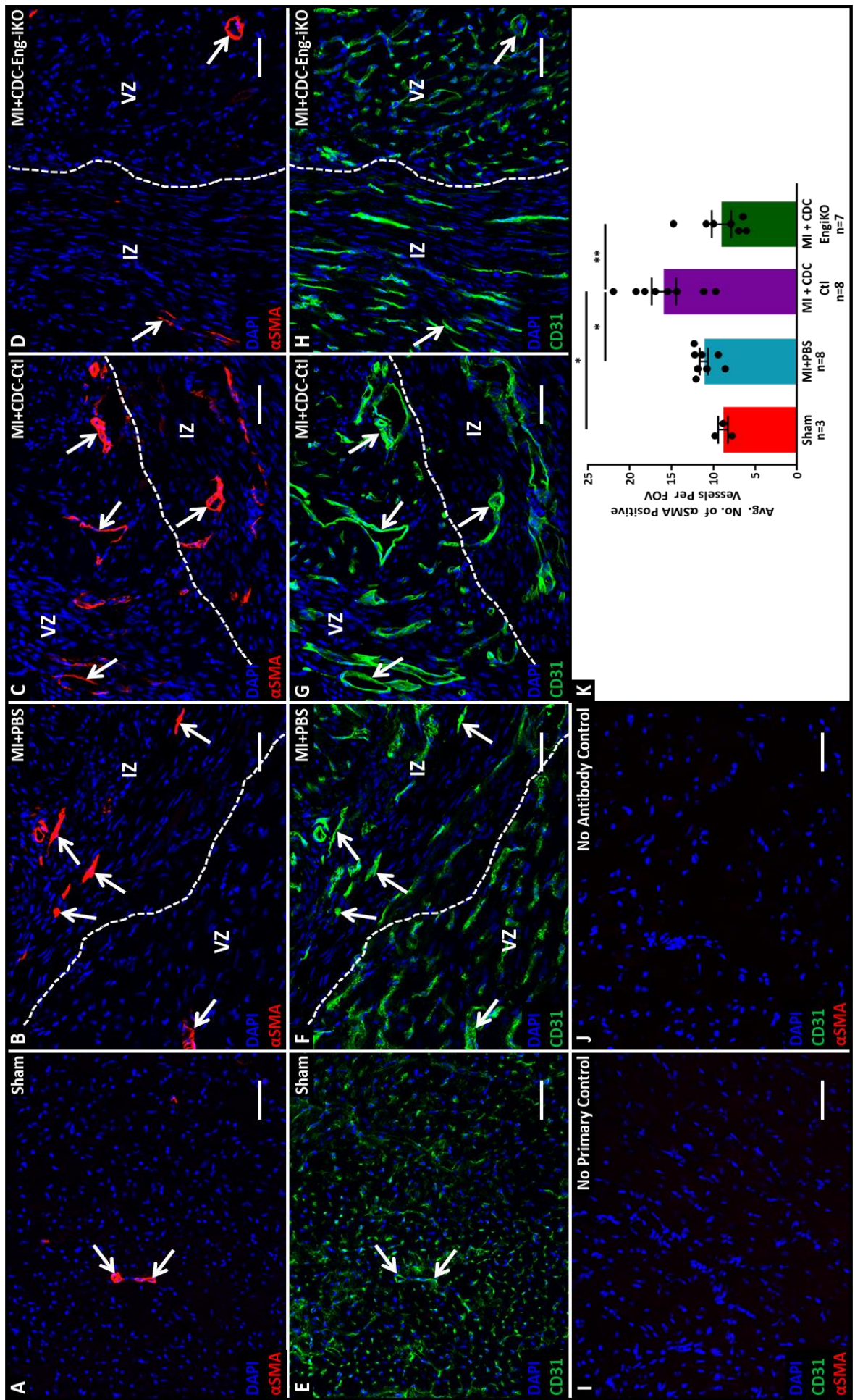


**Figure 6.7: Whole-view tiled image of 4-week sham and MI hearts showing the analysis area.** Adult sham and MI heart sections stained anti- $\alpha$ SMA antibody to mark SMCs (red) and counterstained with DAPI (blue). **(A)** Whole-view image of sham hearts, showing even distribution of muscularised vessels throughout the heart section and region of heart used for quantification (white boxes). **(B-D)** In MI hearts, transborder region (white boxes) used for quantification, showed the presence of multiple muscularised vessels. *Abbreviations: IVS – Inter Ventricular Septum; LV – Left Ventricle; MI – Myocardial Infarction and RV- Right Ventricle.* Scale bars: A-D = 500 $\mu$ m.

**Figure 6.8: Endoglin loss in donor CDCs led to a reduction of muscularised vessels in the trans-border region of 4 weeks post-MI hearts.** Vascular smooth muscle cells are stained with mouse anti- $\alpha$ SMA antibody (red, white arrows), endothelial cells marked using rat anti-CD31 (green) and nuclei are stained with DAPI (blue). Representative split channel images showing (A,E) sham-operated, un-injured heart with low baseline number of muscularised vessels (n=3, image taken at comparable region of trans-border zone); (B,F) PBS-injected infarcted heart showing an increased number of muscularised vessels (white arrows) in the trans-border region (viable and infarcted zone; n=8); (C,G) Post-MI heart injected with control CDCs resulting in a marked increase in number of muscularised vessels (white arrows, n=8) and (D,H) attenuation of control CDC effect on muscularised vessel number in the absence of endoglin (n=7). (I) No primary and (J) no antibody staining controls. (K) Muscularised vessels ( $\alpha$ SMA positive) were counted in multiple fields of view/heart sections per group. The number of  $\alpha$ SMA positive vessels was observed to be similar in sham-operated, un-injured control hearts ( $8.833 \pm 0.585$ , n=3), PBS only ( $11.11 \pm 0.492$ , n=8) and Eng-iKO CDCs recipient ( $9.033 \pm 1.180$ , n=7) hearts. Whereas, MI hearts injected with control CDCs ( $15.92 \pm 1.451$ , n=8) showed a significant increase in the number of  $\alpha$ SMA-positive vessels compared to sham ( $p = 0.0109$ ), MI+PBS ( $p = 0.0217$ ) and MI+CDC-Eng-iKO group ( $p = 0.0011$ ). Data shown as mean  $\pm$  SEM and analysed using one-way ANOVA (\*  $p < 0.05$ , \*\*  $p < 0.01$ ). Abbreviations: CDC – Cardiosphere Derived Cells; IZ – Infarcted Zone; MI – Myocardial Infarction; and VZ – Viable Zone. Scale bars: A-J – 50 $\mu$ m.



Statistical analysis confirmed a significant increase in the average number of muscularised vessels in the trans-border zone region of ‘MI+CDC-Ctl’ groups compared to ‘MI+PBS’ ( $p = 0.0217$ ) and ‘Sham’ ( $p = 0.0109$ , Figure 6.8) groups. This positive effect of control CDCs on vessel stabilisation was lost in ‘MI+CDC-Eng-iKO’ group ( $p = 0.0011$ ). A summary of this quantification is showed in Table 6.2.

**Table 6.2: Summary of the average number of muscularised/ $\alpha$ SMA positive vessels in the trans-border zone 4wks post-MI with and without CDCs, with and without endoglin KO.** Images were taken along the trans-border zone region (mid-ventricle) of MI hearts at x20 and in similar region of Sham hearts. Only the vessels stained positive for both CD31 and  $\alpha$ SMA were counted. Each cell of the table represents an individual mouse heart and is an average of at least 25 images. Grey coloured cells represent the hearts from pilot study and white colour cell represent the hearts analysed during the current study.

	SHAM	MI Only	MI + CDC-Ctl	MI + CDC-Eng-iKO
<b>Average Number of <math>\alpha</math>SMA positive vessels per FOV</b>	7.80	8.63	15.52	14.83
	9.83	11.39	11.17	7.92
	8.88	9.44	22.00	6.50
		12.25	17.00	6.08
		12.10	19.29	10.89
		12.33	9.75	10.00
		10.82	18.24	7.00
		11.92	14.41	
<b>Average <math>\pm</math> SEM</b>	8.83 $\pm$ 0.58	11.11 $\pm$ 0.49	15.92 $\pm$ 1.45	9.03 $\pm$ 1.18

However, as observed earlier in the study, CDCs promote neovascularisation in transborder zone in post-MI hearts (Figure 6.5); so, it is possible that this direct comparison of vessels number potentially be showing a false positive effect of control CDCs on muscularisation. Therefore, to confirm this phenotype I calculated density of muscularised vessels per FOV (average number of muscularised vessels/ average CD31 stained area x 100). A summary of this data is shown in the Table 6.3.

**Table 6.3: Summary of density of muscularised vessels per FOV in the trans-border zone 4-weeks post-MI hearts with and without CDCs, with and without endoglin KO.** The number of muscularised vessels was normalised using the mean CD31 stained area for each heart. Grey coloured cells represent the hearts from pilot study and white colour cell represent the hearts analysed during the current study.

	Sham	MI + PBS	MI + CDC-Ctl	MI + CDC <sup>Eng-iKO</sup>
<b>Density of muscularised vessels per FOV (no. of muscularised vessels/ CD31 stained area)</b>	0.0063	0.0161	0.0174	0.0191
	0.0087	0.0170	0.0175	0.0131
	0.0074	0.0126	0.0224	0.0102
		0.0191	0.0214	0.0094
		0.0195	0.0243	0.0125
		0.0214	0.0103	0.0127
		0.0188	0.0231	0.0111
		0.0202	0.0154	
<b>Average <math>\pm</math> SEM</b>	<b>0.0075 <math>\pm</math>0.0007</b>	<b>0.0181 <math>\pm</math>0.0010</b>	<b>0.0189 <math>\pm</math>0.0017</b>	<b>0.0126 <math>\pm</math>0.0012</b>

Consistent with the previous analysis, the statistical analysis of normalised data showed a significantly high density of muscularised vessels in MI+CDC-Ctl group compared to sham and MI+CDC-EngiKO hearts (Figure 6.9). However, in contrast to previous analysis (Figure 6.8K) no difference in the density of muscularised vessels was observed in between PBS injected and control CDCs injected hearts. Interestingly, in Eng-iKO CDCs group a significant drop in the muscularised vessels density was observed compared to ‘MI+PBS’ group (Figure 6.9). This data suggests that endoglin in CDCs might not be able to promote muscularisation in post MI hearts. However, lack of endoglin in CDCs does inhibit the process of vessel muscularisation. This could be a direct or indirect effect; however further studies are required to unveil the mechanism behind it.

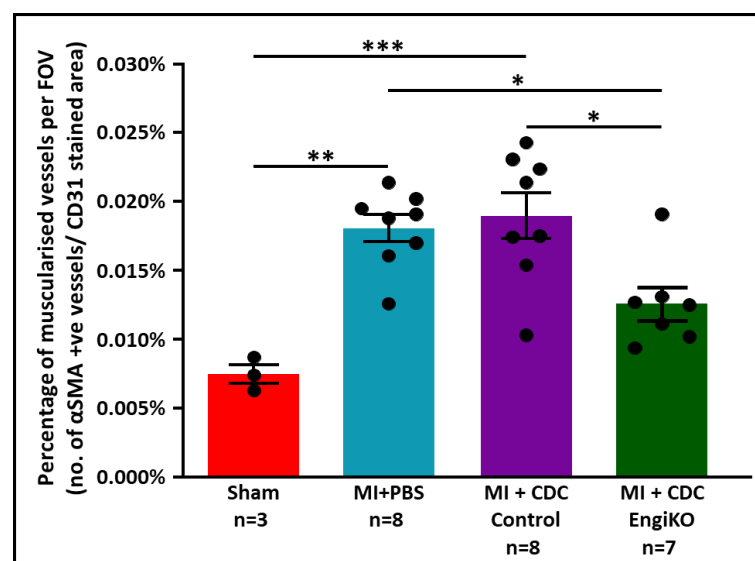


**Figure 6.9: Quantification showed a significant reduction in percentage of muscularised vessels in MI hearts after transplantation of Eng-iKO CDCs.** The percentage of muscularised vessels was calculated by normalising the number of muscularised vessels (Table 6.2) using mean CD31 stained area for each heart (Table 6.1). In contrast to the previous results, following infarction a significant increase in the density of muscularised vessels was observed in the trans-border-zone region of the PBS injected ( $0.0181 \pm 0.0010$ ;  $n=8$ ;  $p = 0.0012$ ) and control CDCs injected ( $0.0190 \pm 0.0017$ ,  $n=8$ ;  $p = 0.0005$ ) hearts. Furthermore, no difference was observed between PBS injected and control CDCs injected ( $p > 0.9999$ ) hearts. Consistent with previous results, injection of Eng-iKO CDCs ( $0.0126 \pm 0.0012$ ,  $n=7$ ) led to a significant reduction in the density of muscularised vessels compared to both PBS injected ( $p = 0.0382$ ) and control CDCs injected ( $p = 0.0121$ ) MI hearts. Percentage of muscularised vessels in Eng-iKO CDCs injected MI hearts was observed to be similar to sham hearts ( $p = 0.2823$ ). Data shown as mean  $\pm$  SEM and analysed using one-way ANOVA (\*  $p < 0.05$ , \*\*  $p < 0.01$ , \*\*\*  $p < 0.001$ ).

### 6.3. Discussion

CDCs are currently being tested in CADUCEUS (CARDiosphere-Derived aUtologous stem CELls to reverse ventricular dySfunction) clinical setting for their ability to protect against ventricular dysfunction after MI (226). In this trial, myocardial infarction patients (over 18yrs of age) undergone successful PPCI with left ventricular ejection fraction of 25–45% were enrolled (2 to 4wks after MI). The patients with less than 3yrs life expectancy were excluded. During this trial, CDCs are delivered to the heart by intracoronary injection (3 to 5wks) and this

---

led to reduction in scar mass and increased viable myocardium mass. But unlike animal models, no significant change in the LV function was observed 6 and 12 months after the injection (226). A possible explanation for lack of translation of the beneficial of CDCs from pre-clinical studies is delay in transplantation of these cells. Therefore, another clinical trial (ALLSTAR) is underway using allogenic CDCs by the same group (227). Patients with similar criteria as CADUCEUS trial are enrolled with a history of MI in last 4 to 12 months. During this study, allogenic CDCs are injected via an intra-coronary route post-MI.

In case of most acute MI patients, PPCI is the most common treatment along with therapeutics (208). This treatment is effective but does not reverse the muscle damage and for better prognosis, PPCI need to be achieved at the earliest time possible. This is not always feasible leading complications such as heart failure. The best way to improve cardiac healing would be by reducing CM death post-MI (or initiating CM regeneration). One of the treatment strategies believed to be beneficial is transplantation of stem cells during or after PPCI and have proved to be beneficial in the clinical setting (220). The aim of this chapter was to further characterise these cells, specifically to understand the importance of endoglin in CDCs.

All human CDCs express endoglin (327) while in this study 70% of murine CDCs express endoglin (Figure 6.2A) consistent with previous publications (326). As mentioned in the introduction (section 1.5.1), endothelial endoglin is essential during angiogenesis. The upregulation of endoglin expression was not only observed in angiogenic phases but also during inflammation and remains high throughout the phase (335). They also showed a significant increase in endoglin expression in diseased human skin, liver and lung tissue samples (335). This increase in endoglin was directly correlated with inflammatory cell infiltration. For instance, in skin samples, strong endoglin expression was observed in the ECs in the regions with increased infiltration of macrophages and T cells (335).

In this chapter I show that endoglin is also essential in CDCs, a heterogeneous mesenchymal cell population, to promote a significant increase in vessel density in the infarct border zone following MI (Figure 6.5). This result confirms that the pro-angiogenic effect of CDCs was endoglin dependent. Endoglin is known to promote BMP9/ALK1 mediated signalling to trigger ECs proliferation (130). In addition to this, it could also be promoting VEGF signalling in the infarct zone as discussed in the Chapter 5, section 5.3.4. Therefore, it would improve ECs proliferation in the infarcted zone. To test increased ECs proliferation, the sections from above hearts could be stained for proliferative marker pHH3 or mice could be injected with BrDU then hearts could be stained with BrDU and ECs cell marker PECAM1. It might also be

---

beneficial to understand which angiogenic factors (such as VEGF, angiotensin 1, FGF) are promoted by performing qPCR on cDNA or western blots/ angiogenic factor ELISA on protein lysates harvested from infarcted myocardium.

Similar to other studies (225, 327, 336), genetic tracing using GFP-expressing CDCs in my host laboratory showed that very few differentiated myocardial cells including endothelial cells or vSMCs originating from CDCs were observed in 4-weeks post-MI hearts (150), leading to the postulation that the pro-angiogenic effect of CDCs was driven via a paracrine route. To further confirm that CDCs act via paracrine route, CDCs conditional media was collected from control and Eng-iKO CDCs and added to matrigel seeded with mouse endothelial lung cells. This matrigel mixture was then subdermally injected into the mouse flanks and analysis of matrigel plugs after two weeks showed higher vessel density in matrigel supplemented with control CDC conditioned media compared to media from Eng-iKO CDCs (150). This experiment showed that CDCs drive angiogenic responses via a paracrine route consistent with previous studies (225) and confirmed that the pro-angiogenic effect of CDCs is endoglin dependent.

The formation of new vessels is not sufficient for proper healing, because if these new vessels are not stabilised, they tend to regress after the proliferation phase (209). Vessels are stabilised through the recruitment of pericytes or vSMCs (depending on vessel type). During the vessel maturation phase, growth factors secreted by endothelium and SMCs play a critical role (30). Any disturbance in signalling of these molecules leads to leaky or ruptured vessels. For example, lack of smooth muscle derived PDGF leads to a defective smooth muscle layer (337). Similarly, lack of endoglin during embryogenesis is fatal due to problems with SMC recruitment (128). A similar requirement for endoglin during SMC recruitment is also reported in other studies (129, 330-333). I, therefore, studied the role of endoglin in CDC mediated vessel maturation. Based on the studies above, I hypothesised that loss of CDC-specific endoglin would lead to a reduction or delay in vessel maturation in post-MI hearts. Immunofluorescent image analysis revealed an increased density of muscularised vessels in control CDCs injected hearts (Figure 6.8, C&G) however this phenotype is potentially not due to CDCs as similar density of muscularised vessels were observed in PBS injected MI hearts (Figure 6.9). Interestingly, injection of endoglin knockdown CDCs showed a significantly reduced density of muscularised cells (Figure 6.9).

The reduced number of muscularised vessels in 'MI+CDC-Eng-iKO' group was surprising. This could be direct or an indirect effect from Eng-iKO CDCs could cause either due to lack

---

angiogenic factors (Vegf, angiopoietin 1, FGF) or secretion of anti-angiogenic factors such as thrombospondin-2 (338). The presence of anti-angiogenic or absence of pro-angiogenic factors could be affecting signalling between the endothelium and mural cells required for recruitment of SMCs. To test this hypothesis *in vitro*, first conditional media collected from control and Eng-iKO CDCs would need to be analysed for the expression of these factors. Next, to study the signalling between endothelial and mural cells, contact co-culture would be carried using ECs and mural cells in presence of CDCs conditional media. Furthermore, to assess this hypothesis *in vivo*, MI hearts injected with control or Eng-iKO CDCs would need to be collected at different time points from early to later time points (e.g. day 1, 3, 5 & 7 then week 2, 3 & 4). Once harvested, expression of angiogenic (for example, VEGF, FGF and CD105) and anti-angiogenic (for example, soluble endoglin and thrombospondin-2) factors would need to be measured either using qPCR or western blots. Another explanation for reduced number of muscularised vessels in Eng-iKO CDCs groups could be a delay in the maturation process. To test this, hearts from all four groups would need to be harvested at a later time point, for instance around 6, 8 or 12 weeks post-MI, and subjected to the same analysis as above. During this study, it might also be beneficial to analyse vessel perfusion by and time required for perfusion. As this could affect the muscularisation of vessels as well.

Although the immunofluorescent data showed a positive effect of control CDCs on angiogenesis and potentially on vessel maturation; unfortunately, cardiac MRI analysis revealed there was no difference in cardiac function between all three MI groups analysed (150). Similarly, histological analysis using masson trichrome staining did not show any difference in scar size at 4-weeks post MI between the three MI groups (Arthur Lab, unpublished data). Lack of functional improvement following CDC treatment runs counter to previous publications (225, 327, 336) and could be partly due to the experimental design. Firstly, animals with large infarcts (judged by the paler of the myocardium after ligation of LAD) were selected for this study to reduce the variability in the group (339). Large permanent infarcts affect almost all the free left ventricular wall, making it extremely challenging to gain functional improvement. Second, CDCs/ PBS injections were given via intra-myocardial route which could also trigger an inflammatory response that could lead to a longer inflammatory phase resulting in poor heart function. Repeating the experiment on mice with small and moderate sized infarcts and including an MI only control group (without any intra-myocardial injections) would help to address these possible factors. Alternatively, as our data agree with the clinical studies using CDCs which reveal no functional benefit, our data may reflect the limited capacity of CDCs to promote heart repair. Another factor to be consider is the time

---

between cardiomyocyte death and angiogenesis induction. Hypoxia caused due to MI leads to CM death potentially within 2hrs however, this not enough time for formation of new stable vessels. Therefore, angiogenesis alone probably would not be able to rescue the heart function post MI. However, increased angiogenesis would definitely help to reduce the apoptosis of surrounding CMs and may be improve function in smaller infarcts.

Another possibility for lack of functional improvement using CDCs could be lack of coronary reperfusion, as the permanent ligation model was used for this study. As mentioned above, reperfusion is essential for better prognosis (203, 340). To test this hypothesis, the experiment would need to be repeated using an ischemia-reperfusion (IR) mouse model. This model mimics the clinical setting and would aid in generating useful data for better translation of CDC therapy into the clinical setting. In another study, CDCs were injected intra-myocardially in a rat IR model (341). Results from this study showed significantly higher ejection fraction in CDC treated group compared to control mice at 6 weeks after CDC transplantation. In contrast, in the current study mice were tested only 4 weeks after injection. Considering this, as mentioned previously, for future studies it would be beneficial to study the heart function at later time-points, potentially at 8- or 12-weeks post-MI. Another difference between current and Carr *et al.* (341) study was that, CDCs were injected in two waves via two different routes: (i) immediately after reperfusion via intra-myocardial route which potentially increased angiogenesis and (ii) 2 days after reperfusion via a systemic route. This would significantly boost the quantity of paracrine factors released by CDCs during cardiac healing.

Despite the lack of functional improvement, it is evident from this study that CDCs help in revascularisation of the infarcted region and may be have an indirect effect on stabilisation of neo-vessels. This positive effect of CDCs on angiogenesis was endoglin dependent. Endoglin as mentioned in the introduction (Sections 1.4.2 and 1.5.1), is a TGF $\beta$  type 3 co-receptor. In ECs endoglin promotes signalling via ALK1 receptor and supresses ALK5 mediated signalling (144). In my host laboratory, in vitro experiments using control and Eng-iKO CDCs showed that this positive effect of CDCs secreted endoglin on vasculature repair in post-MI hearts was due to BMP9 signalling via SMAD1/5/8 (Figure 1.19). Another striking effect of this pathway is the positive feedback loop between endoglin and BMP9. Endoglin promotes the binding of BMP9 to ALK1 which helps to maintain a high level of endoglin expression (150). This is crucial result as expression of high levels of endoglin would help to obtain most pro-angiogenic benefits from CDCs during clinical trials.

---

# **Chapter 7. Final Discussion and Future Work**

---

The aim of the work described in this thesis was to understand the importance of endoglin in coronary vasculature development, in adult ECs homeostasis and in stem cell mediated cardiac repair.

In chapter 3, I mapped the expression of endoglin in developing, post-natal and adult heart in different cell types. The expression of endoglin was observed in endothelium and endocardium throughout development and in adult hearts. The quantification of this expression showed strongest endoglin expression in coronary vein ECs and capillaries while a weaker expression was observed in coronary arteries. I speculated that as venous ECs start to express arterial markers, endoglin expression will be reduced. I also observed expression of endoglin in the mesenchymal cells of developing AV cushions and in developing myocardium. These myocardial mesenchymal cells were presumed as EPDCs as they migrate through the myocardium from E12 onwards (54) and express endoglin *in vitro* (64). Interestingly, quantification of this data showed that expression of endoglin in these mesenchymal cells was significantly lower than the adjacent endocardium/endothelium. In valvular mesenchymal cells, endoglin is required for endocardial cell EMT, mesenchymal cell migration and proliferation (127, 128, 161, 239, 242). However, the importance of endoglin in EPDCs *in vivo* is unknown and was analysed in chapter 4. Based on endoglin's role in valvular mesenchymal cells, I hypothesised a similar role of endoglin in EPDCs.

*In vivo* analysis showed expression of endoglin in minor subset of EPDCs and depletion of endoglin in these EPDCs using *Wt1<sup>Cre-ERT2</sup>* did lead to reduced number of EPDCs in E15.5 hearts. However, this loss of EPDCs did not lead to any cardiac, endothelium or SMCs related defects in E17.5 hearts. This data suggested that endoglin might play a role potentially during some EPDCs proliferation however, it is not required for EPDC differentiation. It might also be possible that another factor might have compensated in the absence of endoglin such as  $\beta$ -glycan. EPDCs also known to differentiate into cardiac fibroblasts (54, 70-75) and expression of endoglin is reported in myofibroblasts after an injury (215, 216). Therefore, it is possible endoglin knockdown in EPDCs could affect the cardiac fibroblasts population however further studies are required to analyse this.

In chapter 5, I analysed the role of endoglin during development of coronary ECs in embryonic and early post-natal development as well as the importance of endoglin in adult vascular maintenance. I hypothesized that lack of endothelial endoglin would have a detrimental effect on coronary vessels development and would imbalance the vascular homeostasis in adult mice. However, the mouse line (*Dll4in3<sup>Cre-ERT2</sup>*) used to study the embryonic coronary development

---

was not efficient and knockdown of endoglin in ECs using of *VE-Cad*<sup>Cre-ERT2</sup> mouse line in post-natal mice did not lead to any coronary vasculature related defects. These results could either mean that endoglin is not necessary this late in coronary vessel development or else development of coronary vessels is not dependent on endoglin expression. The latter option is unlikely as various *in vivo* (131, 213, 214, 335) and *in vitro* (144, 342) studies showed the importance of endoglin in ECs. To elucidate this, further studies would be required to be performed during embryonic development preferably using a mouse line specific to coronary vasculature. Interestingly, *Eng*<sup>fl/fl</sup>; *VE-Cad*<sup>Cre-ERT2</sup> mouse line used during this study is also used to as an inducible mouse model to study HHT1. However, the cardiac phenotype (enlarged hearts coupled with CM hypertrophy) observed during the current project was not reported in any previous studies (188, 294). In the current study, these mice were speculated to be suffering from eccentric cardiomyopathy due to increase cardiac workload caused by reduced systemic resistance initiated by formation of AVMs. However, cardiac functional studies are required to confirm eccentric cardiomyopathy phenotype.

As mentioned above, endoglin knockdown in early post-natal life (P2&P4) led to formation of systemic vasculature abnormalities (AVMs) that did affect the cardiac development/maturation. Occurrence of AVMs due to endoglin deficiency are associated with HHT1. Patients suffering from HHT1 have a haplo-deficiency of endoglin and suffer from various vascular malformation including AVMs. In some HHT patients, larger AVMs in liver also lead to HOHF (170-172). Interestingly, in the current study depletion of endoglin in ECs using *VE-Cad*<sup>Cre-ERT2</sup> mouse line slightly later in post-natal development (P5&P6) or in adult quiescent ECs (10 to 12wks) also led to similar cardiac phenotype (enlarged hearts coupled with CM hypertrophy) coupled with AV shunts. In adult mice, this cardiac phenotype was confirmed to be HOHF by performing cardiac functional analysis using MRI. The data generated from the current study shows that continuous endoglin expression is vital during development and to maintain adult vasculature.

This study also provides a non-invasive HOHF mouse model. HOHF is a rare complication in HHT patients (170-172). It is generally caused due to reduced vascular resistance linked with either anaemia, vasodilation or formation of AVMs and if left untreated could lead to cardiac arrest (295-297). However, this defect is not well characterised and currently multiple studies are underway to understand the mechanism behind HOHF (297). Furthermore, to study HOHF mouse models are generated by surgical intervention (343). However, the mouse model used during this study leads to development of HOHF in short time and with 100% efficiency.

---

In chapter 5, I also observed HHT1 phenotype (AVMs and enlarged hearts) in a novel mouse line (*Apj*<sup>Cre-ERT2</sup>). This mouse line allows to knockdown endoglin only in venous and capillaries ECs. Interestingly, the presence of endoglin in arterial cells did not prevent the incidence of this phenotype. This result along with higher endoglin expression observed in veins and capillaries during the expression analysis in chapter 3 and 5, strongly indicate that endoglin expression in veins and capillaries is vital for normal vascular development. Further assessment of this mouse model would provide invaluable insights into the role of venous and capillary endoglin on AVM formation. It would also be useful to assess if similar phenotype occurs after arterial ECs specific endoglin knockdown.

The results generated so far strongly indicate that this cardiac phenotype observed after ECs specific endoglin knockdown was due to AV shunts or dilated vessels. Therefore, I hypothesised that therapeutic interventions to treat these AVMs would ameliorate the cardiac phenotype. Endoglin has high affinity for BMP9 and BMP10 (130, 134) and is known to signal via Alk1 receptor in ECs (144, 344). Lack of BMP9 and BMP10 ligands also led to development of retinal and cerebral AVMs (192, 293). Therefore, I postulate that treatment with exogenous BMP9 would either rescue or prevent the AV shunts which in turn would rescue the cardiac phenotype. Unfortunately, this pilot study was not successful due to technical difficulties. Nevertheless, it is a viable hypothesis based on the evidence so far generated through various studies. Long *et al.* (313) showed that IP injection of BMP9 was able to treat PAH phenotype observed in *Bmpr2*<sup>+/*R899X*</sup> mice. Therefore, it might have a similar effect on the HHT1 mice. To analyse this, further studies potentially involving IP injection of BMP9 would help to accept or dismiss this hypothesis.

In chapter 6, I analysed the role of endoglin in cardiac stem cells (CDCs) mediated heart repair post MI with primary focus on angiogenesis. Multiple studies have shown that transplantation of CDCs in post-MI hearts led to functional improvements as well as increased angiogenesis in animal models (225, 327, 336, 341). However, full benefits of CDCs are not observed in the clinical settings (226, 227). Therefore, I characterised these cells further during this project. CDCs are shown to express high level of endoglin (326) and coupled with previous studies, I hypothesised that the proangiogenic effect of CDCs is endoglin dependent. Consistent with previous studies, *in vivo* analysis in 4-weeks post-MI hearts showed an increase angiogenesis in the transborder zone region after CDC injection. This pro-angiogenic effect was lost in the absence of endoglin thus confirming the initial hypothesis. Furthermore, I also analysed the effect of CDCs on vessels muscularisation. Surprising, my results showed that CDCs do not promote this process however, Eng-iKO CDCs had a detrimental effect on vessel

---

muscularisation. This interesting finding would need further investigation to identify the proteins involved during this process. This study did not show any functional improvement in 4-weeks post-MI hearts potentially due to the size of the infarct. This result does suggest that functional improvement with CDCs are potentially linked with the size and severity of the infarct. This hypothesis would need to be tested in animal studies with small to moderate sized infarcts.

In conclusion, this thesis showed that endoglin is expressed in the endothelium from development onwards and that this expression of endoglin is vital for normal vascular development as well as to maintain normal adult vasculature. Endoglin is also responsible for pro-angiogenic effect seen during stem cells mediated cardiac repair. In addition to this, the current study as also provides a novel mouse model for HHT1 research and well as a non-invasive model for HOHF research.

---

# APPENDIX

**Appendix 1: List of Solutions**

<b>Solution</b>	<b>Preparation</b>	<b>Comments</b>
0.5M NaOH	500mg of NaOH in 25ml of Millipore filtered H <sub>2</sub> O	Autoclaved and stored at RT
Solution 1	2.5ml of 0.5M NaOH + 20µl of 0.5M EDTA in 50ml of autoclaved Millipore filtered H <sub>2</sub> O (approximate pH 12)	Stored at RT
0.5M Tris-HCl	3.94gms of Tris-HCL in 50ml of Millipore filtered H <sub>2</sub> O	Autoclaved and stored at RT
Solution 2	4ml of 0.5M Tris-HCl in 46ml of autoclaved Millipore filtered H <sub>2</sub> O (approximate pH 5)	Stored at RT
50x TAE	242.0gms Trizma Base + 57.1ml Acetic Acid + 100.0ml 0.5M EDTA in 1L (~840ml) of Millipore filtered H <sub>2</sub> O	Autoclaved and stored at RT
1x TAE	20ml of 50x TAE in 980ml of Millipore filtered H <sub>2</sub> O	Stored at RT
100bp DNA Ladder	50ul of Loading Dye into 250ul of DNA ladder solution	Stored at RT
Acid-Alcohol	3ml of 37% HCl + 297ml of 70% EtOH	Always use fresh, stored at RT
10xPBS	80.0gms NaCl + 2.0gms KCl + 11.5gms Na <sub>2</sub> HPO <sub>4</sub> + 2.0gms KH <sub>2</sub> PO <sub>4</sub> in 1L of Millipore filtered H <sub>2</sub> O (pH to 7.4 using 5M NaOH or 1M HCl)	Autoclaved and stored at RT
1xPBS	100ml of 10xPBS (pH 7.4) in 900ml of Millipore filtered H <sub>2</sub> O	Stored at RT
2xPBS	200ml of 10xPBS (pH 7.4) in 900ml of Millipore filtered H <sub>2</sub> O	Stored at RT
0.1M KCl	75.0mgs of KCl in 100ml of autoclaved 1xPBS (pH 7.4)	Autoclaved and stored at RT
4% PFA (in 1xPBS)	40.0gms of PFA in 1L of autoclaved 1xPBS	50ml aliquots stored at -20°C
1% PFA	50ml of 4% PFA diluted in 150ml of autoclaved 1xPBS (pH7.4)	50ml aliquots stored at -20°C
0.2% PFA	50ml of 4% PFA diluted in 950ml of autoclaved 1xPBS (pH7.4)	50ml aliquots stored at -20°C
4% PFA (in 2xPBS)	20.0gms of PFA in 500ml of autoclaved 2xPBS	15ml aliquots stored at -20°C
30% Sucrose	300gms of sucrose in 1L of autoclaved 1xPBS (pH7.4)	50ml aliquots stored at -20°C
15% Sucrose	50ml of 30% Sucrose in 50ml of autoclaved 1xPBS (pH7.4)	50ml aliquots stored at -20°C
1M Tris-HCL (pH7.5)	121g Trizma Base in 1L of Millipore filtered H <sub>2</sub> O (pH to 7.5 using 1M HCl)	Autoclaved and stored at RT
1xTBS	100ml 1M Tris-HCL (pH7.5) + 30ml 5M NaCl in 870ml of Millipore filtered H <sub>2</sub> O	Stored at RT
TBS-Tx	1L TBS plus 5ml Triton x-100	Stored at RT
3% H <sub>2</sub> O <sub>2</sub>	90ml of 30% Stock solution (stored at 4°C) in 210ml of 1xPBS	Always use fresh
5M NaCl	290g NaCl in 1L of Millipore filtered H <sub>2</sub> O	Autoclaved and stored at RT
1M HCl	16.6ml of 37% HCl in 183.4ml of autoclaved Millipore filtered H <sub>2</sub> O	Stored at RT
0.01M Citrate Buffer (pH6 to 6.3)	1.92g citric acid in 1L of Millipore filtered H <sub>2</sub> O (pH with 5M NaOH)	Autoclaved and stored at RT
5M NaOH	100.0gms of NaOH in 500ml of Millipore filtered H <sub>2</sub> O	Autoclaved and stored at RT
AB Complex (Standard)	250µl 1M Tris-HCL (pH7.5) + 4.75ml of autoclaved Millipore filtered H <sub>2</sub> O + 1 drop A + 1 drop B (stored at 4°C)	Make 30 minutes before use

Liquid DAB	0.25ml of DAB substrate + 1 drop of H <sub>2</sub> O <sub>2</sub> + 2 drops of Liquid DAB (kit stored at 4°C) in 25ml of autoclaved Millipore filtered H <sub>2</sub> O	Always use fresh
50% EtOH	150ml of absolute ethanol + 150ml of Millipore filtered H <sub>2</sub> O	Stored at RT
70% EtOH	210ml of absolute ethanol + 90ml of Millipore filtered H <sub>2</sub> O	Stored at RT
90% EtOH	270ml of absolute ethanol + 30ml of Millipore filtered H <sub>2</sub> O	Stored at RT
95% EtOH	285ml of absolute ethanol + 15ml of Millipore filtered H <sub>2</sub> O	Stored at RT
PBSTTx	0.3% Triton X-100 + 0.5% Tween-20 in 2xPBS	Always use fresh, stored at RT

**Appendix 2: CDC Cell Culture**

<b>Culture Media</b>	<b>Growth Factor</b>	<b>Final Concentration</b>
Complete Explant Media (CEM)	IMDM media with L-glutamine	500ml
	Heat inactivated FBS	20%
	Penicillin/ Streptomycin	1%
	2-mercaptoethanol	0.1mM
Cardiospheres Growth Medium (CGM)	Cardiotrophin	25ng/ml
	FGF	20ng/ml
	EGF	10ng/ml
	Thrombin	1%
	2-mercaptoethanol	0.1mM
	B27	2%
	CEM	17.5%
	IMDM without serum	17.5%
DMEM/F-12 (with 1% L-glutamine and 1% Pen/Strep)	65%	
FBS Stock	Heat inactivated for 30mins at 56°C	50ml aliquots stored at -20°C

**Appendix 3: List of Chemicals and Consumables**

<b>Item Name</b>	<b>Company</b>	<b>Cat. No.</b>
0.05% Trypsin-EDTA (1x) phenol red	ThermoFisher	25300054
0.5M EDTA	Sigma Aldrich	E7889
100bp DNA Ladder	Promega	G2101
1ml Syringe	VWR	613-4897
30% Hydrogen Peroxide (H <sub>2</sub> O <sub>2</sub> )	VWR	23622.298
4-Hydroxy Tamoxifen	SLS Ltd	H7904
AB Complex (Standard)	Vector Labs	PK-4000
Absolute Ethanol	VWR	85651.32
Accutase	eBioscience	00-4555-56
Acetic Acid	VWR	20102.292
Agarose	nbs biologicals	NBS-AG500
B27	ThermoFisher	17504-044
Basal Serum Albumin (low in endotoxins)	VWR	422381B
Basic Fibroblast Growth Factor (FGF)	Peprotech	100-18B
BMP9	Peprotech	
Bovine Serum Albumin lyophilized powder	Sigma Aldrich	A7638
Citric Acid	Sigma Aldrich	C0759
DMEM/ F-12	ThermoFisher	31330-038
Eosin (aqueous 1%)	RA Lamb	LAMB-100-D
Epidermal Growth Factor (EGF)	Peprotech	AF100-15
Ethidium Bromide (EtBr)	Sigma Aldrich	E7637
Foetal Bovine Serum, qualified, E.U.- approved, South America origin	ThermoFisher	10270106
Fibronectin	Sigma	F1141
Fluoresbrite® YG Microspheres 45.0µm	Polysciences, Inc.	18242-2
FluoSpheres™ Polystyrene Microspheres, 15µm, carmine fluorescent (580/620), for blood flow determination	ThermoFisher	F21013
Foetal Bovine Serum (Heat Inactivated) Origin: EU Approved (South American)	ThermoFisher	10500064
Genotyping Primers	IDT	n/a
GoTaq Master Mix	Promega	M7422
Hamilton Syringe (10 µL, Model 1701 LT SYR)	Hamilton	80001
Histobond Twinfrosted adhesion slides	VWR	631-0624
Histoclear	SLS Ltd	HS-202
Histomount	SLS Ltd	HS-103
Hypodermic needle 25G 16mm	Greiner Bio-One Ltd	N2516
Hypodermic needle 27G 20mm	VWR	613-2013
Hypodermic needle 30G 12mm	VWR	613-2011
ImmEdge Pen (hydrophobic barrier pen)	Vector Labs	H-4000
Insulin Syringe with 29G needle	VWR	613-4897
Iscove's modified Dulbecco's medium (IMDM)	ThermoFisher	21980032
Liquid DAB Substrate Pack, Concentrated	BioGenex	HK153-5K
Mayer's Haematoxylin	Sigma-Aldrich	MHS16
Methanol	VWR	20864.32
Monobasic potassium phosphate (KH <sub>2</sub> PO <sub>4</sub> )	Sigma-Aldrich	P5655
MX35 Premier Disposable Low-Profile Microtome Blades	ThermoFisher	3051835
Normal Donkey Serum	Sigma Aldrich	D9663
Normal Goat Serum	Vector Labs	S-1000

OCT	CellPath	KMA-0100-00A
Peanut Oil	Sigma Aldrich	P2144
Penicillin-Streptomycin	ThermoFisher	15070063
Plastic and Glassware	VWR, ThermoFisher and Scientific Laboratory Supplies	
Poly-D-Lysine	Sigma	P7280
Potassium Chloride (KCl)	Sigma Aldrich	P9541
Prolong gold antifade agent	ThermoFisher	P36930
Prolong gold antifade agent with DAPI	ThermoFisher	P36931
Recombinant Murine Cardiotrophin-1	Peprtech	250-25
Sodium Chloride (NaCl)	Sigma Aldrich	S9625
Sodium Hydroxide (NaOH)	VWR	28244.295
Sodium phosphate dibasic (Na <sub>2</sub> HPO <sub>4</sub> )	Sigma-Aldrich	S0876
Sterile PBS (pH 7.2)	ThermoFisher	20012019
Sterile PBS (pH 7.4)	ThermoFisher	10010023
Sucrose	Sigma Aldrich	S0389
Superfrost slides	Fisher Scientific	10149870
Tamoxifen	Sigma-Aldrich	T5648
Thrombin	Sigma-Aldrich	T4393
Tris-HCl	Sigma Aldrich	T3253
Triton X-100	Sigma Aldrich	T9284
Trizma Base	Sigma Aldrich	20252.244
Tween-20	Sigma Aldrich	P1379
Versene	ThermoFisher	15040033
Water, Molecular Biology Reagent	Sigma Aldrich	W1754

---

## **REFERENCES**

- 
1. Miquerol L, Kelly RG. Organogenesis of the vertebrate heart. *Wiley Interdisciplinary Reviews: Developmental Biology*. 2013;2(1):17-29.
  2. Savolainen SM, Foley JF, Elmore SA. Histology Atlas of the Developing Mouse Heart with Emphasis on E11.5 to E18.5. *Toxicologic Pathology*. 2009;37(4):395-414.
  3. Kaufman MH, Navaratnam V. Early differentiation of the heart in mouse embryos. *Journal of Anatomy*. 1981;133(2):235 - 46.
  4. Hoogaars WMH, Barnett P, Moorman AFM, Christoffels VM. Cardiovascular development: towards biomedical applicability. *Cell Mol Life Sci*. 2007;64(6):646-60.
  5. Risau W, Sariola H, Zerwes HG, Sasse J, Ekblom P, Kemler R, et al. Vasculogenesis and angiogenesis in embryonic-stem-cell-derived embryoid bodies. *Development*. 1988;102(3):471.
  6. Patel-Hett S, D'Amore PA. Signal transduction in vasculogenesis and developmental angiogenesis. *The International Journal of Developmental Biology*. 2011;55:353-63.
  7. Patan S. Vasculogenesis and Angiogenesis as Mechanisms of Vascular Network Formation, Growth and Remodeling. *J Neurooncol*. 2000;50(1-2):1-15.
  8. Carmeliet P. Mechanisms of angiogenesis and arteriogenesis. *Nat Med*. 2000;6(4):389-95.
  9. Caprioli A, Minko K, Drevon C, Eichmann A, Dieterlen-Lièvre F, Jaffredo T. Hemangioblast Commitment in the Avian Allantois: Cellular and Molecular Aspects. *Developmental Biology*. 2001;238(1):64-78.
  10. Poole TJ, Coffin JD. Vasculogenesis and angiogenesis: Two distinct morphogenetic mechanisms establish embryonic vascular pattern. *Journal of Experimental Zoology*. 1989;251(2):224-31.
  11. Pardanaud L, Altmann C, Kitos P, Dieterlen-Lievre F, Buck CA. Vasculogenesis in the early quail blastodisc as studied with a monoclonal antibody recognizing endothelial cells. *Development*. 1987;100(2):339-49.
  12. Pardanaud L, Dieterlen-Lievre F. Emergence of endothelial and hemopoietic cells in the avian embryo. *Anatomy and embryology*. 1993;187(2):107-14.
  13. Carmeliet P, Ferreira V, Breier G, Pollefeyt S, Kieckens L, Gertsenstein M, et al. Abnormal blood vessel development and lethality in embryos lacking a single VEGF allele. *Nature*. 1996;380(6573):435-9.
  14. Ferrara N, Carver-Moore K, Chen H, Dowd M, Lu L, O'Shea KS, et al. Heterozygous embryonic lethality induced by targeted inactivation of the VEGF gene. *Nature*. 1996;380(6573):439-42.
  15. Senger DR, Connolly DT, Van De Water L, Feder J, Dvorak HF. Purification and NH<sub>2</sub>-Terminal Amino Acid Sequence of Guinea Pig Tumor-secreted Vascular Permeability Factor. *Cancer Research*. 1990;50(6):1774-8.
  16. Miquerol L, Gertsenstein M, Harpal K, Rossant J, Nagy A. Multiple Developmental Roles of VEGF Suggested by a LacZ-Tagged Allele. *Developmental Biology*. 1999;212(2):307-22.
  17. Flamme I, Breier G, Risau W. Vascular Endothelial Growth Factor (VEGF) and VEGF Receptor 2(flk-1) Are Expressed during Vasculogenesis and Vascular Differentiation in the Quail Embryo. *Developmental Biology*. 1995;169(2):699-712.
  18. Shalaby F, Rossant J, Yamaguchi TP, Gertsenstein M, Wu X-F, Breitman ML, et al. Failure of blood-island formation and vasculogenesis in Flk-1-deficient mice. *Nature*. 1995;376(6535):62-6.
  19. Fong G-H, Rossant J, Gertsenstein M, Breitman ML. Role of the Flt-1 receptor tyrosine kinase in regulating the assembly of vascular endothelium. *Nature*. 1995;376(6535):66-70.
  20. Ten Dijke P, Arthur HM. Extracellular control of TGF[ $\beta$ ] signalling in vascular development and disease. *Nat Rev Mol Cell Biol*. 2007;8(11):857-69.
  21. Risau W. Mechanisms of angiogenesis. *Nature*. 1997;386:671-4.
  22. Karamysheva AF. Mechanisms of Angiogenesis. *Biochemistry (Moscow)*. 2008;73(7):751-62.
  23. Smart N, Dubé KN, Riley PR. Coronary vessel development and insight towards neovascular therapy. *International Journal of Experimental Pathology*. 2009;90(3):262-83.
  24. Shawber CJ, Das I, Francisco E, Kitajewski JAN. Notch Signaling in Primary Endothelial Cells. *Annals of the New York Academy of Sciences*. 2003;995(1):162-70.
  25. Krebs LT, Xue Y, Norton CR, Shutter JR, Maguire M, Sundberg JP, et al. Notch signaling is essential for vascular morphogenesis in mice. *Genes & development*. 2000;14(11):1343-52.
-

- 
26. Uyttendaele H, Ho J, Rossant J, Kitajewski J. Vascular patterning defects associated with expression of activated Notch4 in embryonic endothelium. *Proceedings of the National Academy of Sciences*. 2001;98(10):5643-8.
  27. Krebs LT, Shutter JR, Tanigaki K, Honjo T, Stark KL, Gridley T. Haploinsufficient lethality and formation of arteriovenous malformations in Notch pathway mutants. *Genes & development*. 2004;18(20):2469-73.
  28. Liu ZJ, Shirakawa T, Li Y, Soma A, Oka M, Dotto GP, et al. Regulation of Notch1 and Dll4 by vascular endothelial growth factor in arterial endothelial cells: implications for modulating arteriogenesis and angiogenesis. *Molecular and cellular biology*. 2003;23(1):14-25.
  29. Suchting S, Freitas C, le Noble F, Benedito R, Breant C, Duarte A, et al. The Notch ligand Delta-like 4 negatively regulates endothelial tip cell formation and vessel branching. *Proceedings of the National Academy of Sciences of the United States of America*. 2007;104(9):3225-30.
  30. Hellstrom M, Kalen M, Lindahl P, Abramsson A, Betsholtz C. Role of PDGF-B and PDGFR-beta in recruitment of vascular smooth muscle cells and pericytes during embryonic blood vessel formation in the mouse. *Development*. 1999;126(14):3047-55.
  31. Kelly BD, Hackett SF, Hirota K, Oshima Y, Cai Z, Berg-Dixon S, et al. Cell Type-Specific Regulation of Angiogenic Growth Factor Gene Expression and Induction of Angiogenesis in Nonischemic Tissue by a Constitutively Active Form of Hypoxia-Inducible Factor 1. *Circulation Research*. 2003;93(11):1074-81.
  32. Iyer NV, Kotch LE, Agani F, Leung SW, Laughner E, Wenger RH, et al. Cellular and developmental control of O<sub>2</sub> homeostasis by hypoxia-inducible factor 1 alpha. *Genes & development*. 1998;12(2):149-62.
  33. Wang HU, Chen Z-F, Anderson DJ. Molecular Distinction and Angiogenic Interaction between Embryonic Arteries and Veins Revealed by ephrin-B2 and Its Receptor Eph-B4. *Cell*. 1998;93(5):741-53.
  34. Gerety SS, Wang HU, Chen Z-F, Anderson DJ. Symmetrical Mutant Phenotypes of the Receptor EphB4 and Its Specific Transmembrane Ligand ephrin-B2 in Cardiovascular Development. *Molecular cell*. 1999;4(3):403-14.
  35. Herzog Y, Guttman-Raviv N, Neufeld G. Segregation of arterial and venous markers in subpopulations of blood islands before vessel formation. *Developmental Dynamics*. 2005;232(4):1047-55.
  36. Fiss DM. Normal coronary anatomy and anatomic variations. *Applied Radiology*. 2007;Supplement(1):14 - 26.
  37. Gray H. *Gray's - Anatomy of Human Body*. 20 ed. Lewis WH, editor: Philadelphia: Lea & Febiger; 2002.
  38. Bogers AJC, Gittenberger-de Groot AC, Poelmann RE, Péault BM, Huysmans HA. Development of the origin of the coronary arteries, a matter of ingrowth or outgrowth? *Anatomy and embryology*. 1989;180(5):437-41.
  39. Kumar D, Hacker TA, Buck J, Whitesell LF, Kaji EH, Douglas PS, et al. Distinct mouse coronary anatomy and myocardial infarction consequent to ligation. *Coronary Artery Disease*. 2005;16(1):41-4.
  40. Magazine MM. Coronary Circulation Anatomy Medchrome Medical Magazine website: Medchrome Medical Magazine; 2013 [Available from: <http://tube.medchrome.com/2011/04/coronary-circulation-anatomy.html>].
  41. Mak GS, Hill AJ, Moisiuc F, Krishnan SC. Variations in Thebesian valve anatomy and coronary sinus ostium: implications for invasive electrophysiology procedures. *Europace*. 2009;11(9):1188-92.
  42. Minnesota Uo. Cardiac Veins Minnesota2010 [updated 14/09/12. Available from: <http://www.vhlab.umn.edu/atlas/cardiac-veins/index.shtml>].
  43. Red-Horse K, Ueno H, Weissman IL, Krasnow MA. Coronary arteries form by developmental reprogramming of venous cells. *Nature*. 2010;464(7288):549-53.
  44. Chen HI, Sharma B, Akerberg BN, Numi HJ, Kivelä R, Saharinen P, et al. The sinus venosus contributes to coronary vasculature through VEGFC-stimulated angiogenesis. *Development*. 2014;141(23):4500-12.
  45. Carmeliet P, Ng Y-S, Nuyens D, Theilmeier G, Brusselmans K, Cornelissen I, et al. Impaired myocardial angiogenesis and ischemic cardiomyopathy in mice lacking the vascular endothelial growth factor isoforms VEGF164 and VEGF188. *Nat Med*. 1999;5(5):495-502.
-

- 
46. Reese DE, Mikawa T, Bader DM. Development of the Coronary Vessel System. *Circulation Research*. 2002;91(9):761-8.
  47. Kirby ML, Waldo K. *Cardiac Development*. Oxford: Oxford University Press; 2007.
  48. Carmona R, Guadix JA, Cano E, Ruiz-Villalba A, Portillo-Sánchez V, Pérez-Pomares JM, et al. The embryonic epicardium: an essential element of cardiac development. *Journal of Cellular and Molecular Medicine*. 2010;14(8):2066-72.
  49. Muñoz-Chápuli R. Epicardial development. *European Journal of Anatomy*. 2011;15:10-6.
  50. Pérez-Pomares JM, Phelps A, Sedmerova M, Wessels A. Epicardial-like cells on the distal arterial end of the cardiac outflow tract do not derive from the proepicardium but are derivatives of the cephalic pericardium. *Developmental Dynamics*. 2003;227(1):56-68.
  51. Komiyama M, Ito K, Shimada Y. Origin and development of the epicardium in the mouse embryo. *Anatomy and embryology*. 1987;176(2):183-9.
  52. Masters M, Riley PR. The epicardium signals the way towards heart regeneration. *Stem Cell Research*. 2014;13(3, Part B):683-92.
  53. Rodgers LS, Lalani S, Runyan RB, Camenisch TD. Differential growth and multicellular villi direct proepicardial translocation to the developing mouse heart. *Developmental Dynamics*. 2008;237(1):145-52.
  54. Wessels A, van den Hoff MJB, Adamo RF, Phelps AL, Lockhart MM, Sauls K, et al. Epicardially derived fibroblasts preferentially contribute to the parietal leaflets of the atrioventricular valves in the murine heart. *Developmental Biology*. 2012;366(2):111-24.
  55. Pérez-Pomares JM, de la Pompa JL. Signaling During Epicardium and Coronary Vessel Development. *Circulation Research*. 2011;109(12):1429-42.
  56. Moore AW, McInnes L, Kreidberg J, Hastie ND, Schedl A. YAC complementation shows a requirement for *Wt1* in the development of epicardium, adrenal gland and throughout nephrogenesis. *Development*. 1999;126(9):1845-57.
  57. Martínez-Estrada OM, Lettice LA, Essafi A, Guadix JA, Slight J, Velecela V, et al. *Wt1* is required for cardiovascular progenitor cell formation through transcriptional control of *Snail* and *E-cadherin*. *Nature Genetics*. 2009;42:89.
  58. Brown CB, Boyer AS, Runyan RB, Barnett JV. Antibodies to the Type II TGF $\beta$  Receptor Block Cell Activation and Migration during Atrioventricular Cushion Transformation in the Heart. *Developmental Biology*. 1996;174(2):248-57.
  59. Jiao K, Langworthy M, Batts L, Brown CB, Moses HL, Baldwin HS. Tgf $\beta$  signaling is required for atrioventricular cushion mesenchyme remodeling during in vivo cardiac development. *Development*. 2006;133(22):4585.
  60. Somyoth Sridurongrit, Jonas Larsson, Robert Schwartz, Pilar Ruiz-Lozano, Kaartinena V. Signaling via the Tgf-beta type I receptor *Alk5* in heart development. *Development Biology*. 2008;322(1):208 - 18.
  61. Austin AF, Compton LA, Love JD, Brown CB, Barnett JV. Primary and immortalized mouse epicardial cells undergo differentiation in response to TGF $\beta$ . *Developmental Dynamics*. 2008;237(2):366-76.
  62. Compton Leigh A, Potash Dru A, Mundell Nathan A, Barnett Joey V. Transforming growth factor- $\beta$  induces loss of epithelial character and smooth muscle cell differentiation in epicardial cells. *Developmental Dynamics*. 2005;235(1):82-93.
  63. Dokic D, Dettman RW. VCAM-1 inhibits TGF $\beta$  stimulated epithelial-mesenchymal transformation by modulating Rho activity and stabilizing intercellular adhesion in epicardial mesothelial cells. *Developmental Biology*. 2006;299(2):489-504.
  64. Bax NM, Oorschot AM, Maas S, Braun J, Tuyn J, Vries AF, et al. In vitro epithelial-to-mesenchymal transformation in human adult epicardial cells is regulated by TGF $\beta$ -signaling and *WT1*. *Basic Res Cardiol*. 2011;106(5):829-47.
  65. Azhar M, Schultz JEJ, Grupp I, Dorn GW, Meneton P, Molin DGM, et al. Transforming growth factor beta in cardiovascular development and function. *Cytokine & Growth Factor Reviews*. 2003;14(5):391-407.
  66. Arthur HM, Bamforth SD. TGF $\beta$  signaling and congenital heart disease: Insights from mouse studies. *Birth Defects Research Part A: Clinical and Molecular Teratology*. 2011;91(6):423-34.
-

- 
67. Tan EJ, Olsson A-K, Moustakas A. Reprogramming during epithelial to mesenchymal transition under the control of TGF $\beta$ . *Cell Adhesion & Migration*. 2015;9(3):233-46.
  68. Mercado-Pimentel ME, Runyan RB. Multiple Transforming Growth Factor- $\beta$  Isoforms and Receptors Function during Epithelial-Mesenchymal Cell Transformation in the Embryonic Heart. *Cells Tissues Organs*. 2007;185(1-3):146-56.
  69. Garside VC, Chang AC, Karsan A, Hoodless PA. Co-ordinating Notch, BMP, and TGF- $\beta$  signaling during heart valve development. *Cellular and molecular life sciences : CMLS*. 2013;70(16):2899-917.
  70. Mikawa T, Gourdie RG. Pericardial Mesoderm Generates a Population of Coronary Smooth Muscle Cells Migrating into the Heart along with Ingrowth of the Epicardial Organ. *Developmental Biology*. 1996;174(2):221-32.
  71. Swonger JM, Liu JS, Ivey MJ, Tallquist MD. Genetic tools for identifying and manipulating fibroblasts in the mouse. *Differentiation*. 2016;92(3):66-83.
  72. Wu S-P, Dong X-R, Regan JN, Su C, Majesky MW. Tbx18 regulates development of the epicardium and coronary vessels. *Developmental Biology*. 2013;383(2):307-20.
  73. Zhou B, von Gise A, Ma Q, Hu YW, Pu WT. Genetic fate mapping demonstrates contribution of epicardium-derived cells to the annulus fibrosus of the mammalian heart. *Developmental Biology*. 2010;338(2):251-61.
  74. Groot ACG-d, Peeters M-PFMV, Mentink MMT, Gourdie RG, Poelmann RE. Epicardium-derived cells contribute a novel population to the myocardial wall and the atrioventricular cushions. *Circulation research*. 1998;82(10):1043-52.
  75. Dettman RW, Denetclaw W, Ordahl CP, Bristow J. Common Epicardial Origin of Coronary Vascular Smooth Muscle, Perivascular Fibroblasts, and Intermyocardial Fibroblasts in the Avian Heart. *Developmental Biology*. 1998;193(2):169-81.
  76. Männer J. Does the subepicardial mesenchyme contribute myocardioblasts to the myocardium of the chick embryo heart? A quail-chick chimera study tracing the fate of the epicardial primordium. *The Anatomical Record*. 1999;255(2):212-26.
  77. Pérez-Pomares JM, Phelps A, Sedmerova M, Carmona R, González-Iriarte M, Muñoz-Chápuli R, et al. Experimental Studies on the Spatiotemporal Expression of WT1 and RALDH2 in the Embryonic Avian Heart: A Model for the Regulation of Myocardial and Valvuloseptal Development by Epicardially Derived Cells (EPDCs). *Developmental Biology*. 2002;247(2):307-26.
  78. Zhou B, Ma Q, Rajagopal S, Wu SM, Domian I, Rivera-Feliciano J, et al. Epicardial progenitors contribute to the cardiomyocyte lineage in the developing heart. *Nature*. 2008;454(7200):109-13.
  79. Tian X, Hu T, Zhang H, He L, Huang X, Liu Q, et al. Subepicardial endothelial cells invade the embryonic ventricle wall to form coronary arteries. *Cell Res*. 2013;23(9):1075-90.
  80. Cai C-L, Martin JC, Sun Y, Cui L, Wang L, Ouyang K, et al. A myocardial lineage derives from Tbx18 epicardial cells. *Nature*. 2008;454:104.
  81. Zhou B, Gise Av, Ma Q, Rivera-Feliciano J, Pu WT. Nkx2-5- and Isl1-expressing cardiac progenitors contribute to proepicardium. *Biochemical and Biophysical Research Communications*. 2008;375(3):450-3.
  82. Rudat C, Kispert A. Wt1 and Epicardial Fate Mapping. *Circulation Research*. 2012;111(2):165-9.
  83. Christoffels VM, Grieskamp T, Norden J, Mommersteeg MTM, Rudat C, Kispert A. Tbx18 and the fate of epicardial progenitors. *Nature*. 2009;458:E8.
  84. Morabito CJ, Kattan J, Bristow J. Mechanisms of embryonic coronary artery development. *Current Opinion in Cardiology*. 2002;17(3):235-41.
  85. Olivey HE, Svensson EC. Epicardial-Myocardial Signaling Directing Coronary Vasculogenesis. *Circulation Research*. 2010;106(5):818-32.
  86. Mu H, Ohashi R, Lin P, Yao Q, Chen C. Cellular and molecular mechanisms of coronary vessel development. *Vascular Medicine*. 2005;10(1):37-44.
  87. Pinco KA, Liu S, Yang JT.  $\alpha$ 4 integrin is expressed in a subset of cranial neural crest cells and in epicardial progenitor cells during early mouse development. *Mechanisms of Development*. 2001;100(1):99-103.
  88. Yang JT, Rayburn H, Hynes RO. Cell adhesion events mediated by alpha 4 integrins are essential in placental and cardiac development. *Development*. 1995;121(2):549-60.
-

- 
89. Sengbusch JK, He W, Pinco KA, Yang JT. Dual functions of  $\alpha 4\beta 1$  integrin in epicardial development: initial migration and long-term attachment. *The Journal of cell biology*. 2002;157(5):873-82.
  90. Reese DE, Zavaljevski M, Streiff NL, Bader D. Bves: A Novel Gene Expressed during Coronary Blood Vessel Development. *Developmental Biology*. 1999;209(1):159-71.
  91. Wada AM, Reese DE, Bader DM. Bves: prototype of a new class of cell adhesion molecules expressed during coronary artery development. *Development*. 2001;128(11):2085-93.
  92. Osler ME, Chang MS, Bader DM. Bves modulates epithelial integrity through an interaction at the tight junction. *Journal of Cell Science*. 2005;118(20):4667.
  93. Li WEI, Waldo K, Linask KL, Chen T, Wessels A, Parmacek MS, et al. An essential role for connexin43 gap junctions in mouse coronary artery development. *Development*. 2002;129(8):2031.
  94. Wu H, Lee SH, Gao J, Liu X, Iruela-Arispe ML. Inactivation of erythropoietin leads to defects in cardiac morphogenesis. *Development*. 1999;126(16):3597.
  95. Lie-Venema H, Gittenberger-de Groot Adriana C, van Empel Louis JP, Boot Marit J, Kerkdijk H, de Kant E, et al. Ets-1 and Ets-2 Transcription Factors Are Essential for Normal Coronary and Myocardial Development in Chicken Embryos. *Circulation Research*. 2003;92(7):749-56.
  96. Torlopp A, Schlueter J, Brand T. Role of fibroblast growth factor signaling during proepicardium formation in the chick embryo. *Developmental Dynamics*. 2010;239(9):2393-403.
  97. Tomanek RJ, Zheng W. Role of Growth Factors in Coronary Morphogenesis. *Texas Heart Institute Journal*. 2002;29(4):250 - 4.
  98. Tevosian SG, Deconinck AE, Tanaka M, Schinke M, Litovsky SH, Izumo S, et al. FOG-2, a Cofactor for GATA Transcription Factors, Is Essential for Heart Morphogenesis and Development of Coronary Vessels from Epicardium. *Cell*. 2000;101(7):729-39.
  99. Watt AJ, Battle MA, Li J, Duncan SA. GATA4 is essential for formation of the proepicardium and regulates cardiogenesis. *Proceedings of the National Academy of Sciences of the United States of America*. 2004;101(34):12573-8.
  100. Trembley MA, Velasquez LS, de Mesy Bentley KL, Small EM. Myocardin-related transcription factors control the motility of epicardium-derived cells and the maturation of coronary vessels. *Development*. 2015;142(1):21.
  101. Wagner K-D, Wagner N, Pagnotta S, Michiels J-F, Schedl A, Morrison H, et al. The podocyte protein nephrin is required for cardiac vessel formation. *Human Molecular Genetics*. 2011;20(11):2182-94.
  102. Zhao Z, Rivkees SA. Rho-associated kinases play an essential role in cardiac morphogenesis and cardiomyocyte proliferation. *Developmental Dynamics*. 2003;226(1):24-32.
  103. Lu J, Landerholm TE, Wei JS, Dong X-R, Wu S-P, Liu X, et al. Coronary Smooth Muscle Differentiation from Proepicardial Cells Requires RhoA-Mediated Actin Reorganization and p160 Rho-Kinase Activity. *Developmental Biology*. 2001;240(2):404-18.
  104. Landerholm TE, Dong XR, Lu J, Belaguli NS, Schwartz RJ, Majesky MW. A role for serum response factor in coronary smooth muscle differentiation from proepicardial cells. *Development*. 1999;126(10):2053.
  105. Pontén A, Walsh S, Malan D, Xian X, Schéele S, Tarnawski L, et al. FACS-based isolation, propagation and characterization of mouse embryonic cardiomyocytes based on VCAM-1 surface marker expression. *PloS one*. 2013;8(12):e82403-e.
  106. Kwee L, Baldwin HS, Shen HM, Stewart CL, Buck C, Buck CA, et al. Defective development of the embryonic and extraembryonic circulatory systems in vascular cell adhesion molecule (VCAM-1) deficient mice. *Development*. 1995;121(2):489-503.
  107. Tomanek RJ, Ratajska A, Kitten GT, Yue X, Sandra A. Vascular endothelial growth factor expression coincides with coronary vasculogenesis and angiogenesis. *Developmental Dynamics*. 1999;215(1):54-61.
  108. Tomanek Robert J, Sandra A, Zheng W, Brock T, Bjercke Robert J, Holifield Jennifer S. Vascular Endothelial Growth Factor and Basic Fibroblast Growth Factor Differentially Modulate Early Postnatal Coronary Angiogenesis. *Circulation Research*. 2001;88(11):1135-41.
-

- 
109. Drake CJ, Little CD. Exogenous vascular endothelial growth factor induces malformed and hyperfused vessels during embryonic neovascularization. *Proceedings of the National Academy of Sciences of the United States of America*. 1995;92(17):7657-61.
  110. Miquerol L, Langille BL, Nagy A. Embryonic development is disrupted by modest increases in vascular endothelial growth factor gene expression. *Development*. 2000;127(18):3941.
  111. Wu B, Zhang Z, Lui W, Chen X, Wang Y, Chamberlain AA, et al. Endocardial Cells Form the Coronary Arteries by Angiogenesis through Myocardial-Endocardial VEGF Signaling. *Cell*. 2012;151(5):1083-96.
  112. Aase K, Lymboussaki A, Kaipainen A, Olofsson B, Alitalo K, Eriksson U. Localization of VEGF-B in the mouse embryo suggests a paracrine role of the growth factor in the developing vasculature. *Developmental Dynamics*. 1999;215(1):12-25.
  113. Bellomo D, Headrick John P, Silins Ginters U, Paterson Carol A, Thomas Penny S, Gartside M, et al. Mice Lacking the Vascular Endothelial Growth Factor-B Gene (*Vegfb*) Have Smaller Hearts, Dysfunctional Coronary Vasculature, and Impaired Recovery From Cardiac Ischemia. *Circulation Research*. 2000;86(2):e29-e35.
  114. Muhl L, Moessinger C, Adzemovic MZ, Dijkstra MH, Nilsson I, Zeitelhofer M, et al. Expression of vascular endothelial growth factor (VEGF)-B and its receptor (VEGFR1) in murine heart, lung and kidney. *Cell and Tissue Research*. 2016;365(1):51-63.
  115. Kurotsu S, Osakabe R, Isomi M, Tamura F, Sadahiro T, Muraoka N, et al. Distinct expression patterns of *Flk1* and *Flt1* in the coronary vascular system during development and after myocardial infarction. *Biochemical and Biophysical Research Communications*. 2018;495(1):884-91.
  116. von Gise A, Zhou B, Honor LB, Ma Q, Petryk A, Pu WT. WT1 regulates epicardial epithelial to mesenchymal transition through  $\beta$ -catenin and retinoic acid signaling pathways. *Developmental biology*. 2011;356(2):421-31.
  117. Zeng B, Ren X-f, Cao F, Zhou X-y, Zhang J. Developmental patterns and characteristics of epicardial cell markers *Tbx18* and *Wt1* in murine embryonic heart. *Journal of biomedical science*. 2011;18(1):67-.
  118. Takeichi M, Nimura K, Mori M, Nakagami H, Kaneda Y. The Transcription Factors *Tbx18* and *Wt1* Control the Epicardial Epithelial-Mesenchymal Transition through Bi-Directional Regulation of *Slug* in Murine Primary Epicardial Cells. *PLoS ONE*. 2013;8(2):e57829.
  119. Lavine KJ, Long F, Choi K, Smith C, Ornitz DM. Hedgehog signaling to distinct cell types differentially regulates coronary artery and vein development. *Development*. 2008;135(18):3161-71.
  120. Zhang H, Pu W, Li G, Huang X, He L, Tian X, et al. Endocardium Minimally Contributes to Coronary Endothelium in the Embryonic Ventricular Free Walls. *Circulation Research*. 2016;118(12):1880-93.
  121. del Monte G, Harvey Richard P. An Endothelial Contribution to Coronary Vessels. *Cell*. 2012;151(5):932-4.
  122. Tian X, Hu T, Zhang H, He L, Huang X, Liu Q, et al. De novo formation of a distinct coronary vascular population in neonatal heart. *Science*. 2014;345(6192):90-4.
  123. Lebrin F, Deckers M, Bertolino P, ten Dijke P. TGF- $\beta$  receptor function in the endothelium. *Cardiovascular Research*. 2005;65(3):599-608.
  124. Hinck AP, Mueller TD, Springer TA. Structural Biology and Evolution of the TGF- $\beta$  Family. *Cold Spring Harbor Perspectives in Biology*. 2016;8(12).
  125. Nickel J, ten Dijke P, Mueller TD. TGF- $\beta$  family co-receptor function and signaling. *Acta Biochimica et Biophysica Sinica*. 2017;50(1):12-36.
  126. Mahmoud M, Upton PD, Arthur HM. Angiogenesis regulation by TGF $\beta$  signalling: clues from an inherited vascular disease. *Biochemical Society Transactions*. 2011;39(6):1659-66.
  127. Li DY, Sorensen LK, Brooke BS, Urness LD, Davis EC, Taylor DG, et al. Defective Angiogenesis in Mice Lacking *Endoglin*. *Science*. 1999;284(5419):1534-7.
  128. Arthur HM, Ure J, Smith AJH, Renforth G, Wilson DI, Torsney E, et al. *Endoglin*, an Ancillary TGF $\beta$  Receptor, Is Required for Extraembryonic Angiogenesis and Plays a Key Role in Heart Development. *Developmental Biology*. 2000;217(1):42-53.
-

- 
129. Carvalho RLC, Jonker L, Goumans M-J, Larsson J, Bouwman P, Karlsson S, et al. Defective paracrine signalling by TGF $\beta$  in yolk sac vasculature of endoglin mutant mice: a paradigm for hereditary haemorrhagic telangiectasia. *Development*. 2004;131(24):6237-47.
  130. Saito T, Bokhove M, Croci R, Zamora-Caballero S, Han L, Letarte M, et al. Structural Basis of the Human Endoglin-BMP9 Interaction: Insights into BMP Signaling and HHT1. *Cell Reports*. 2017;19(9):1917-28.
  131. Dijke P, Goumans M-J, Pardali E. Endoglin in angiogenesis and vascular diseases. *Angiogenesis*. 2008;11(1):79-89.
  132. Nassiri F, Cusimano MD, Scheithauer BW, Rotondo F, Fazio A, Yousef GM, et al. Endoglin (CD105): A Review of its Role in Angiogenesis and Tumor Diagnosis, Progression and Therapy. *Anticancer Research*. 2011;31(6):2283-90.
  133. López-Novoa JM, Bernabeu C. The physiological role of endoglin in the cardiovascular system. *American Journal of Physiology - Heart and Circulatory Physiology*. 2010;299(4):H959-H74.
  134. Castonguay R, Werner ED, Matthews RG, Presman E, Mulivor AW, Solban N, et al. Soluble Endoglin Specifically Binds Bone Morphogenetic Proteins 9 and 10 via Its Orphan Domain, Inhibits Blood Vessel Formation, and Suppresses Tumor Growth. *The Journal of Biological Chemistry*. 2011;286(34):30034-46.
  135. Hawinkels LJAC, Kuiper P, Wiercinska E, Verspaget HW, Liu Z, Pardali E, et al. Matrix Metalloproteinase-14 (MT1-MMP)-Mediated Endoglin Shedding Inhibits Tumor Angiogenesis. *Cancer Research*. 2010;70(10):4141-50.
  136. Li C, Guo B, Ding S, Rius C, Langa C, Kumar P, et al. TNF alpha down-regulates CD105 expression in vascular endothelial cells: a comparative study with TGF beta 1. *Anticancer Res*. 2003;23(2B):1189-96.
  137. Jonker L, Arthur HM. Endoglin expression in early development is associated with vasculogenesis and angiogenesis. *Mechanisms of Development*. 2002;110(1-2):193-6.
  138. St-Jacques S, Cymerman U, Pece N, Letarte M. Molecular characterization and in situ localization of murine endoglin reveal that it is a transforming growth factor-beta binding protein of endothelial and stromal cells. *Endocrinology*. 1994;134(6):2645-57.
  139. Duff SE, Li C, Garland JM, Kumar S. CD105 is important for angiogenesis: evidence and potential applications. *Faseb J*. 2003;17(9):984-92.
  140. Chen CZ, Li M, de Graaf D, Monti S, Gottgens B, Sanchez MJ, et al. Identification of endoglin as a functional marker that defines long-term repopulating hematopoietic stem cells. *Proceedings of the National Academy of Sciences of the United States of America*. 2002;99(24):15468-73.
  141. Mahmoud M, Borthwick GM, Hislop AA, Arthur HM. Endoglin and activin receptor-like-kinase 1 are co-expressed in the distal vessels of the lung: implications for two familial vascular dysplasias, HHT and PAH. *Lab Invest*. 2008;89(1):15-25.
  142. Goumans MJ, Valdimarsdottir G, Itoh S, Rosendahl A, Sideras P, Dijke Pt. Balancing the activation state of the endothelium via two distinct TGF- $\beta$  type I receptors. *The EMBO Journal*. 2002;21(7):1743-53.
  143. Benezra R. Role of Id Proteins in Embryonic and Tumor Angiogenesis. *Trends in Cardiovascular Medicine*. 2001;11(6):237-41.
  144. Lebrin F, Goumans M-J, Jonker L, Carvalho RL, Valdimarsdottir G, Thorikay M, et al. Endoglin promotes endothelial cell proliferation and TGF- $\beta$ /ALK1 signal transduction. *The EMBO Journal*. 2004;23(20):3909 - 4125.
  145. Stefansson S, Petitclerc E, Wong MKK, McMahon GA, Brooks PC, Lawrence DA. Inhibition of Angiogenesis in Vivo by Plasminogen Activator Inhibitor-1. *Journal of Biological Chemistry*. 2001;276(11):8135-41.
  146. Wu J, Strawn Tammy L, Luo M, Wang L, Li R, Ren M, et al. Plasminogen Activator Inhibitor-1 Inhibits Angiogenic Signaling by Uncoupling Vascular Endothelial Growth Factor Receptor-2- $\alpha$ V $\beta$ 3 Integrin Cross Talk. *Arteriosclerosis, Thrombosis, and Vascular Biology*. 2015;35(1):111-20.
  147. Oh SP, Seki T, Goss KA, Imamura T, Yi Y, Donahoe PK, et al. Activin receptor-like kinase 1 modulates transforming growth factor- $\beta$ 1 signaling in the regulation of angiogenesis. *Proceedings of the National Academy of Sciences*. 2000;97(6):2626-31.
-

- 
148. Goumans M-J, Lebrin F, Valdimarsdottir G. Controlling the Angiogenic Switch: A Balance between Two Distinct TGF- $\beta$  Receptor Signaling Pathways. *Trends in Cardiovascular Medicine*. 2003;13(7):301-7.
  149. Barbara NP, Wrana JL, Letarte M. Endoglin Is an Accessory Protein That Interacts with the Signaling Receptor Complex of Multiple Members of the Transforming Growth Factor- $\beta$  Superfamily. *Journal of Biological Chemistry*. 1999;274(2):584-94.
  150. Redgrave RE, Tual-Chalot S, Davison BJ, Singh E, Hall D, Amirrasouli MM, et al. Cardiosphere-Derived Cells Require Endoglin for Paracrine-Mediated Angiogenesis. *Stem Cell Reports*. 2017;8(5):1287-98.
  151. Frutkin AD, Shi H, Otsuka G, Levéen P, Karlsson S, Dichek DA. A critical developmental role for *tgfbr2* in myogenic cell lineages is revealed in mice expressing SM22-Cre, not SMMHC-Cre. *Journal of Molecular and Cellular Cardiology*. 2006;41(4):724-31.
  152. Carvalho RLC, Itoh F, Goumans M-J, Lebrin F, Kato M, Takahashi S, et al. Compensatory signalling induced in the yolk sac vasculature by deletion of TGF $\beta$  receptors in mice. *Journal of Cell Science*. 2007;120(24):4269-77.
  153. Dominique Langlois, Mohammad Hneino, Lamia Bouazza, Ara Parlakian, Takako Sasaki, Giampiero Bricca, et al. Conditional inactivation of TGF- $\beta$  type II receptor in smooth muscle cells and epicardium causes lethal aortic and cardiac defects. *Translational Research*. 2010;19(6):1069 - 82.
  154. Oshima M, Oshima H, Taketo MM. TGF- $\beta$  Receptor Type II Deficiency Results in Defects of Yolk Sac Hematopoiesis and Vasculogenesis. *Developmental Biology*. 1996;179(1):297-302.
  155. Per Levéen, Jonas Larsson, Mats Ehinger, Corrado M. Cilio, Martin Sundler, Lottie Jansson Sjöstrand, et al. Induced disruption of the transforming growth factor beta type II receptor gene in mice causes a lethal inflammatory disorder that is transplantable. *Blood*. 2002;100(2).
  156. M.C. Dickson, J.S. Martin, F.M. Cousins, A.B. Kulkarni, and SK, Akhurst RJ. Defective haematopoiesis and vasculogenesis in transforming growth factor-beta 1 knock out mice. *Development*. 1995;121:1845 - 54.
  157. A B Kulkarni CGH, D Becker, Geiser A, Lyght M, Flanders KC, Roberts AB, Sporn MB, et al. Transforming growth factor beta 1 null mutation in mice causes excessive inflammatory response and early death. *Proceedings of the National Academy of Sciences of the United States of America*. 1993;90(2):770 - 4.
  158. Bartram U, Molin DGM, Wisse LJ, Mohamad A, Sanford LP, Doetschman T, et al. Double-Outlet Right Ventricle and Overriding Tricuspid Valve Reflect Disturbances of Looping, Myocardialization, Endocardial Cushion Differentiation, and Apoptosis in TGF- $\beta$ 2-Knockout Mice. *Circulation*. 2001;103(22):2745-52.
  159. Molin DGM, DeRuiter MC, Wisse LJ, Azhar M, Doetschman T, Poelmann RE, et al. Altered apoptosis pattern during pharyngeal arch artery remodelling is associated with aortic arch malformations in *Tgf $\beta$ 2* knock-out mice. *Cardiovascular Research*. 2002;56(2):312-22.
  160. Azhar M, Schultz JEJ, Grupp I, Dorn GW, Meneton P, Molin DGM, et al. Transforming growth factor beta in cardiovascular development and function. *Cytokine & Growth Factor Reviews*. 2003;14(5):391 - 407.
  161. Bourdeau A, Dumont DJ, Letarte M. A murine model of hereditary hemorrhagic telangiectasia. *Journal of Clinical Investigation*. 1999;104(10):1343-51.
  162. Camenisch TD, Molin DGM, Person A, Runyan RB, Gittenberger-de Groot AC, McDonald JA, et al. Temporal and Distinct TGF $\beta$  Ligand Requirements during Mouse and Avian Endocardial Cushion Morphogenesis. *Developmental Biology*. 2002;248(1):170-81.
  163. Sanford LP, Ormsby I, Gittenberger-de Groot AC, Sariola H, Friedman R, Boivin GP, et al. TGFbeta2 knockout mice have multiple developmental defects that are non-overlapping with other TGFbeta knockout phenotypes. *Development*. 1997;124(13):2659-70.
  164. Brown CB, Boyer AS, Runyan RB, Barnett JV. Requirement of Type III TGF- $\beta$  Receptor for Endocardial Cell Transformation in the Heart. *Science*. 1999;283(5410):2080.
  165. Stenvers KL, Tursky ML, Harder KW, Kountouri N, Amatayakul-Chantler S, Grail D, et al. Heart and Liver Defects and Reduced Transforming Growth Factor  $\beta$ 2 Sensitivity in Transforming Growth Factor  $\beta$  Type III Receptor-Deficient Embryos. *Molecular and Cellular Biology*. 2003;23(12):4371.
-

- 
166. Compton Leigh A, Potash Dru A, Brown Christopher B, Barnett Joey V. Coronary Vessel Development Is Dependent on the Type III Transforming Growth Factor  $\beta$  Receptor. *Circulation Research*. 2007;101(8):784-91.
  167. HHT C. Cure HHT Monkton, USA: Cure HHT; 2019 [Available from: <https://curehht.org/>].
  168. McAllister KA, Grogg KM, Johnson DW, Gallione CJ, Baldwin MA, Jackson CE, et al. Endoglin, a TGF- $\beta$  binding protein of endothelial cells, is the gene for hereditary haemorrhagic telangiectasia type 1. *Nature Genetics*. 1994;8:345.
  169. Johnson DW, Berg JN, Baldwin MA, Gallione CJ, Marondel I, Yoon SJ, et al. Mutations in the activin receptor-like kinase 1 gene in hereditary haemorrhagic telangiectasia type 2. *Nature Genetics*. 1996;13(2):189-95.
  170. Wu PR, Horwith A, Mai S, Parikh M, Tyagi G, Pai RG. High-Output Cardiac Failure Due to Hereditary Hemorrhagic Telangiectasia: A Case of an Extra-Cardiac Left to Right Shunt. *The International Journal of Angiology: Official Publication of the International College of Angiology, Inc*. 2017;26(2):125-9.
  171. Elwir S, Martin CM, Chinnakotla S, Reding M, Lake J, Hassan M. Liver Transplantation for High Output Heart Failure Secondary to HHT: A Case Report and Review of the Literature. *Journal of Gastrointestinal & Digestive System*. 2015;5(5).
  172. Cho D, Kim S, Kim M, Seo YH, Kim W, Kang SH, et al. Two Cases of High Output Heart Failure Caused by Hereditary Hemorrhagic Telangiectasia. *Korean Circulation Journal*. 2012;42(12):861-5.
  173. Braverman IM, Keh A, Jacobson BS. Ultrastructure and Three-Dimensional Organization of the Telangiectases of Hereditary Hemorrhagic Telangiectasia. *Journal of Investigative Dermatology*. 1990;95(4):422-7.
  174. Shovlin CL, Guttmacher AE, Buscarini E, Faughnan ME, Hyland RH, Westermann CJJ, et al. Diagnostic criteria for hereditary hemorrhagic telangiectasia (Rendu-Osler-Weber syndrome). *American Journal of Medical Genetics*. 2000;91(1):66-7.
  175. Ruiz-Llorente L, Gallardo-Vara E, Rossi E, Smadja DM, Botella LM, Bernabeu C. Endoglin and Alk1 as therapeutic targets for hereditary hemorrhagic telangiectasia Expert Opinion on Therapeutic Targets. 2017;21(10):933-47.
  176. Letteboer TGW, Mager JJ, Snijder RJ, Koeleman BPC, Lindhout D, Ploos van Amstel JK, et al. Genotype-phenotype relationship in hereditary haemorrhagic telangiectasia. *Journal of Medical Genetics*. 2006;43(4):371-7.
  177. Lesca G, Olivieri C, Burnichon N, Pagella F, Carette M-F, Gilbert-Dussardier B, et al. Genotype-phenotype correlations in hereditary hemorrhagic telangiectasia: Data from the French-Italian HHT network. *Genetics In Medicine*. 2007;9:14.
  178. Shovlin CL. Hereditary haemorrhagic telangiectasia: Pathophysiology, diagnosis and treatment. *Blood Reviews*. 2010;24(6):203-19.
  179. Komiyama M, Ishiguro T, Yamada O, Morisaki H, Morisaki T. Hereditary hemorrhagic telangiectasia in Japanese patients. *Journal Of Human Genetics*. 2013;59:37.
  180. Govani FS, Shovlin CL. Hereditary haemorrhagic telangiectasia: a clinical and scientific review. *European Journal Of Human Genetics*. 2009;17:860.
  181. Jonker L. TGF- $\beta$  & BMP Receptors Endoglin and ALK1: Overview of their Functional Role and Status as Antiangiogenic Targets. *Microcirculation*. 2014;21(2):93-103.
  182. Tual-Chalot S, Oh P, Arthur HM. Mouse Models of Hereditary Haemorrhagic Telangiectasia: Recent Advances and Future Challenges. *Frontiers in Genetics*. 2015;6.
  183. Cunha Sara I, Magnusson Petra U, Dejana E, Lampugnani Maria G. Deregulated TGF- $\beta$ /BMP Signaling in Vascular Malformations. *Circulation Research*. 2017;121(8):981-99.
  184. Sorensen LK, Brooke BS, Li DY, Urness LD. Loss of distinct arterial and venous boundaries in mice lacking endoglin, a vascular-specific TGF $\beta$  coreceptor. *Developmental Biology*. 2003;261(1):235-50.
  185. Urness LD, Sorensen LK, Li DY. Arteriovenous malformations in mice lacking activin receptor-like kinase-1. *Nature Genetics*. 2000;26:328.
  186. Park SO, Wankhede M, Lee YJ, Choi E-J, Fliess N, Choe S-W, et al. Real-time imaging of de novo arteriovenous malformation in a mouse model of hereditary hemorrhagic telangiectasia. *The Journal of clinical investigation*. 2009;119(11):3487-96.
-

- 
187. Tual-Chalot S, Mahmoud M, Allinson KR, Redgrave RE, Zhai Z, Oh SP, et al. Endothelial Depletion of Acvrl1 in Mice Leads to Arteriovenous Malformations Associated with Reduced Endoglin Expression. *PLoS ONE*. 2014;9(6):e98646.
  188. Mahmoud M, Allinson KR, Zhai Z, Oakenfull R, Ghandi P, Adams RH, et al. Pathogenesis of Arteriovenous Malformations in the Absence of Endoglin. *Circulation Research*. 2010;106(8):1425-33.
  189. Choi E-J, Walker EJ, Shen F, Oh SP, Arthur HM, Young WL, et al. Minimal homozygous endothelial deletion of Eng with VEGF stimulation is sufficient to cause cerebrovascular dysplasia in the adult mouse. *Cerebrovascular diseases (Basel, Switzerland)*. 2012;33(6):540-7.
  190. Walker EJ, Su H, Shen F, Choi E-J, Oh SP, Chen G, et al. Arteriovenous malformation in the adult mouse brain resembling the human disease. *Annals of Neurology*. 2011;69(6):954-62.
  191. Thomas JM, Surendran S, Abraham M, Rajavelu A, Kartha CC. Genetic and epigenetic mechanisms in the development of arteriovenous malformations in the brain. *Clinical epigenetics*. 2016;8:78-.
  192. Ricard N, Ciais D, Levet S, Subileau M, Mallet C, Zimmers TA, et al. BMP9 and BMP10 are critical for postnatal retinal vascular remodeling. *Blood*. 2012;119(25):6162.
  193. Guttmacher AE, Marchuk DA, White RI. Hereditary Hemorrhagic Telangiectasia. *New England Journal of Medicine*. 1995;333(14):918-24.
  194. Bhattacharya JJ, Jenkins S, Zampakis P, Behbahani M, Teasdale E, Papanastassiou V. Endovascular Treatment of AVMs in Glasgow. *Interventional Neuroradiology*. 2005;11(1\_suppl):73-80.
  195. Zaki Ghali MG. Endovascular therapy for brainstem arteriovenous malformations. *World Neurosurgery*. 2018.
  196. Whitehead KJ, Sautter NB, McWilliams JP, Chakinala MM, Merlo CA, Johnson MH, et al. Effect of Topical Intranasal Therapy on Epistaxis Frequency in Patients With Hereditary Hemorrhagic Telangiectasia: A Randomized Clinical Trial. *Intranasal Therapy for Epistaxis in Patients With Hereditary Hemorrhagic Telangiectasia*. *JAMA*. 2016;316(9):943-51.
  197. Riss D, Burian M, Wolf A, Kranebitter V, Kaider A, Arnoldner C. Intranasal submucosal bevacizumab for epistaxis in hereditary hemorrhagic telangiectasia: A double-blind, randomized, placebo-controlled trial. *Head & Neck*. 2015;37(6):783-7.
  198. Han C, Choe S-W, Kim YH, Acharya AP, Keselowsky BG, Sorg BS, et al. VEGF neutralization can prevent and normalize arteriovenous malformations in an animal model for hereditary hemorrhagic telangiectasia 2. *Angiogenesis*. 2014;17(4):823-30.
  199. Ola R, Dubrac A, Han J, Zhang F, Fang JS, Larrivée B, et al. PI3 kinase inhibition improves vascular malformations in mouse models of hereditary haemorrhagic telangiectasia. *Nature Communications*. 2016;7:13650.
  200. BHF. Cardiovascular Disease Statistics 2018: British Heart Foundation; 2018 [updated February 2018. Available from: <https://www.bhf.org.uk/research/heart-statistics>.
  201. Thygesen K, Alpert JS, White HD. Universal Definition of Myocardial Infarction. *Journal of the American College of Cardiology*. 2007;50(22):2173-95.
  202. Kulick DL. Heart Attack. *MedicineNet*: MedicineNet; 2014 [Available from: [http://www.medicinenet.com/heart\\_attack/page2.htm#what\\_causes\\_a\\_heart\\_attack](http://www.medicinenet.com/heart_attack/page2.htm#what_causes_a_heart_attack).
  203. Lassen JF, Bøtker HE, Terkelsen CJ. Timely and optimal treatment of patients with STEMI. *Nature Reviews Cardiology*. 2012;10:41.
  204. Bujak M, Frangogiannis NG. The role of TGF- $\beta$  signaling in myocardial infarction and cardiac remodeling. *Cardiovascular Research*. 2007;74(2):184-95.
  205. Frangogiannis NG. The role of transforming growth factor (TGF)- $\beta$  in the infarcted myocardium. *Journal of Thoracic Disease*. 2016:S52-S63.
  206. Frangogiannis NG. Regulation of the Inflammatory Response in Cardiac Repair. *Circulation Research*. 2012;110(1):159.
  207. Prabhu SD, Frangogiannis NG. The Biological Basis for Cardiac Repair After Myocardial Infarction. *Circulation Research*. 2016;119(1):91.
  208. Liehn EA, Postea O, Curaj A, Marx N. Repair After Myocardial Infarction, Between Fantasy and Reality: The Role of Chemokines. *Journal of the American College of Cardiology*. 2011;58(23):2357-62.
-

- 
209. Frangogiannis NG. The immune system and cardiac repair. *Pharmacological Research*. 2008;58(2):88-111.
  210. Frantz S, Hu K, Adamek A, Wolf J, Sallam A, Kg Maier S, et al. Transforming growth factor beta inhibition increases mortality and left ventricular dilatation after myocardial infarction. *Basic Res Cardiol*. 2008;103(5):485-92.
  211. Dobaczewski M, Chen W, Frangogiannis NG. Transforming growth factor (TGF)- $\beta$  signaling in cardiac remodeling. *Journal of Molecular and Cellular Cardiology*. 2011;51(4):600-6.
  212. Frangogiannis NG. The inflammatory response in myocardial injury, repair, and remodelling. *Nature Reviews Cardiology*. 2014;11:255.
  213. Dallas NA, Samuel S, Xia L, Fan F, Gray MJ, Lim SJ, et al. Endoglin (CD105): A Marker of Tumor Vasculature and Potential Target for Therapy. *Clinical Cancer Research*. 2008;14(7):1931.
  214. Ollauri-Ibáñez C, López-Novoa JM, Pericacho M. Endoglin-based biological therapy in the treatment of angiogenesis-dependent pathologies. *Expert Opinion on Biological Therapy*. 2017;17(9):1053-63.
  215. Ma X, Labinaz M, Goldstein J, Miller H, Keon Wilbert J, Letarte M, et al. Endoglin Is Overexpressed After Arterial Injury and Is Required for Transforming Growth Factor- $\beta$ -Induced Inhibition of Smooth Muscle Cell Migration. *Arteriosclerosis, Thrombosis, and Vascular Biology*. 2000;20(12):2546-52.
  216. van Laake LW, van den Driesche S, Post S, Feijen A, Jansen MA, Driessens MH, et al. Endoglin Has a Crucial Role in Blood Cell-Mediated Vascular Repair. *Circulation*. 2006;114(21):2288-97.
  217. Davison BJ. *The Importance of Endoglin for Cardiac Structure and Function*. Newcastle upon Tyne, UK: Newcastle University; 2013.
  218. Carmeliet P. Angiogenesis in life, disease and medicine. *Nature*. 2005;438(7070):932-6.
  219. Pfister O, Della Verde G, Liao R, Kuster GM. Regenerative therapy for cardiovascular disease. *Translational Research*. 2014;163(4):307-20.
  220. Lefer DJ, Marbán E. Is Cardioprotection Dead? *Circulation*. 2017;136(1):98.
  221. Wöhrle J, Merkle N, Mailänder V, Nusser T, Schauwecker P, von Scheidt F, et al. Results of Intracoronary Stem Cell Therapy After Acute Myocardial Infarction. *The American Journal of Cardiology*. 2010;105(6):804-12.
  222. Traverse JH, Henry TD, Ellis SG, et al. Effect of intracoronary delivery of autologous bone marrow mononuclear cells 2 to 3 weeks following acute myocardial infarction on left ventricular function: The latetime randomized trial. *JAMA*. 2011;306(19):2110-9.
  223. Traverse JH, Henry TD, Pepine CJ, Willerson JT, Zhao DXM, Ellis SG, et al. Effect of the Use and Timing of Bone Marrow Mononuclear Cell Delivery on Left Ventricular Function After Acute Myocardial Infarction: The TIME Randomized Trial. *JAMA : the journal of the American Medical Association*. 2012;308(22):2380-9.
  224. Lee J-W, Lee S-H, Youn Y-J, Ahn M-S, Kim J-Y, Yoo B-S, et al. A Randomized, Open-Label, Multicenter Trial for the Safety and Efficacy of Adult Mesenchymal Stem Cells after Acute Myocardial Infarction. *J Korean Med Sci*. 2014;29(1):23-31.
  225. Chimenti I, Smith RR, Li T-S, Gerstenblith G, Messina E, Giacomello A, et al. Relative Roles of Direct Regeneration Versus Paracrine Effects of Human Cardiosphere-Derived Cells Transplanted Into Infarcted Mice. *Circulation Research*. 2010;106(5):971-80.
  226. Makkar RR, Smith RR, Cheng K, Malliaras K, Thomson LEJ, Berman D, et al. Intracoronary cardiosphere-derived cells for heart regeneration after myocardial infarction (CADUCEUS): a prospective, randomised phase 1 trial. *The Lancet*. 2012;379(9819):895-904.
  227. Chakravarty T, Makkar RR, Ascheim DD, Traverse JH, Schatz R, Demaria A, et al. ALLogeneic Heart STem Cells to Achieve Myocardial Regeneration (ALLSTAR) Trial: Rationale and Design. *Cell Transplantation*. 2017;26(2):205-14.
  228. Ishigami S, Ohtsuki S, Eitoku T, Ousaka D, Kondo M, Kurita Y, et al. Intracoronary Cardiac Progenitor Cells in Single Ventricle Physiology: The PERSEUS (Cardiac Progenitor Cell Infusion to Treat Univentricular Heart Disease) Randomized Phase 2 Trial. *Circulation Research*. 2017;120(7):1162.
  229. Tarui S, Ishigami S, Ousaka D, Kasahara S, Ohtsuki S, Sano S, et al. Transcoronary infusion of cardiac progenitor cells in hypoplastic left heart syndrome: Three-year follow-up of the Transcoronary
-

- 
- Infusion of Cardiac Progenitor Cells in Patients With Single-Ventricle Physiology (TICAP) trial. *The Journal of Thoracic and Cardiovascular Surgery*. 2015;150(5):1198-208.e2.
230. Srinivas S, Watanabe T, Lin C-S, William C, Tanabe Y, Jessell T, et al. Cre reporter strains produced by targeted insertion of EYFP and ECFP into the ROSA26 locus. *BMC Developmental Biology*. 2001;1(1):4.
231. Allinson KR, Carvalho RLC, van den Brink S, Mummery CL, Arthur HM. Generation of a floxed allele of the mouse endoglin gene. *genesis*. 2007;45(6):391-5.
232. Levéen P, Larsson J, Ehinger M, Cilio CM, Sundler M, Sjöstrand LJ, et al. Induced disruption of the transforming growth factor beta type II receptor gene in mice causes a lethal inflammatory disorder that is transplantable. *Blood*. 2002;100(2):560-8.
233. Sacilotto N, Monteiro R, Fritzsche M, Becker PW, Sanchez-del-Campo L, Liu K, et al. Analysis of Dll4 regulation reveals a combinatorial role for Sox and Notch in arterial development. *Proceedings of the National Academy of Sciences*. 2013;110(29):11893-8.
234. Wang Y, Nakayama M, Pitulescu ME, Schmidt TS, Bochenek ML, Sakakibara A, et al. Ephrin-B2 controls VEGF-induced angiogenesis and lymphangiogenesis. *Nature*. 2010;465:483.
235. Muzumdar MD, Tasic B, Miyamichi K, Li L, Luo L. A global double-fluorescent Cre reporter mouse. *genesis*. 2007;45(9):593-605.
236. Tual-Chalot S, Allinson KR, Fruttiger M, Arthur HM. Whole Mount Immunofluorescent Staining of the Neonatal Mouse Retina to Investigate Angiogenesis In vivo. *Journal of Visualized Experiments : JoVE*. 2013(77):50546.
237. Redgrave RE, Davison B, Amirrasouli M, Keavney B, Blamire A, Arthur HM. Cardiosphere-Derived Cell Transplantation Rescues Cardiac Function Post-MI Independently of Endoglin Expression. *Heart*. 2012;98(Suppl 5):A1.
238. Gougos A, Letarte M. Primary structure of endoglin, an RGD-containing glycoprotein of human endothelial cells. *Journal of Biological Chemistry*. 1990;265(15):8361-4.
239. Nomura-Kitabayashi A, Anderson GA, Sleep G, Mena J, Karabegovic A, Karamath S, et al. Endoglin is dispensable for angiogenesis, but required for endocardial cushion formation in the midgestation mouse embryo. *Developmental Biology*. 2009;335(1):66-77.
240. Qu R, Silver MM, Letarte M. Distribution of endoglin in early human development reveals high levels on endocardial cushion tissue mesenchyme during valve formation. *Cell and Tissue Research*. 1998;292(2):333-43.
241. Wei T-C, Lin H-Y, Lu C-C, Chen C-M, You L-R. Expression of Crip2, a LIM-domain-only protein, in the mouse cardiovascular system under physiological and pathological conditions. *Gene Expression Patterns*. 2011;11(7):384-94.
242. Mercado-Pimentel M, Hubbard A, Runyan R. Endoglin and Alk5 regulate epithelial-mesenchymal transformation during cardiac valve formation. *Developmental Biology*. 2007;304(1):420 - 32.
243. Chen K, Mehta JL, Li D, Joseph L, Joseph J. Transforming Growth Factor  $\beta$  Receptor Endoglin Is Expressed in Cardiac Fibroblasts and Modulates Profibrogenic Actions of Angiotensin II. *Circulation Research*. 2004;95(12):1167-73.
244. Vecchi A, Garlanda C, Lampugnani MG, Resnati M, Matteucci C, Stoppacciaro A, et al. Monoclonal antibodies specific for endothelial cells of mouse blood vessels. Their application in the identification of adult and embryonic endothelium. *European journal of cell biology*. 1994;63(2):247-54.
245. Braitsch CM, Combs MD, Quaggin SE, Yutzey KE. Pod1/Tcf21 is regulated by retinoic acid signaling and inhibits differentiation of epicardium-derived cells into smooth muscle in the developing heart. *Developmental Biology*. 2012;368(2):345-57.
246. Solway J, Seltzer J, Samaha FF, Kim S, Alger LE, Niu Q, et al. Structure and Expression of a Smooth Muscle Cell-specific Gene, SM22 $\alpha$ . *Journal of Biological Chemistry*. 1995;270(22):13460-9.
247. Kühbandner S, Brummer S, Metzger D, Chambon P, Hofmann F, Feil R. Temporally controlled somatic mutagenesis in smooth muscle. *genesis*. 2000;28(1):15-22.
248. Duband J-L, Gimona M, Scatena M, Sartore S, Small JV. Calponin and SM22 as differentiation markers of smooth muscle: spatiotemporal distribution during avian embryonic development. *Differentiation*. 1993;55(1):1-11.
-

- 
249. Van Tuyn J, Atsma DE, Winter EM, van der Velde-van Dijke I, Pijnappels DA, Bax NAM, et al. Epicardial Cells of Human Adults Can Undergo an Epithelial-to-Mesenchymal Transition and Obtain Characteristics of Smooth Muscle Cells In Vitro. *STEM CELLS*. 2007;25(2):271-8.
250. Kaufman MH. *The Atlas of Mouse Development*. London: Academic Press Limited; 1998.
251. Krishnan A, Samtani R, Dhanantwari P, Lee E, Yamada S, Shiota K, et al. A detailed comparison of mouse and human cardiac development. *Pediatric Research*. 2014;76:500.
252. Dominici M, Le Blanc K, Mueller I, Slaper-Cortenbach I, Marini FC, Krause DS, et al. Minimal criteria for defining multipotent mesenchymal stromal cells. The International Society for Cellular Therapy position statement. *Cytotherapy*. 2006;8(4):315-7.
253. Zhou B, Pu WT. Genetic Cre-loxP Assessment of Epicardial Cell Fate Using Wt1-Driven Cre Alleles. *Circulation Research*. 2012;111(11):e276-e80.
254. Eisenberg LM, Markwald RR. Molecular Regulation of Atrioventricular Valvuloseptal Morphogenesis. *Circulation Research*. 1995;77(1):1.
255. GeneCard W. TAGLN Gene (Protein Coding): Weizmann Institute of Science; 2018 [updated 2018. Available from: <http://www.genecards.org/cgi-bin/carddisp.pl?gene=TAGLN>.
256. Vrancken Peeters M-PFM, Gittenberger-de Groot AC, Mentink MMT, Hungerford JE, Little CD, Poelmann RE. Differences in development of coronary arteries and veins. *Cardiovascular Research*. 1997;36(1):101-10.
257. Luttun A, Carmeliet P. De novo vasculogenesis in the heart. *Cardiovascular Research*. 2003;58(2):378-89.
258. Sharma B, Chang A, Red-Horse K. Coronary Artery Development: Progenitor Cells and Differentiation Pathways. *Annual review of physiology*. 2017;79:1-19.
259. Marieb EN. *Anatomy and Physiology*. 6th Edition ed. New Jersey: Pearson Benjamin Cummings; 2004.
260. Dubé KN, Thomas TM, Munshaw S, Rohling M, Riley PR, Smart N. Recapitulation of developmental mechanisms to revascularize the ischemic heart. *JCI Insight*. 2017;2(22).
261. Payne S, De Val S, Neal A. Endothelial-Specific Cre Mouse Models. *Arteriosclerosis, Thrombosis, and Vascular Biology*. 2018;38(11):2550-61.
262. Wessels A, Pérez-Pomares JM. The epicardium and epicardially derived cells (EPDCs) as cardiac stem cells. *The Anatomical Record Part A: Discoveries in Molecular, Cellular, and Evolutionary Biology*. 2004;276A(1):43-57.
263. Massagué J, Chen YG. Controlling TGF- $\beta$  signaling. *Genes and Development*. 2000;14(6):627-44.
264. Derynck R, Feng XH. TGF- $\beta$  receptor signaling. *Biochimica et Biophysica Acta - Reviews on Cancer*. 1997;1333(2):F105-F50.
265. Lie-Venema H, van den Akker NMS, Bax NAM, Winter EM, Maas S, Kekarainen T, et al. Origin, Fate, and Function of Epicardium-Derived Cells (EPDCs) in Normal and Abnormal Cardiac Development. *TheScientificWorldJOURNAL*. 2007;7.
266. Allinson KR, Carvalho RL, van den Brink S, Mummery CL, Arthur HM. Generation of a floxed allele of the mouse Endoglin gene. *Genesis*. 2007;45(6):391-5.
267. Srinivas S, Watanabe T, Lin CS, William CM, Tanabe Y, Jessell TM, et al. Cre reporter strains produced by targeted insertion of EYFP and ECFP into the ROSA26 locus. *BMC Dev Biol*. 2001;1:4.
268. Hayashi S, McMahon AP. Efficient Recombination in Diverse Tissues by a Tamoxifen-Inducible Form of Cre: A Tool for Temporally Regulated Gene Activation/Inactivation in the Mouse. *Developmental Biology*. 2002;244(2):305-18.
269. Huh WJ, Khurana SS, Geahlen JH, Kohli K, Waller RA, Mills JC. Tamoxifen induces rapid, reversible atrophy, and metaplasia in mouse stomach. *Gastroenterology*. 2012;142(1):21-4.e7.
270. Goodpaster T, Legesse-Miller A, Hameed MR, Aisner SC, Randolph-Habecker J, Collier HA. An immunohistochemical method for identifying fibroblasts in formalin-fixed, paraffin-embedded tissue. *The journal of histochemistry and cytochemistry : official journal of the Histochemistry Society*. 2008;56(4):347-58.
271. Feng Q, Di R, Tao F, Chang Z, Lu S, Fan W, et al. PDK1 Regulates Vascular Remodeling and Promotes Epithelial-Mesenchymal Transition in Cardiac Development. *Molecular and cellular biology*. 2010;30(14):3711-21.
-

- 
272. Kaur H, Takefuji M, Ngai CY, Carvalho J, Bayer J, Wietelmann A, et al. Targeted Ablation of Periostin-Expressing Activated Fibroblasts Prevents Adverse Cardiac Remodeling in Mice. *Circulation Research*. 2016;118(12):1906-17.
273. Kokkinopoulos I, Ishida H, Saba R, Coppens S, Suzuki K, Yashiro K. Cardiomyocyte differentiation from mouse embryonic stem cells using a simple and defined protocol. *Developmental Dynamics*. 2016;245(2):157-65.
274. Lam ML, Hashem SI, Claycomb WC. Embryonic stem cell-derived cardiomyocytes harbor a subpopulation of niche-forming Sca-1+ progenitor cells. *Mol Cell Biochem*. 2011;349(1-2):69-76.
275. Boyer JG, Bhanot K, Kothary R, Boudreau-Larivière C. Hearts of Dystonia musculorum Mice Display Normal Morphological and Histological Features but Show Signs of Cardiac Stress. *PLOS ONE*. 2010;5(3):e9465.
276. MacDonald ST, Bamforth SD, Bragança J, Chen C-M, Broadbent C, Schneider JE, et al. A cell-autonomous role of Cited2 in controlling myocardial and coronary vascular development. *European Heart Journal*. 2013;34(32):2557-65.
277. Lawler S, Candia AF, Ebner R, Shum L, Lopez AR, Moses HL, et al. The murine type II TGF-beta receptor has a coincident embryonic expression and binding preference for TGF-beta 1. *Development*. 1994;120(1):165.
278. Mummery CL. Transforming growth factor  $\beta$  and mouse development. *Microscopy Research & Technique*. 2001;52:374-86.
279. Roelen BAJ, Lin HY, Knežević V, Freund E, Mummery CL. Expression of TGF- $\beta$ s and Their Receptors during Implantation and Organogenesis of the Mouse Embryo. *Developmental Biology*. 1994;166(2):716-28.
280. Seki T, Hong K-H, Oh SP. Nonoverlapping expression patterns of ALK1 and ALK5 reveal distinct roles of each receptor in vascular development. *Laboratory Investigation*. 2005;86:116.
281. Wang Y-Q, Sizeland A, Wang X-F, Sassoon D. Restricted expression of type-II TGF $\beta$  receptor in murine embryonic development suggests a central role in tissue modeling and CNS patterning. *Mechanisms of Development*. 1995;52(2):275-89.
282. Vrancken Peeters M-PFM, Gittenberger-de Groot AC, Mentink MMT, Poelmann RE. Smooth muscle cells and fibroblasts of the coronary arteries derive from epithelial-mesenchymal transformation of the epicardium. *Anatomy and embryology*. 1999;199(4):367-78.
283. Ivey MJ, Tallquist MD. Defining the Cardiac Fibroblast: A New Hope. *Circulation journal : official journal of the Japanese Circulation Society*. 2016;80(11):2269-76.
284. Merki E, Zamora M, Raya A, Kawakami Y, Wang J, Zhang X, et al. Epicardial retinoid X receptor  $\alpha$  is required for myocardial growth and coronary artery formation. *Proceedings of the National Academy of Sciences of the United States of America*. 2005;102(51):18455-60.
285. Dudas M, Kim J, Li WY, Nagy A, Larsson J, Karlsson S, et al. Epithelial and ectomesenchymal role of the type I TGF- $\beta$  receptor ALK5 during facial morphogenesis and palatal fusion. *Developmental Biology*. 2006;296(2):298-314.
286. Ito Y, Yeo JY, Chytil A, Han J, Bringas P, Nakajima A, et al. Conditional inactivation of Tgfr2 in cranial neural crest causes cleft palate and calvaria defects. *Development*. 2003;130(21):5269-80.
287. Lin AH, Luo J, Mondschein LH, ten Dijke P, Vivien D, Contag CH, et al. Global Analysis of Smad2/3-Dependent TGF- $\beta$  Signaling in Living Mice Reveals Prominent Tissue-Specific Responses to Injury. *The Journal of Immunology*. 2005;175(1):547.
288. Liu Z, Lebrin F, Maring JA, van den Driesche S, van der Brink S, van Dinther M, et al. ENDOGLIN Is Dispensable for Vasculogenesis, but Required for Vascular Endothelial Growth Factor-Induced Angiogenesis. *PLoS ONE*. 2014;9(1):e86273.
289. Hong K-H, Seki T, Oh SP. Activin receptor-like kinase 1 is essential for placental vascular development in mice. *Laboratory Investigation*. 2007;87:670 - 9.
290. Shutter JR, Scully S, Fan W, Richards WG, Kitajewski J, DeBlandre GA, et al. Dll4, a novel Notch ligand expressed in arterial endothelium. *Genes & development*. 2000;14(11):1313-8.
291. Benedito R, Duarte A. Expression of Dll4 during mouse embryogenesis suggests multiple developmental roles. *Gene Expression Patterns*. 2005;5(6):750-5.
292. Eva M, Garrido-Martin, Ha-Long Nguyen, Tyler A. Cunningham, Se-woon Choe, Zhihua Jiang, Helen M. Arthur, et al. Common and distinctive pathogenetic features of arteriovenous malformations
-

- 
- in hereditary hemorrhagic telangiectasia 1 and hereditary hemorrhagic telangiectasia 2 animal models-  
-brief report. *Arteriosclerosis, thrombosis, and vascular biology*. 2014;34:2232-6.
293. Ruiz S, Zhao H, Chandakkar P, Chatterjee PK, Papoin J, Blanc L, et al. A mouse model of hereditary hemorrhagic telangiectasia generated by transmammary-delivered immunoblocking of BMP9 and BMP10. *Scientific reports*. 2016;5:37366-.
294. Jin Y, Muhl L, Burmakin M, Wang Y, Duchez A-C, Betsholtz C, et al. Endoglin prevents vascular malformation by regulating flow-induced cell migration and specification through VEGFR2 signalling. *Nature Cell Biology*. 2017;19:639.
295. Anand IS, Florea VG. High output cardiac failure. *Current Treatment Options in Cardiovascular Medicine*. 2001;3(2).
296. Mehta PA, Dubrey SW. High output heart failure. *QJM: An International Journal of Medicine*. 2009;102(4):235-41.
297. Reddy YNV, Melenovsky V, Redfield MM, Nishimura RA, Borlaug BA. High-Output Heart Failure: A 15-Year Experience. *Journal of the American College of Cardiology*. 2016;68(5):473-82.
298. Jackson DG, Prevo R, Clasper S, Banerji S. LYVE-1, the lymphatic system and tumor lymphangiogenesis. *Trends in Immunology*. 2001;22(6):317-21.
299. Rossi MA, Carillo SV. Cardiac hypertrophy due to pressure and volume overload: distinctly different biological phenomena? *International Journal of Cardiology*. 1991;31(2):133-41.
300. Fruttiger M. Development of the retinal vasculature. *Angiogenesis*. 2007;10(2):77-88.
301. Crist AM, Young C, Meadows SM. Characterization of arteriovenous identity in the developing neonate mouse retina. *Gene Expression Patterns*. 2017;23-24:22-31.
302. Saint-Geniez M, Argence CB, Knibiehler B, Audigier Y. The msr/apj gene encoding the apelin receptor is an early and specific marker of the venous phenotype in the retinal vasculature. *Gene Expression Patterns*. 2003;3(4):467-72.
303. Sapienza P. Eyeing central neurons in vascular growth and reparative angiogenesis. *Blood*. 2012;120(11):2182.
304. Kline TL, Knudsen BE, Anderson JL, Vercnocke AJ, Jorgensen SM, Ritman EL. Anatomy of hepatic arteriolo-portal venular shunts evaluated by 3D micro-CT imaging. *Journal of Anatomy*. 2014;224(6):724-31.
305. Medical U. The venous system within the cardiovascular system Loughborough Urgo Medical; 2009 [updated 02/08/2018. Available from: <http://www.urgo.co.uk/260-the-venous-system-within-the-cardiovascular-system>.
306. Coppoolse ER, de Vroomen MJ, van Gennip F, Hersmus BJM, van Haaren MJJ. Size Does Matter: Cre-mediated Somatic Deletion Efficiency Depends on the Distance Between the Target lox-Sites. *Plant Molecular Biology*. 2005;58(5):687-98.
307. Wang S-z, Liu B-h, Tao HW, Xia K, Zhang LI. A Genetic Strategy for Stochastic Gene Activation with Regulated Sparseness (STARS). *PLOS ONE*. 2009;4(1):e4200.
308. Zheng B, Sage M, Sheppard EA, Jurecic V, Bradley A. Engineering Mouse Chromosomes with Cre-loxP: Range, Efficiency, and Somatic Applications. *Molecular and cellular biology*. 2000;20(2):648.
309. Schlabach MR, Hu JK, Li M, Elledge SJ. Synthetic design of strong promoters. *Proceedings of the National Academy of Sciences of the United States of America*. 2010;107(6):2538-43.
310. Turlo KA, Gallaher SD, Vora R, Laski FA, Iruela-Arispe ML. When Cre-Mediated Recombination in Mice Does Not Result in Protein Loss. *Genetics*. 2010;186(3):959-67.
311. Tian J, An X, Niu L. Myocardial fibrosis in congenital and pediatric heart disease. *Experimental and Therapeutic Medicine*. 2017;13(5):1660-4.
312. Hombrebueno JR, Luo C, Guo L, Chen M, Xu H. Intravitreal Injection of Normal Saline Induces Retinal Degeneration in the C57BL/6J Mouse. *Translational vision science & technology*. 2014;3(2):3-.
313. Long L, Ormiston ML, Yang X, Southwood M, Gräf S, Machado RD, et al. Selective enhancement of endothelial BMPR-II with BMP9 reverses pulmonary arterial hypertension. *Nature Medicine*. 2015;21:777.
314. Lane KB, Machado RD, Pauculo MW, Thomson JR, Phillips JA, Loyd JE, et al. Heterozygous germline mutations in BMPR2, encoding a TGF- $\beta$  receptor, cause familial primary pulmonary hypertension. *Nature Genetics*. 2000;26:81.
-

- 
315. Deng Z, Morse JH, Slager SL, Cuervo N, Moore KJ, Venetos G, et al. Familial Primary Pulmonary Hypertension (Gene *PPH1*) Is Caused by Mutations in the Bone Morphogenetic Protein Receptor-II Gene. *The American Journal of Human Genetics*. 2000;67(3):737-44.
316. NHS-UK G. Arteriovenous malformations London, UK: NHS; 2018 [updated 2018. Available from: <https://www.gosh.nhs.uk/conditions-and-treatments/conditions-we-treat/arteriovenous-malformations>.
317. Sobczak M, Dargatz J, Chrzanowska-Wodnicka M. Isolation and Culture of Pulmonary Endothelial Cells from Neonatal Mice. *Journal of Visualized Experiments : JoVE*. 2010(46):2316.
318. Cai X, Bai B, Zhang R, Wang C, Chen J. Apelin receptor homodimer-oligomers revealed by single-molecule imaging and novel G protein-dependent signaling. *Scientific reports*. 2017;7:40335-.
319. Sopeña B, Pérez-Rodríguez MT, Portela D, Rivera A, Freire M, Martínez-Vázquez C. High prevalence of pulmonary hypertension in patients with hereditary hemorrhagic telangiectasia. *European Journal of Internal Medicine*. 2013;24(3):e30-e4.
320. Cirulli A, Liso A, D'Ovidio F, Mestice A, Pasculli G, Gallitelli M, et al. Vascular Endothelial Growth Factor Serum Levels Are Elevated in Patients with Hereditary Hemorrhagic Telangiectasia. *Acta Haematologica*. 2003;110(1):29-32.
321. Sadick H, Riedel F, Naim R, Goessler U, Hormann K, Hafner M, et al. Patients with hereditary hemorrhagic telangiectasia have increased plasma levels of vascular endothelial growth factor and transforming growth factor-beta1 as well as high ALK1 tissue expression. *Haematologica*. 2005;90(6):818.
322. Sánchez-Elsner T, Botella LM, Velasco B, Langa C, Bernabéu C. Endoglin Expression Is Regulated by Transcriptional Cooperation between the Hypoxia and Transforming Growth Factor- $\beta$  Pathways. *Journal of Biological Chemistry*. 2002;277(46):43799-808.
323. A A, J N, MK J, X D, AS T. Impaired angiogenesis in aging myocardial microvascular endothelial cells is associated with reduced importin alpha and decreased nuclear transport of HIF1 alpha: mechanistic implications. *Journal of physiology and pharmacology*. 2010;61(2):133-9.
324. Marti HJH, Bernaudin M, Bellail A, Schoch H, Euler M, Petit E, et al. Hypoxia-Induced Vascular Endothelial Growth Factor Expression Precedes Neovascularization after Cerebral Ischemia. *The American Journal of Pathology*. 2000;156(3):965-76.
325. Shweiki D, Itin A, Soffer D, Keshet E. Vascular endothelial growth factor induced by hypoxia may mediate hypoxia-initiated angiogenesis. *Nature*. 1992;359:843.
326. Jakob P, Landmesser U. Current Status of Cell-Based Therapy for Heart Failure. *Curr Heart Fail Rep*. 2013;10(2):165-76.
327. Smith RR, Barile L, Cho HC, Leppo MK, Hare JM, Messina E, et al. Regenerative Potential of Cardiosphere-Derived Cells Expanded From Percutaneous Endomyocardial Biopsy Specimens. *Circulation*. 2007;115(7):896-908.
328. Redgrave R. Role of endoglin in CDC mediated heart repair. Newcastle upon Tyne, UK: Newcastle University; 2013.
329. Brant R. Inference for Means: Comparing Two Independent Samples The University of British Columbia, Vancouver [Available from: <https://www.stat.ubc.ca/~rollin/stats/ssize/n2.html>].
330. Ma X, Labinaz M, Goldstein J, Miller H, Keon WJ, Letarte M, et al. Endoglin Is Overexpressed After Arterial Injury and Is Required for Transforming Growth Factor- $\beta$ -Induced Inhibition of Smooth Muscle Cell Migration. *Arteriosclerosis, Thrombosis, and Vascular Biology*. 2000;20(12):2546-52.
331. Mancini Maria L, Terzic A, Conley Barbara A, Oxburgh Leif H, Nicola T, Vary Calvin PH. Endoglin plays distinct roles in vascular smooth muscle cell recruitment and regulation of arteriovenous identity during angiogenesis. *Developmental Dynamics*. 2009;238(10):2479-93.
332. Rossi E, Smadja DM, Boscolo E, Langa C, Arevalo MA, Pericacho M, et al. Endoglin regulates mural cell adhesion in the circulatory system. *Cell Mol Life Sci*. 2016;73(8):1715-39.
333. Núñez-Gómez E, Pericacho M, Ollauri-Ibáñez C, Bernabéu C, López-Novoa JM. The role of endoglin in post-ischemic revascularization. *Angiogenesis*. 2017;20(1):1-24.
334. Karrowni W, El Accaoui RN, Chatterjee K. Coronary collateral circulation: Its relevance. *Catheterization and Cardiovascular Interventions*. 2013;82(6):915-28.
335. Torsney E, Charlton R, Parums D, Collis M, Arthur HM. Inducible expression of human endoglin during inflammation and wound healing in vivo. *Inflammation Research*. 2002;51(9):464-70.
-

- 
336. Tseliou E, Reich H, de Couto G, Terrovitis J, Sun B, Liu W, et al. Cardiospheres reverse adverse remodeling in chronic rat myocardial infarction: roles of soluble endoglin and Tgf- $\beta$  signaling. *Basic Res Cardiol*. 2014;109(6):443.
337. Lindahl P, Johansson BR, Levéen P, Betsholtz C. Pericyte Loss and Microaneurysm Formation in PDGF-B-Deficient Mice. *Science*. 1997;277(5323):242.
338. Streit M, Riccardi L, Velasco P, Brown LF, Hawighorst T, Bornstein P, et al. Thrombospondin-2: A potent endogenous inhibitor of tumor growth and angiogenesis. *Proceedings of the National Academy of Sciences*. 1999;96(26):14888.
339. Redgrave RE, Tual-Chalot S, Davison BJ, Greally E, Santibanez-Koref M, Schneider JE, et al. Using MRI to predict future adverse cardiac remodelling in a male mouse model of myocardial infarction. *IJC Heart & Vasculature*. 2016;11:29-34.
340. Boukouaci W, Lauden L, Siewiera J, Dam N, Hocine H-R, Khaznadar Z, et al. Natural killer cell crosstalk with allogeneic human cardiac-derived stem/progenitor cells controls persistence. *Cardiovascular Research*. 2014;104(2):290-302.
341. Carr CA, Stuckey DJ, Tan JJ, Tan SC, Gomes RSM, Camelliti P, et al. Cardiosphere-Derived Cells Improve Function in the Infarcted Rat Heart for at Least 16 Weeks – an MRI Study. *PLoS ONE*. 2011;6(10):e25669.
342. Li C, Issa R, Kumar P, Hampson IN, Lopez-Novoa JM, Bernabeu C, et al. CD105 prevents apoptosis in hypoxic endothelial cells. *Journal of Cell Science*. 2003;116(13):2677.
343. Gomes AC, Falcão-Pires I, Pires AL, Brás-Silva C, Leite-Moreira AF. Rodent models of heart failure: an updated review. *Heart Failure Reviews*. 2013;18(2):219-49.
344. Letarte AGaM. Primary structure of endoglin, an RGD-containing glycoprotein of human endothelial cells. *Journal of Biological Chemistry*. 1990;265(15):8361-4.